

174
210

Unsteady Pressure and Vorticity Fields in

Blade-Vortex Interactions

by

Matthew M. Pesce

Thesis submitted to the Faculty of the

Virginia Polytechnic Institute and State University

in partial fulfillment of the requirements for the degree of

Master of Science

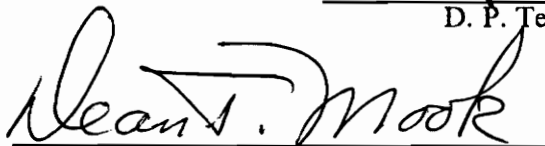
in

Engineering Mechanics

APPROVED:



D. P. Telionis, Chairman



D. T. Mook



R. D. Kriz

December, 1990

Blacksburg, Virginia

LD
5655
V855
1990
P452
C.2

Unsteady Pressure and Vorticity Fields in

Blade-Vortex Interactions

by

Matthew M. Pesce

D. P. Telionis, Chairman

Engineering Mechanics

(ABSTRACT)

The unsteady interaction of a vortex core with a NACA 0015 airfoil is studied in two dimensions. A two-component, three-beam Helium-Neon laser-Doppler Velocimetry system is used to take data in a water tunnel. Ensemble-averaged velocity fields are obtained in the region of the leading edge of the airfoil. Finite-difference algorithms were written to obtain vorticity and pressure in the data field. Computer animation of the unsteady vorticity was accomplished first with a Fortran code written for an Apple Macintosh computer and later with a commercial software package for a SUN Microsystems graphics terminal.

Dedication

Dedicated to my Parents, Ralph and Mary, my sister, Rachael, and my brothers, Adam and Thaddeus

Proof that the human spirit can overcome all adversity and persevere

Acknowledgements

I wish to express my gratitude to Dr. Demetri P. Telionis for the opportunity, guidance, and support to reach an advanced degree.

Thanks also to Drs. Kriz and Mook for serving on my committee and their criticisms concerning this work. Extra thanks to Dr. Kriz for his assistance in data animation.

The work presented here was funded by Boeing Helicopter; without their support I would not have been able to eat.

Special thanks to Michael Wilder, Ngoc Hoang, Othon Rediniotis, Ron Swecker and other notables for their help and friendship.

Finally, thanks to Tracey A. Mitchell for her endurance through the years of our acquaintance. I will always remember.

Table of Contents

| | |
|---|-----------|
| 1. Introduction and Literature Review | 1 |
| 2. Facilities and Equipment | 5 |
| 2.1 The Water Tunnel | 5 |
| 2.2 The Models | 6 |
| 2.3 Laser-Doppler Velocimetry | 7 |
| 2.3.1 The DISA Laser System | 9 |
| 2.3.2 The TSI Laser System | 10 |
| 3. Data Acquisition, Reduction, and Analysis | 12 |
| 3.1 Data Acquisition | 12 |
| 3.2 Vorticity Calculations | 13 |
| 3.3 Pressure Distribution | 14 |
| 3.4 Animation | 17 |
| 3.4.1 Macintosh Animation | 18 |
| 3.4.2 SUN Animation | 19 |

| | |
|---|------------|
| 4. Results and Discussion | 21 |
| 4.1 Introduction | 21 |
| 4.2 Velocity and Vorticity | 22 |
| 4.3 Pressure | 24 |
| 4.4 Conclusions | 27 |
| | |
| Bibliography | 29 |
| | |
| Appendix A. Vorticity Code | 32 |
| | |
| Appendix B. Pressure Code | 39 |
| | |
| Appendix C. Macintosh Animation Code | 49 |
| | |
| Appendix D. SUN Animation Code | 60 |
| | |
| Appendix E. Figures | 64 |
| | |
| Vita | 216 |

1. Introduction and Literature Review

The interaction of vortices with wings, propellers, and helicopter rotor blades comprises an important class of non-uniformities in unsteady aerodynamics. Concentrated filaments of vorticity are shed from sharp surfaces, such as the trailing edge of a wing or the tip of a blade. Under normal flight conditions, the vortex cores dissipate; however, when two aircraft fly in close proximity or when vorticity remains in the helicopter rotor plane, as in powered descent (Figure 1.1), the vortex filaments induce rapidly fluctuating airfoil pressures and noise. In helicopter aerodynamics, in particular, vorticity interactions cause vibrational loadings that can damage rotors and amplify fatigue of materials.

The interactions of vortices with wings or rotors exist between two extreme conditions, the vortex perpendicular to the blade axis and the vortex parallel to the blade axis (Figure 1.2). The perpendicular condition affects only a small region of the blade but presents itself as a three-dimensional problem. The parallel condition affects the entire blade but is only a two-dimensional problem. As a vortex comes closer to a blade, the area affected by the vortex, the structural loading, and the noise increase.

Work has been done in an effort to closely simulate the real helicopter-blade interaction problem. Neuwerth and Muller (1985) generated vortices which interact with rotating blades in a wind tunnel. This arrangement resembles the actual conditions of helicopter flight, but accurate study of the flow character near the rotors is difficult due to the three-dimensional flowfield and the motion of the model relative to an inertial reference plane. Simpler, numerical and experimental simulations of a two-dimensional parallel interaction can provide detailed flow information in the vicinity of the airfoil's leading edge. A popular method for studying the 2-D parallel interaction is to generate vortices by pitching an airfoil upstream of a second airfoil. A street of alternating positive and negative vortices follow the freestream and alters the flow around the second, or target, airfoil (Figure 1.3). The 2-D, parallel, vortex interaction is generally known as the Blade-Vortex Interaction (BVI) problem. The initial strength and location of the vortex, with respect to the target airfoil, vary widely in the literature.

Numerical solutions to Blade-Vortex Interactions include Navier-Stokes and discrete-vortex dynamics methods. Work by Caradonna (1984), Tang and Sankar (1987), and Rai (1987) are representative of Navier-Stokes solutions. Unmodified N-S solvers numerically dissipate the strong gradients across the vortices. Since numerical dissipation is the order of the grid spacing to the 4th power, this effect is much worse for the coarse grids used in the outer flow than for the fine grids used in the airfoil boundary layer. A vortex released upstream of the target airfoil will be numerically dispersed before it interacts unless modifications are made. However, fixing the path or strength of the vortex, a modification used by many researchers, produces incorrect results for close interactions. In their unsteady, compressible Navier-Stokes algorithm, Tang and Sankar employ artificial viscosity terms to a modified velocity field; this allows the vortex to retain its sharp features until the actual interaction. Rai, however, used a 5th-order, thin-layer solver. Very fine grids were needed to prevent numerical diffusion of the vortex core.

Work by Mook et al. (1987,1990), Lee and Smith (1987), and Poling et al. (1988) are representative of discrete-vortex dynamics. Velocities and pressures induced by clouds of point vortices

are calculated. Mook et al. modeled the flow over a pitching airfoil with a panel method. The airfoil was represented by a piecewise linear distribution of vorticity. As the airfoil pitches, it sheds vorticity from the trailing edge. The shed vorticity is modeled by vortex cores or blobs of vorticity. As the cores move away, they may spread too far apart or move too close together; cores are added or combined, eliminating discontinuities, and the vorticity is redistributed. Lee and Smith and Poling et al. modeled the interaction process of a vortex striking an airfoil. A cloud of ideal vortices, simulating one of the vortices in the unsteady wake, is convected with the freestream over the target airfoil. Poling et al. modeled the airfoil with a Joukowski transformation; the circle theorem is employed to solve the problem in complex coordinates. The cloud is modeled as a Gaussian distribution of vorticity strength in an effort to more closely resemble a real vortex. Lee and Smith modeled the target airfoil with a panel method. As the cloud warps and moves closer to the airfoil, the strengths and sizes of the panels are redistributed. The point vorticities in the cloud begin with equal strength. Discrete-vortex dynamics yields accurate solutions but does not capture airfoil separation. Common problems are cloud instability and singularities at the center of the point vorticities.

Experimental work has also been done on the 2-D parallel interaction problem. Booth and Yu (1986), Poling (1985), and others have employed flow visualization to study the roll-up of vorticities behind a pitching airfoil and the interaction of vortex cores with stationary airfoils. Booth and Yu establish three interaction regions--the collision zone, the distortion zone, and the deflection zone. A vortex moving within the collision zone, a small band above and below the target airfoil's leading edge, will split across the nose of the airfoil. A vortex moving in the deflection zone, the outermost region, is only displaced along with the freestream. In the distortion zone, the interacting vortex deforms and displaces. The interaction regions are sensitive to the strength, size, and initial position of the vortex as well as the loading of the airfoil.

Meier and Timm (1985) created a Karman vortex street with a stationary square cylinder and single start-up vorticities using an airfoil in a shock-tube chamber. Meier and Timm found that when

a vortex moves in the deflection zone, the suction region on the airfoil is reduced. But as the vortex gets closer, it mixes with the vorticity of the boundary layer and induces a separation bubble. This secondary vortex collapses as the vortex moves over the airfoil. In the collision zone, the impinging vortex core disintegrates, leaving only scattered vorticity. Later work by Booth (1986, 1987), Wilder et al. (1990), and Mayle et al. (1990) obtained quantitative experimental velocity, vorticity, and pressure fields in the wake of the pitching airfoil and in the vicinity of a target airfoil placed in the wake.

In the experimental work presented here, we use a NACA 0015 target airfoil at 10° angle of attack and vortex cores created with a NACA 0012 airfoil pitching upstream of the target airfoil with a reduced frequency of 2. The reduced frequency, $k = \frac{\omega c}{2U_\infty}$, is a similarity parameter comparing freestream velocity to the pitching airfoil's frequency and chord length. Laser-Doppler Velocimetry (LDV) measurements are taken on a fine spacial grid to establish the unsteady, ensemble-averaged velocity flowfield in the vicinity of the target airfoil. The case of a positive vortex passing above the target airfoil within the distortion zone is explored. Finite differences are used to calculate flow derivatives to create vorticity as well as pressure coefficients. Previous experimental research could not supply large amounts of qualitative data on BVI. The work presented here provides detailed velocity measurements in the vicinity of target airfoil's leading edge. The fundamentals of the interaction process are studied and conclusions are presented.

2. Facilities and Equipment

2.1 The Water Tunnel

The water tunnel (Figure 2.1.1) was built in 1976 by the Engineering Science and Mechanics Department with the support of the Army Research Office. The basic designs can be found in the work of Koromilas (1978) and Mezaris (1979). Recent modifications are described by Poling (1985). The tunnel contains 570 gallons of water and is built of poly-vinyl chloride (PVC) pipe and plexiglass. The test section and parts of the lower tunnel are made of plexiglass to allow flow visualization and laser velocimetry studies.

Speed control is accomplished with both a butterfly valve and a variable-speed DC electric motor driving a centrifugal pump. Speeds can range between 0 and 5 m/s by changing the valve openings and pump speeds; however, high valve openings cause higher turbulence levels. There is a temperature control unit that can heat the water and increase the temperature at the rate of 3 degrees Celcius per hour.

The settling chamber contracts at a six-to-one ratio into the test section. There are turning vanes as well as screens and 3 cm² aluminum hexagonal honeycombs to reduce the turbulence level and turbulence scales. Moreover, a small honeycomb section with 1/4-inch cells and three screens precede the test section. These further reduce turbulence levels and increase flow uniformity.

The test section has a cross-section of 10 inches by 12 inches and is 28 inches long (Figure 2.1.2). It was constructed with false walls to bleed off the side-wall boundary-layer and reduce end effects. Flaps at the ends of the false walls control the bleed-flow and limit separation at the leading edges of the false walls. The flaps are kept at 10° to minimize the boundary layer thickness as mentioned in Kim (1985) and Poling (1985). The boundary-layer thickness is then at most 4% of the span of the tunnel. The turbulence levels in the test section are on the order of 0.4% to 0.65% for u' and v' components between ± 3 inches from the center of the tunnel.

2.2 The Models

Two symmetrical airfoils are mounted in the test section of the water tunnel. The first is a NACA 0012 with a 4-inch chord, the other is a NACA 0015 with a 6-inch chord placed 8 inches downstream of the trailing edge of the first airfoil (Figure 2.2.1). The NACA 0012 pitches about its quarter chord to generate a street of positive and negative vorticity. A shaft connects the airfoil to a four-bar linkage system running off a 3/4 hp Morse DC electric motor (Figure 2.2.2). The motor is connected to a 16:1-ratio gear box and to a 6-inch aluminum flywheel. The four-bar linkage acts to reduce vibrations entering the flowfield during airfoil oscillations. A push-bar connects the four-bar linkage to the aluminum flywheel. Pitching amplitude can be selected by connecting the push-bar to any radial position on the flywheel; an amplitude of 20 degrees is used for the data collected here. A Datel electric shaft encoder coupled with a photo-diode on the flywheel triggers the data-aquisition system at the beginning of a new pitching cycle.

The NACA 0015 acts as a target airfoil for the generated vortex street. Connected to a rotating mount embedded into the inner false wall of the test section, the airfoil can be adjusted to various angles of attack. The rotating mount is fixed into position with two set screws. A third set screw pushes the model tight against the water tunnel.

2.3 *Laser-Doppler Velocimetry*

Velocity data are gathered with a laser-Doppler velocimetry system. When two or more laser beams intersect, an interference pattern of alternating light and dark fringes occurs (Figure 2.3.1). Particles travelling in a moving fluid refract light and dark as they pass through this intersection. The scattered light is received by a photodetector and converted to an electric signal. The signal contains low- and high-frequency noise, a pedestal voltage, and the Doppler frequency (Figure 2.3.2). After processing, the Doppler frequency, f_D , is removed from the signal and directly converted to velocity.

Both forward- and backward-scatter modes are used in LDV systems (Figure 2.3.3). In forward-scatter the photodetector and light receiving optics are on the opposite side of the beam intersection from the laser. Forward-scatter requires less laser power for good signal quality but is difficult to traverse. In backward-scatter the photodetector and optics are on the same side as the laser. The backward-scatter systems need more power for good signals but traverse much more easily.

Laser-Doppler velocimetry systems have several desirable advantages. LDV has high-frequency response and high signal-to-noise ratio, and no calibrations are required since the particle velocity is directly proportional to the frequency of the signal. Also, the control volume of intersection is small, thereby, allowing detailed measurements. Finally, the laser beams do not physically interfere

with the flow--this is especially important in flows with vortex structures where hot-wire or 5-hole probes can alter the vortex path or cause early core breakdown. However, laser systems are initially expensive and difficult to setup.

With LDV systems, flow reversal can be detected by the frequency shifting of one or more of the intersecting beams, which adds a known frequency to the signal. Without frequency shifting, particles moving with the same speed but in opposite directions will scatter light at the same Doppler frequency, but with frequency shifting, the scattered light will have different Doppler frequencies. Therefore, flow reversal can be measured accurately, and the frequency shift can then be removed during processing.

Another important consideration in LDV is prevention of particle-lag errors. A particle that is too heavy or large can fall due to gravity and produce an extraneous component of velocity, or it may not respond to quick movements of the flow. Particle lag is reduced by using small, neutrally buoyant particles, i.e. particle density near that of the fluid density, dispersed in the fluid in a way that prevents aggregation of the particles. The signals scattered from particles that are too large or too small can be rejected during signal processing.

The experimental setup of the present effort includes DISA and TSI optical systems. The DISA system consists of a 5 mW laser in forward-scatter mode while the TSI system has a 15 mW laser in backward-scatter mode. Both systems use He-Ne lasers with 632.8 nm wavelength. The DISA laser system monitors the free-stream velocity. The laser control volume is fixed and the system uses tracker-type signal processing. The TSI laser system is used to take the two independent components of unsteady velocity data. It consists of several optical components to insure high signal-to-noise ratio and detection of flow reversals. The system uses linear variable direct transducers (LVDT) for computer-controlled stepping through space, and the two independent Doppler signals are processed with counter-type signal processors. Neutrally buoyant 1.5 micron silicon carbide particles are used to seed the flow for better signal quality.

The fluid velocity is proportional to the Doppler frequency f_D and the interference-fringe spacing, d_f , such that $V = d_f f_D$, where $d_f = \frac{\lambda}{2 \sin k}$. The wavelength of the laser-light and the half-angle between the two intersecting beams are λ and k , respectively.

2.3.1 The DISA Laser System

A DISA laser system (Figure 2.3.4) is used to monitor the freestream velocity, which is then employed for on-line non-dimensionalizing of the data as well as helping reduce errors due to low-frequency fluctuations in the freestream. A 5 mW laser beam is split into two equal-intensity beams by a DISA 55L01 beam splitter. The beams focus through a 300 mm focal-length lens into the water tunnel, upstream of the pitching airfoil. The scattered light is collected in forward-scatter through a 0.1 mm pin-hole into the DISA 55L10 photomultiplier. A DISA 55L15 high-voltage source supplies continuously adjustable DC voltage to the photomultiplier. The signal from the photomultiplier enters the preamplifier (DISA 55L30). The preamp contains narrow-band filtering, preset for the selectable Doppler frequency ranges available with the frequency tracker (DISA 55L35). The measured Doppler signals can range from 2.25 kHz to 15 MHz and are tracked with seven selectable ranges. Velocity fluctuations of up to 70% of the mean in a given range can be followed. For low density seeding situations, signal drop-out circuitry can be set to keep only the clearest signals. An output voltage proportional to the Doppler frequency is then sent as analog output to the MINC 11 analog-to-digital converter. The freestream velocity data are accepted at constant time steps and saved on disk along with the u and v velocity components from the TSI system.

The laser and photomultiplier are arranged in forward-scatter mode and are manually positioned on an optical bench. The silicon carbide seeding gives a very high data rate in forward-scatter mode.

This, paradoxically, can lead to higher noise since the photodetector could saturate. Lowering the power to the photodetector compensates for this.

2.3.2 The TSI Laser System

A TSI system is employed to collect data around the NACA 0015 model (Figure 2.3.5). A 15 mW laser beam is split into 3 beams, and two independent velocity components are measured using a single photomultiplier in backward-scatter. The 15 mW beam is collimated (TSI 9108) to prevent beam divergence and to place the beam waist, the thinnest diameter, at the beam intersection. This decreases the size of the control volume, increases signal to noise ratio, and keeps the fringes parallel and straight for accurate Doppler frequency refraction. The beam then passes through two quarter-wave plates (TSI 9178-2) that linearly polarize the light. Next, a polarization rotator (TSI 9102-2) rotates the polarization plane of the incoming beam relative to the two split beams coming out of the variable-intensity beam splitter (TSI 9216-2). The rotation optimizes the intensity split to 2/3 to 1/3. The variable-intensity beam splitter offsets the 1/3 beam 25 mm from the optical axis and leaves the 2/3 beam on-axis to be split again (TSI 9115-2) into two equal-intensity beams. Both beams are set off the axis by 25 mm. The first 1/3 intensity beam is rotated again (TSI 9103-2) to ensure that it is plane-polarized with the last two beams. Two of the three beams are now frequency shifted with 40 and 60 MHz Bragg cells (TSI 9182-2 and TSI 9282). This puts the fringes in motion at 20 MHz and 40 MHz in the two independent directions used for measurements. The photomultiplier (TSI 9162) follows next in the optic assembly. The refracted light is received in backward scatter along the optic-axis. The photomultiplier system can sense frequencies up to 200 MHz and amplify weak signals. The beams are then displaced inward (TSI 9114-2) and their diameters are expanded (TSI 9188A). This decreases the intersection size and increases the signal-to-noise ratio of the system.

The expanded beams reflect through the mirror tower (Figure 2.3.6) and out through an achromatic focusing lens (TSI 9118) into the test section. The lens has a focal length of 250 mm. Scattered light is received through the same optics into the photomultiplier. The signal is then down-mixed to remove the 20 MHz and 40 MHz frequency shifts and a selectable frequency is left with the signal. This allows for detection of flow reversals and is removed during data reduction. The signals are then processed with TSI Model 1990 counters. The counters remove the high- and low-frequency noise from the Doppler signal and then count the number of times the signal crosses and re-crosses zero (Figure 2.3.7). Once the signal crosses zero twice, the logic gate is opened and the zero crossings are counted. When the signal crosses zero a preset number of times, the signal is considered valid and is counted. The counted signals are converted from digital to analog in the TSI counters and sent to the MINC 11 laboratory computer.

The analog signal must be converted back to digital to be processed and stored on disk. The MINC 11 expects data at fixed times during data acquisition; however, the signals arrive randomly due to the dispersion of particles in the flow. With digital input, if no signal is available at acquisition time, the computer will substitute zero. To prevent this situation, the digital-to-analog-to-digital set-up is used. Now, if a new signal is not available, the counter keeps sending the previous value. Acquisition is triggered at the beginning of each pitching period, and the velocities are ensemble-averaged. This removes the velocity fluctuations and leaves the mean-velocity components.

Traversing is accomplished horizontally by moving the optical bench while vertical traversing is performed with two mirrors, one mirror moves and the other is fixed to the laser table. The movement is performed with LVDT's connected to the MINC-11 with feedback circuitry. The position of the control volume is monitored and corrected as needed.

3. Data Acquisition, Reduction, and Analysis

3.1 Data Acquisition

After the raw data are obtained, the voltages stored on diskette by the MINC 11 lab computer are converted to velocity. The voltages are reduced on the IBM 3090 mainframe computer using programs written by Wilder (1988). The IBM 3090 allows faster computing and greater storage. Processed data can then be plotted on the Versatec Color and B/W electrostatic plotters available with the VPI & SU computing facilities.

The u and v components of velocity, those components parallel and perpendicular to the primary flow direction, and the freestream velocity are stored as voltages at each time level and at each grid position. The measurement grid is a rectangular, orthogononal mesh with its x - y origin centered at the leading edge of the target airfoil, where x points downstream and y points up (Figure 3.1.1). Voltages corresponding to beams blocked by the airfoil are steady with time. Data from these spacial locations are recognized by this feature and are tossed out. However, to keep the data field uniform, a weighting parameter is stored for each location. If this parameter is equal to one, the data are good; for all other cases the data are bad. The region of blockage occurs only near the

airfoil surface. The three converging beams encompass more space than does the control volume itself. When the control volume is outside of the airfoil surface, at least one beam can strike the airfoil. To diminish the size of the blocked region during data acquisition, the beams are tilted in the vertical plane (Figure 3.1.2). The beams enter the focusing lense at an angle, although still parallel to each other. The velocities are now measured out of the x-y plane, but this can be corrected analytically. With this modification data can now be taken closer to the airfoil, thus, reducing the bad data region around the airfoil. The rest of the voltages are converted to velocity directly from the equations presented in Sections 2.4.1 and 2.4.2. These velocities are smoothed by using IMSL subroutines to eliminate any sharp discontinuities in the velocities.

3.2 Vorticity Calculations

A finite-difference algorithm was written to calculate the two-dimensional vorticity field from the measured, unsteady velocity field (Appendix A). The vorticity expression

$$\vec{\omega} = \frac{1}{2} \nabla \times \vec{V}$$

simplified for two-dimensional flow

$$\omega = \frac{\partial v}{\partial x} - \frac{\partial u}{\partial y} \quad (3.2.1)$$

is evaluated in space at each time level. The derivatives are represented by the following 2nd Order central, forward, and backward finite-difference expressions:

$$\text{Central: } \left. \frac{\partial f}{\partial z} \right|_i = \frac{f_{i+1} - f_{i-1}}{2\Delta z} + O(\Delta z^2) \quad (3.2.2)$$

$$\text{Forward: } \frac{\partial f}{\partial z} \Big|_i = \frac{-f_{i+2} + 4f_{i+1} - 3f_i}{2\Delta z} + O(\Delta z^2) \quad (3.2.3)$$

$$\text{Backward: } \frac{\partial f}{\partial z} \Big|_i = \frac{f_{i-2} - 4f_{i-1} + 3f_i}{2\Delta z} + O(\Delta z^2). \quad (3.2.4)$$

where f represents a dependent variable and z represents any independent variable. The subscripts $i, i + 1, i + 2$, etc., indicate the grid-node where the quantity is evaluated. The spacing, Δz , is constant.

Logical expressions route the program to the correct derivatives. With good data on either side of the point evaluated, central differences are used, and when a blocked data point exists, a one sided difference is used (Figure 3.2.1). The derivatives above, though shown in one direction, are substituted for the two dimensional spacial vorticity derivatives by changing the dependent and independent variables to u or v and x or y , respectively. There are nine independent conditions to consider (Figure 3.2.2) and, therefore, nine combinations of the finite-difference expressions to be used. Figure 3.2.1 shows how the derivatives would be used in one direction, but Figure 3.2.2 shows the actual 2-D decisions to be made. The vorticity is set to zero where correct derivatives cannot be computed. Vorticity iso-bars are then plotted at each time level of the pitching period.

3.3 Pressure Distribution

The ensemble-averaged velocity data are employed in the 2-D non-dimensionalized Euler equations to evaluate the convective terms and solve for the pressure gradients,

$$\frac{\partial p}{\partial x} = - \left(T \frac{\partial u}{\partial t} + u \frac{\partial u}{\partial x} + v \frac{\partial u}{\partial y} \right) \quad (3.2.5)$$

and

$$\frac{\partial p}{\partial y} = - \left(T \frac{\partial v}{\partial t} + u \frac{\partial v}{\partial x} + v \frac{\partial v}{\partial y} \right). \quad (3.2.6)$$

where u and v and x , y , and t are dimensionless velocity components, space, and time, respectively, and T is a dimensionless parameter, often referred to as the Strouhal Number.

The physical quantities are non-dimensionalized according to the formulae

$$\begin{aligned} x &= \frac{x^*}{c} & p &= \frac{p^*}{\rho^* U_\infty^{*2}} & u &= \frac{u^*}{U_\infty^*} \\ y &= \frac{y^*}{c} & \rho &= \frac{\rho^*}{\rho_\infty^*} = 1 & v &= \frac{v^*}{U_\infty^*} \\ t &= \frac{t^*}{\tau} \end{aligned}$$

The dimensional terms x^* and y^* are the actual distances in the water tunnel while c is the chord length of the target airfoil. Similarly, t^* is real time measured while τ^* is the pitching period. The physical pressure p^* is non-dimensionalized with the dynamic pressure $\rho^* U_\infty^{*2}$. The velocities are non-dimensionalized with the freestream velocity while the density is eliminated during the non-dimensionalization. The non-dimensional Euler equations retain the same form as the dimensional equations except for Strouhal Number in front of the time dependant term, $T = \frac{c^*}{\tau^* U_\infty^*}$.

The derivatives are evaluated as defined by Equations (3.2.2), (3.2.3), and (3.2.4) in Section 3.2. Central differences are used when there are no blocked data on either side of the point where the derivative is calculated; one-sided differences are used on the boundaries and near the airfoil. Moreover, the non-linear terms are evaluated at the point where the derivative is evaluated. For example, $u \frac{\partial u}{\partial x}$ is represented as $u_{i,j} \frac{\partial u}{\partial x} \Big|_{i,j}$, where $\frac{\partial u}{\partial x} \Big|_{i,j}$ is evaluated as a finite difference and the point (i,j) is an arbitrary grid point in the data field.

Once the values of $\frac{\partial p}{\partial x}$ and $\frac{\partial p}{\partial y}$ are known everywhere, the pressure coefficients $C_p(x,y,t)$ can be evaluated with partial integration or algebraic approximations on the derivatives. Partial integration of the differential pressure terms is accomplished by the trapezoidal-rule. The trapezoidal-rule provides 2nd-order accuracy and requires two differential pressure values and a starting value for pressure. Since no experimental or numerical pressure solutions were available, the farthest point upstream of and above the airfoil is used as a reference pressure, p_∞ . Although this point is unsteady, it is assumed constant from one time step to the next; this permits time frame comparisons. Also, the vortex only indirectly affects this point, so trends in C_p should remain accurate.

The horizontal and vertical integration equations are

$$\frac{p(x_i, y_j, t) - p(x_{i-1}, y_j, t)}{\rho U_\infty^2} = \int_{x_1}^{x_2} \frac{\partial p}{\partial x} dx,$$

and

$$\frac{p(x_i, y_j, t) - p(x_i, y_{j-1}, t)}{\rho U_\infty^2} = \int_{y_1}^{y_2} \frac{\partial p}{\partial y} dy,$$

respectively, where U_∞ is the freestream velocity, and $i, j, i-1$, and $j-1$ are arbitrary locations in the data grid. The integrals are then approximated with the trapezoidal-rule,

$$\Delta C_p)_{ij} = \frac{\Delta x}{2} \left[\frac{\partial p}{\partial x}_{ij} + \frac{\partial p}{\partial x}_{i-1,j} \right] \quad (3.2.7)$$

and

$$\Delta C_p)_{ij} = \frac{\Delta y}{2} \left[\frac{\partial p}{\partial y}_{ij} + \frac{\partial p}{\partial y}_{i,j-1} \right] \quad (3.2.8)$$

Integration starts with the reference pressure, p_∞ , and continues down into the data field. All the finite ΔC_p values are summed from the reference location to a general grid location to get total C_p based on the reference pressure.

An important consideration is the direction in which to integrate through space. In the data presented here, differential pressures are integrated first in the positive x-direction, downstream, and then in the negative y-direction, toward the upper airfoil surface. This prevents integration through the vortex except when necessary for C_p calculations. Different path directions for integration yield a variety of results, especially in x-direction integrations. This may be due to the course grid spacing in this direction or integration through the vortex core.

Other methods were tried and compared to the trapezoidal-rule method. A sixth-order Simpson's rule integration scheme as well as a finite-difference approximation to the derivatives were used. Both had the same trends as the trapezoidal-rule solution but had different magnitudes. Simpson's rule needed six integrand values preceding the solution point and gave results differing by as much as 20%. Since no exact comparisons could be made, the simplest algorithm was used.

3.4 Animation

Computer animation is the rapid painting and repainting of graphic images on a computer screen, creating the impression of moving figures. The general procedure is to take the physical quantity to be animated and convert it to a discrete pixel representation; the calculations are generally done in a two-step procedure. First, the data are transferred to the screen by converting physical quantities to graphic images. The pixels on the computer screen are allocated memory space; each pixel has a location, color, and brightness associated to it. The screen is then stored as a bitmap, to be recalled as a block quantity, containing only the information needed to locate

and shade the pixels. A second program reads the bitmaps and displays them. Since there are no calculations in the second program, animation is faster than when using only the first program.

Animating vorticity has several advantages over animation of velocity or pressure. The vortical structure of the flow and the separation regions on the airfoil are readily visualized. Also, changes in the position, size, and strength of the vortex are observable along the vortex path. Available colors are scaled continuously from positive to negative vorticity maximums. Moreover, small flow disturbances as well as the large distortions due to the airfoil can be visualized. The entire pitching cycle can be visualized continuously.

3.4.1 Macintosh Animation

Animation of vorticity was achieved first on the Apple Macintosh IIx computer with an Apple high-resolution RGB color monitor. The monitor is a 13-inch diagonal with 640 by 480 pixel resolution and a vertical refresh rate of 66.7 Hz. The computer is based on the 32-bit NuBus with a Motorola MC68020 processor and MC68881 Math co-processor. Although the system is built for speed and expandability, all instructions pass through the NuBus to be processed. Mathematical and graphics intensive applications must vie for processing time. In animation, where mathematics and graphics are combined, the processing is slow.

A Fortran code, Microsoft Fortran Version 2.0, was written to take advantage of the Macintosh II graphics toolbox utilities. The code (Appendix C) draws color pixels into a graphics window for levels of vorticity. At each time step, the data are searched and assigned a color based on its vorticity; this color is drawn onto the screen in locations scaled to the data. The target airfoil is drawn into the graphics image by available line drawing utilities.

The Fortran code is concise and useful, and provides a first look into the animation process and knowledge into alternative methods. Software changes could be made easily to the source code; color and processing ideas could be vented at this level of software. However, since all calculations and drawings are done at the time of animation, the images are refreshed slowly; screens are not saved as bitmaps to optimize animation time. Also, resolution is limited by the lack of speed; only real data of 25 by 41 spacial points could be animated, resulting in chunky images. The data set is interpolated on the IBM 3090 with a bi-cubic spline to 350 by 250 spacial points for animation on the SUN computer.

3.4.2 SUN Animation

Animation of vorticity data is done on the SUN Microsystems SPARC color workstation. The monitor is a 16-inch diagonal with a 1152 by 900 pixel resolution and a vertical refresh rate of 66 Hz. The computer is a 32-bit SUN-4 system with a SPARC architecture. The SUN-4 Central Processing Unit (CPU) combines an integer unit for basic processing and a floating-point unit for floating-point arithmetic. The SPARC (Scalable Processor Architecture) combines simple instruction formats with delayed instruction control transfers in registers, overlapping registers, and single-cycle execution of most instructions.

The commercial software PV-Wave from Precision Visuals was used to animate the vorticity data on the SUN (Appendix D). PV-Wave is a general purpose analysis and visualization system. Commands and keywords, entered both interactively and in programs, act on variables referring to collections of data. The scientific data, seen as scalars, vectors, and arrays, are expressed and manipulated as single entities or as data structures. Error checking and error messages are available, and PV-Wave uses only the ASCII character set.

Once on the SUN, the vorticity data are converted to pixel-image, pixel-shade, and contour representations. In a pixel-image, the vorticity range is mapped onto a color table of 256 distinct colors. Each datum point is assigned a color based on its vorticity level. The data points, for example, for vorticity values ranging from -5 to -5.2 might have a color level of 11 which could be a reference to light blue. The pixel-shade maps the vorticity in and out of the plane of data based on sign and magnitude; a positive vortex will rise out of the plane as a mountain, the summit representing the maximum vorticity at the core. Imaginary light strikes the formed surfaces projecting shadows. Small gradients are readily seen this way, however, the operations are math intensive and slower. The contour representation are lines of constant vorticity traced thru the data set.

There are many advantages and disadvantages to PV-Wave. The program is concise and powerful; the commands can be quickly altered for picture size, location, and color. Simple animations and analyses take very little knowledge of the program while the programmer can grow into the program's power and agility. PV-Wave, however, requires the data to be uniformly spaced. Also, non-data information cannot be incorporated into the graphics. For example, the target airfoil could not be drawn on the screen with the data using PV-Wave. Changing all the values of vorticity between the top and bottom of the airfoil to the same level but different from zero compensated for the program's limitation. PV-Wave acted as if this were real data and formed an airfoil of a constant color. Finally, PV-Wave could only animate one physical quantity at a time; velocity, vorticity, and pressure could not be animated all at once.

4. Results and Discussion

4.1 Introduction

Taken in the vicinity of a NACA 0015 airfoil at $\alpha = 10^\circ$, the ensemble-averaged velocity data collected from LDV measurements is presented here as velocity vectors, vorticity contours, $\frac{\partial p}{\partial x}$ and $\frac{\partial p}{\partial y}$ contours, and pressure coefficient plots. The leading edge of the target airfoil is offset above the zero-degree axis of the pitching airfoil by $y/c = 0.12$, where y is the vertical distance from the leading edge of the NACA 0015 airfoil and c is the chord length (Figure 4.1.1). The freestream velocity and Reynolds number, based on the target airfoil chord, are 0.128 m/s and 19550, respectively. The pitching schedule is sinusoidal with a period of 1.24 seconds, an amplitude of 20° , and a reduced frequency, k , of 2. A positive vortex enters the data at $y/c = 0$, level with the nose of the airfoil, and is pulled above the blade by the lower pressures; however, it does not collide with the leading edge. Fifty samples are obtained over one pitching period and ensemble averaged 20 times at each spacial location. Each sample is referred to as a time level between 1 and 50, where time level 1 is the first sample taken in the period and time level 50 is the last. The TSI laser beams are tilted down 4° to get data closer to the airfoil; this allows data to be taken upstream of and

above the target airfoil, but causes excessive blockage of the laser beams in the region below the airfoil. For this reason, almost no data are taken below the leading edge of the target airfoil.

The velocity data are acquired in two blocks (Figure 4.1.2). Between $x/c = -0.3$ and $x/c = 0.05$, vertical columns of data are taken between $y/c = -0.1375$ and $y/c = 0.3625$, for 41 rows and 15 columns. Between $x/c = 0.075$ and $x/c = 0.3$, vertical columns of data are taken between $y/c = 0$ and $y/c = 0.3625$, for 29 rows and 10 columns. The latter data block has fewer rows, having saved time during acquisition by ignoring the blocked region inside and below the target airfoil. The grid spacings, $\Delta x/c$ and $\Delta y/c$, are 0.025 and 0.0125, respectively. Better resolution in the normal direction allows better detail of the boundary layer and airfoil-vortex interaction region.

A vortex affects the behavior of flow around an airfoil by changing the apparent direction of the freestream velocity. The vortex induces higher velocities and changing angles of attack, α , as it approaches. For a positive vortex, a positive increase in α occurs. Previous research has proved the formation of a vortex induced separation bubble as well as rapidly fluctuating velocity and pressure fields. The following results confirm previous work, but also yield insight into the fundamentals of the blade-vortex interaction problem.

4.2 *Velocity and Vorticity*

The velocity vectors and vorticity contours are shown in Figures 4.2.1 through 4.2.50. The vortex-induced velocity and apparent angle of attack are already significant in the first time level of the pitching period. The dimensionless velocity vectors are not parallel to the freestream velocity anywhere upstream of the airfoil. The velocity profile of the $x/c = -0.3$ column shows a positive v-component of velocity (perpendicular to U_∞), due to the positive rotation of the vortex, everywhere between $y/c = -0.1375$ and $y/c = 0.3625$. The velocity increases below and decreases

slightly above $y/c = 0$, indicating the center of the approaching vortex. Above the airfoil, the flow is relatively undisturbed and the boundary layer is thin. The airfoil shields this region from the unsteady effects of the vortex, while imposing its own flow characteristics. This region remains steady until the vortex passes above the airfoil and becomes unsteady only in the vicinity of the vortex.

With the entrance of the vortex at time level 5, Figure 4.2.5, the boundary layer has grown in size and negative vorticity strength, seen as an enlarging region of vorticity less than -20. This indicates an increase in the induced velocity and induced angle of attack on the airfoil. A small accelerated flow region above the airfoil surface, between $x/c = 0$ and $x/c = 0.15$, forms, but the flow above the blade remains steady, dominated by the freestream velocity. The velocity profiles shorten and lengthen above and below the vortex position, respectively. Upstream of the vortex, the v -components of the velocities decrease reducing the angles of the velocity vectors relative to the freestream direction, thereby, revealing the very localized influence of the vortex and indicating freestream dominance in the wake of the passing vortex.

By time level 10, Figure 4.2.10, the vortex has moved to $x/c = -0.175$ and $y/c = 0.025$. The velocities downstream of the vortex are increasing and pointing upward, while upstream the velocities above the vortex are dominated by the freestream, and those below turn downward, complimented by the vortex rotation. The shortening and lengthening moves along with the vortex while the profiles at $x/c = -0.3$ are quickly steadying under the freestream's influence. A separation bubble is now fully formed, due to the increasing vortex-induced angle of attack. The vortex accelerates quickly between time levels 11 and 16 (Figures 4.2.11-4.2.16 and 4.2.51), pulled into and distorted by the low-pressure region above the airfoil. Once there, however, the positive rotation feeds the separation bubble causing it to grow in strength. Moreover, the low pressure preceding the vortex pulls the separation bubble above the airfoil surface.

At time level 17, Figure 4.2.17, the separation bubble has grown to cover 20% of the chord. A high-velocity region exists between the vortex and the separation bubble. Since the two regions rotate in opposite directions, the intersection creates a fluid jet between the vortex structures. The fastest velocity and, therefore, the largest pressure gradient is between the two vortex structures. Due to the uneven pressure distribution, the vortex stretches lengthwise in passing above the airfoil. The core of the vortex rotates eccentrically within the structure, causing it to move from back to front by time level 20. The secondary vortex, now attached only to the airfoil near its point of formation, is pulled by the low pressure preceding the primary vortex and moves downstream.

In the last 40% of the period, time levels 30-50, little occurs on the first three-tenths of the chord. The vortex pulls the separation region downstream, leaving the boundary layer to stabilize upstream. The negative vortex follows the positive vortex but is too far away to influence the suction surface of the airfoil. The path the vortex follows in one complete period is plotted in Figure 4.2.51.

4.3 Pressure

Pressure gradient contours are shown in Figures 4.3.1 to 4.3.50, where two concentric circles are drawn based on the vorticity data to mark the average location of the vortex core. Before the vortex enters the data field, there is a strong localized pressure gradient on the nose of the airfoil. The pressure decreases towards the upper, leading-edge surface causing $\frac{\partial p}{\partial x}$ to be negative and $\frac{\partial p}{\partial y}$ to be positive. This low pressure region is also seen in the pressure-coefficient plots, Figures 4.3.51 to 4.3.75, where C_p becomes more negative near the leading-edge of the airfoil. The lowest pressure is located at $x/c = 0.05$, the center of the positive $\frac{\partial p}{\partial y}$ region, with $C_p = -0.9$. A portion of this suction can be attributed to the vortex-induced velocity and angle of attack; however, this early in

the pitching downstroke, the freestream-airfoil interaction characterizes the flow in this region and, therefore, dictates the local pressures.

By the time the vortex enters at time levels 6 and 7, Figures 4.3.6-4.3.7 and 4.3.53-4.3.54, a positive $\frac{\partial p}{\partial x}$ region forms at $x/c = 0.125$, while the negative region grows in strength and size. This indicates a rise in pressure just past $x/c = 0.1$ while the induced angle of attack increases, decreasing the pressure near the nose. The positive $\frac{\partial p}{\partial y}$ region grows fuller by this time, confirming the decreasing pressure above the airfoil. A large decrease in $\frac{\partial p}{\partial y}$ just below the nose is due to the growing pressure below the airfoil; the stagnation point is moving away from the leading edge along the bottom of the airfoil. The minimum C_p decreases by 50% to -1.3 at $x/c = 0.05$, where the lowest pressure and the center of the positive $\frac{\partial p}{\partial y}$ region are located.

As the vortex moves closer, the pressure gradients increase in magnitude and influence. When the vortex comes within $0.15c$ of the leading edge at time level 10, Figures 4.3.10 and 4.3.55, a sharp discontinuity from negative to positive develops in $\frac{\partial p}{\partial x}$ above the airfoil at $x/c = 0.1$; this is the center of the separation bubble in the vorticity contours, the center of the positive $\frac{\partial p}{\partial y}$ region, and the position of minimum pressure. Also, the $\frac{\partial p}{\partial y}$ positive region starts to move above the airfoil surface at this time; this indicates the largest pressure gradients are no longer inside the separation bubble but are in the fluid jet between the separation bubble and the vortex. The minimum C_p continues to decrease with increasing induced angle of attack and moves from $x/c = 0.05$ to $x/c = 0.1$.

At time 15, the vortex begins to disrupt the shapes of the $\frac{\partial p}{\partial x}$ and $\frac{\partial p}{\partial y}$ contours, which are now affecting 20% of the airfoil. The negative $\frac{\partial p}{\partial y}$ region has pulled in very tightly to the leading edge, indicating a strong increase in pressure. The pressure coefficients continue to decrease to a minimum at time level 17, where the secondary vortex begins to move both away from the surface and downstream; then, the pressure coefficients begin to increase as the minimum moves with the sec-

ondary vortex further toward the trailing edge. The decreased local pressure in front of the vortex pulls the separation bubble free of the airfoil and downstream.

As the vortex passes over the blade, time levels 17-24, Figures 4.3.17-4.3.24, the pressure gradients are pulled along with it, leaving small regions of irregular flow. This parallels the breakdown of the secondary vortex in Figures 4.2.17-4.2.24. The velocity ahead of the vortex is still considerably faster than the freestream which causes low pressure; behind the vortex, the flow stabilizes toward freestream conditions. This effect is also seen in Figures 4.3.59-4.3.62, where the pressure over the front of the blade, in the wake of the exiting vortex, increases rapidly. Pressure coefficients vary little once the vortex has passed.

The positive vortex influences the first 20% of the airfoil's suction surface even when it is 0.3c away from the leading edge. However, once above the airfoil, it has little effect behind its location and strong effects ahead. This is due to the positive rotation; fast moving fluid is forced down into the boundary layer and then up and ahead of the vortex. Anything behind the vortex is immediately settled down by the freestream velocity. Once above the leading edge, the vortex begins to strengthen the secondary vortex by feeding fluid between the nose and $x/c = 0.05$. Once the vortex is fully above the separation bubble, the bubble is at its maximum size and strength. This is indicated by the enlarged regions of $\frac{\partial p}{\partial x}$ and $\frac{\partial p}{\partial y}$ and the minimum pressure coefficient. Once the bubble starts to move, it can no longer be fed from the positive vortex; the pressures start to increase. In Figures 4.3.76-4.3.78, pressure coefficients at $y/c = 0.0625$ are shown together for various time samples. The minimum C_p stays between $x/c = 0.05$ and $x/c = 0.1$ until the secondary vortex moves downstream, where it follows the bubble. Also, the minimum decreases until this point and then begins to increase.

The last 40% of the period, time levels 30-50, shows almost no variation in $\frac{\partial p}{\partial x}$, $\frac{\partial p}{\partial y}$, and C_p but is included for completeness. The negative vortex, released upstream by the pitching airfoil, is too far away to have a significant affect on the top of the airfoil.

4.4 Conclusions

In the non-collision case of blade-vortex interaction, three physical phenomena are identified and studied (Figures 4.4.1 and 4.4.2). First, the free vortex influences its surroundings by inducing a decrease and an increase in the local velocity above and below its center, respectively, as well as by adding a vertical velocity component to the flow. This is seen in the first 20% of the period, time levels 1-10. The induced velocity and induced angle of attack on the airfoil continues to increase until a separation bubble forms on the suction side of the airfoil. Second, the vortex is pulled into the low-pressure region above the airfoil and begins to interact with the leading edge and the upstream end of the separation bubble. This region is dominated by the localized influence of the vortex. Once above the leading edge of the airfoil, the vortex feeds the boundary layer with fast moving fluid, decreasing the already low pressures and increasing the size of the separation bubble. The strong pressure variations pull the vortex unevenly, distorting its shape. Above $y/c = 0.2$, in the freestream/airfoil dominated flow, the vortex has little influence due to its stretched form. The radius of influence depends on the reduced frequency of the vortex-freestream formation. In the last phenomenon, the vortex continuously feeds fast moving fluid into the wall region, increasing the size and strength of the secondary vortex, until, finally, the vortex has pushed enough energy into the wall region that the separation bubble lifts free of the airfoil and starts moving downstream. The primary and secondary vortices now interact as independent structures. The flow between them accelerates, moving the minimum pressure gradient to this point; however, once the separation bubble is free of the airfoil, it can no longer grow in strength; the vortex is too far past the bubble/airfoil attachment point to add fluid, and the minimum pressure starts to increase as the vortex moves toward the trailing edge. The low pressure region pulls the primary and secondary vortices downstream while the freestream velocity re-establishes the steady-flow condition upstream.

The results of the near-collision or distortion-zone solution yields important conclusions that can be applied to both the pure collision and the deflection regimes in order to understand the basic fundamentals of Blade-Vortex Interactions. A vortex in the deflection zone follows the freestream/airfoil streamlines. Since the vortex never enters the low pressure region above the blade while in the deflection zone, it is not distorted. However, a vortex in the collision zone is pulled by the low pressure above the airfoil but strikes the leading edge. This leaves two smaller regions of vorticity moving over the airfoil. In the positive vortex case, the top vortex portion will move counter to the boundary layer, decreasing the pressure, while the lower vortex portion will rotate in the same direction as the boundary layer, acting against the freestream, and will increase the pressure. The net effect is a sharp, temporary increase in lift and vibrational loading on the airfoil.

Bibliography

- Booth, E. R., 1987, "Experimental Observations of Two Dimensional Blade Vortex Interactions," AIAA Paper 87-2745.
- Booth, E. R., 1987, "Measurement of Velocity and Vorticity Fields in the Wake of an Airfoil in Periodic Pitching Motion," NASA TP-2780.
- Booth, E. R., 1986, "Surface Pressure Measurement During Low Speed Two-Dimensional Blade-Vortex Interaction," AIAA Paper 86-1856.
- Booth, E. R. and Yu, J. C., 1986, "New Technique for Experimental Generation of Two-Dimensional Blade-Vortex Interaction at Low Reynolds Numbers," NASA TP-2551.
- Caradonna, F. X., Laub, G. H., and Tung, C., "An Experimental Investigation of the Parallel Blade-Vortex Interaction," 10th European Rotorcraft Forum, The Hague, 1984.
- Chow, C. Y. and Huang, M. K., 1983, "Unsteady Flow About a Joukowski Airfoil in the Presence of Moving Vortices," AIAA Paper No. 83-0129.
- Hsu, T. M. and Wu, J. C., 1986, "Theoretical and Numerical Studies of a Vortex-Airfoil Interaction Problem," AIAA Paper No. 86-1094.
- Karamcheti, K., 1966, *Principles of Ideal-Fluid Aerodynamics*, J. Wiley and Sons.
- Kim, B. K., 1985, "Boundary Layer Analysis and Measurement of Non-Newtonian Fluids," Ph.D. Dissertation, VPI & SU.
- Kim, M. J., 1985, "Application of Panel Methods for Subsonic Aerodynamics," Ph.D. Dissertation, VPI & SU.
- Kim, M. J. and Mook, D. T., 1986, "Application of Continuous Vorticity Panels to General Unsteady Incompressible Two-Dimensional Lifting Flows," *Journal of Aircraft*, Vol. 23, pp. 464-471.
- Koromilas, Constantinos A., 1978, "Experimental Investigation of Unsteady Separation," Ph.D. Dissertation, VPI & SU.
- Lee, D. J. and Roberts, L., 1985, "Interaction of a Turbulent Vortex with a Lifting Surface," AIAA Paper 85-0004.
- Lee, D. J. and Smith, C. A., 1987, "Distortion of the Vortex Core During Blade-Vortex Interaction," AIAA Paper 87-1243.

- McAlister, K. W. and Tung, C., 1984, "Airfoil Interaction with an Impinging Vortex," NASA TP-227 3, AVSCOM TR-83-A-17.
- Meier, G. E. A. and Timm, R., 1985, "Unsteady Vortex Airfoil Interaction," AGARD CP-386.
- Mezaris, Thomas Basil, 1979, "Visualization and LDV Measurements of Separating Oscillatory Laminar Flows," M.S. Thesis, VPI & SU.
- Mook, D. T. and Dong, B., 1990, "Application of Vortex Dynamics to Simulations of Two-Dimensional Wakes," submitted for publication.
- Mook, D. T., Roy, S., Choksi, G., and Alexander, D. M., 1987, "On the Numerical Simulation of the Unsteady Wake Behind an Airfoil," AIAA Paper 87-0190.
- Neuwerth, G. and Muller, R., 1985, "Pressure Fluctuations on Rotor Blades Generated by Blade-Vortex Interaction," *Vertica*, Vol. 9, pp. 227-239.
- Panaras, A. G., 1987, "Numerical Modeling of the Vortex/Airfoil Interaction," *AIAA Journal*, Vol. 25.
- Poling, D. R., 1985, "Unsteady Airfoil Interference," Ph.D. Dissertation, VPI & SU.
- Poling, D. R., Dadone, L., and Telionis, D. P., 1987, "Blade-Vortex Interaction," AIAA Paper No. 87-0497.
- Poling, D. R., Wilder, M. C., Telionis, D. P., 1988, "Two-Dimensional Interaction of Vortices With a Blade," AIAA Paper 88-0040.
- Rai, M. M., 1987, "Navier-Stokes Simulations of Blade Vortex Interaction Using High Order Accurate Upwind Schemes," AIAA Paper 87-0543.
- Rosenhead, L., 1931, "The Formation of Vortices from a Surface of Discontinuity," Proceedings of the Royal Society of London, A134, pp. 170-192.
- Straus, J., Renzoni, P., and Mayle, R. E., 1990, "Airfoil Pressure Measurements during a Blade Vortex Interaction and Comparison with Theory," *AIAA Journal*, Vol. 28, No. 2, pp. 222-228.
- Srinivasan, G. R. and McCroskey, W. J., "Computations of Blade-Vortex Interaction by Different Methods," U.S. Army Research Office Workshop on Blade-Vortex Interactions, NASA Ames Research Center, Moffett Field, California, Oct. 29-31, 1984.
- Srinivasan, G. R., McCroskey, W. J., and Kutler, P., 1984, "Numerical Simulation of the Interaction of a Vortex with a Stationary Airfoil in Transonic Flow," AIAA Paper No. 84-0254.
- Tang, W. and Sankar, L. N., "Strong Blade-Vortex Interactions Including Collision," in Forum on Unsteady Flow Separation, ed. K. N. Ghia, ASME, June 1987.
- Wilder, M. C., Mathioulakis, D. S., Poling, D. R., Dong, B., Mook, D. T., and Telionis, D. P., "On the Wake of a Pitching Airfoil," submitted for publication.
- Wilder, M. C., Pesce, M. M., and Telionis, D. P., 1990, "Blade-Vortex Interaction Experiments-Velocity and Vorticity Fields," AIAA Paper 90-0030.
- Wu, J. C., Sankar, N. L., and Hsu, T. M., 1985, "Unsteady Aerodynamics of an Airfoil Encountering a Passing Vortex," AIAA Paper No. 85-0203.

Wu, J. C. and Thompson, J. F., 1973, "Numerical Solutions of Time-Dependent Incompressible Navier-Stokes Equations Using an Integro-Differential Formulation," *Computer and Fluids*, Vol. 1, pp. 197-215.

Appendix A. Vorticity Code

```
C=====
C PROGRAM TO CALCULATE VORTICITY FROM VELOCITY FILES USING   =
C FINITE DIFFERENCE APPROXIMATIONS FOR DERIVATIVES           =
C                                                             =
C                                                             =
C MATTHEW M. PESCE                                           =
C MASTER OF SCIENCE CANDIDATE                               =
C ENGINEERING SCIENCE AND MECHANICS                         =
C VIRGINIA POLYTECHNIC INSTITUTE AND STATE UNIVERSITY       =
C                                                             =
C September 1990                                            =
C=====
C                                                             =
C                                                             =
C This code reads in u and v velocities and calculates       =
C two-dimensional vorticity. The logic statements            =
C allow only good data points to be used in the             =
C calculations.                                             =
C                                                             =
C Description of Variables:                                  =
C                                                             =
C DUDY      2nd order derivative of u with respect to y     =
C DVDX      2nd order derivative of v with respect to x     =
C U         Velocity in primary flow direction              =
C V         Velocity in                                     =
C VFILL     Input parameter to supply vorticity at bad data =
C           locations (usually zero)                         =
C VORT      Vorticity                                       =
C WEIGHT    Weighting parameter for bad data locations      =
C                                                             =
C DX       Discretized differential x                       =
```

```

C      DX2      DX multiplied by 2      =
C      DY      Discretized differential y      =
C      DY2      DY multiplied by 2      =
C      FLAG     Flag to make sure all vorticities are calculated      =
C      I        Integer for looping in x direction      =
C      ITIME    Looping variable for reading data      =
C      J        Integer for looping in y direction      =
C      K        Integer for looping in time direction      =
C      K1       First time level to begin evaluating vorticity      =
C      K2       Final time level to stop evaluating vorticity      =
C      KDELTA   Integer step between K1 and K2      =
C      NI       Number of data columns in the x direction      =
C      NJ       Number of data rows in the y direction      =
C      NT       Number of time levels      =
C      NX1      Columns of data in the first data file      =
C      NX2      Columns of data in the second data file      =
C      NXMAX    Total possible data columns in array space      =
C      NY1      Rows of data in the first data file      =
C      NY2      Rows of data in the second data file      =
C      NYMAX    Total possible data rows in array space      =
C      NTMAX    Total possible time levels in array space      =
C      XD       Array holding x locations      =
C      YD       Array holding y locations      =
C      UFS      Average of freestream velocities      =
C      UFS1     Freestream velocity from first data file      =
C      UFS2     Freestream velocity from second data file      =
C
C      ISAVE    Number of time samples saved per period      =
C      ISMPL    Number of samples taken per period      =
C      PERIOD   Pitching period (in seconds)      =
C      REYNOL   Reynolds number      =
C      RFREQ    Reduced frequency      =
C      TBD      Time between data      =
C
C

```

```

C      PARAMETER(NXMAX=50,NYMAX=50,NTMAX=102)

```

```

C      DIMENSION U(NXMAX,NYMAX,NTMAX),V(NXMAX,NYMAX,NTMAX)
C      DIMENSION VORT(NXMAX,NYMAX,NTMAX),WEIGHT(NXMAX,NYMAX)
C      DIMENSION XD(NXMAX),YD(NYMAX)

```

```

C-----
C      INITIALIZE U,V, AND WEIGHT
C-----

```

```

C
C      DO 60 I = 1,NXMAX
C        DO 60 J = 1,NYMAX
C          WEIGHT(I,J) = 1000.
C          DO 60 K = 1,NTMAX
C            U(I,J,K) = 0.

```



```

        V(I,J,K) = 0.
60 CONTINUE
    WRITE(6,*) 'INITIALIZATION OK'
C
C-----
C    READ IN VELOCITY DATA FILES
C-----
C
C
C    FILE 1
C
    READ(1,*) TBD, ISMPL, ISAVE, PERIOD
    READ(1,*) NX1, NY1, NT
    READ(1,1000) UFS1
    WRITE(6,*) UFS1
    DO 10 I = 1, NX1
        DO 10 J = 1, NY1
            READ(1,1010) XD(I), YD(J)
            DO 10 ITIME = 1, NT, 3
                READ(1,1020) (U(I,J,K), V(I,J,K), K=ITIME, ITIME+2)
10 CONTINUE
C
    READ(1,*) ((WEIGHT(I,J), J=1, NY1), I=1, NX1)
    WRITE(6,*) 'FILE 1 READING COMPLETE'
C
C    FILE 2
C
    READ(2,*) TBD, ISMPL, ISAVE, PERIOD
    READ(2,*) NX2, NY2, NT
    READ(2,1000) UFS2
    DO 110 I = NX1+1, NX1+NX2
        DO 110 J = NY1-NY2+1, NY1
            READ(2,1010) XD(I), YD(J)
            DO 110 ITIME = 1, NT, 3
                READ(2,1020) (U(I,J,K), V(I,J,K), K=ITIME, ITIME+2)
110 CONTINUE
    READ(2,*) ((WEIGHT(I,J), J=NY1-NY2+1, NY1), I=NX1+1, NX1+NX2)
C
    DO 150 I = NX1+1, NX1+NX2
        DO 150 J = 1, NY1-NY2
            WEIGHT(I,J) = 1000.
            DO 150 K = 1, NT
                U(I,J,K) = 0.
                V(I,J,K) = 0.
150 CONTINUE
C
    WRITE(6,*) 'FILE 2 READING COMPLETE'
C
C    FIND FLOW VARIABLES
C

```

```

UFS = (UFS1+UFS2)/2.
REYNOL = UFS*0.1524/1.007E-06
RFREQ = 2.
C
C-----
C   CALCULATE VORTICITIES
C-----
C
DX = 0.025
DY = 0.0125
DX2 = 2.*DX
DY2 = 2.*DY
NI = NX1+NX2
NJ = NY1
C
WRITE(6,*) 'ENTER VORTICITY FOR BAD DATA POINTS'
READ(5,*) VFILL
WRITE(6,*) 'ENTER 1ST AND LAST TIME AND STEP DESIRED'
READ(5,*) K1,K2,KDELTA
C
FLAG = 0.
DO 500 K = K1,K2,KDELTA
DO 500 J = 1,NJ
DO 500 I = 1,NI
IF(WEIGHT(I,J).GT.1.) THEN
VORT(I,J,K) = VFILL
GO TO 500
END IF
IF(I.EQ.1.AND.J.EQ.1) THEN
DVDX = (-V(I+2,J,K)+4.*V(I+1,J,K)-3.*V(I,J,K))/DX2
DUDY = (-U(I,J+2,K)+4.*U(I,J+1,K)-3.*U(I,J,K))/DY2
VORT(I,J,K) = DVDX - DUDY
FLAG = -1.
END IF
IF(J.EQ.1.AND.I.GT.1) THEN
IF(WEIGHT(I,J+2).GT.1..OR.WEIGHT(I,J+1).GT.1.) THEN
VORT(I,J,K) = VFILL
GO TO 500
END IF
IF(WEIGHT(I+1,J).GT.1.) THEN
DVDX = (V(I-2,J,K)-4.*V(I-1,J,K)+3.*V(I,J,K))/DX2
ELSE
DVDX = (V(I+1,J,K)-V(I-1,J,K))/DX2
END IF
DUDY = (-U(I,J+2,K)+4.*U(I,J+1,K)-3.*U(I,J,K))/DY2
VORT(I,J,K) = DVDX-DUDY
FLAG = -1.
END IF
IF(I.EQ.1.AND.J.GT.1.AND.J.LT.NJ) THEN
DVDX = (-V(I+2,J,K)+4.*V(I+1,J,K)-3.*V(I,J,K))/DX2

```

```

DUDY = ( U(I,J+1,K)-U(I,J-1,K))/DY2
VORT(I,J,K) = DVDX-DUDY
FLAG = -1.
END IF
IF(I.GT.1.AND.I.LT.NI.AND.J.GT.1.AND.J.LT.NJ) THEN
  IF(WEIGHT(I+1,J).GT.1.) THEN
    DVDX = (V(I-2,J,K)-4.*V(I-1,J,K)+V(I,J,K))/DX2
  ELSE
    DVDX = (V(I+1,J,K)-V(I-1,J,K))/DX2
  END IF
  DUDY = (U(I,J+1,K)-U(I,J-1,K))/DY2
  IF(WEIGHT(I,J+1).GT.1.) THEN
    DUDY = (U(I,J-2,K)-4.*U(I,J-1,K)+3.*U(I,J,K))/DY2
  END IF
  IF(WEIGHT(I,J-1).GT.1.) THEN
    DUDY = (-U(I,J+2,K)+4.*U(I,J+1,K)-3.*U(I,J,K))/DY2
  END IF
  VORT(I,J,K) = DVDX - DUDY
  FLAG = -1.
END IF
IF(I.EQ.1.AND.J.EQ.NJ) THEN
  DVDX = (-V(I+2,J,K)+4.*V(I+1,J,K)-3.*V(I,J,K))/DX2
  DUDY = ( U(I,J-2,K)-4.*U(I,J-1,K)+3.*U(I,J,K))/DY2
  VORT(I,J,K) = DVDX - DUDY
  FLAG = -1.
END IF
IF(I.GT.1.AND.I.LT.NI.AND.J.EQ.NJ) THEN
  IF(WEIGHT(I,J-2).GT.1..OR.WEIGHT(I,J-1).GT.1.) THEN
    VORT(I,J,K) = VFILL
    GO TO 500
  END IF
  DUDY = (U(I,J-2,K)-4.*U(I,J-1,K)+3.*U(I,J,K))/DY2
  DVDX = (V(I+1,J,K)-V(I-1,J,K))/DX2
  VORT(I,J,K) = DVDX - DUDY
  FLAG = -1.
END IF
IF(I.EQ.NI.AND.J.EQ.NJ) THEN
  IF(WEIGHT(I,J-2).GT.1..OR.WEIGHT(I,J-1).GT.1.) THEN
    VORT(I,J,K) = VFILL
    GO TO 500
  END IF
  DVDX = (V(I-2,J,K)-4.*V(I-1,J,K)+3.*V(I,J,K))/DX2
  DUDY = (U(I,J-2,K)-4.*U(I,J-1,K)+3.*U(I,J,K))/DY2
  VORT(I,J,K) = DVDX - DUDY
  FLAG = -1.
END IF
IF(I.EQ.NI.AND.J.GT.1.AND.J.LT.NJ) THEN
  IF(WEIGHT(I,J+1).GT.1..OR.WEIGHT(I-1,J).GT.1..OR.
    WEIGHT(I-2,J).GT.1.) THEN
    VORT(I,J,K) = VFILL

```

```

      GO TO 500
      END IF
      IF(WEIGHT(I,J-1).GT.1.) THEN
        DUDY = (-U(I,J+2,K)+4.*U(I,J+1,K)-3.*U(I,J,K))/DY2
      ELSE
        DUDY = ( U(I,J+1,K)-U(I,J-1,K))/DY2
      END IF
      DVDX = (V(I-2,J,K)-4.*V(I-1,J,K)+3.*V(I,J,K))/DX2
      VORT(I,J,K) = DVDX - DUDY
      FLAG = -1.
      END IF
C
C   NOTE:  THE CASE I=NI, J=1 IS COVERED IN ANOTHER CASE SINCE
C           IT IS KNOWN THAT J=1 TO J=12 ARE BAD DATA POINTS
C
      IF(FLAG.EQ.-1.) THEN
        FLAG = 0.
      ELSE
        VORT(I,J,K) = VFILL
      END IF
500 CONTINUE
C
      WRITE(6,*) 'VORTICITY CALCULATIONS COMPLETE'
C
C-----
C   WRITE VORTICITIES TO A FILE
C-----
C
      WRITE(6,*) 'WRITING VORTICITY FILE . . .'
C
      WRITE(10,802) UFS,REYNOL,RFREQ
      DO 700 K = K1,K2,KDELTA
        WRITE(10,801) NI,NJ,K
C       WRITE(10,*) 'A',K
        DO 700 I = 1,NI
          WRITE(10,802) (XD(I),YD(J),VORT(I,J,K),J=1,NJ)
600 CONTINUE
C
      WRITE(6,*) 'WRITING COMPLETE'
C
C-----
C   FORMAT STATEMENTS
C-----
C
      800 FORMAT(3(5X,E14.7))
      801 FORMAT(3(5X,I3))
      802 FORMAT(3(5X,E14.7))
      803 FORMAT(6E13.5)
      1000 FORMAT(/E15.7)
      1010 FORMAT(2E15.7)

```

```
1020 FORMAT(3(3E13.5))
```

```
C
```

```
STOP
```

```
END
```

Appendix B. Pressure Code

```
C
C-----
C PROGRAM TO CALCULATE PRESSURES USING EULER AND          =
C NAVIER-STOKES FINITE DIFFERENCE DERIVATIVES AND        =
C USING TRAPEZOIDAL RULE NUMERICAL INTEGRATION            =
C (2ND ORDER)                                             =
C                                                         =
C                                                         =
C MATTHEW M. PESCE                                       =
C MASTER OF SCIENCE CANDIDATE                             =
C ENGINEERING SCIENCE AND MECHANICS                       =
C VIRGINIA POLYTECHNIC INSTITUTE AND STATE UNIVERSITY     =
C                                                         =
C September 1990                                         =
C-----
C                                                         =
C                                                         =
C The code reads in u and v velocities and calculates    =
C differential pressures by solving the Euler or          =
C Navier-Stokes equations. The logic statements          =
C allow only calculations using good data points.        =
C The differential pressure is then integrated to         =
C get pressure everywhere in the field.                  =
C                                                         =
C                                                         =
C Description of Variables:                               =
C                                                         =
C DUDX      1st derivative of u with respect to x        =
C D2UDX2    2nd derivative of u with respect to x        =
C DUDY      1st derivative of u with respect to y        =
C D2UDY2    2nd derivative of u with respect to y        =
C DVDX      1st derivative of v with respect to x        =
C D2VDX2    2nd derivative of v with respect to x        =
```

| | | | |
|---|--------|--|---|
| C | DVDY | 1st derivative of v with respect to y | = |
| C | D2VDY2 | 2nd derivative of v with respect to y | = |
| C | DPDX | Derivative of pressure with respect to x | = |
| C | DPDY | Derivative of pressure with respect to y | = |
| C | P | Numerically integrated pressure | = |
| C | PW | Pressure on airfoil surface | = |
| C | U | Velocity in primary flow direction (u) | = |
| C | UIJ | Scalar for U(I,J,K) | = |
| C | UI0J | Scalar for U(I-1,J,K) | = |
| C | UI1J | Scalar for U(I+1,J,K) | = |
| C | UI2J | Scalar for U(I+2,J,K) | = |
| C | UIJ0 | Scalar for U(I,J-1,K) | = |
| C | UIJ1 | Scalar for U(I,J+1,K) | = |
| C | UIJ2 | Scalar for U(I,J+2,K) | = |
| C | V | Velocity perpendicular to primary flow (v) | = |
| C | VIJ | Scalar for V(I,J,K) | = |
| C | VI0J | Scalar for V(I-1,J,K) | = |
| C | VI1J | Scalar for V(I+1,J,K) | = |
| C | VI2J | Scalar for V(I+2,J,K) | = |
| C | VIJ0 | Scalar for V(I,J-1,K) | = |
| C | VIJ1 | Scalar for V(I,J+1,K) | = |
| C | VIJ2 | Scalar for V(I,J+2,K) | = |
| C | WT | Weighting parameter for bad data locations | = |
| C | | | = |
| C | DX | Discretized differential x | = |
| C | DX2 | DX multiplied by 2 | = |
| C | DXDX | DX squared | = |
| C | DY | Discretized differential y | = |
| C | DY2 | DY multiplied by 2 | = |
| C | DYDY | DY squared | = |
| C | DT | Discretized differential time | = |
| C | DT2 | DT multiplied by 2 | = |
| C | I | Integer for looping in x direction | = |
| C | ITIME | Looping variable for reading data | = |
| C | J | Integer for looping in y direction | = |
| C | K | Integer for looping in time direction | = |
| C | K1 | First time level to begin evaluating pressures | = |
| C | K2 | Final time level to stop evaluating pressures | = |
| C | KDELTA | Integer step between K1 and K2 | = |
| C | NAVIER | Parameter whether do Euler or Laminar N-S | = |
| C | NI | Number of data columns in the x direction | = |
| C | NJ | Number of data rows in the y direction | = |
| C | NX1 | Columns of data in the first data file | = |
| C | NX2 | Columns of data in the second data file | = |
| C | NXMAX | Total possible data columns in array space | = |
| C | NY1 | Rows of data in the first data file | = |
| C | NY2 | Rows of data in the second data file | = |
| C | NYMAX | Total possible data rows in array space | = |
| C | NT | Number of time levels | = |
| C | NTMMAX | Total possible time levels in array space | = |

```

C     PSUM      Variable for summing pressures in a loop      =
C     XD        Array holding x locations                    =
C     YD        Array holding y locations                    =
C     UFS       Average of freestream velocities             =
C     UFS1      Freestream velocity from first data file    =
C     UFS2      Freestream velocity from second data file   =
C
C     CHORD     Chord length of the target airfoil          =
C     ISAVE     Number of time samples saved per period     =
C     ISMPL     Number of samples taken per period          =
C     PERIOD    Pitching period (in seconds)                 =
C     RE        Reynolds number                              =
C     RFREQ     Reduced frequency                            =
C     TBD       Time between data                            =
C     TIMCON    Non-dimensional Strouhal number             =
C
C
C     PARAMETER(NXMAX=30,NYMAX= 41,NTMAX=102)
C
C     DIMENSION U(NXMAX,NYMAX,NTMAX),V(NXMAX,NYMAX,NTMAX)
C     DIMENSION WT(NXMAX,NYMAX),XD(NXMAX),YD(NYMAX)
C     DIMENSION DPDX(NXMAX,NYMAX,NTMAX)
C     DIMENSION DPDY(NXMAX,NYMAX,NTMAX)
C     DIMENSION P(NXMAX,NYMAX,NTMAX),PW(NXMAX,NTMAX)
C
C-----
C     INITIALIZE U,V, AND WEIGHT
C-----
C
C     DO 60 I = 1,NXMAX
C       DO 60 J = 1,NYMAX
C         WT(I,J) = 1000.
C         DO 60 K = 1,NTMAX
C           U(I,J,K) = 0.
C           V(I,J,K) = 0.
C           DPDX(I,J,K) = 0.
C           DPDY(I,J,K) = 0.
C     60 CONTINUE
C     WRITE(6,*) 'INITIALIZATION OK'
C
C-----
C     READ IN VELOCITY DATA FILES
C-----
C
C     FILE 1
C
C     READ(1,*) TBD,ISMPL,ISAVE,PERIOD
C     READ(1,*) NX1,NY1,NT
C     READ(1,1000) UFS1

```



```

WRITE(6,*) UFS1
DO 10 I = 1,NX1
  DO 10 J = 1,NY1
    READ(1,1010) XD(I),YD(J)
    DO 10 ITIME = 1,NT,3
      READ(1,1020) (U(I,J,K),V(I,J,K),K=ITIME,ITIME+2)
10 CONTINUE
C
  READ(1,*) ((WT(I,J),J=1,NY1),I=1,NX1)
  WRITE(6,*) 'FILE 1 READING COMPLETE'
C
C   FILE 2
C
  READ(2,*) TBD,ISMPL,ISAVE,PERIOD
  READ(2,*) NX2,NY2,NT
  READ(2,1000) UFS2
  DO 110 I = NX1+1,NX1+NX2
    DO 110 J = NY1-NY2+1,NY1
      READ(2,1010) XD(I),YD(J)
      DO 110 ITIME = 1,NT,3
        READ(2,1020) (U(I,J,K),V(I,J,K),K=ITIME,ITIME+2)
110 CONTINUE
  READ(2,*) ((WT(I,J),J=NY1-NY2+1,NY1),I=NX1+1,NX1+NX2)
C
  DO 150 I = NX1+1,NX1+NX2
    DO 150 J = 1,NY1-NY2
      WT(I,J) = 1000.
      DO 150 K = 1,NT
        U(I,J,K) = 0.
        V(I,J,K) = 0.
150 CONTINUE
  WRITE(6,*) 'FILE 2 READING COMPLETE'
C
C   FIND FLOW VARIABLES
C
  UFS = (UFS1+UFS2)/2.
  RE = UFS*0.1524/1.007E-06
  RFREQ = 2.
  CHORD = 0.1524
  TIMCON = CHORD/(PERIOD*UFS)
C
  DX = 0.025
  DY = 0.0125
  DT = FLOAT(ISAVE)*TBD/PERIOD
  NI = NX1+NX2
  NJ = NY1
C
  WRITE(6,*) 'ENTER 1ST AND LAST TIME AND STEP DESIRED'
  READ(5,*) K1,K2,KDELTA
C

```

```

C-----
C   CALCULATE DIFFERENTIAL
C   PRESSURES
C-----
C
C
C   DX2 = 2.*DX
C   DY2 = 2.*DY
C   DT2 = 2.*DT
C   DXDX = DX*DX
C   DYDY = DY*DY
C
C   NAVIER = 1
C
C   GET DP/DX AND DP/DY ALONG J=NJ LINE
C
C   J = NJ
C   DO 400 K = K1,K2,KDELTA
C   DO 400 I = 1,NI
C
C   UIJ = U(I,J,K)
C   VIJ = V(I,J,K)
C   IF(I.GT.1) THEN
C     UI0J = U(I-1,J,K)
C     VI0J = V(I-1,J,K)
C   END IF
C   IF(I.LT.NI) THEN
C     UI1J = U(I+1,J,K)
C     VI1J = V(I+1,J,K)
C   END IF
C   IF(I.LT.NI-1) THEN
C     UI2J = U(I+2,J,K)
C     VI2J = V(I+2,J,K)
C   END IF
C
C   IF(J.GT.1) THEN
C     UIJ0 = U(I,J-1,K)
C     VIJ0 = V(I,J-1,K)
C   END IF
C   IF(J.LT.NJ) THEN
C     UIJ1 = U(I,J+1,K)
C     VIJ1 = V(I,J+1,K)
C   END IF
C   IF(J.LT.NJ-1) THEN
C     UIJ2 = U(I,J+2,K)
C     VIJ2 = V(I,J+2,K)
C   END IF
C
C   DUDY = ( U(I,J-2,K)-4.*UIJ0+3.*UIJ)/DY2
C   DVDY = ( V(I,J-2,K)-4.*VIJ0+3.*VIJ)/DY2

```

```

D2UDY2 = (UIJ-2.*UIJO+U(I,J-2,K))/DYDY
D2VDY2 = (VIJ-2.*VIJO+V(I,J-2,K))/DYDY
C
IF(K.EQ.1) THEN
  DUDT = (-U(I,J,K+2)+4.*U(I,J,K+1)-3.*UIJ)/DT2
  DVDT = (-V(I,J,K+2)+4.*V(I,J,K+1)-3.*VIJ)/DT2
ELSE
  DUDT = (U(I,J,K+1)-U(I,J,K-1))/DT2
  DVDT = (V(I,J,K+1)-V(I,J,K-1))/DT2
END IF
C
IF(I.EQ.1) THEN
  DUDX = (-UI2J+4.*UI1J-3.*UIJ)/DX2
  DVDX = (-VI2J+4.*VI1J-3.*VIJ)/DX2
  D2UDX2 = (UIJ-2.*UI1J+UI2J)/DXDX
  D2VDX2 = (VIJ-2.*VI1J+VI2J)/DXDX
ELSE
  IF(I.GT.1.AND.I.LT.NI) THEN
    DUDX = (UI1J-UI0J)/DX2
    DVDX = (VI1J-VI0J)/DX2
    D2UDX2 = (UI1J-2.*UIJ+UI0J)/DXDX
    D2VDX2 = (VI1J-2.*VIJ+VI0J)/DXDX
  END IF
  IF(I.EQ.NI) THEN
    DUDX = ( U(I-2,J,K)-4.*UI0J+3.*UIJ)/DX2
    DVDX = ( V(I-2,J,K)-4.*VI0J+3.*VIJ)/DX2
    D2UDX2 = (UIJ-2.*UI0J+U(I-2,J,K))/DXDX
    D2VDX2 = (VIJ-2.*VI0J+V(I-2,J,K))/DXDX
  END IF
END IF
C
DPDX(I,J,K) = -(TIMCON*DUDT + UIJ*DUDX + VIJ*DUDY)
               +FLOAT(NAVIER)*(D2UDX2 + D2UDY2)/RE
DPDY(I,J,K) = -(TIMCON*DVDT + UIJ*DVDX + VIJ*DVDY)
               +FLOAT(NAVIER)*(D2VDX2 + D2VDY2)/RE
400 CONTINUE
C
DO 500 K = K1,K2,KDELTA
DO 500 I = 1,NI
DO 500 J = NJ-1,1,-1
C
  UIJ = U(I,J,K)
  VIJ = V(I,J,K)
  IF(I.GT.1) THEN
    UI0J = U(I-1,J,K)
    VI0J = V(I-1,J,K)
  END IF
  IF(I.LT.NI) THEN
    UI1J = U(I+1,J,K)
    VI1J = V(I+1,J,K)

```

```

END IF
IF(I.LT.NI-1) THEN
  UI2J = U(I+2,J,K)
  VI2J = V(I+2,J,K)
END IF

```

C

```

IF(J.GT.1) THEN
  UIJ0 = U(I,J-1,K)
  VIJ0 = V(I,J-1,K)
END IF
IF(J.LT.NJ) THEN
  UIJ1 = U(I,J+1,K)
  VIJ1 = V(I,J+1,K)
END IF
IF(J.LT.NJ-1) THEN
  UIJ2 = U(I,J+2,K)
  VIJ2 = V(I,J+2,K)
END IF
WTIJ = WT(I,J)

```

C

```

IF(K.EQ.1) THEN
  DUDT = (-U(I,J,K+2)+4.*U(I,J,K+1)-3.*UIJ)/DT2
  DVDT = (-V(I,J,K+2)+4.*V(I,J,K+1)-3.*VIJ)/DT2
ELSE
  DUDT = (U(I,J,K+1)-U(I,J,K-1))/DT2
  DVDT = (V(I,J,K+1)-V(I,J,K-1))/DT2
END IF

```

C

```

IF(I.EQ.1) THEN
  DUDX = (-UI2J+4.*UI1J-3.*UIJ)/DX2
  DVDX = (-VI2J+4.*VI1J-3.*VIJ)/DX2
  D2UDX2 = (UIJ-2.*UI1J+UI2J)/DXDX
  D2VDX2 = (VIJ-2.*VI1J+VI2J)/DXDX
ELSE
  IF(I.GT.1.AND.I.LT.NI) THEN
    DUDX = (UI1J-UI0J)/DX2
    DVDX = (VI1J-VI0J)/DX2
    D2UDX2 = (UI1J-2.*UIJ+UI0J)/DXDX
    D2VDX2 = (VI1J-2.*VIJ+VI0J)/DXDX
  IF(WT(I+1,J).GT.1..AND.WTIJ.EQ.1..AND.I.GT.2) THEN
    DUDX = ( U(I-2,J,K)-4.*UI0J+3.*UIJ)/DX2
    DVDX = ( V(I-2,J,K)-4.*VI0J+3.*VIJ)/DX2
    D2UDX2 = (UIJ-2.*UI0J+U(I-2,J,K))/DXDX
    D2VDX2 = (VIJ-2.*VI0J+V(I-2,J,K))/DXDX
  END IF
  IF(WT(I-1,J).GT.1..AND.WTIJ.EQ.1..AND.I.LT.NI-1) THEN
    DUDX = (-UI2J+4.*UI1J-3.*UIJ)/DX2
    DVDX = (-VI2J+4.*VI1J-3.*VIJ)/DX2
    D2UDX2 = (UIJ-2.*UI1J+UI2J)/DXDX
    D2VDX2 = (VIJ-2.*VI1J+VI2J)/DXDX
  END IF

```

```

      END IF
    END IF
    IF(I.EQ.NI) THEN
      DUDX = ( U(I-2,J,K)-4.*UI0J+3.*UIJ)/DX2
      DVDX = ( V(I-2,J,K)-4.*VI0J+3.*VIJ)/DX2
      D2UDX2 = (UIJ-2.*UI0J+U(I-2,J,K))/DXDX
      D2VDX2 = (VIJ-2.*VI0J+V(I-2,J,K))/DXDX
    END IF
  END IF

```

C

```

    IF(J.EQ.1) THEN
      DUDY = (-UIJ2+4.*UIJ1-3.*UIJ)/DY2
      DVDY = (-VIJ2+4.*VIJ1-3.*VIJ)/DY2
      D2UDY2 = (UIJ-2.*UIJ1+UIJ2)/DYDY
      D2VDY2 = (VIJ-2.*VIJ1+VIJ2)/DYDY
    ELSE
      IF(J.GT.1.AND.J.LT.NI) THEN
        DUDY = (UIJ1-UIJ0)/DY2
        DVDY = (VIJ1-VIJ0)/DY2
        D2UDY2 = (UIJ1-2.*UIJ+UIJ0)/DYDY
        D2VDY2 = (VIJ1-2.*VIJ+VIJ0)/DYDY
        IF(WT(I,J+1).GT.1..AND.WTIJ.EQ.1..AND.J.GT.2) THEN
          DUDY = ( U(I,J-2,K)-4.*UIJ0+3.*UIJ)/DY2
          DVDY = ( V(I,J-2,K)-4.*VIJ0+3.*VIJ)/DY2
          D2UDY2 = (UIJ-2.*UIJ0+U(I,J-2,K))/DYDY
          D2VDY2 = (VIJ-2.*VIJ0+V(I,J-2,K))/DYDY
        END IF
        IF(WT(I,J-1).GT.1..AND.WTIJ.EQ.1..AND.J.LT.NJ-1) THEN
          DUDY = (-UIJ2+4.*UIJ1-3.*UIJ)/DY2
          DVDY = (-VIJ2+4.*VIJ1-3.*VIJ)/DY2
          D2UDY2 = (UIJ-2.*UIJ1+UIJ2)/DYDY
          D2VDY2 = (VIJ-2.*VIJ1+VIJ2)/DYDY
        END IF
      END IF
      IF(J.EQ.NJ) THEN
        DUDY = ( U(I,J-2,K)-4.*UIJ0+3.*UIJ)/DY2
        DVDY = ( V(I,J-2,K)-4.*VIJ0+3.*VIJ)/DY2
        D2UDY2 = (UIJ-2.*UIJ0+U(I,J-2,K))/DYDY
        D2VDY2 = (VIJ-2.*VIJ0+V(I,J-2,K))/DYDY
      END IF
    END IF

```

C

```

    DPDX(I,J,K) = -(TIMCON*DUDT + UIJ*DUDX + VIJ*DUDY)
                  +FLOAT(NAVIER)*(D2UDX2+D2UDY2)/RE
    DPDY(I,J,K) = -(TIMCON*DVDY + UIJ*DVDX + VIJ*DVDY)
                  +FLOAT(NAVIER)*(D2VDX2+D2VDY2)/RE

```

500 CONTINUE

C

C-----

C

CALCULATE PRESSURES

```

C-----
C
C
C
C   TRAPEZOIDAL RULE OF INTEGRATION
C
DO 600 K = K1,K2,KDELTA
  P(1,NJ,K) = 0.
  PSUM = 0.
  DO 600 I = 2,NI
    PSUM = PSUM + DX/2.*(DPDX(I,NJ,K)+DPDX(I-1,NJ,K))
    P(I,NJ,K) = PSUM
600 CONTINUE
C
DO 650 K = K1,K2,KDELTA
  DO 650 I = 1,NI
    PSUM = P(I,NJ,K)
    DO 650 J = NJ-1,1,-1
      IF(WT(I,J).GT.1.) THEN
        P(I,J,K) = P(I,J+1,K)
      ELSE
        PSUM = PSUM - DY/2.*(DPDY(I,J,K)+DPDY(I,J+1,K))
        P(I,J,K) = PSUM
      END IF
650 CONTINUE
C
C-----
C   WRITE OUTPUT
C-----
C
C
C   PRINT OUT DATA AT Y/C = 0.3625, 0.2625, 0.1625, AND 0.0625
C
DO 700 K = K1,K2,KDELTA
  WRITE(11,804) K
  WRITE(11,805) NI
  DO 675 I = 1,NI
675  WRITE(11,803) XD(I),P(I,NJ,K),P(I,NJ-8,K),P(I,NJ-16,K),
      P(I,NJ-24,K)
700 CONTINUE
C
C   TIME TRACE ON BLADE
C
DO 740 I = 17,25,2
  WRITE(12,1000) XD(I)
  NUMPTS = (K2-K1)/KDELTA + 1
  WRITE(12,805) NUMPTS
  DO 740 K = K1,K2,KDELTA
740  WRITE(12,803) FLOAT(K),P(I,1,K)
C
C-----

```

C FORMAT STATEMENTS

C-----

C
800 FORMAT(3(5X,E14.7))
801 FORMAT(3(5X,I3))
802 FORMAT(3(5X,E14.7))
803 FORMAT(6E13.5)
804 FORMAT(/3X,I3)
805 FORMAT(3X,I3)
1000 FORMAT(/E15.7)
1010 FORMAT(2E15.7)
1020 FORMAT(3(3E13.5))

C
 STOP
 END

Appendix C. Macintosh Animation Code

```
C
C
C PROGRAM TO ANIMATE DISCRETE FIELD VALUES AT SEQUENTIAL      =
C TIMES USING A MACINTOSH II COMPUTER AND MICROSOFT           =
C FORTRAN V2.2                                                 =
C                                                               =
C                                                               =
C MATTHEW M. PESCE                                           =
C MASTER OF SCIENCE CANDIDATE                                =
C ENGINEERING SCIENCE AND MECHANICS                          =
C VIRGINIA POLYTECHNIC INSTITUTE AND STATE UNIVERSITY        =
C                                                               =
C September 1990                                             =
C
C
C
C
C This code reads in position X and Y and two-dimensional     =
C vorticity Z for each time level of the data period.        =
C The vorticity is then drawn to the screen as blocks        =
C of colored pixels representing a range of vorticity.       =
C The pixels are then replaced with the pixels representing   =
C the next time level.                                       =
C
C
C
C Description of Variables:                                   =
C
C COLORS      Color scheme sent to subroutine PIXS          =
C COLOR1     Color scheme for positive vorticity only       =
C COLOR2     Color scheme for negative vorticity only       =
C COLOR3     Color scheme for both positive and negative    =
C            vorticity together                             =
```



```

C      W          Width of pixel block                      =
C      H          Height of pixel block                     =
C      IMAX       Dimension of X direction                 =
C      JMAX       Dimension of Y direction                 =
C      KMAX       Dimension in time                       =
C      NCOLOR     Number of colors used in pixel image    =
C      NCLEVL     Number of vorticity levels               =
C      YMAXO      Value of Y used to convert coordinate    =
C                system to that of screen                 =
C      X          Array holding x locations                =
C      Y          Array holding y locations                =
C      Z          Vorticity                                =
C      CC         Levels of vorticity to display           =
C      XE         Extended x array, four point average    =
C      YE         Extended y array, four point average    =
C      ZE         Extended vorticity array, four point average =
C      XMAX       Maximum X value                          =
C      XMIN       Minimum X value                          =
C      YMAX       Maximum Y value                          =
C      YMIN       Minimum Y value                          =
C      XORIG      X position of image origin               =
C      YORIG      Y position of image origin               =
C      F          Scaling factor for image                 =
C
C      Other variables are part of MS-Fortran V2.2 Toolbox =
C      routines or are supplemental variables for looping =
C      and decision control                                =
C
C
C      INTEGER*4  COLORS(8),COLOR1(8),COLOR2(8),COLOR3(8),W,H
C      COMMON /STUFF1/  IMAX,JMAX,KMAX
C      COMMON /STUFF2/  W,H,NCOLOR,NCLEVL,YMAXO
C      COMMON /STUFF3/  X(30),Y(41),Z(30,41,30),CC(10)
C      COMMON /STUFF4/  XE(30),YE(41),ZE(30,41,30)
C      COMMON /COORD/  XMAX,XMIN,YMAX,YMIN,XORIG,YORIG,F
C
C      DEFINE THE COLOR SCEMES FOR THE PARTICLES
C
C      DATA COLOR1/205,341,69,409,273,137,33,30/
C      DATA COLOR2/409,273,33,205,341,69,137,30/
C      DATA COLOR3/409,273,33,30,205,341,69,33/
C
C-----
C      GET THE DATA FROM FILES
C-----
C
C      CALL INPUT
C
C-----
C      LOOPING TO DO POSITIVE VORTICITY, NEGATIVE VORTICITY,

```

```

C      AND BOTH
C-----
C
      KOUNT = 1
300  CONTINUE
      CALL FOIL
C
C      POSITIVE VORTICITY LOOP
C
      IF(KOUNT.EQ.1) THEN
          ZMIN = 3.
          ZMAX = 28.
          NCLEVEL = 4
          NCOLOR = 3
          DO 233 ICOLS = 1,8
233   COLORS(ICOLS) = COLOR1(ICOLS)
          END IF
C
C      NEGATIVE VORTICITY LOOP
C
      IF(KOUNT.EQ.2) THEN
          ZMIN = -28.
          ZMAX = -4.
          NCLEVEL = 4
          NCOLOR = 3
          DO 234 ICOLS = 1,8
234   COLORS(ICOLS) = COLOR2(ICOLS)
          END IF
C
C      COMBINATION LOOP
C
      IF(KOUNT.EQ.3) THEN
          ZMIN = -28.
          ZMAX = 28.
          NCLEVEL = 8
          NCOLOR = 7
          DO 235 ICOLS = 1,8
235   COLORS(ICOLS) = COLOR3(ICOLS)
          END IF
C
C-----
C      SET CONTOUR LEVELS
C-----
C
      R = ABS(ZMAX-ZMIN)/FLOAT(NCLEVEL-1)
      RR = ZMIN - R
      DO 440 II = 1,NCLEVEL
          RR = RR + R
440  CC(II) = RR
C

```

```

C-----
C   CALL PIXEL DRAWING ROUTINES
C-----
C
C   DO 200 K = 1,KMAX-1
C     CALL PIXS(COLORS,K)
200 CONTINUE
C
C   KOUNT = KOUNT + 1
C   IF(KOUNT.GT.3) KOUNT=1
C
C   PAUSE
C   GO TO 300
C   STOP
C   END
C
C-----
C
C   SUBROUTINE INPUT
C
C   INTEGER*4 W,H
C   CHARACTER*5 JUNK
C   COMMON /STUFF1/ IMAX,JMAX,KMAX
C   COMMON /STUFF2/ W,H,NCOLOR,NCLEVL,YMAXO
C   COMMON /STUFF3/ X(30),Y(41),Z(30,41,30),CC(10)
C   COMMON /STUFF4/ XE(30),YE(41),ZE(30,41,30)
C   COMMON /STUFF5/ ILABLE,IAVERG
C   COMMON /COORD/ XMAX,XMIN,YMAX,YMIN,XORIG,YORIG,F
C
C   OPEN(11,FILE='COLOR.INP',STATUS='OLD')
C   OPEN(12,FILE='VORT1.DATA',STATUS='OLD')
C
C-----
C   READ IN INPUT PARAMETERS:  MAKE SURE THERE IS A BLANK
C                               AT THE END OF THE FILE
C-----
C
C   READ(11,*) JUNK
C   READ(11,*) IMAX,JMAX,KMAX,YMAXO,ZMIN,ZMAX
C   READ(11,*) JUNK
C   READ(11,*) NCOLOR,NCLEVL,XORIG,YORIG,F
C   READ(11,*) JUNK
C   READ(11,*) W,H,ILABLE,IAVERG
C   CLOSE(11)
C
C-----
C   READ IN FIRST FILE
C-----
C
C

```

```

IF(KMAX.GT.25) THEN
  KF1 = 25
ELSE
  KF1 = KMAX
END IF
C
  READ(12,*) JUNK
  DO 60 K = 1,KF1
  READ(12,*) IMAX,JMAX,KDUM
  DO 50 I = 1,IMAX
    DO 50 J = 1,JMAX
      READ(12,*) X(I),Y(J),Z(I,J,K)
50 CONTINUE
60 CONTINUE
  CLOSE(12)
C
  IF(KMAX.LE.25) GO TO 68
C
C-----
C  READ IN SECOND FILE
C-----
C
C
C
  OPEN(13,FILE='VORT2.DATA',STATUS='OLD')
  READ(13,*) JUNK
  DO 65 K = 26,KMAX
    READ(13,*) IMAX,JMAX,KDUM
    DO 55 I = 1,IMAX
      DO 55 J = 1,JMAX
        READ(13,*) X(I),Y(J),Z(I,J,K)
55 CONTINUE
65 CONTINUE
  CLOSE(13)
C
68 CONTINUE
C
C-----
C  SHIFT COORDINATES TO MATCH SCREEN
C  (0,0 IN UPPER LEFT CORNER)
C-----
C
C
C
  DO 70 J = 1,JMAX
    Y(J) = YMAXO - Y(J)
70 CONTINUE
C
  XMIN = X(1)
  XMAX = X(IMAX)
  YMIN = Y(JMAX)

```

```

      YMAX = Y(1)
C
C-----
C      USE FOUR POINT AVERAGING TO GET BETTER RESOLUTION
C-----
C
C
      IAVERG = 1
      IF(IAVERG.EQ.1) THEN
      DO 200 J = 1, JMAX
      YE(J) = 0.5*(Y(J)+Y(J+1))
      DO 200 I = 1, IMAX
      IF(I.EQ.IMAX) THEN
      XE(I) = X(I)
      ELSE
      XE(I) = 0.5*(X(I)+X(I+1))
      END IF
      DO 200 K = 1, KMAX
      IF(I.EQ.IMAX) THEN
      ZE(I,J,K) = 0.5*(Z(I,J,K)+Z(I,J+1,K))
      ELSE
      ZE(I,J,K) = 0.25*(Z(I,J,K)+Z(I+1,J,K)+Z(I,J+1,K)+
      Z(I+1,J+1,K))
      END IF
200 CONTINUE
      END IF
C
      RETURN
      END
C
C-----
C
      SUBROUTINE FOIL
C
      INCLUDE TOOLBX.PAR
C
      CHARACTER*256 LABEL
      INTEGER*4 FBYTE, BYTCNT, SRCOPY, W, H, TSIZE
      INTEGER*2 RECT(4)
      COMMON /COORD/ XMAX, XMIN, YMAX, YMIN, XORIG, YORIG, F
      COMMON /STUFF2/ W, H, NCOLOR, NCLEVEL, YMAXO
C
      DRAW INNER BOX
C
      RECT(1) = INT(YMIN*F+YORIG)-H-1
      RECT(2) = INT(XMIN*F+XORIG)-W-1
      RECT(3) = INT(YMAX*F+YORIG)+H+1
      RECT(4) = INT(XMAX*F+XORIG)+W+1
      CALL TOOLBX(FRAMERECT, RECT)
C

```

```

C      DRAW OUTER BOX
C
RECT(1) = INT(YMIN*F+YORIG)-H-6
RECT(2) = INT(XMIN*F+XORIG)-W-6
RECT(3) = INT(YMAX*F+YORIG)+H+6
RECT(4) = INT(XMAX*F+XORIG)+W+6
CALL TOOLBX(FRAMERECT,RECT)

C
C-----
C      DRAW AIRFOIL
C-----
C
C
XZERO = 0.
YZERO = YMAXO

C
CALL TOOLBX(MOVETO,INT(XZERO*F+XORIG),INT(YZERO*F+YORIG))
PALF = 10./180.*ACOS(-1.)
PALF = -PALF
A1 = 0.2969
A2 = -0.126
A3 = -0.3516
A4 = 0.2843
A5 = -0.1015
XAF = 0.
DAF = 0.0005
100 YAF = 15./20.*(A1*SQRT(XAF)+(((A5*XAF+A4)*XAF+A3)*XAF+A2)*XAF)
XX = COS(PALF)*XAF + SIN(PALF)*YAF
YY = -SIN(PALF)*XAF + COS(PALF)*YAF
XAFP = XX + XZERO
YAFF = YY + YZERO
CALL TOOLBX(LINETO,INT(XAFP*F+XORIG),INT(YAFF*F+YORIG))
XAF = XAF + DAF
IF(XX.LT.XMAX+FLOAT(W)/F) GO TO 100

C
CALL TOOLBX(MOVETO,INT(XZERO*F+XORIG),INT(YZERO*F+YORIG))
XAF = 0.
110 YAF = 15./20.*(A1*SQRT(XAF)+(((A5*XAF+A4)*XAF+A3)*XAF+A2)*XAF)
XX = COS(PALF)*XAF + SIN(PALF)*(-YAF)
YY = -SIN(PALF)*XAF + COS(PALF)*(-YAF)
XAFP = XX + XZERO
YAFF = YY + YZERO
CALL TOOLBX(LINETO,INT(XAFP*F+XORIG),INT(YAFF*F+YORIG))
XAF = XAF + DAF
IF(XX.LT.XMAX+FLOAT(W)/F) GO TO 110

C
C-----
C      DRAW PLOT LABELS
C-----

```

```

C
C
      ILABLE = 0
      IF(ILABLE.EQ.0) GO TO 800
C
      LABLE = CHAR(24)//'BLADE VORTEX INTERACTION'
      CALL TOOLBX(MOVETO,INT(XMAX*F+XORIG)+W+15,INT(YMIN*F+YORIG))
      CALL TOOLBX(DRAWSTRING,LABLE)
C
      LABLE = CHAR(18)//'VORTICITY CONTOURS'
      CALL TOOLBX(MOVETO,INT(XMAX*F+XORIG)+W+15,INT(YMIN*F+YORIG)+12)
      CALL TOOLBX(DRAWSTRING,LABLE)
C
      LABLE = CHAR(24)//'FREESTREAM U = 0.126 M/S'
      CALL TOOLBX(MOVETO,INT(XMAX*F+XORIG)+W+15,INT(YMIN*F+YORIG)+36)
      CALL TOOLBX(DRAWSTRING,LABLE)
C
      LABLE = CHAR(23)//'REYNOLDS NUMBER = 19950'
      CALL TOOLBX(MOVETO,INT(XMAX*F+XORIG)+W+15,INT(YMIN*F+YORIG)+48)
      CALL TOOLBX(DRAWSTRING,LABLE)
C
      LABLE = CHAR(6)//'K = 2.'
      CALL TOOLBX(MOVETO,INT(XMAX*F+XORIG)+W+15,INT(YMIN*F+YORIG)+60)
      CALL TOOLBX(DRAWSTRING,LABLE)
C
800 CONTINUE
C
      RETURN
      END
C
C
C-----
C
      SUBROUTINE PIXS(COLORS,K)
C
      INCLUDE TOOLBX.PAR
C
      INTEGER*4 COLOR,COLORS(8),W,H,W1,H1
      COMMON /STUFF1/ IMAX,JMAX,KMAX
      COMMON /STUFF2/ W,H,NCOLOR,NCLEVL,YMAXO
      COMMON /STUFF3/ X(30),Y(41),Z(30,41,30),CC(10)
      COMMON /STUFF4/ XE(30),YE(41),ZE(30,41,30)
      COMMON /STUFF5/ ILABLE,IAVERG
      COMMON /COORD/ XMAX,XMIN,YMAX,YMIN,XORIG,YORIG,F
C
      CALL TOOLBX(PENSIZE,W,H)
C
C-----
C
      DRAW FIRST PICTURE
C-----

```

```

C
C
C   IF(K.EQ.1) THEN
C
C   DO 100 I = 1,IMAX
C     DO 100 J = 1,JMAX
C       ICOLOR = 1
C       ZZ = Z(I,J,K)
C       DO 90 II = 1,NCLEVEL-1
C         IF(II.EQ.4) GO TO 85
C         IF(ZZ.GE.CC(II).AND.ZZ.LT.CC(II+1)) THEN
C           COLOR = COLORS(ICOLOR)
C           CALL TOOLBX(FORECOLOR,COLOR)
C           CALL TOOLBX(MOVETO,INT(X(I)*F+XORIG)-W/2,
C                               INT(Y(J)*F+YORIG)-H/2)
C           CALL TOOLBX(LINE,1,0)
C         END IF
C         IF(IAVERG.EQ.1) THEN
C           ZZE = ZE(I,J,K)
C           IF(ZZE.GE.CC(II).AND.ZZE.LT.CC(II+1)) THEN
C             COLOR = COLORS(ICOLOR)
C             CALL TOOLBX(FORECOLOR,COLOR)
C             CALL TOOLBX(MOVETO,INT(XE(I)*F+XORIG)-W/2,
C                               INT(YE(J)*F+YORIG)-H/2)
C             CALL TOOLBX(LINE,1,0)
C           END IF
C         END IF
C       CONTINUE
C     ICOLOR = ICOLOR + 1
C     IF(ICOLOR.GT.7.OR.ICOLOR.GT.NCOLOR) ICOLOR=1
C   90 CONTINUE
C 100 CONTINUE
C
C   END IF
C
C
C-----
C   START MAIN PICTURE ROUTINE
C-----
C
C
C   DO 200 I = 1,IMAX
C     DO 200 J = 1,JMAX
C
C   ERASE PREVIOUS PIXELS AT LOCATION X,Y
C
C   COLOR = 30
C   CALL TOOLBX(FORECOLOR,COLOR)
C   ZZ = Z(I,J,K)
C   DO 180 II = 1,NCLEVEL-1
C     IF(II.EQ.4) GO TO 180

```



```

IF(ZZ.GE.CC(II).AND.ZZ.LT.CC(II+1)) THEN
  CALL TOOLBX(MOVETO,INT(X(I)*F+XORIG)-W/2,
              INT(Y(J)*F+YORIG)-H/2)
  CALL TOOLBX(LINE,1,0)
END IF
IF(IAVERG.EQ.1) THEN
  ZZE = ZE(I,J,K)
  IF(ZZE.GE.CC(II).AND.ZZE.LT.CC(II+1)) THEN
    CALL TOOLBX(MOVETO,INT(XE(I)*F+XORIG)-W/2,
                INT(YE(J)*F+YORIG)-H/2)
    CALL TOOLBX(LINE,1,0)
  END IF
END IF
180 CONTINUE
C
C PLACE NEW PIXELS AT LOCATION X,Y
C
  ICOLOR = 1
  ZZ1 = Z(I,J,K+1)
  DO 190 II = 1,NCLEVL-1
    IF(II.EQ.4) GO TO 185
    IF(ZZ1.GE.CC(II).AND.ZZ1.LT.CC(II+1)) THEN
      COLOR = COLORS(ICOLOR)
      CALL TOOLBX(FORECOLOR,COLOR)
      CALL TOOLBX(MOVETO,INT(X(I)*F+XORIG)-W/2,
                  INT(Y(J)*F+YORIG)-H/2)
      CALL TOOLBX(LINE,1,0)
    END IF
    IF(IAVERG.EQ.1) THEN
      ZZ1E = ZE(I,J,K+1)
      IF(ZZ1E.GE.CC(II).AND.ZZ1E.LT.CC(II+1)) THEN
        COLOR = COLORS(ICOLOR)
        CALL TOOLBX(FORECOLOR,COLOR)
        CALL TOOLBX(MOVETO,INT(XE(I)*F+XORIG)-W/2,
                    INT(YE(J)*F+YORIG)-H/2)
        CALL TOOLBX(LINE,1,0)
      END IF
    END IF
  185 CONTINUE
  ICOLOR = ICOLOR + 1
  IF(ICOLOR.GT.7.OR.ICOLOR.GT.NCOLOR) ICOLOR=1
  190 CONTINUE
  200 CONTINUE
C
C -----
C ERASE FINAL FRAME BEFORE LEAVING SUBROUTINE
C -----
C
C
C IF(K.EQ.KMAX-1) THEN

```

```

PAUSE
COLOR = 30
CALL TOOLBX(FORECOLOR,COLOR)
C
DO 400 I = 1,IMAX
DO 400 J = 1,JMAX
ZZ = Z(I,J,K+1)
DO 390 II = 1,NCLEVL-1
IF(II.EQ.4) GO TO 390
IF(ZZ.GE.CC(II).AND.ZZ.LT.CC(II+1)) THEN
CALL TOOLBX(MOVETO,INT(X(I)*F+XORIG)-W/2,
INT(Y(J)*F+YORIG)-H/2)
CALL TOOLBX(LINE,1,0)
END IF
IF(IAVERG.EQ.1) THEN
ZZE = ZE(I,J,K+1)
IF(ZZE.GE.CC(II).AND.ZZE.LT.CC(II+1)) THEN
CALL TOOLBX(MOVETO,INT(XE(I)*F+XORIG)-W/2,
INT(YE(J)*F+YORIG)-H/2)
CALL TOOLBX(LINE,1,0)
END IF
END IF
390 CONTINUE
400 CONTINUE
C
END IF
C
COLOR = 33
CALL TOOLBX(FORECOLOR,COLOR)
W1 = 1
H1 = 1
CALL TOOLBX(PENSIZE,W1,H1)
C
RETURN
END
C
C
C

```

Appendix D. SUN Animation Code

```
C=====
C PROGRAMS TO ANIMATE VORTICITY AS PIXEL-IMAGES,      =
C PIXEL-SHADES, AND CONTOURS USING PV-WAVE SCIENTIFIC =
C VISUALIZATION SOFTWARE FOR A SUN MICROSYSTEMS      =
C GRAPHIC WORKSTATION                                =
C                                                     =
C                                                     =
C MATTHEW M. PESCE                                   =
C MASTER OF SCIENCE CANDIDATE                        =
C ENGINEERING SCIENCE AND MECHANICS                 =
C VIRGINIA POLYTECHNIC INSTITUTE AND STATE UNIVERSITY =
C                                                     =
C September 1990                                     =
C=====
C                                                     =
C                                                     =
C The following procedure files read in two-dimensional =
C unsteady vorticity data and convert the data to bit-maps. =
C The bit-maps are then animated with a second procedure =
C file.                                               =
C                                                     =
C                                                     =
C Description of Variables and Commands              =
C                                                     =
C a          Variable holding the picture            =
C assoc      Associates arrays with variable names   =
C ax         Set horizontal viewing angle             =
C az         Set vertical viewing angle              =
C begin      Begin looping of for statement          =
C bytarr     Defines the byte array for the bit-map  =
C close      Close an external file                  =
C contour    Draw 2-D contours                        =
```

```

C    empty      Clears the register memory           =
C    end        End of the procedure           =
C    endfor     End of a for loop             =
C    fltarr     Defines a floating point array =
C    for        Beginning of time loop        =
C    nlevels    Number of contour levels      =
C    openr      Open a file for reading (only) =
C    openw      Open a file for writing (only) =
C    p          Variable holding the picture  =
C    pro        Precedes procedure filename   =
C    readf      Read in formatted data        =
C    return     Return procedure control to PV-Wave interactive =
C              mode                           =
C    shade_surf Converts data to shaded surfaces =
C    tv         Displays gray-scale image     =
C    tvrd       Reads gray-scale image to associated byte array =
C    tvscl      Scales image to 0-255 before displaying image =
C    window     Creates a window with designated parameters =
C    xpos       Horizontal position of lower window corner =
C    xsize      Width of window              =
C    ypos       Vertical position of lower window corner =
C    ysize      Height of window             =
C    z          Variable containing vorticity data =
C              =
C              =

```

Procedure file to draw the pixel-images. A color table is scaled to cover the entire range of the vorticity data. Each vorticity location is then assigned a color pixel, which is then plotted to the screen

```

pro makemovietv
openr,1,'vort.data'
openw,2,'vorttv.by'
z=fltarr(350,250)
p=assoc(2,bytarr(350,250))
window,1,xsize=350,y=250
for i=1,50 do begin
readf,1,z
tvscl,z
p(i)=tvrd(0,0,350,250)
empty
endfor
close,1
close,2
return
end

```

Procedure file to animate the pixel-images. The byte file is read in and painted to the screen, one picture at a time.

```
pro movietv
openr,9,'vorttv.by'
a=assoc(9,bytarr(350,250))
window,9,xsize=350,ysize=250,xpos=740,ypos=400
for i=1,50 do begin
tv,a(i)
empty
endfor
close,9
return
end
```

Procedure file to draw the shade-images. The data is drawn out of the data plane to represent its magnitude.

```
pro makemovieshade
openr,7,'vort.data'
openw,8,'vortshade.by'
z=fltarr(350,250)
p=assoc(8,bytarr(700,500))
window,8,xsize=700,ysize=500,xpos=400,ypos=10
for i=1,50 do begin
readf,7,z
shade_surf,z,az=30,ax=45
p(i)=tvrd(0,0,700,500)
empty
endfor
close,7
close,8
return
end
```

Procedure file to animate the shade-images. The byte file is read in and painted to the screen, one picture at a time.

```
pro movieshade
openr,8,'vortshade.by'
a=assoc(8,bytarr(700,500))
window,8,xsize=700,ysize=500,xpos=0,ypos=370
```

```

for i=1,50 do begin
tv,a(i)
empty
endfor
close,8
return
end

```

Procedure file to draw the contour images. The levels can be set as with standard contouring software.

```

pro makemoviecont
openr,1,'vort.data'
openw,2,'vortcont.by'
z=fltarr(350,250)
p=assoc(2,bytarr(450,350))
window,1,xsize=450,ysize=350,xpos=670,ypos=10
for i=1,50 do begin
readf,1,z
contour,z,nlevels=20
p(i)=tvrd(0,0,450,350)
empty
endfor
close,1
close,2
return
end

```

Procedure file to animate the contour-images. The byte file is read in and painted to the screen, one picture at a time.

```

pro moviecont
openr,7,'vortcont.by'
a=assoc(7,bytarr(450,350))
window,7,xsize=450,ysize=350,xpos=670,ypos=10
for i=1,50 do begin
tv,a(i)
empty
endfor
close,7
return
end

```

Appendix E. Figures

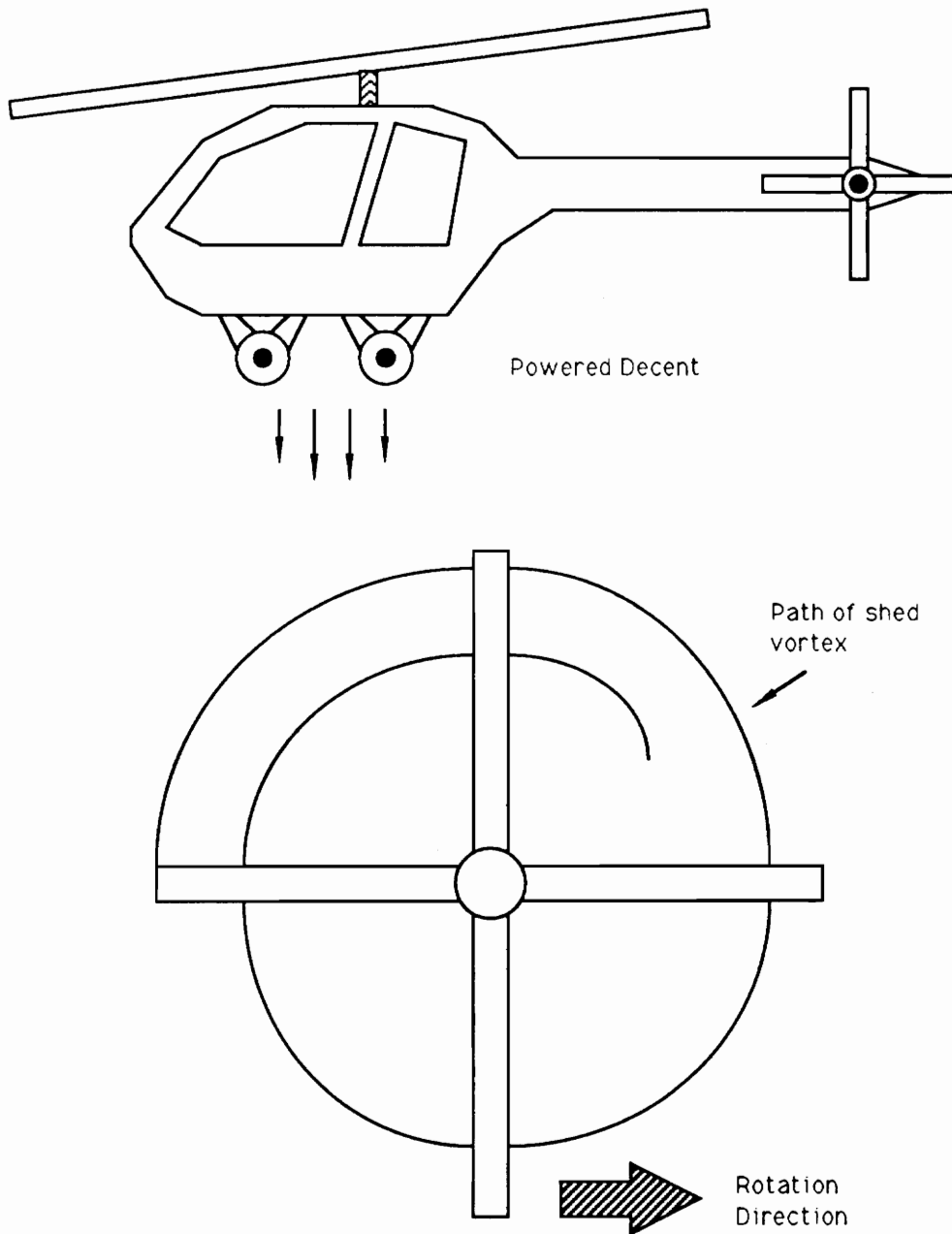
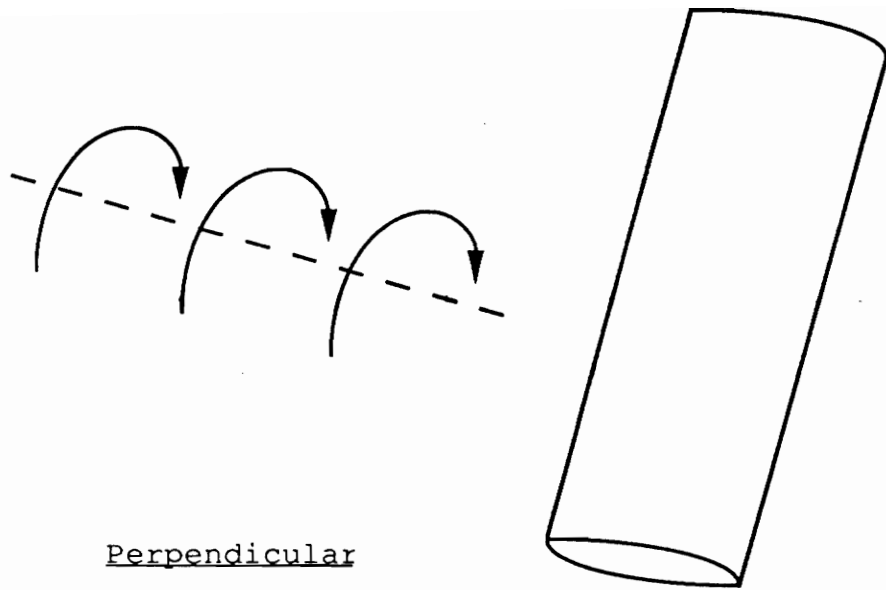
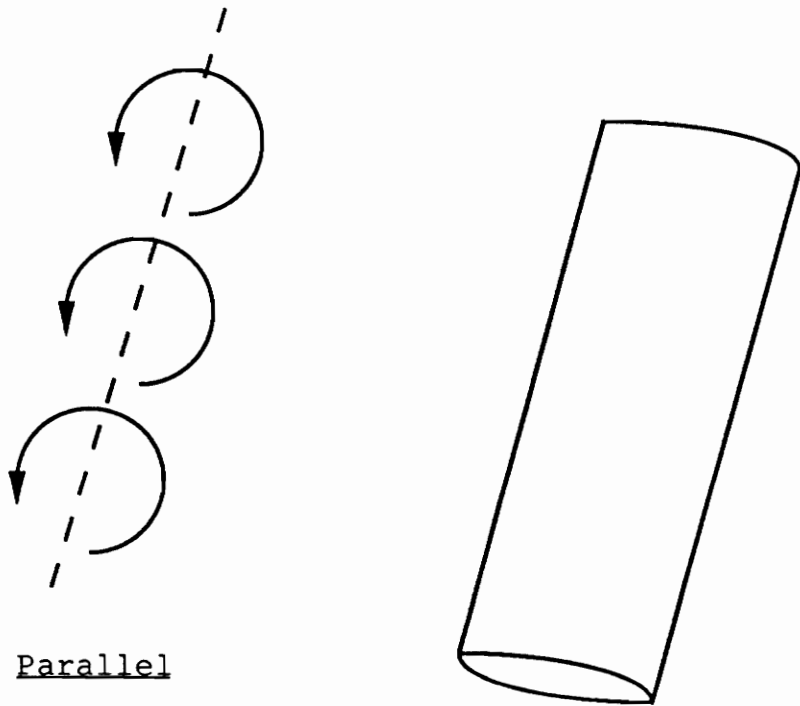


Figure 1.1 The shedding of vorticity from one blade interacts with the following blade in the powered descent condition of helicopter flight

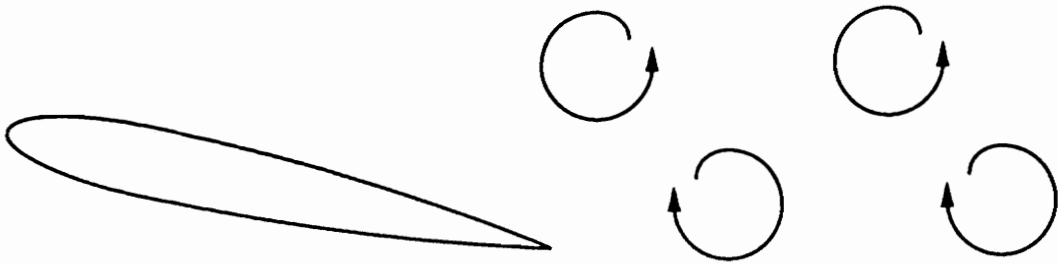


Perpendicular

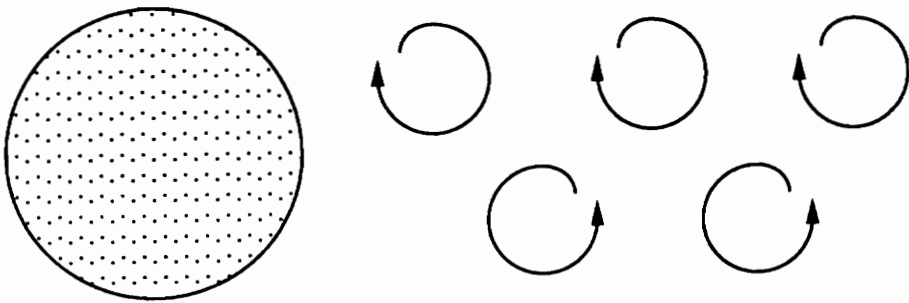


Parallel

Figure 1.2 The extreme conditions of blade-vortex interaction, perpendicular and parallel to the target airfoil axis



Vortex street from airfoil



Von Karman vortex street

Figure 1.3 Vorticity street from a pitching airfoil as compared to a Von Karman vortex street

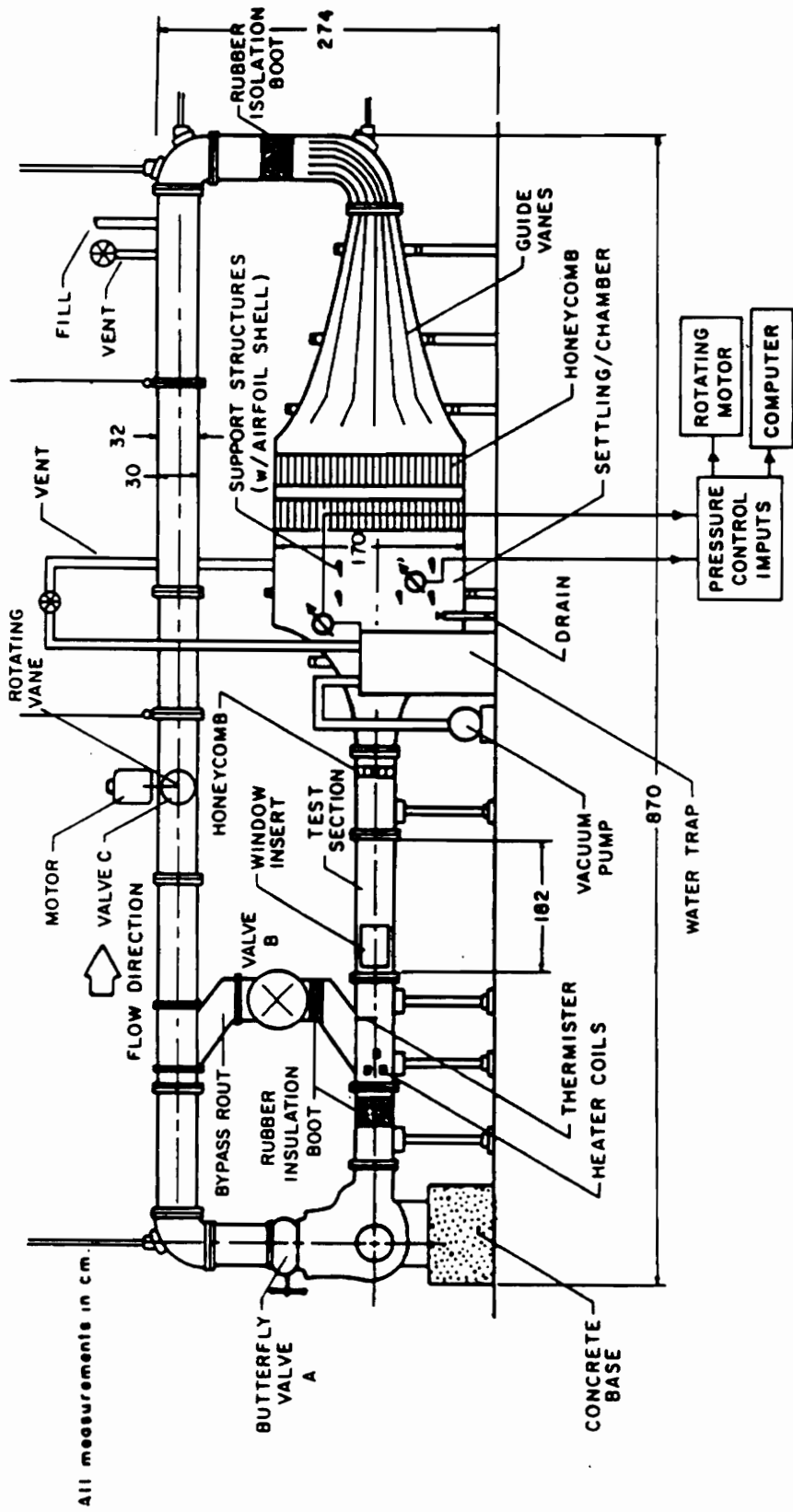


Figure 2.1.1 The ESM water tunnel

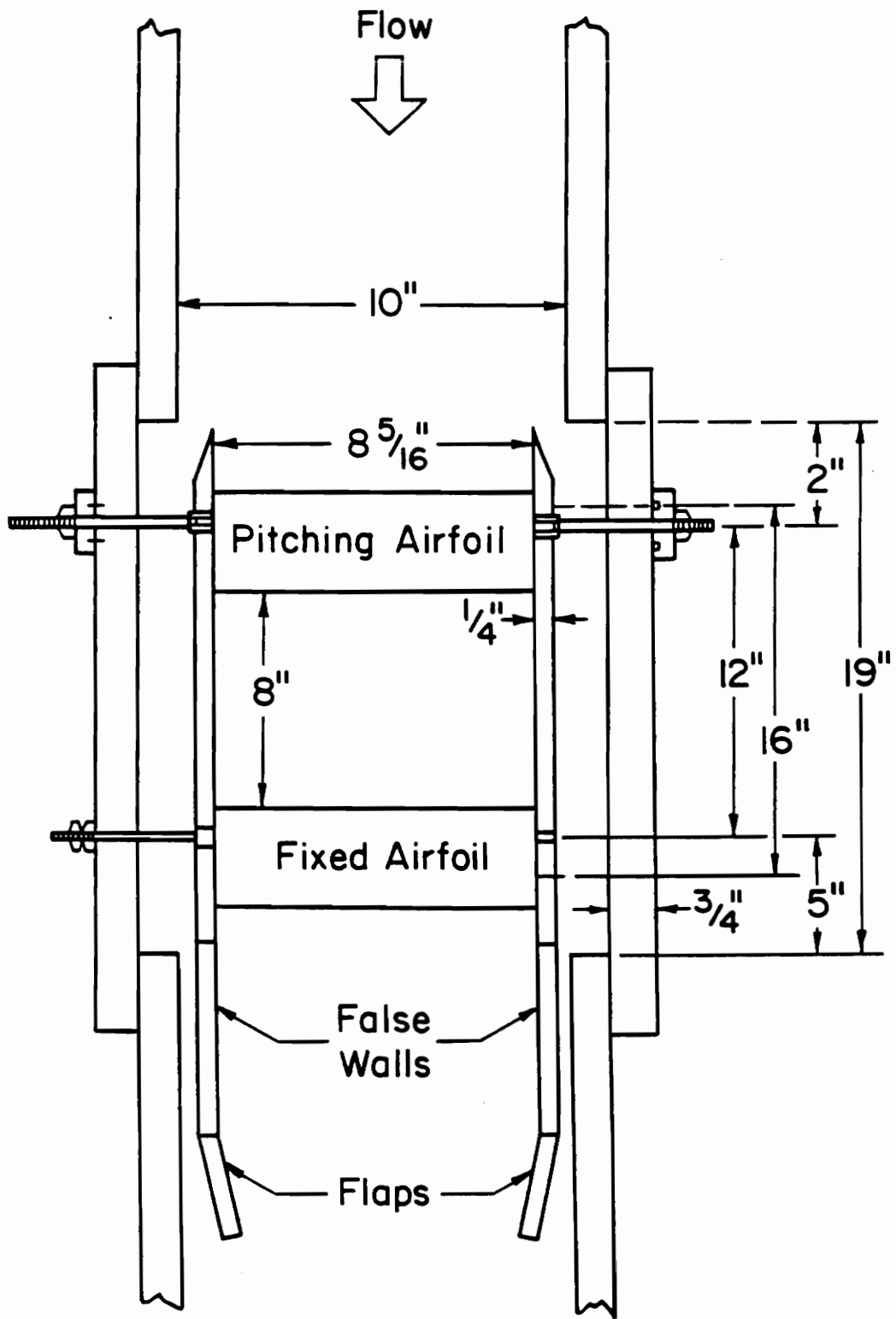


Figure 2.1.2 The test section and false walls

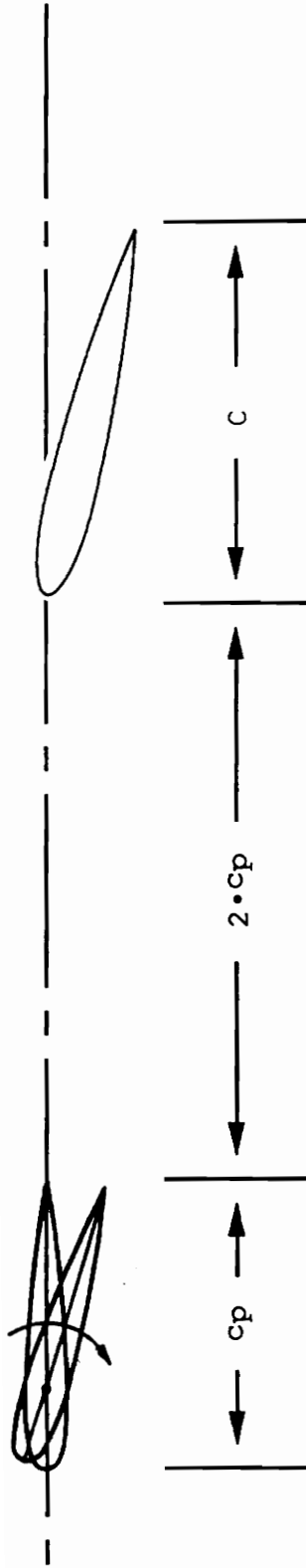


Figure 2.2.1 The pitching airfoil and target airfoil arrangement in the test section

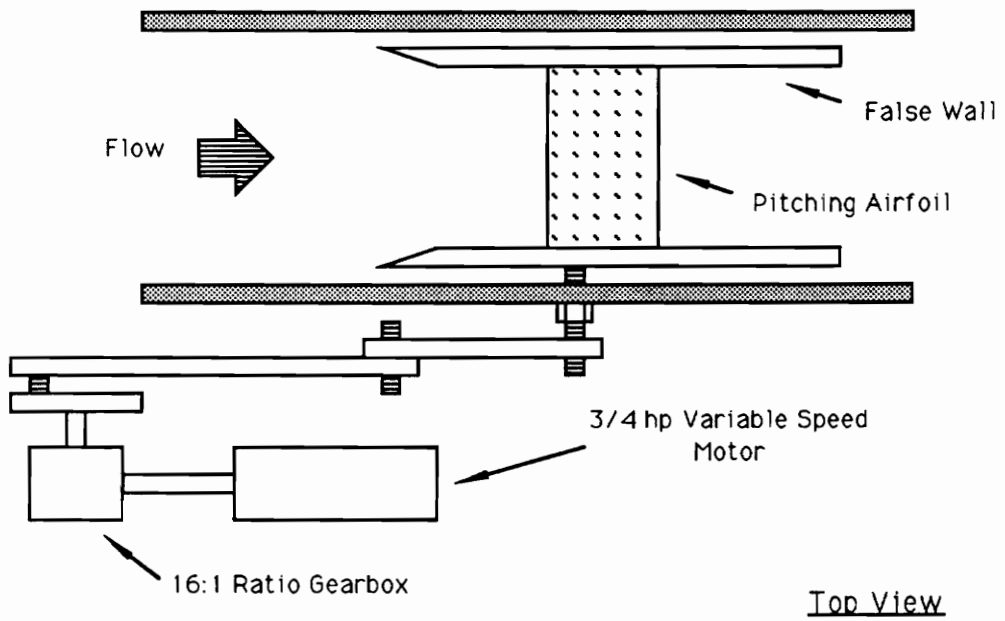
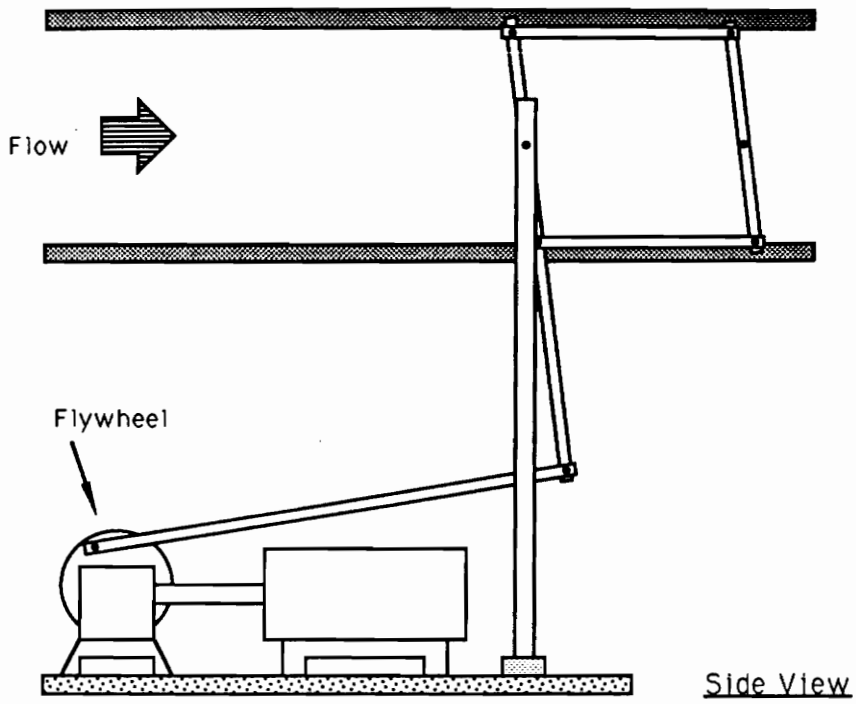


Figure 2.2.2 The four-bar linkage system

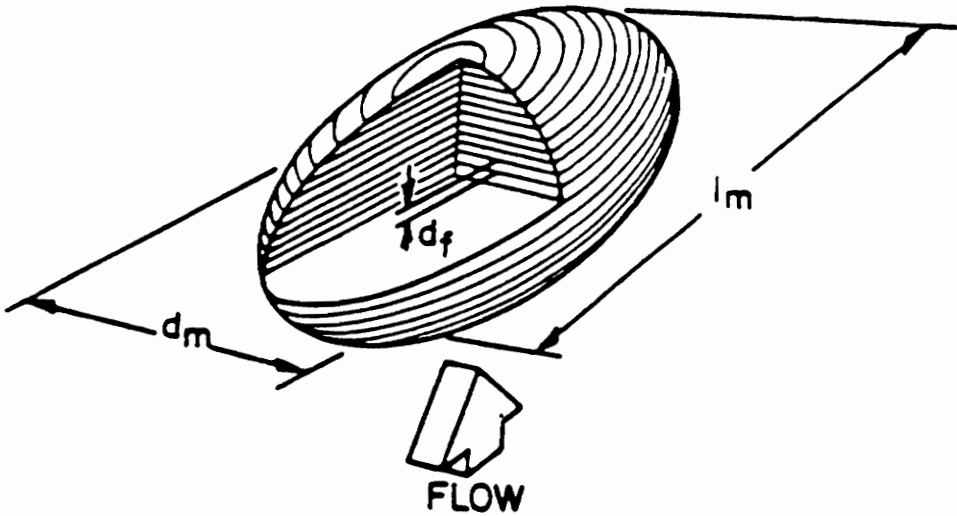
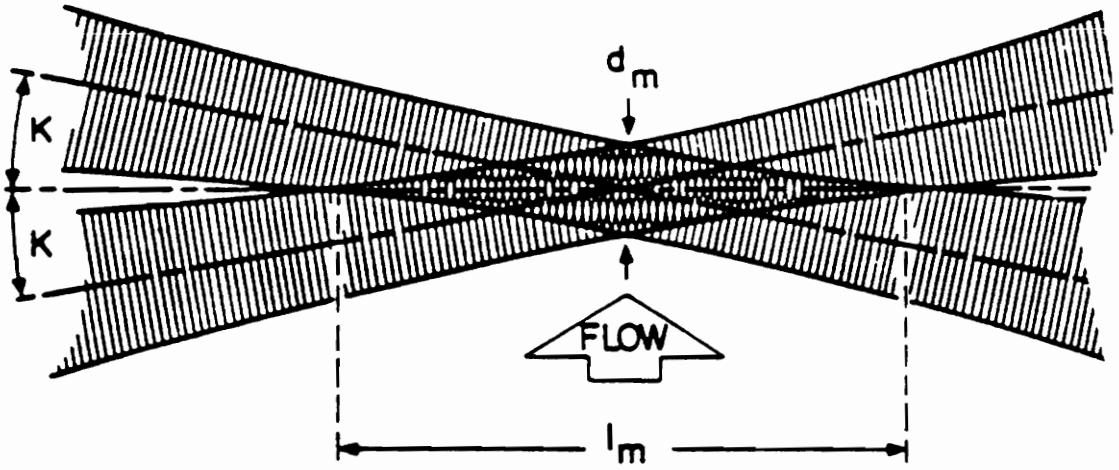


Figure 2.3.1 The wavefronts of two laser beams cause an interference pattern of alternating light and dark fringes. Assuming Gaussian beams, the measuring volume is ellipsoidal with depth and length, d_m and l_m , respectively

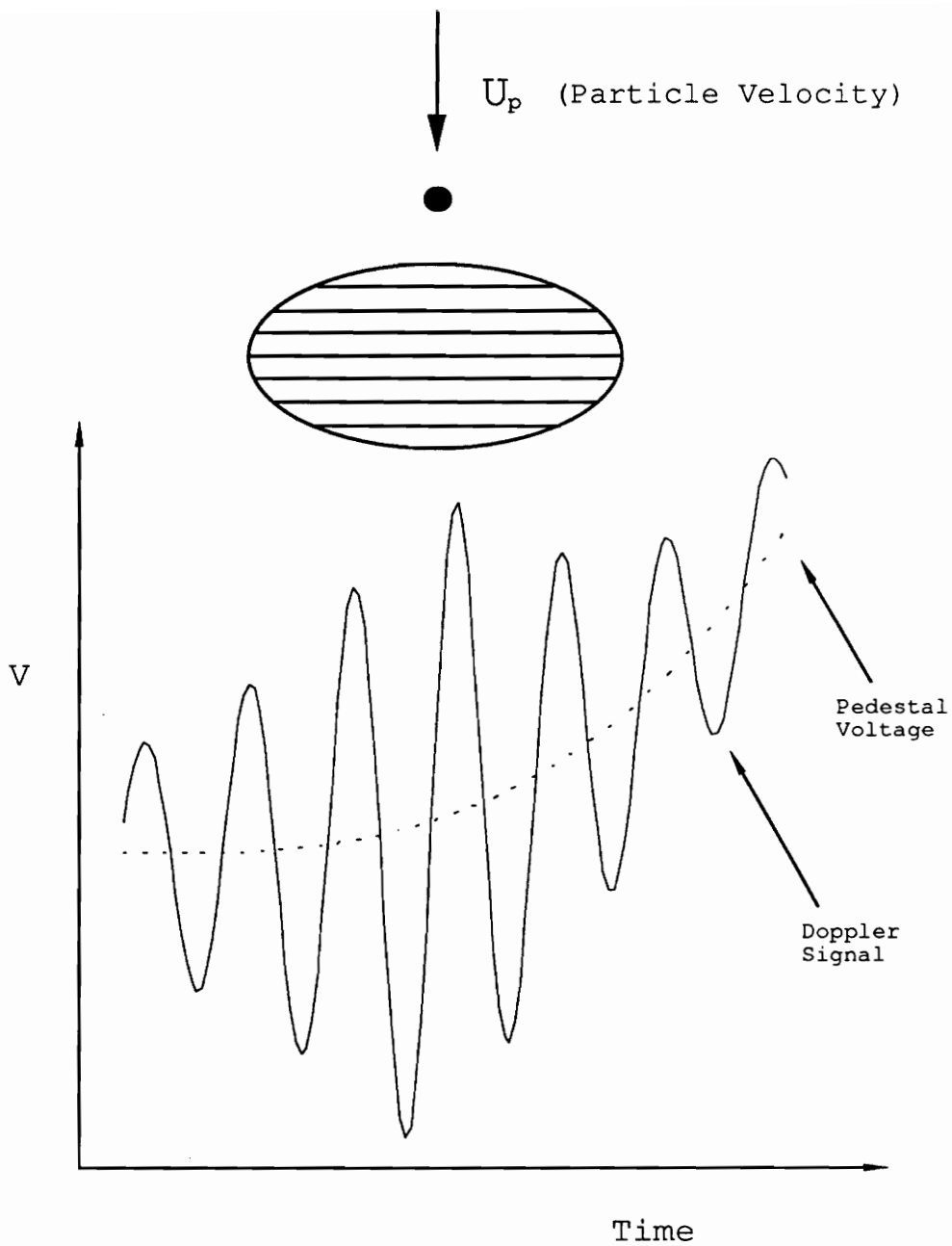
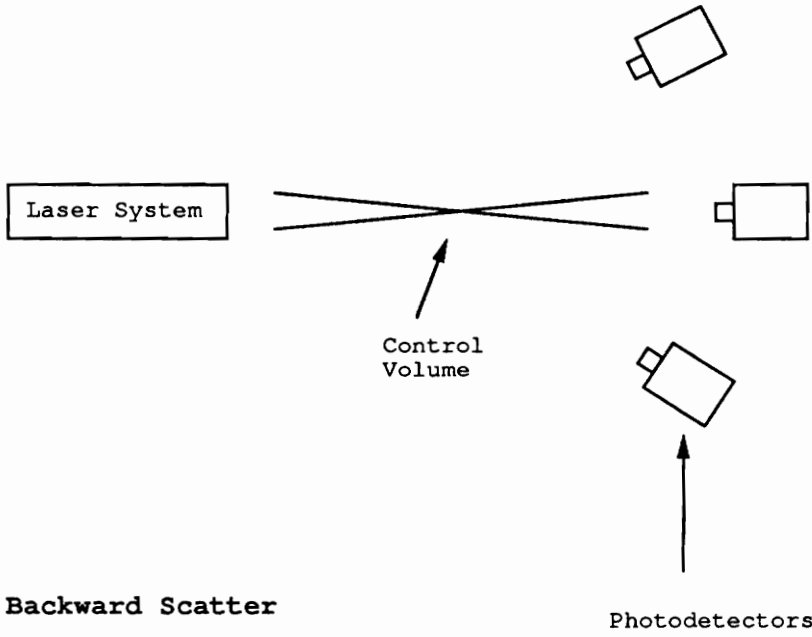


Figure 2.3.2 The signal from the photodetector contains high-frequency noise, the low-frequency pedestal voltage, and the Doppler frequency

Forward Scatter



Backward Scatter

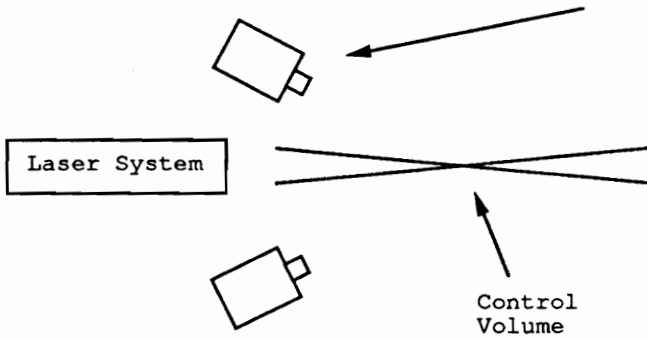


Figure 2.3.3 Forward- and backward-scatter arrangements in LDV

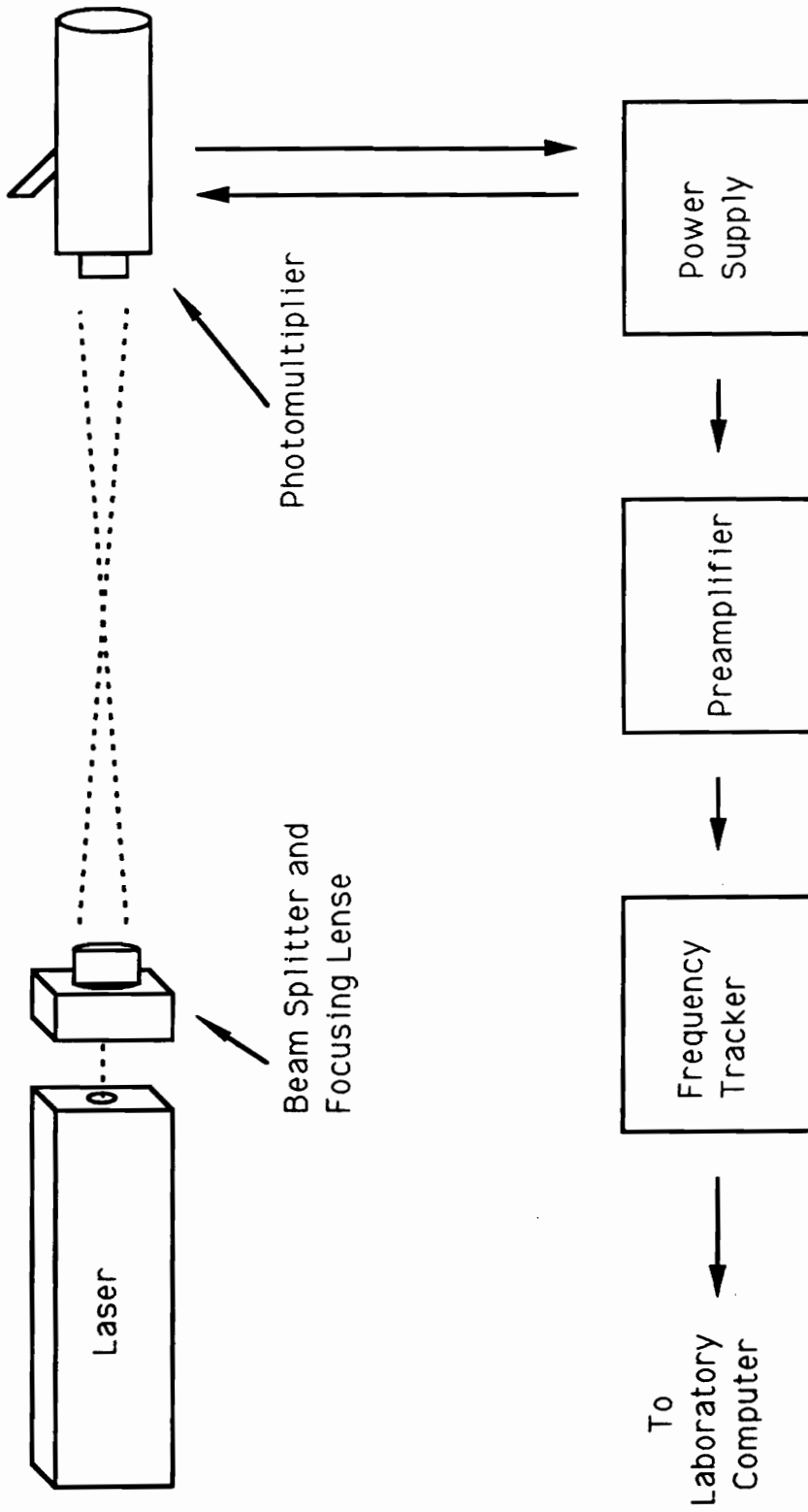
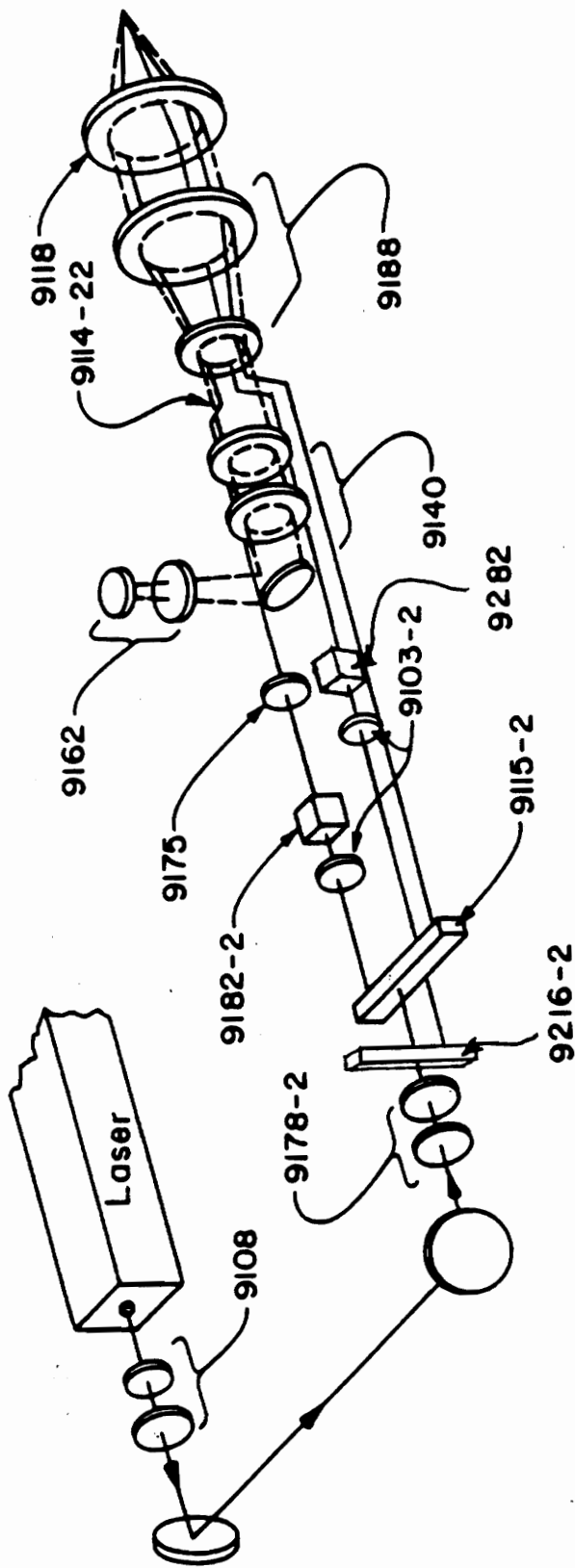


Figure 2.3.4 The DISA laser system



- | | | | |
|---------|---|--------|----------------------------------|
| 9118 | Achromatic lens with focal length 250 mm | 9175 | Beam Steering module |
| 9188 | Beam expander | 9182-2 | Bragg-cell of 40 MHz |
| 9114-22 | Beam spacer | 9103-2 | Polarization rotator |
| 9140 | Receiving assembly | 9115-2 | Beam splitter of equal intensity |
| 9162 | Photodetector | 9178-2 | Rotating mount |
| 9216-2 | Beam splitter | 9108 | Collimator |
| | | 9282 | Bragg-cell of 60 MHz |

Figure 2.3.5 The TSI laser system

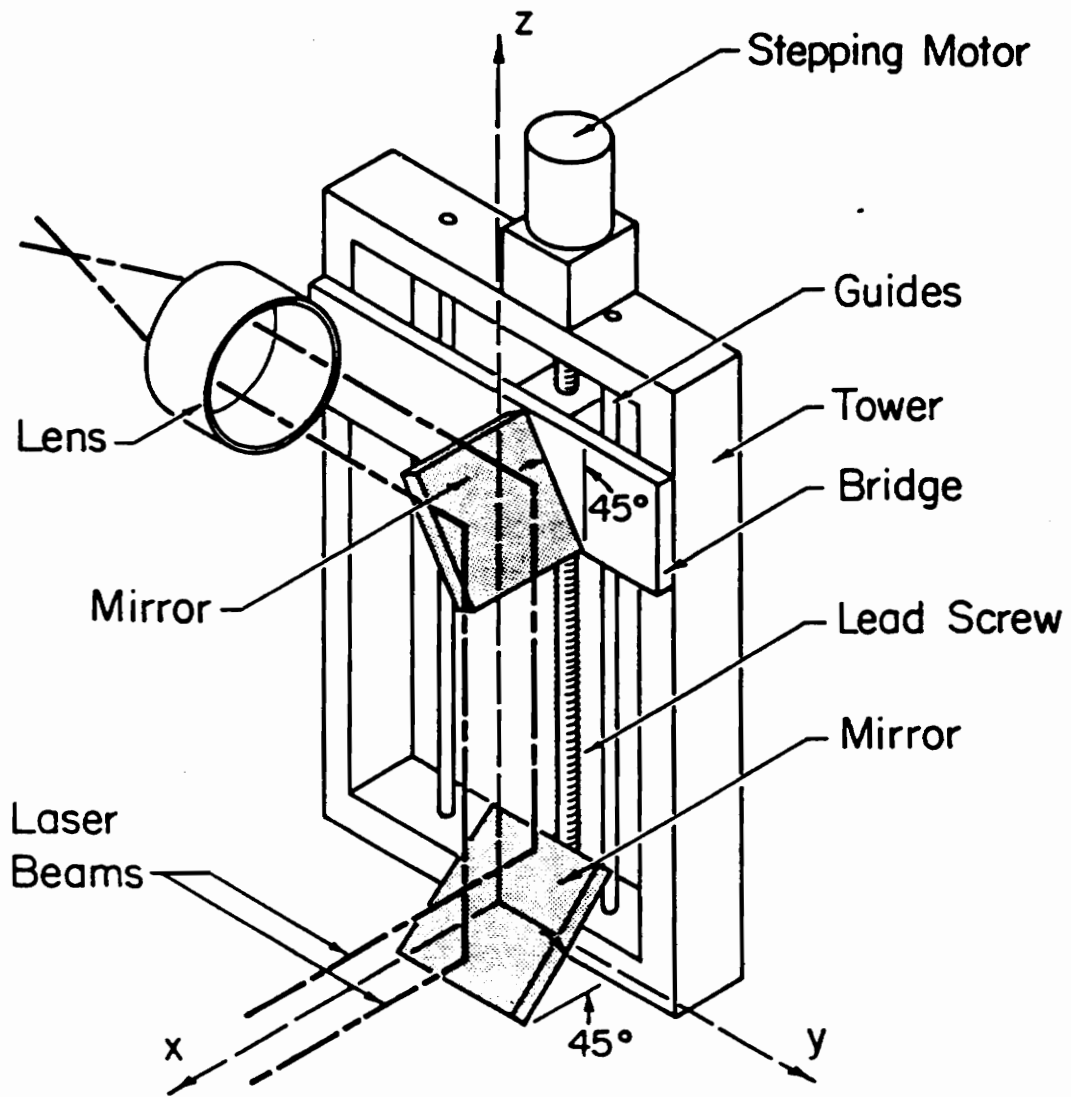


Figure 2.3.6 The mirror tower assembly

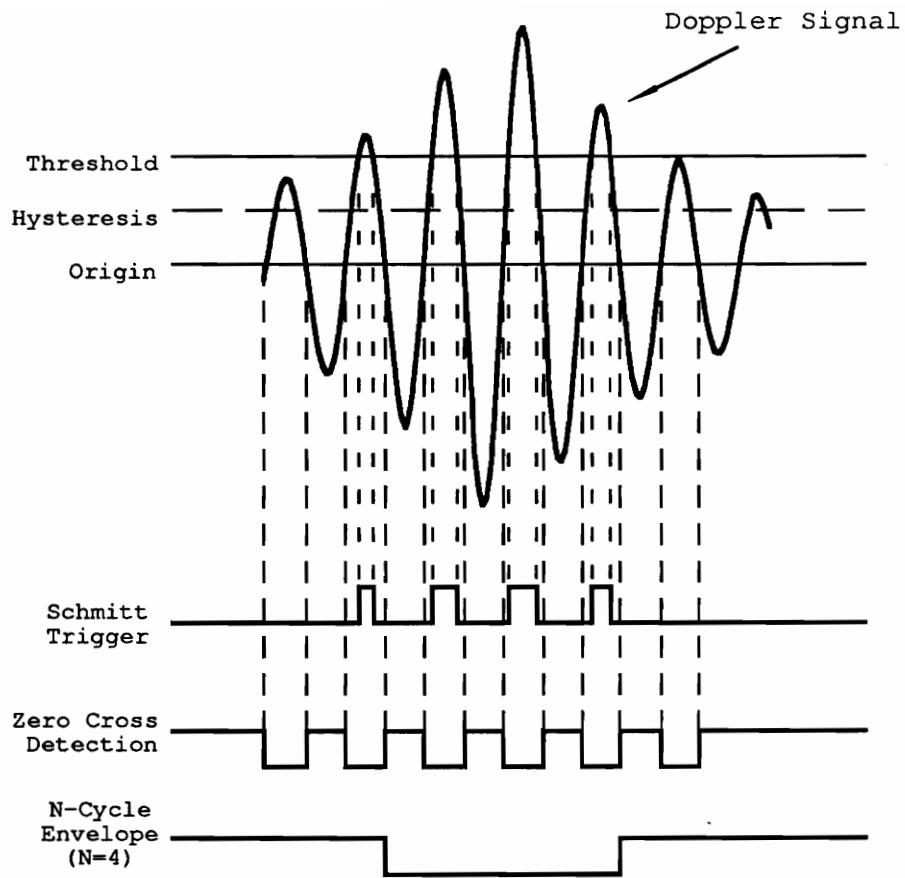


Figure 2.3.7 The counting of signals with counter-type signal processing

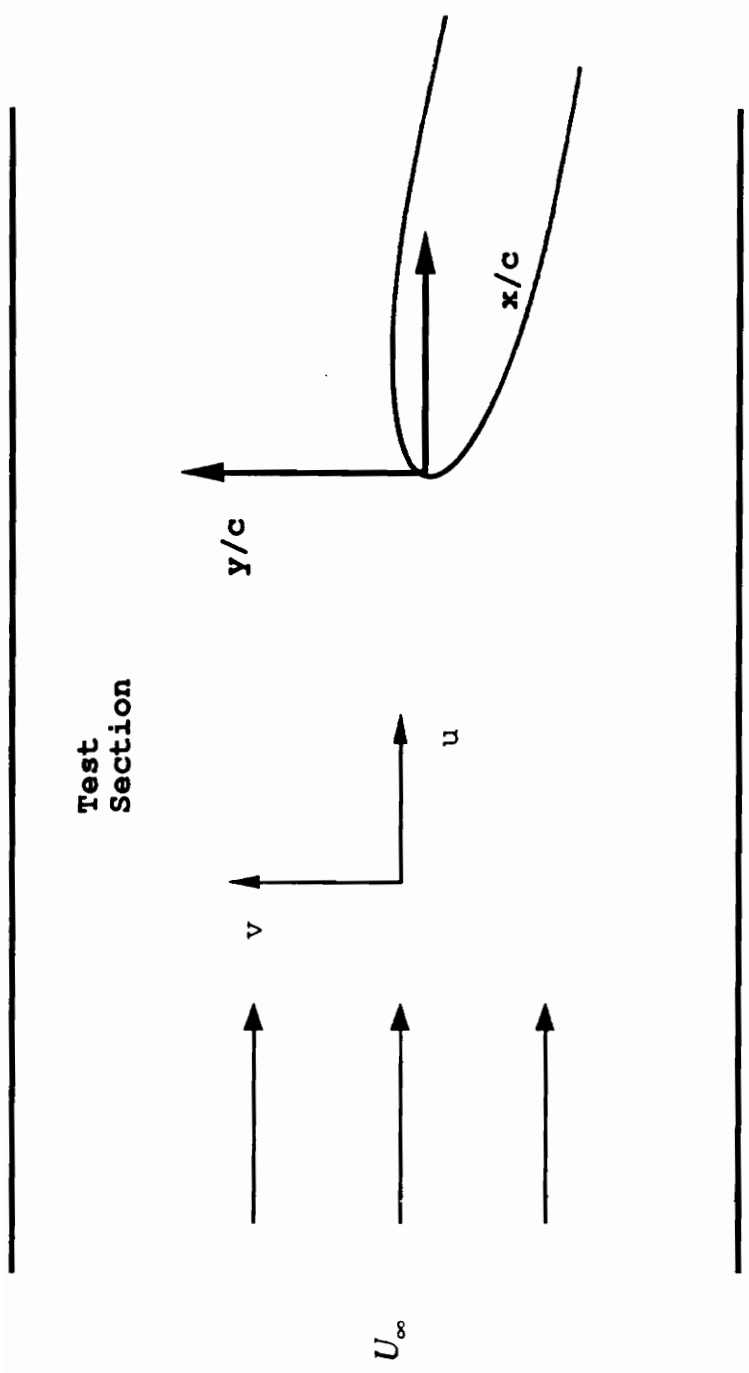
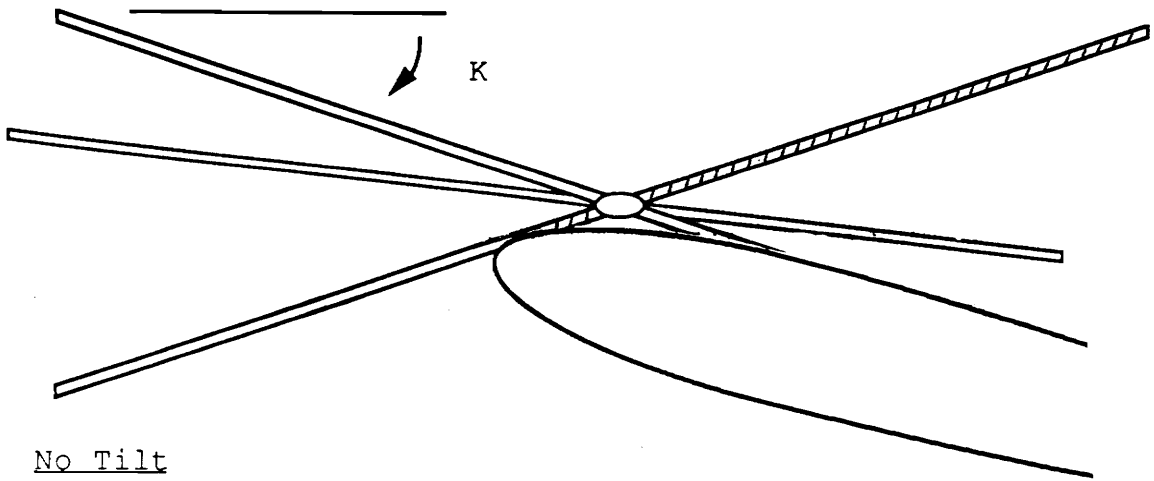


Figure 3.1.1.1 The u and v velocity components relative to the primary flow direction and the coordinate system

K is the half-angle
of the beam intersection



Control
Volume

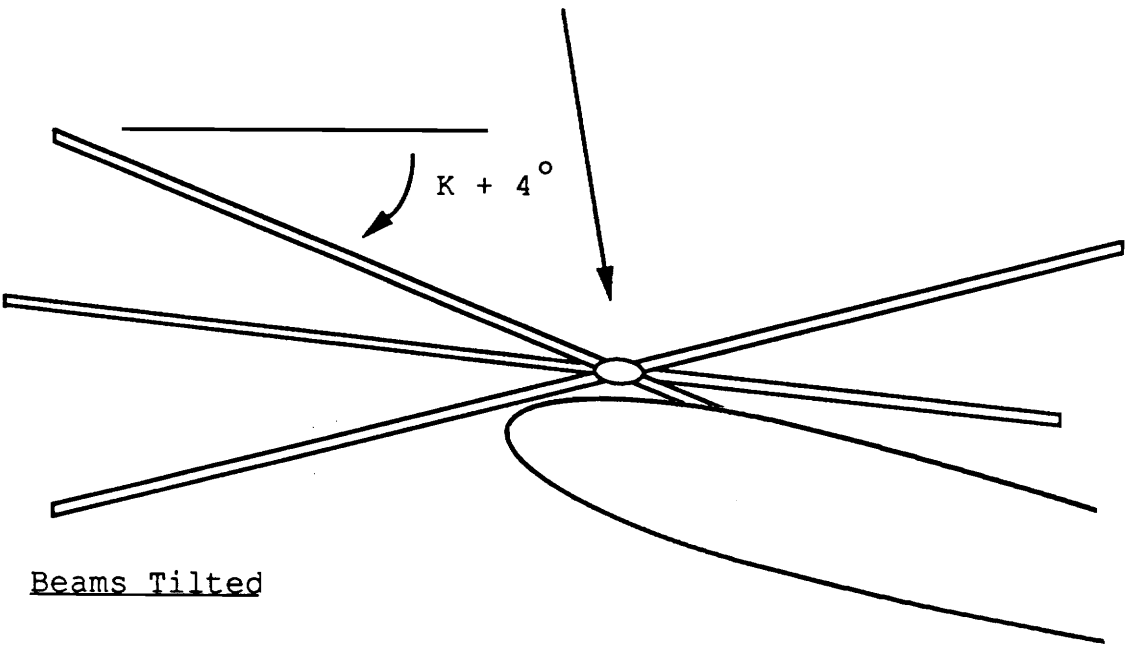


Figure 3.1.2 Tilting of beams to reduce the size of the blocked region

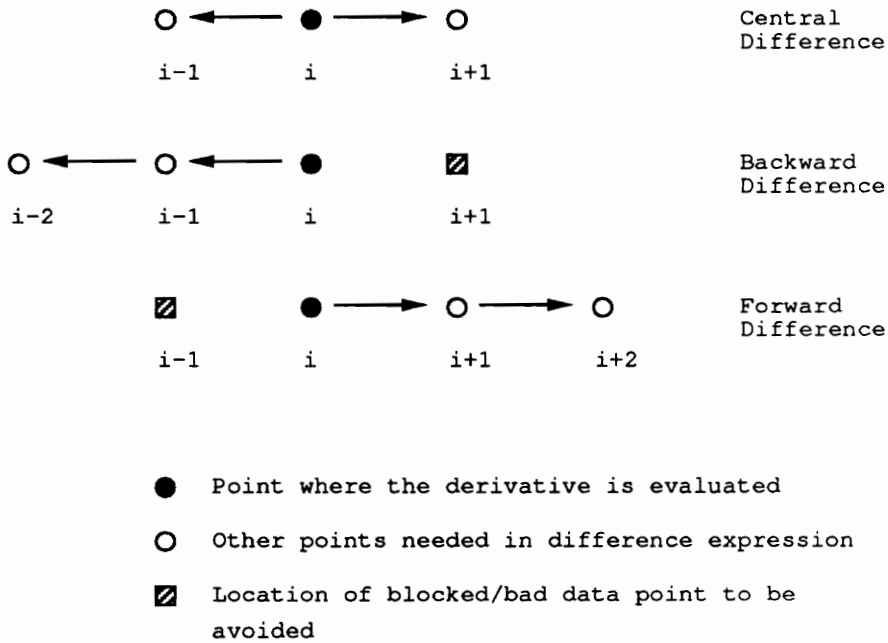
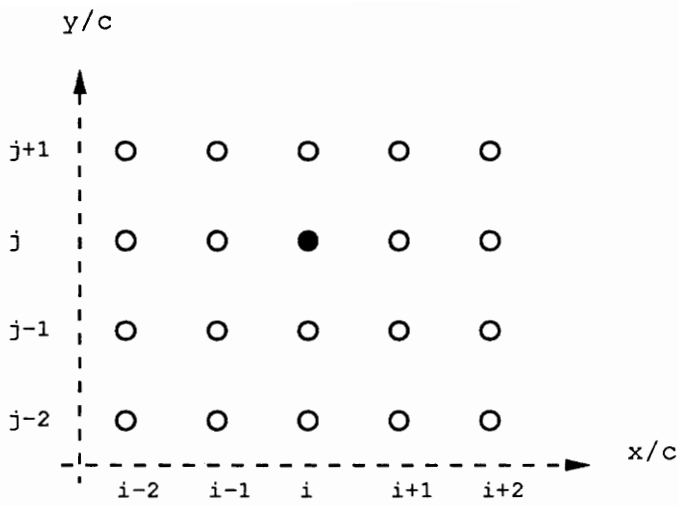
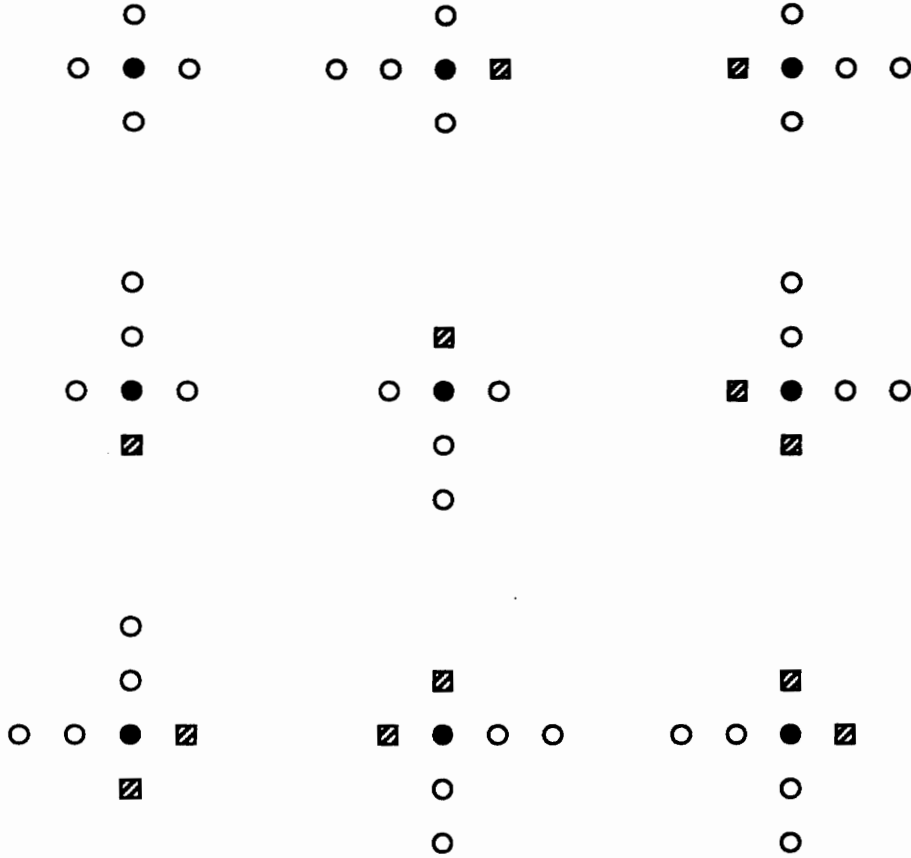


Figure 3.2.1 An arbitrary point (i, j) and its corresponding central-, backward-, and forward-difference representations in the x/c direction



- Point where the derivative is evaluated
- Other points needed in difference expression
- ▨ Location of blocked/bad data point to be avoided

Figure 3.2.2 The nine data conditions to consider when around the airfoil

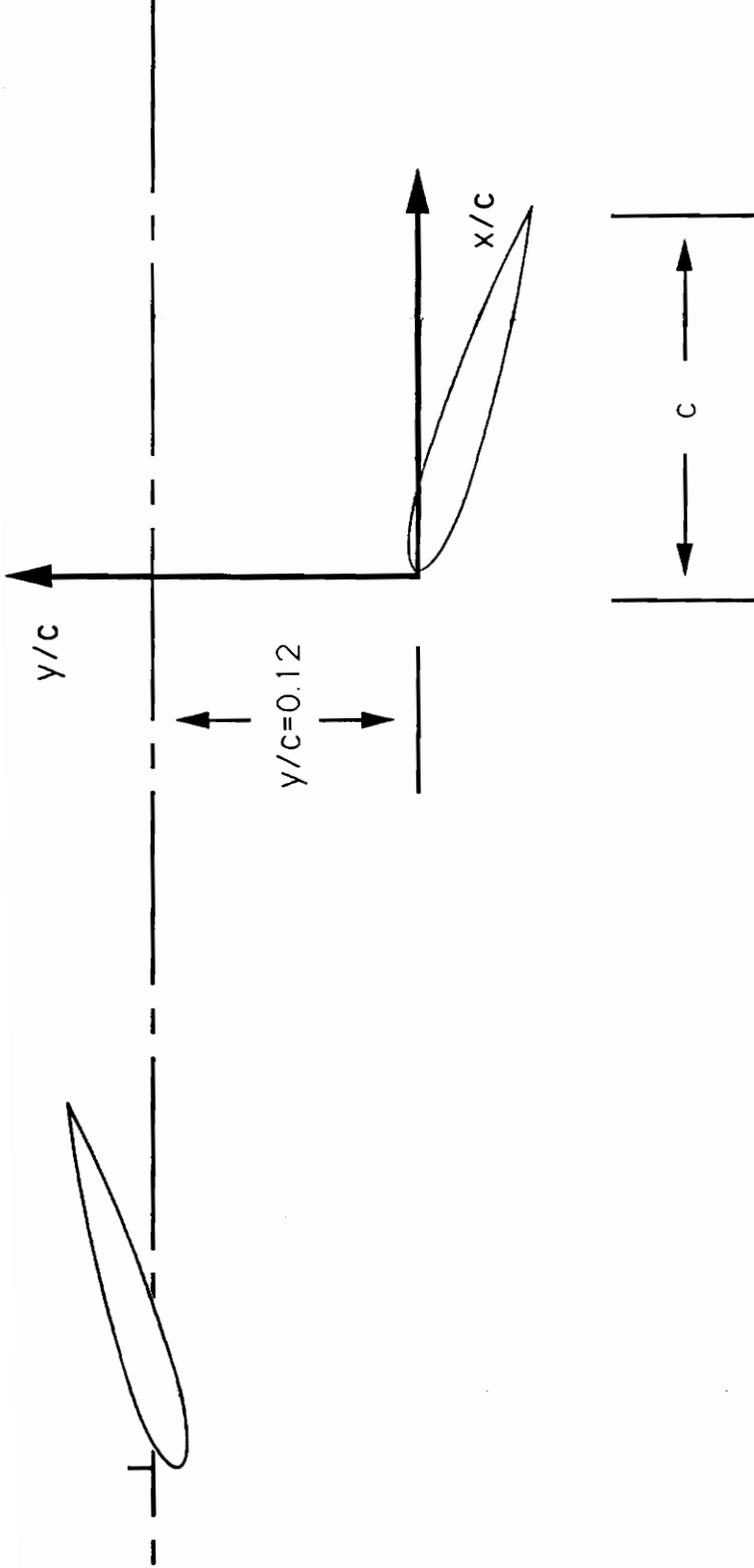


Figure 4.1.1 The pitching and target airfoils and the NACA 0015 based coordinate system

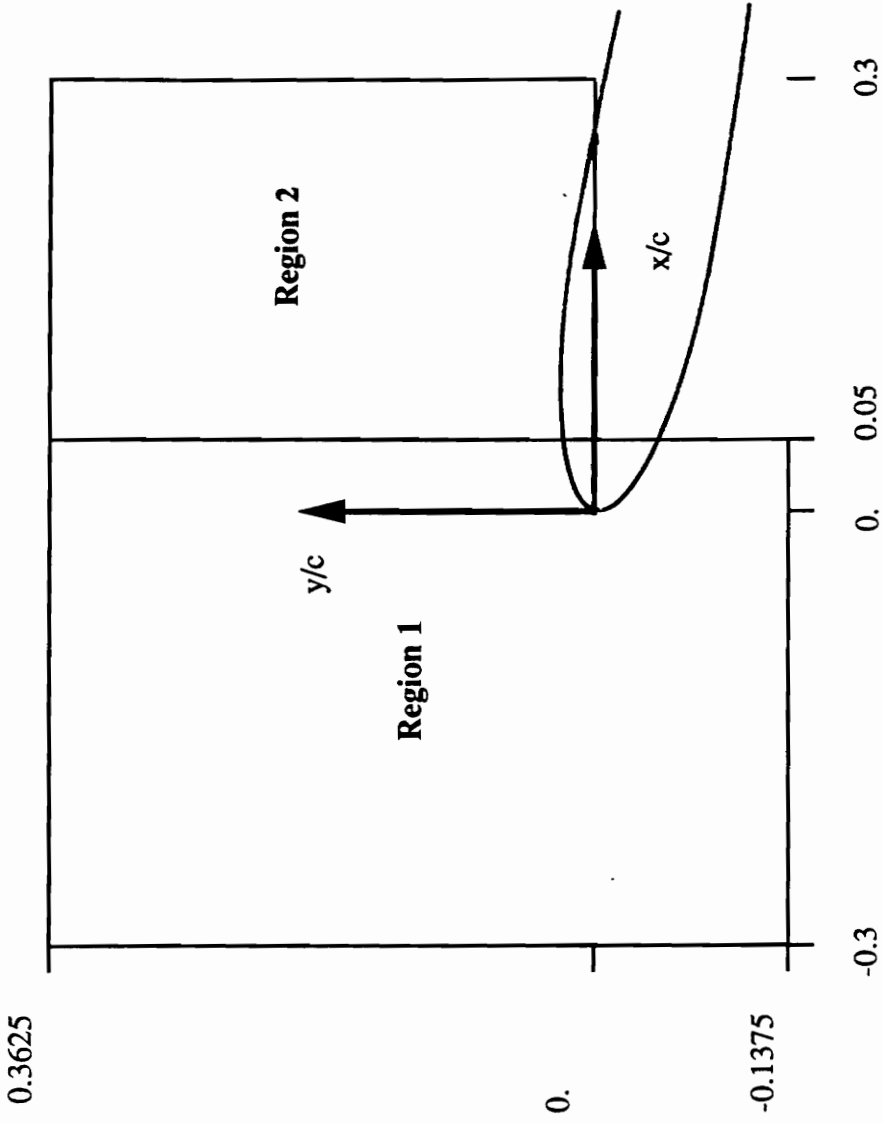


Figure 4.1.1.2 The data set was taken in two pieces, one upstream of the airfoil and the other above the airfoil

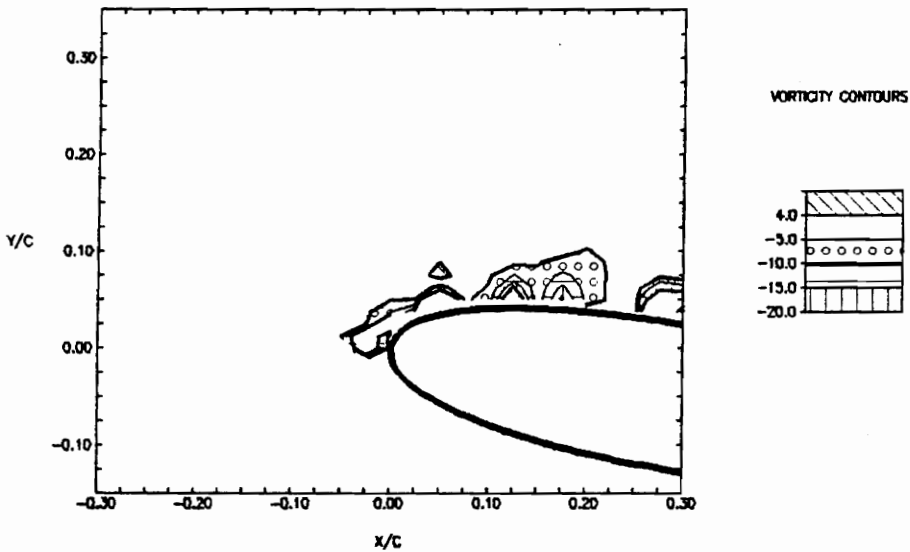
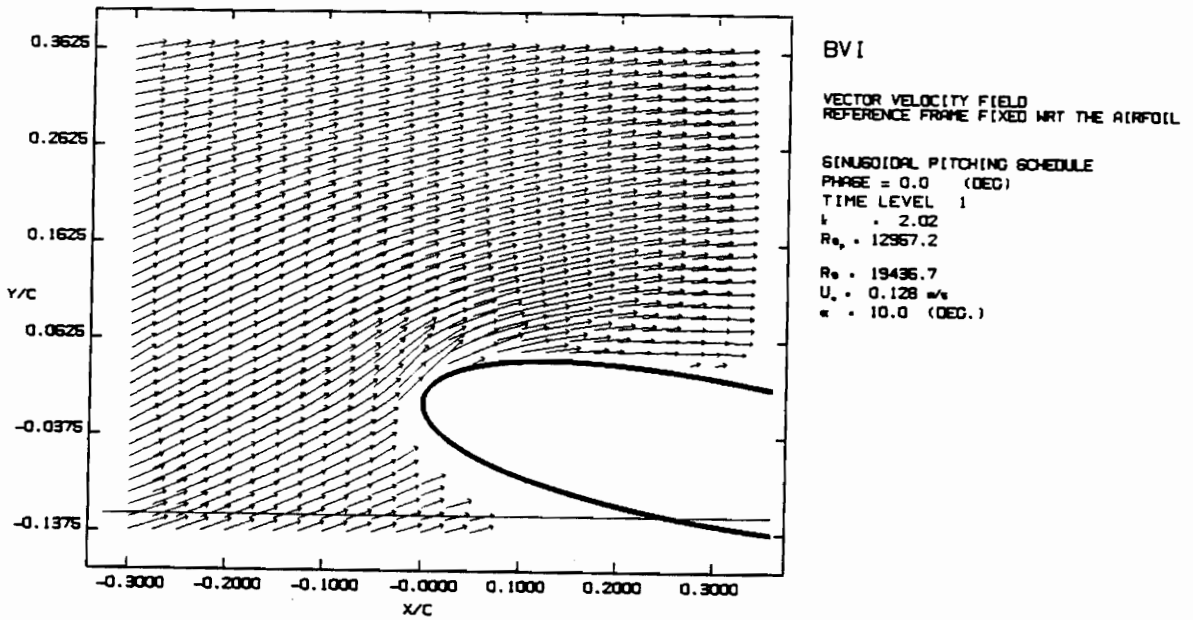
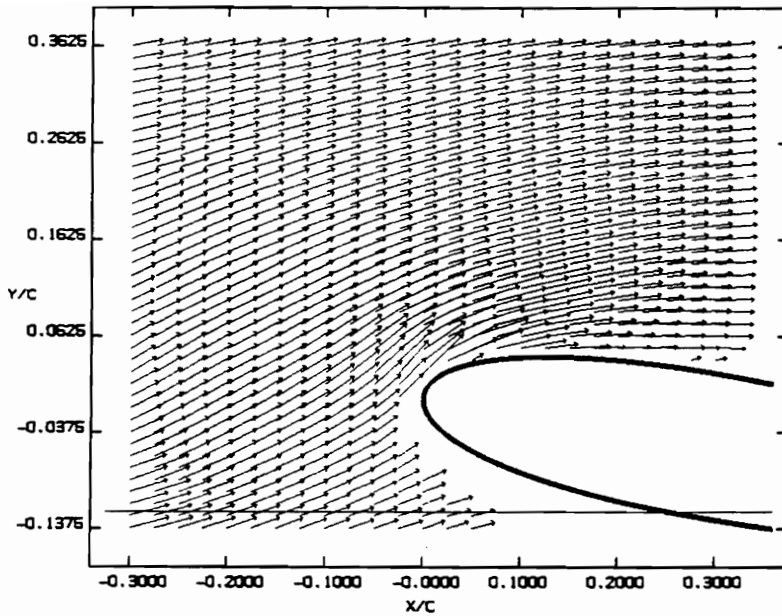


Figure 4.2.1 Velocity vectors and vorticity contours at time level 1 (1/50 of period, $\tau=1.24$ sec.)



BVI

VECTOR VELOCITY FIELD
REFERENCE FRAME FIXED WRT THE AIRFOIL

SINUSOIDAL PITCHING SCHEDULE

PHASE = 7.3 (DEG)

TIME LEVEL 2

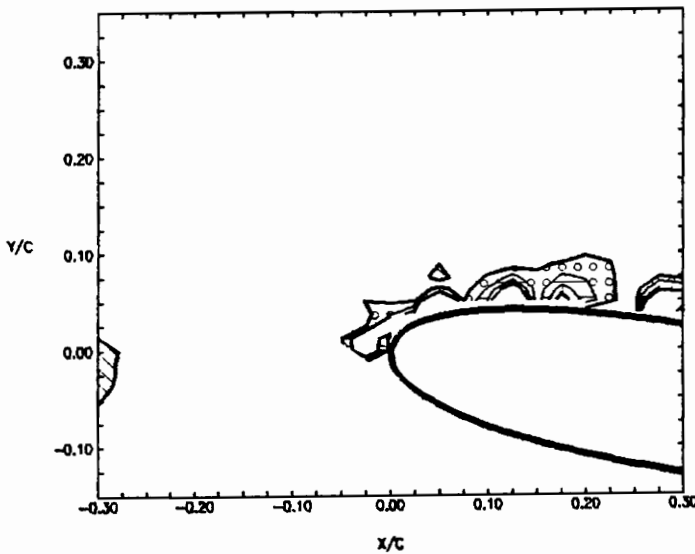
$k = 2.02$

$Re = 12957.2$

$Re = 19436.7$

$U_\infty = 0.128 \text{ m/s}$

$\alpha = 10.0 \text{ (DEG.)}$



VORTICITY CONTOURS

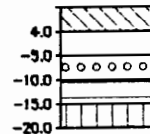
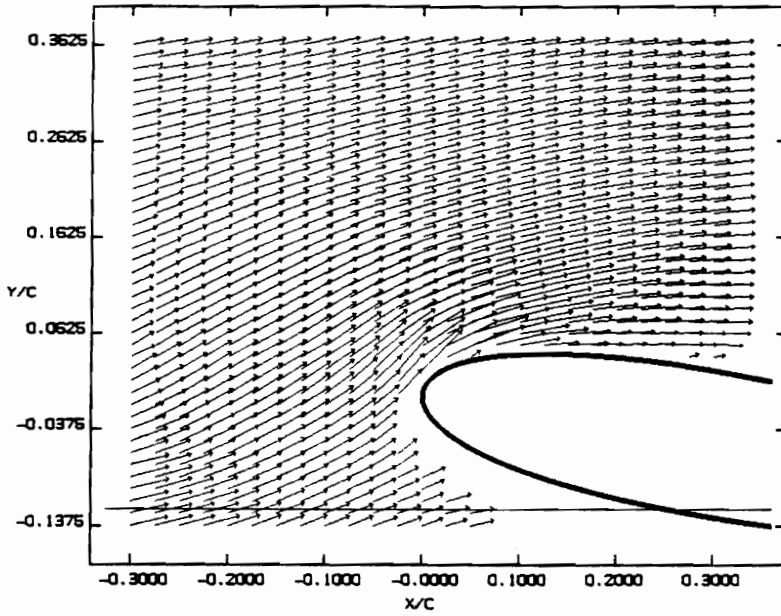


Figure 4.2.2 Velocity vectors and vorticity contours at time level 2 (2/50 of period, $\tau=1.24$ sec.)



BVI

VECTOR VELOCITY FIELD
REFERENCE FRAME FIXED WRT THE AIRFOIL

SINUSOIDAL PITCHING SCHEDULE

PHASE = 14.5 (DEG)

TIME LEVEL 3

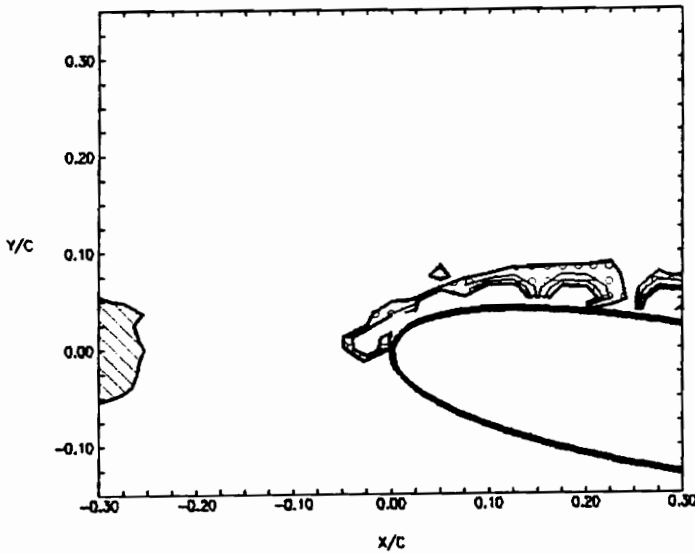
t = 2.02

Re_c = 12957.2

Re = 19435.7

U_∞ = 0.128 m/s

α = 10.0 (DEG.)



VORTICITY CONTOURS

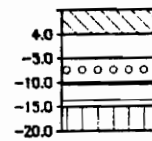
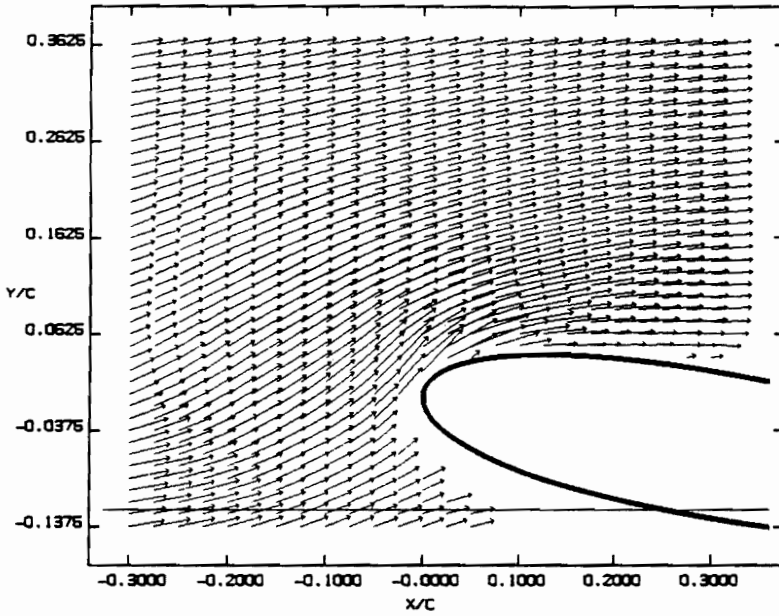


Figure 4.2.3 Velocity vectors and vorticity contours at time level 3 (3/50 of period, $\tau=1.24$ sec.)



BVI

VECTOR VELOCITY FIELD
REFERENCE FRAME FIXED WRT THE AIRFOIL

SINUSOIDAL PITCHING SCHEDULE

PHASE = 21.8 (DEG)

TIME LEVEL 4

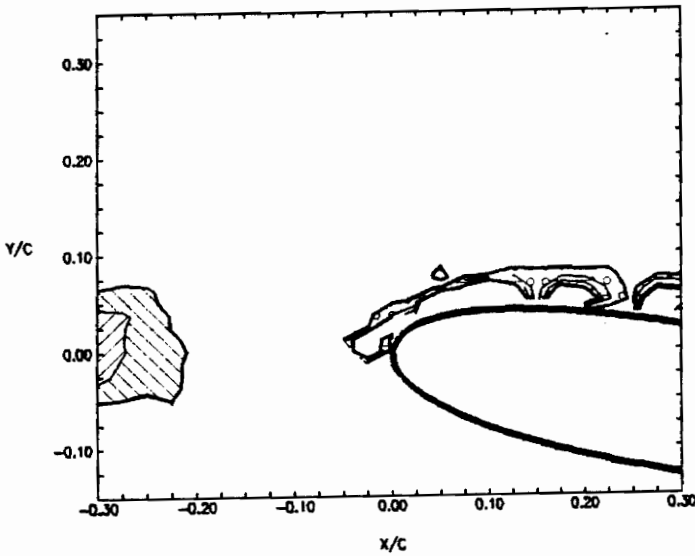
t = 2.02

Re_c = 12957.2

Re = 19435.7

U_∞ = 0.128 m/s

α = 10.0 (DEG.)



VORTICITY CONTOURS

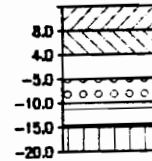
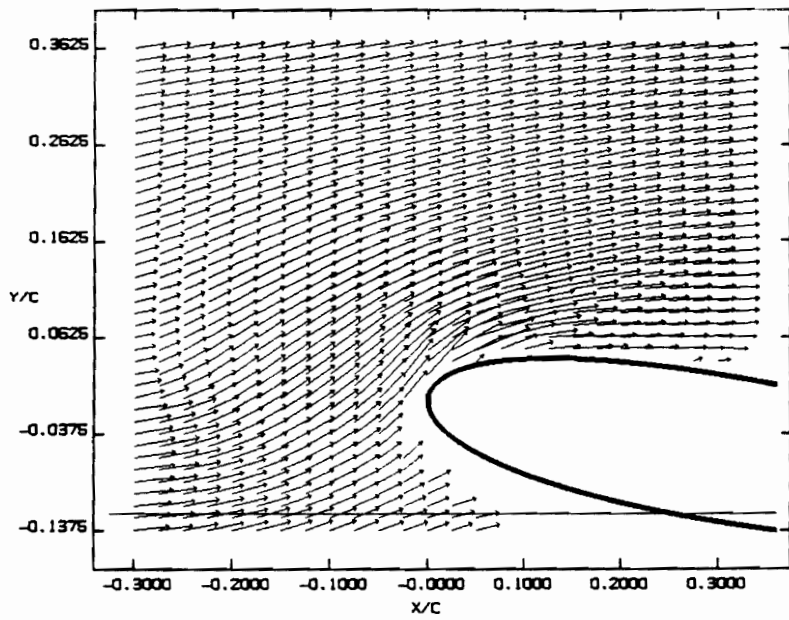


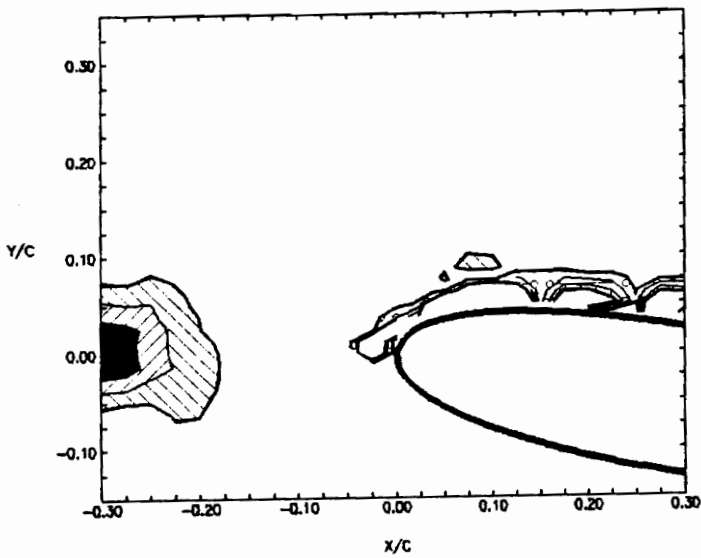
Figure 4.2.4 Velocity vectors and vorticity contours at time level 4 (4/50 of period, $\tau=1.24$ sec.)



BVI

VECTOR VELOCITY FIELD
REFERENCE FRAME FIXED WRT THE AIRFOIL

SINUSOIDAL PITCHING SCHEDULE
 PHASE = 29.0 (DEG)
 TIME LEVEL 5
 t = 2.02
 Re_c = 12957.2
 Re = 19435.7
 U_∞ = 0.128 m/s
 α = 10.0 (DEG.)



VORTICITY CONTOURS

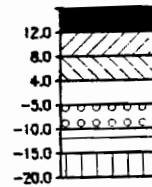
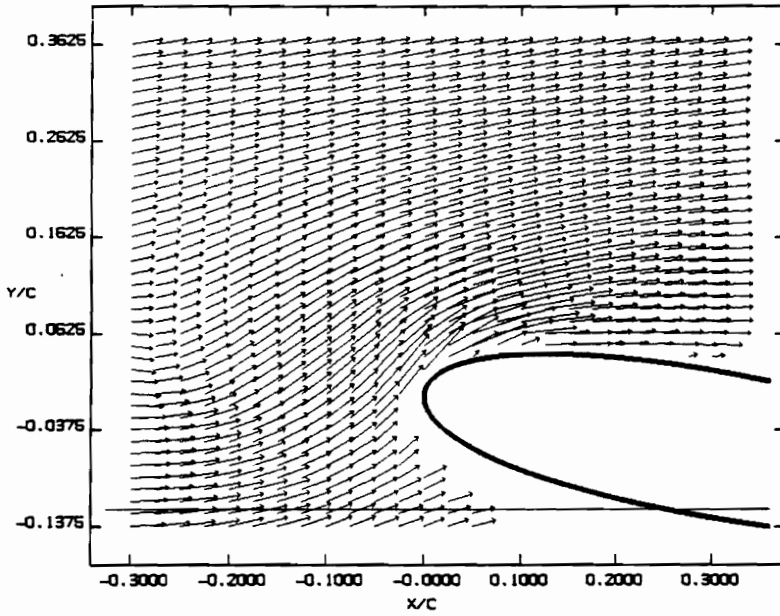


Figure 4.2.5 Velocity vectors and vorticity contours at time level 5 (5/50 of period, $\tau=1.24$ sec.)



BVI

VECTOR VELOCITY FIELD
REFERENCE FRAME FIXED WRT THE AIRFOIL

SINUSOIDAL PITCHING SCHEDULE

PHASE = 36.3 (DEG)

TIME LEVEL 6

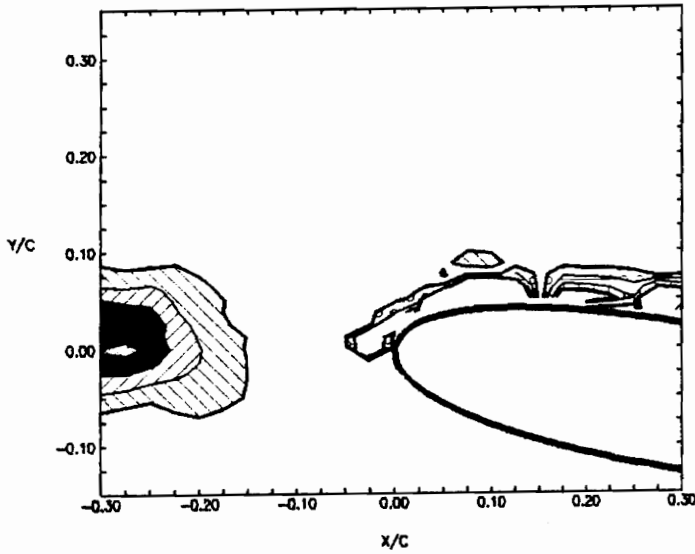
$t = 2.02$

$Re = 12967.2$

$Re = 19436.7$

$U_\infty = 0.128 \text{ m/s}$

$\alpha = 10.0 \text{ (DEG.)}$



VORTICITY CONTOURS

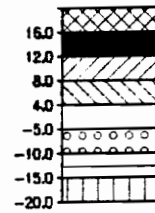
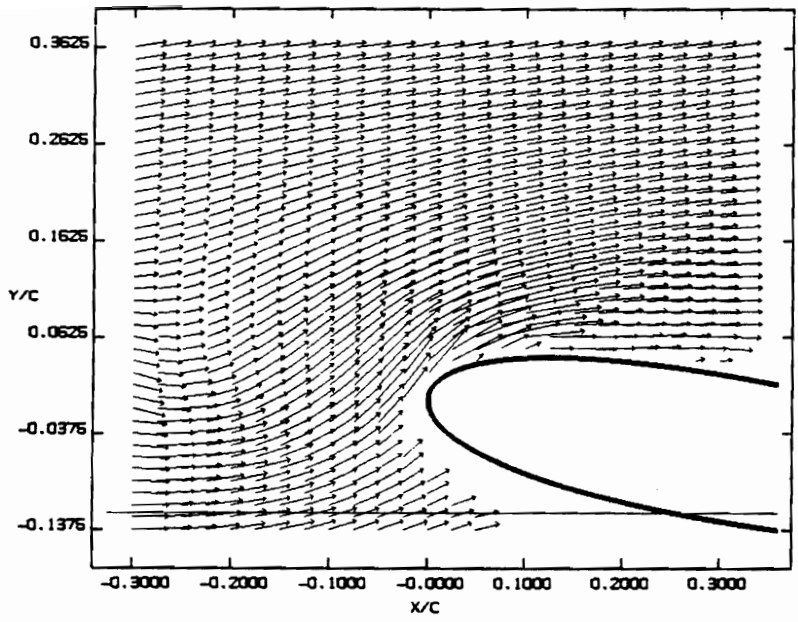


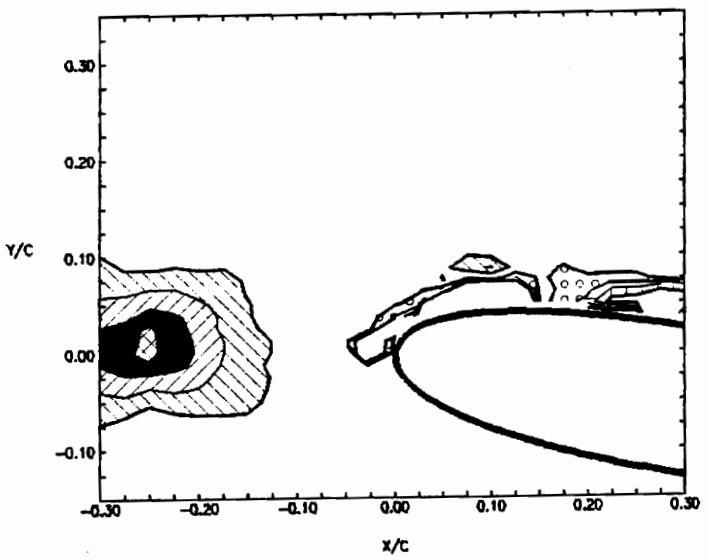
Figure 4.2.6 Velocity vectors and vorticity contours at time level 6 (6/50 of period, $\tau=1.24$ sec.)



BVI

VECTOR VELOCITY FIELD
REFERENCE FRAME FIXED WRT THE AIRFOIL

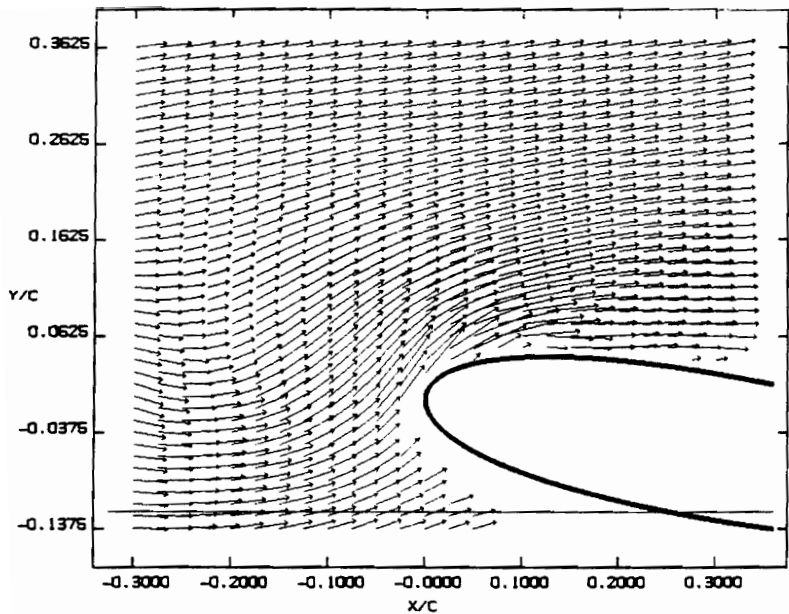
SINUSOIDAL PITCHING SCHEDULE
 PHASE = 43.6 (DEG)
 TIME LEVEL 7
 $t = 2.02$
 $Re_c = 12957.2$
 $Re = 19435.7$
 $U_\infty = 0.128$ m/s
 $\alpha = 10.0$ (DEG.)



VORTICITY CONTOURS

| | |
|-------|-----------------------|
| 16.0 | [Cross-hatch pattern] |
| 12.0 | [Diagonal lines /] |
| 8.0 | [Diagonal lines \] |
| 4.0 | [Horizontal lines] |
| -5.0 | [Vertical lines] |
| -10.0 | [Dotted pattern] |
| -15.0 | [Horizontal lines] |
| -20.0 | [Vertical lines] |

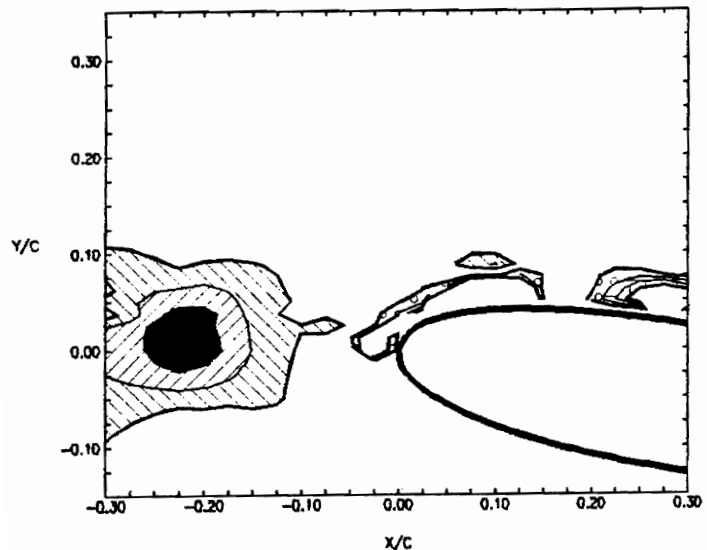
Figure 4.2.7 Velocity vectors and vorticity contours at time level 7 (7/50 of period, $\tau=1.24$ sec.)



BVI

VECTOR VELOCITY FIELD
REFERENCE FRAME FIXED WRT THE AIRFOIL

SINUSOIDAL PITCHING SCHEDULE
 PHASE = 50.8 (DEG)
 TIME LEVEL 8
 $k = 2.02$
 $Re = 12957.2$
 $Re = 19495.7$
 $U_\infty = 0.128 \text{ m/s}$
 $\alpha = 10.0 \text{ (DEG.)}$



VORTICITY CONTOURS

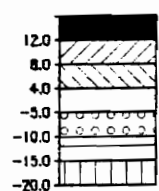
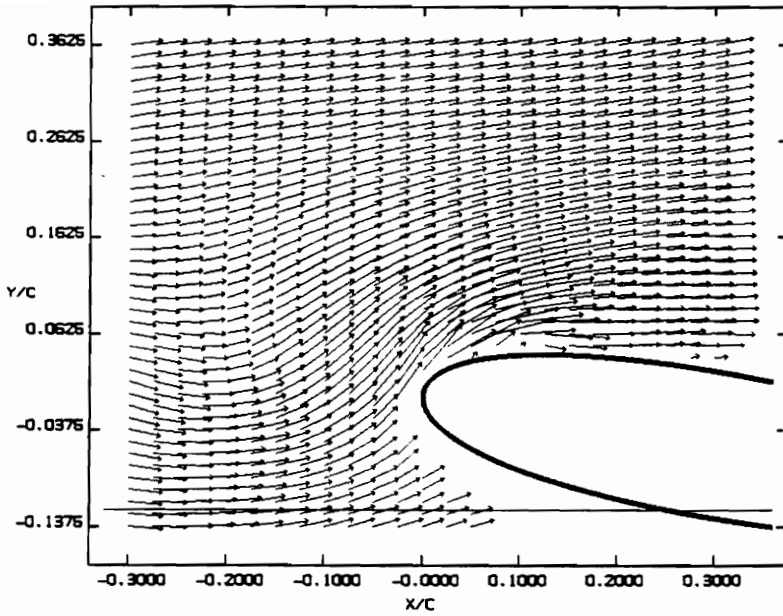


Figure 4.2.8 Velocity vectors and vorticity contours at time level 8 (8/50 of period, $\tau = 1.24 \text{ sec.}$)



BVI

VECTOR VELOCITY FIELD
REFERENCE FRAME FIXED WRT THE AIRFOIL

SINUSOIDAL PITCHING SCHEDULE

PHASE = 58.1 (DEG)

TIME LEVEL 9

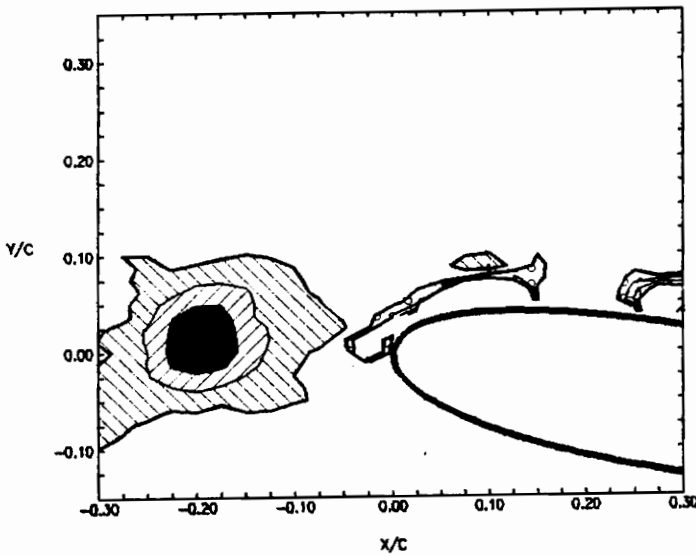
α = 2.02

Re_c = 12967.2

Re = 19436.7

U_∞ = 0.128 m/s

ω = 10.0 (DEG.)



VORTICITY CONTOURS

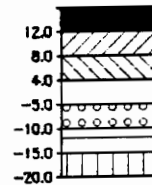
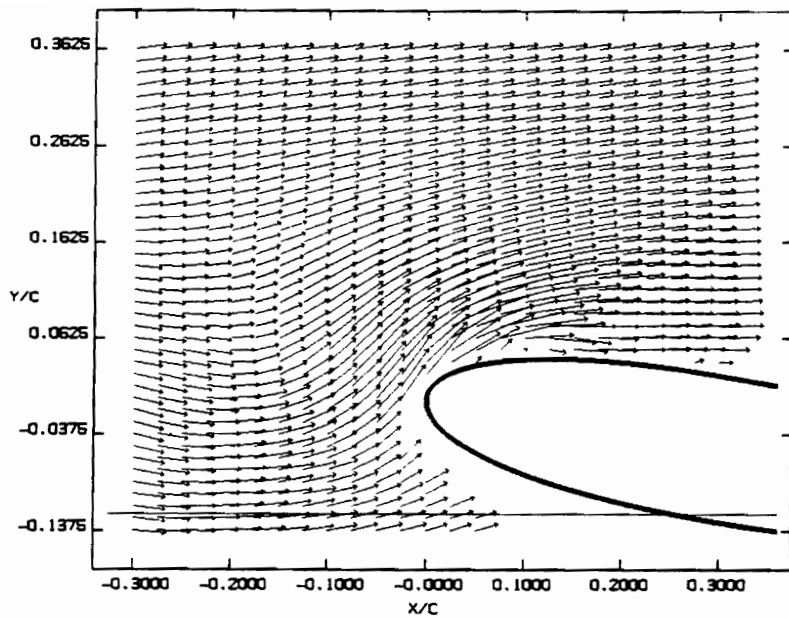


Figure 4.2.9 Velocity vectors and vorticity contours at time level 9 (9/50 of period, $\tau=1.24$ sec.)



BVI

VECTOR VELOCITY FIELD
REFERENCE FRAME FIXED WRT THE AIRFOIL

SINUSOIDAL PITCHING SCHEDULE

PHASE = 66.3 (DEG)

TIME LEVEL 10

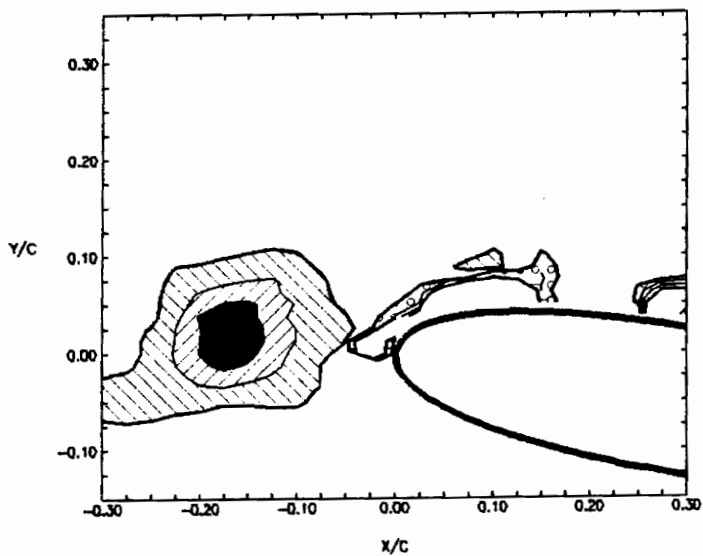
$k = 2.02$

$Re_c = 12967.2$

$Re = 19436.7$

$U_\infty = 0.128 \text{ m/s}$

$\alpha = 10.0 \text{ (DEG.)}$



VORTICITY CONTOURS

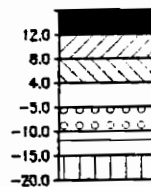
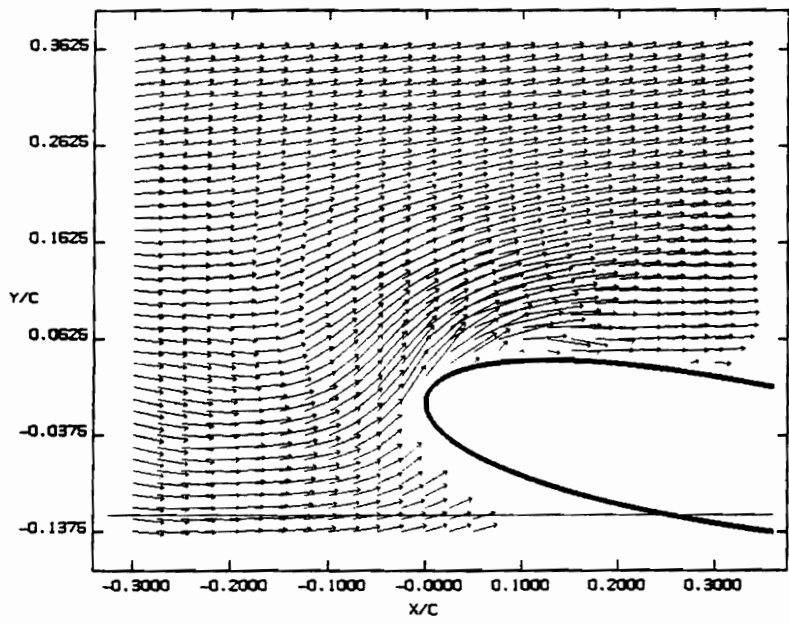


Figure 4.2.10 Velocity vectors and vorticity contours at time level 10 (10/50 of period, $\tau = 1.24 \text{ sec.}$)

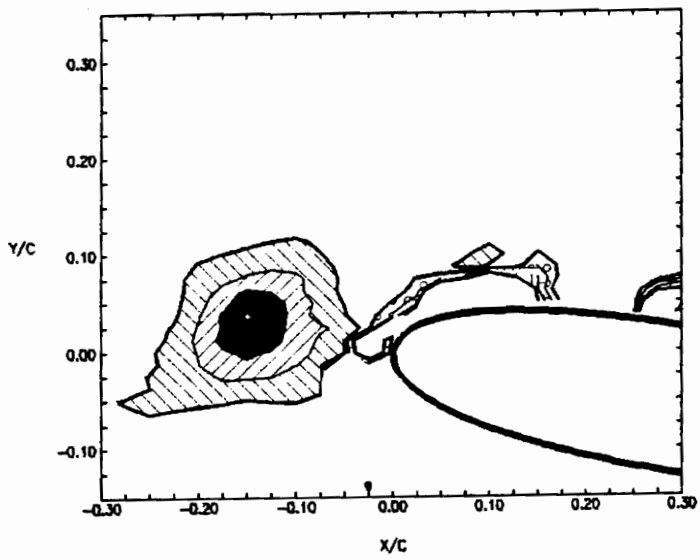


BVI

VECTOR VELOCITY FIELD
REFERENCE FRAME FIXED WRT THE AIRFOIL

SINUSOIDAL PITCHING SCHEDULE
PHASE = 72.6 (DEG)
TIME LEVEL 11
 $t = 2.02$
 $Re = 12957.2$

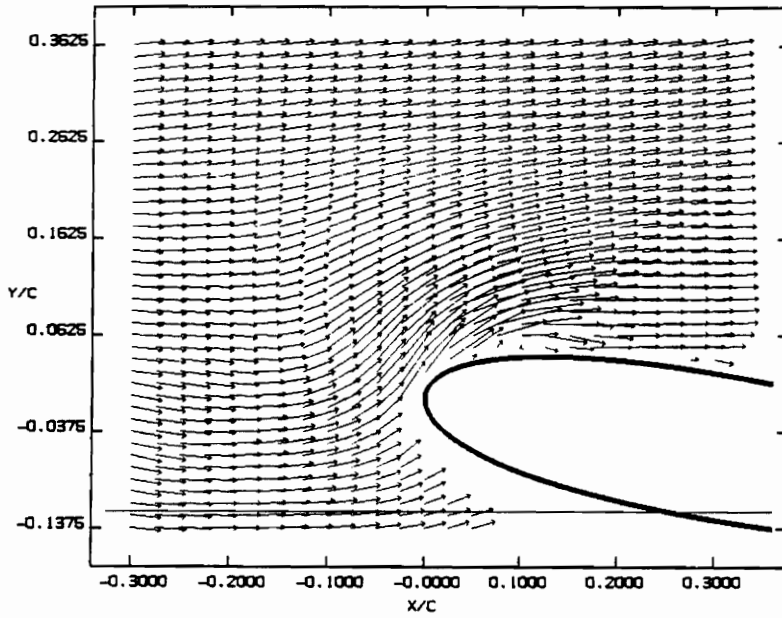
$Re = 19435.7$
 $U_\infty = 0.128 \text{ m/s}$
 $\alpha = 10.0 \text{ (DEG.)}$



VORTICITY CONTOURS

| | |
|-------|-----------------------|
| 16.0 | [Cross-hatch pattern] |
| 12.0 | [Solid black] |
| 8.0 | [Diagonal lines /] |
| 4.0 | [Diagonal lines \] |
| 0.0 | [White] |
| -4.0 | [Dotted pattern] |
| -8.0 | [Horizontal lines] |
| -12.0 | [Vertical lines] |
| -16.0 | [Diagonal lines /] |
| -20.0 | [Diagonal lines \] |

Figure 4.2.11 Velocity vectors and vorticity contours at time level 11 (11/50 of period, $\tau = 1.24$ sec.)



BVI

VECTOR VELOCITY FIELD
REFERENCE FRAME FIXED WRT THE AIRFOIL

SINUSOIDAL PITCHING SCHEDULE

PHASE = 79.8 (DEG)

TIME LEVEL 12

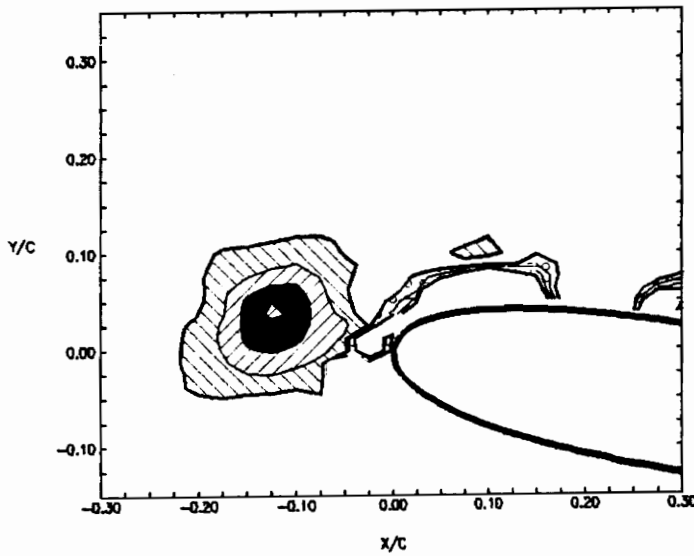
$h = 2.02$

$Re = 12967.2$

$Re = 19436.7$

$U_\infty = 0.128 \text{ m/s}$

$\alpha = 10.0 \text{ (DEG.)}$



VORTICITY CONTOURS

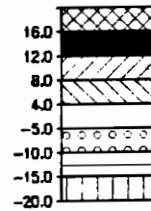
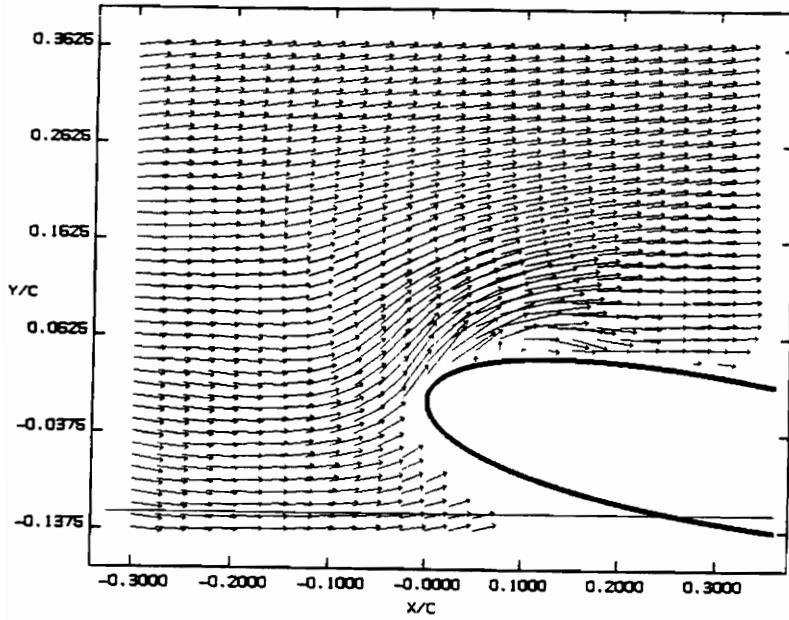


Figure 4.2.12 Velocity vectors and vorticity contours at time level 12 (12/50 of period, $\tau=1.24$ sec.)



BVI

VECTOR VELOCITY FIELD
REFERENCE FRAME FIXED WRT THE AIRFOIL

SINUSOIDAL PITCHING SCHEDULE

PHASE = 87.1 (DEG)

TIME LEVEL 13

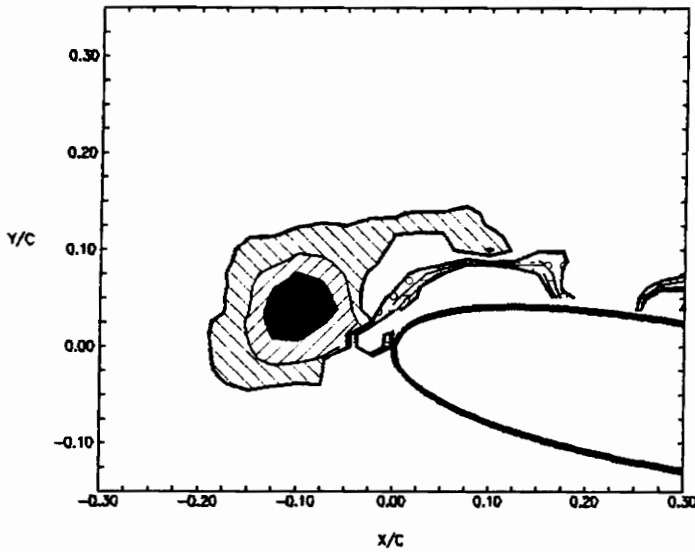
$k = 2.02$

$Re_\infty = 12957.2$

$Re = 19435.7$

$U_\infty = 0.128$ m/s

$\alpha = 10.0$ (DEG.)



VORTICITY CONTOURS

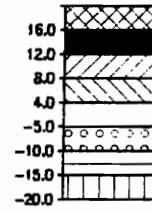
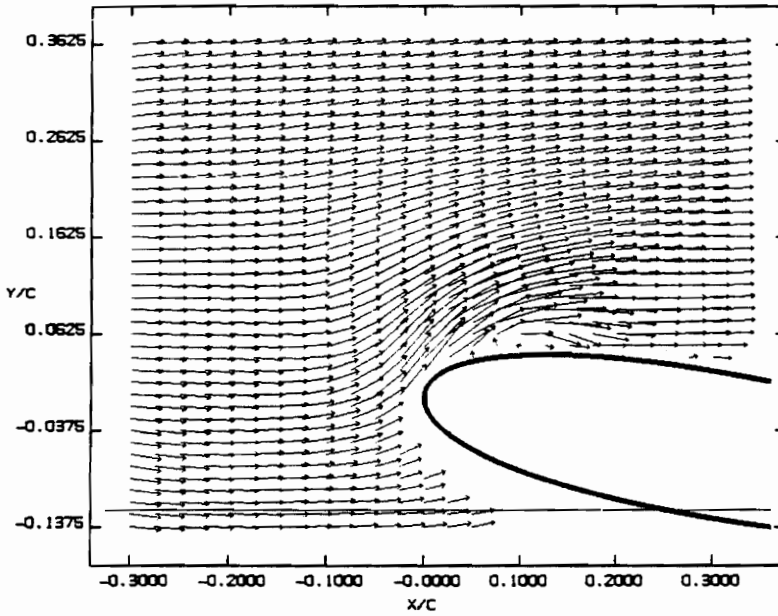


Figure 4.2.13 Velocity vectors and vorticity contours at time level 13 (13/50 of period, $\tau=1.24$ sec.)



BVI

VECTOR VELOCITY FIELD
REFERENCE FRAME FIXED WRT THE AIRFOIL

SINUSOIDAL PITCHING SCHEDULE

PHASE = 94.4 (DEG)

TIME LEVEL 14

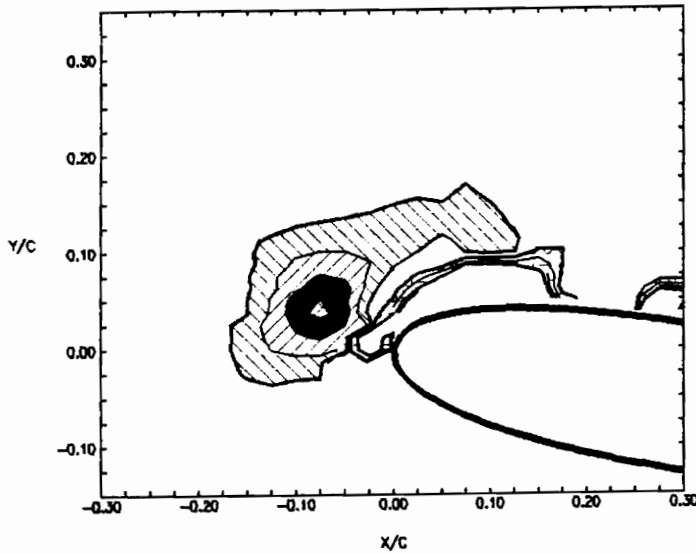
$t = 2.02$

$Re = 12967.2$

$Re = 19435.7$

$U_\infty = 0.128 \text{ m/s}$

$\alpha = 10.0 \text{ (DEG.)}$



VORTICITY CONTOURS

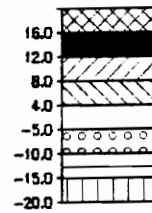
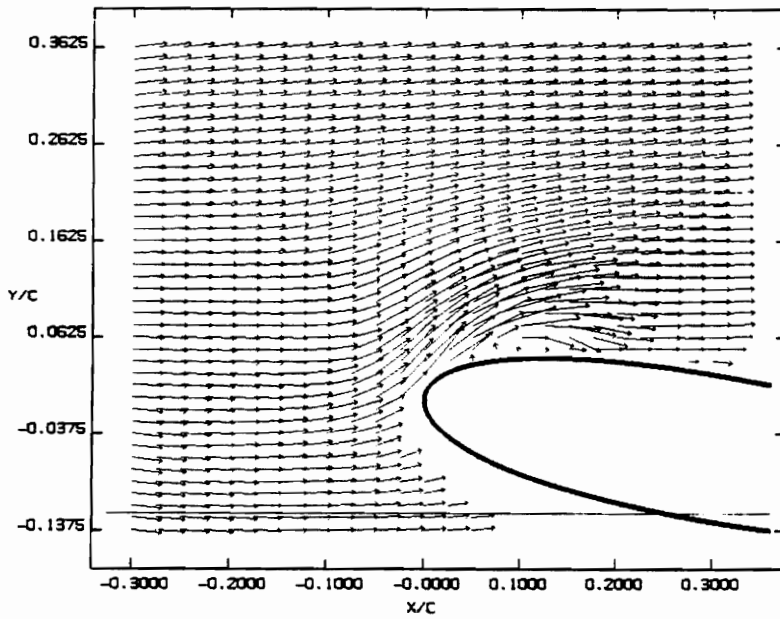


Figure 4.2.14 Velocity vectors and vorticity contours at time level 14 (14/50 of period, $\tau=1.24 \text{ sec.}$)

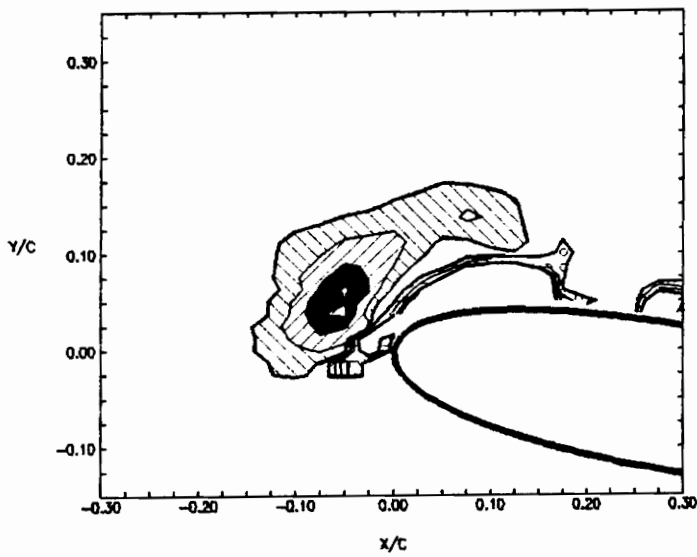


BVI

VECTOR VELOCITY FIELD
REFERENCE FRAME FIXED WRT THE AIRFOIL

SINUSOIDAL PITCHING SCHEDULE
PHASE = 101.6 (DEG)
TIME LEVEL 15
 $t = 2.02$
 $Re_c = 12957.2$

$Re = 19435.7$
 $U_\infty = 0.128 \text{ m/s}$
 $\alpha = 10.0 \text{ (DEG.)}$



VORTICITY CONTOURS

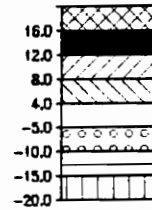
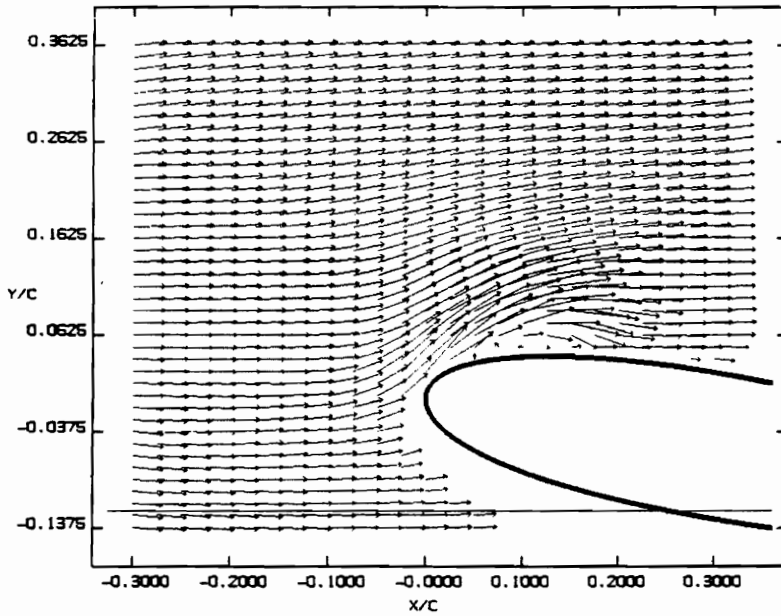


Figure 4.2.15 Velocity vectors and vorticity contours at time level 15 (15/50 of period, $\tau = 1.24 \text{ sec.}$)



BVI

VECTOR VELOCITY FIELD
REFERENCE FRAME FIXED WRT THE AIRFOIL

SINUSOIDAL PITCHING SCHEDULE

PHASE = 108.9 (DEG)

TIME LEVEL 16

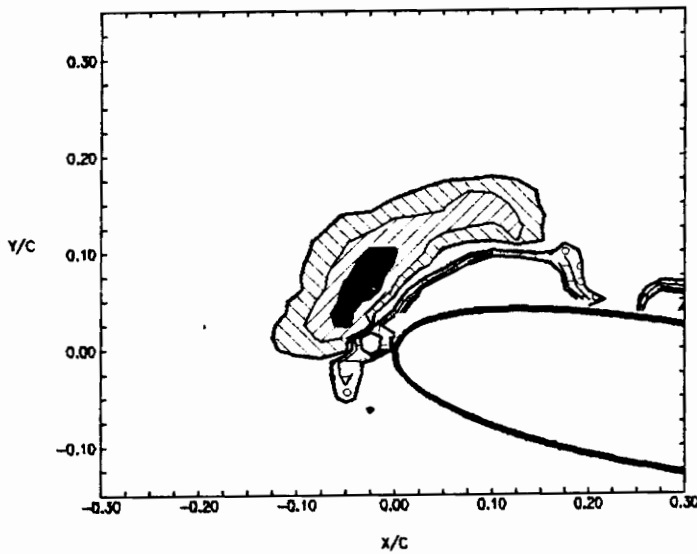
$t = 2.02$

$Re = 12957.2$

$Re = 19435.7$

$U_\infty = 0.128$ m/s

$\alpha = 10.0$ (DEG.)



VORTICITY CONTOURS

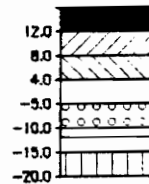
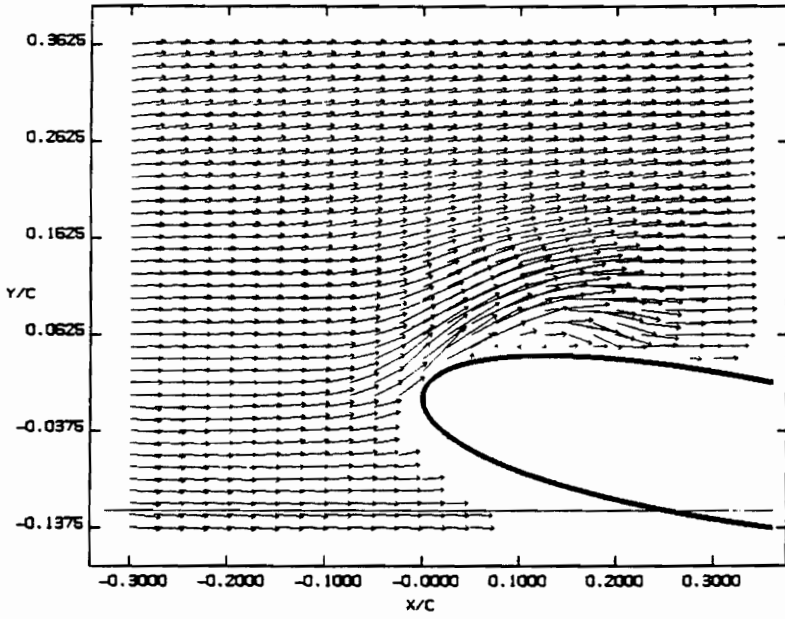


Figure 4.2.16 Velocity vectors and vorticity contours at time level 16 (16/50 of period, $\tau=1.24$ sec.)



BVI

VECTOR VELOCITY FIELD
REFERENCE FRAME FIXED WRT THE AIRFOIL

SINUSOIDAL PITCHING SCHEDULE

PHASE = 116.1 (DEG)

TIME LEVEL 17

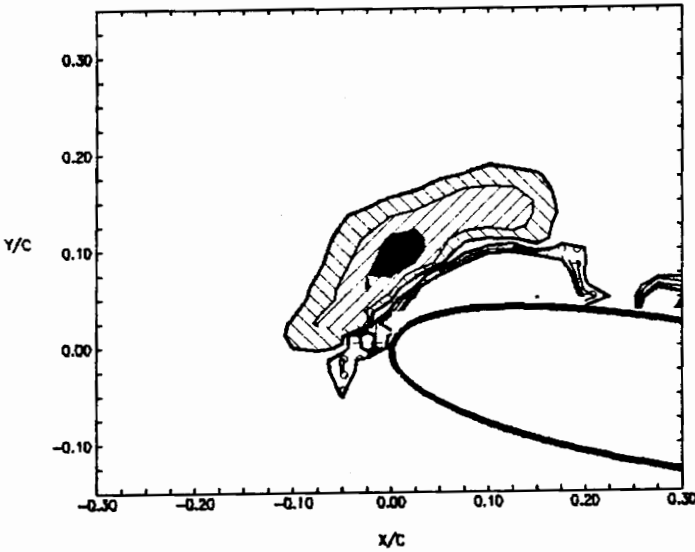
k = 2.02

Re = 12957.2

Re = 19436.7

U_∞ = 0.128 m/s

α = 10.0 (DEG.)



VORTICITY CONTOURS

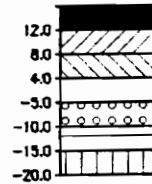
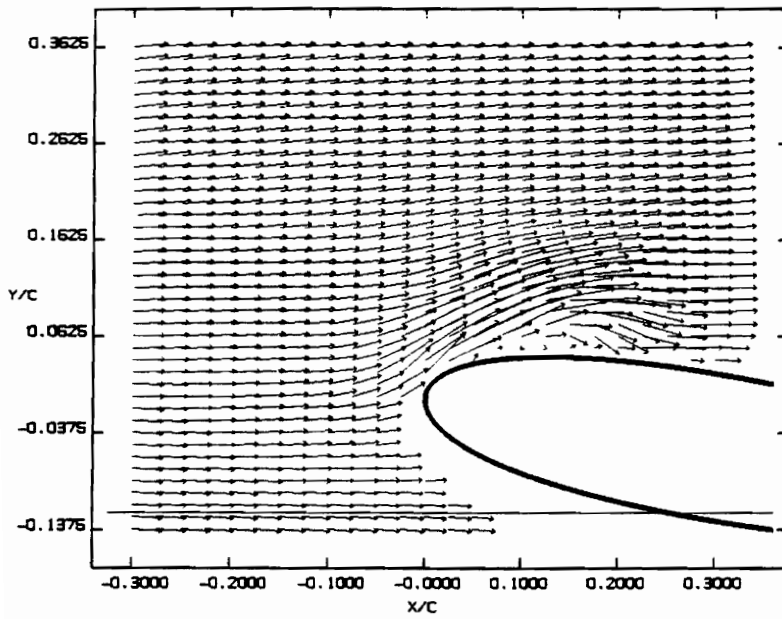


Figure 4.2.17 Velocity vectors and vorticity contours at time level 17 (17/50 of period, $\tau = 1.24$ sec.)



BVI

VECTOR VELOCITY FIELD
REFERENCE FRAME FIXED WRT THE AIRFOIL

SINUSOIDAL PITCHING SCHEDULE

PHASE = 123.4 (DEG)

TIME LEVEL 18

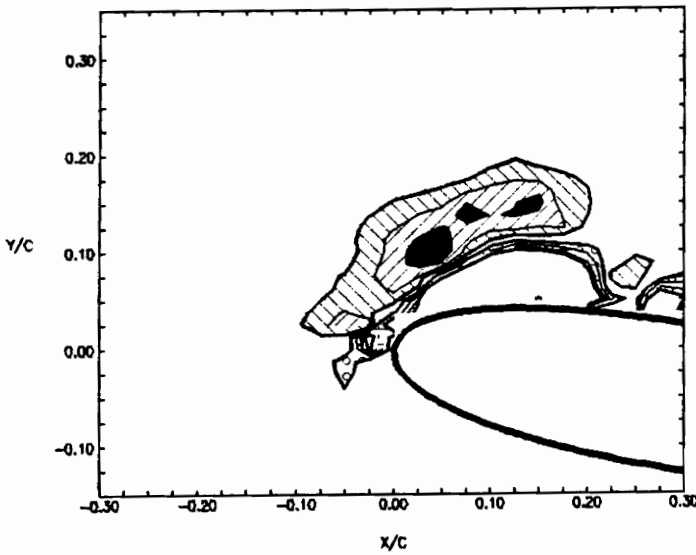
t = 2.02

Re_c = 12957.2

Re = 19435.7

U_∞ = 0.128 m/s

α = 10.0 (DEG.)



VORTICITY CONTOURS

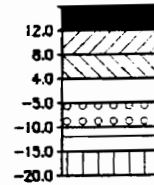
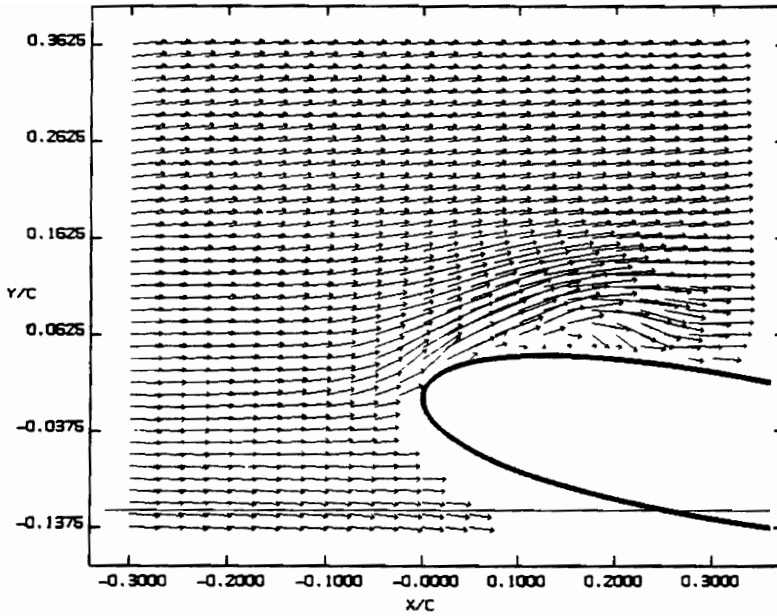


Figure 4.2.18 Velocity vectors and vorticity contours at time level 18 (18/50 of period, $\tau=1.24$ sec.)



BVI

VECTOR VELOCITY FIELD
REFERENCE FRAME FIXED WRT THE AIRFOIL

SINUSOIDAL PITCHING SCHEDULE

PHASE = 130.7 (DEG)

TIME LEVEL 19

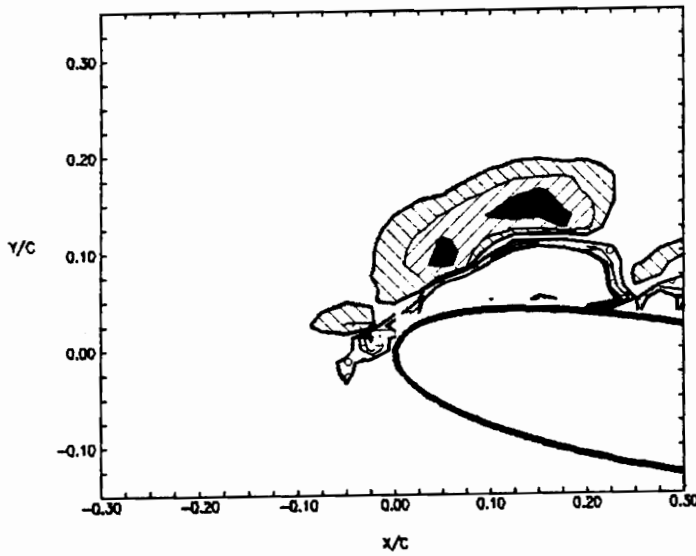
$t = 2.02$

$Re_c = 12957.2$

$Re = 19435.7$

$U_\infty = 0.128 \text{ m/s}$

$\alpha = 10.0 \text{ (DEG.)}$



VORTICITY CONTOURS

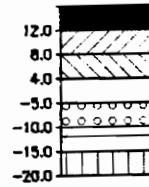
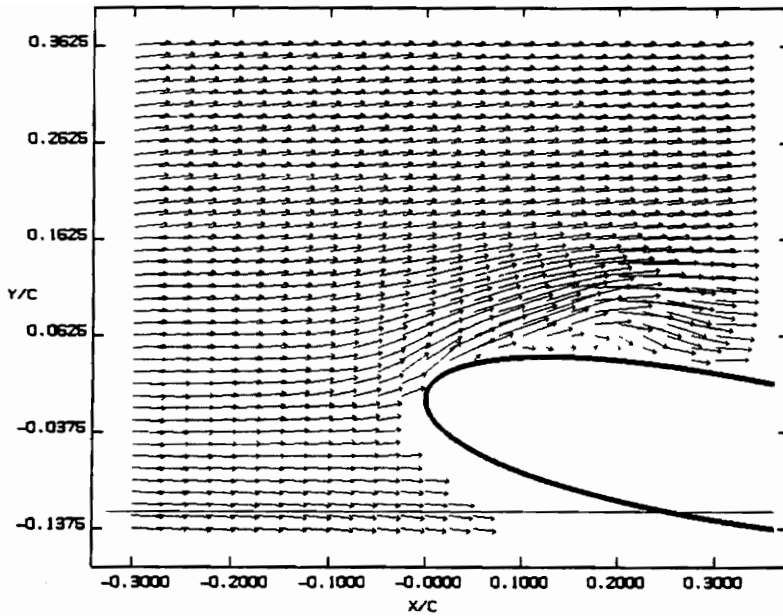


Figure 4.2.19 Velocity vectors and vorticity contours at time level 19 (19/50 of period, $\tau = 1.24 \text{ sec.}$)

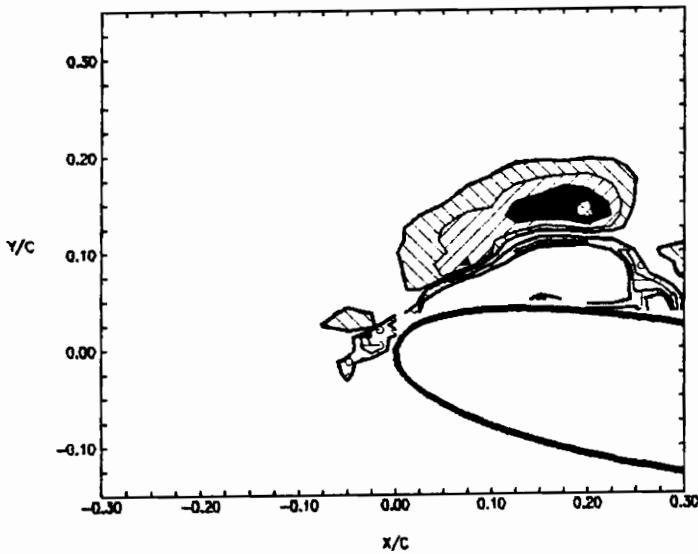


BVI

VECTOR VELOCITY FIELD
REFERENCE FRAME FIXED WRT THE AIRFOIL

SINUSOIDAL PITCHING SCHEDULE
PHASE = 137.9 (DEG)
TIME LEVEL 20
 $t = 2.02$
 $Re = 12957.2$

$Re = 19436.7$
 $U_{\infty} = 0.128 \text{ m/s}$
 $\alpha = 10.0 \text{ (DEG.)}$



VORTICITY CONTOURS

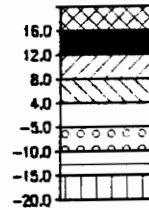
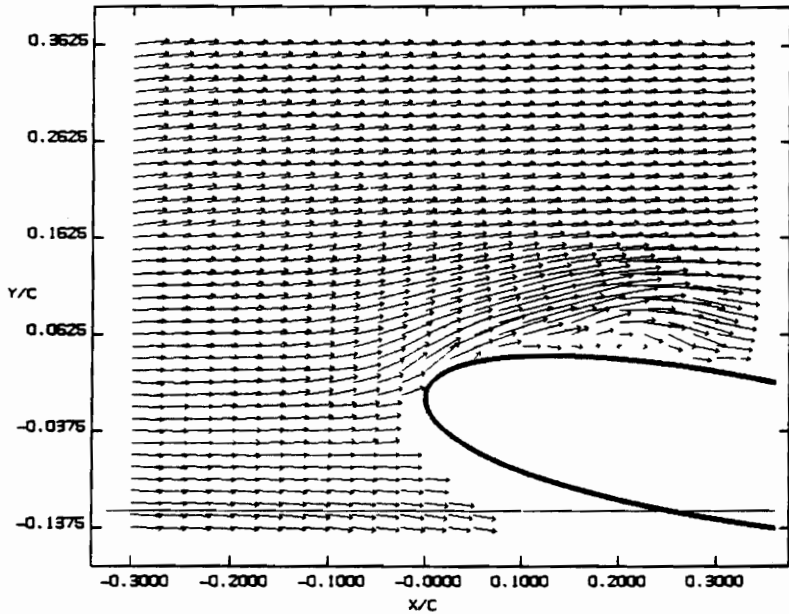


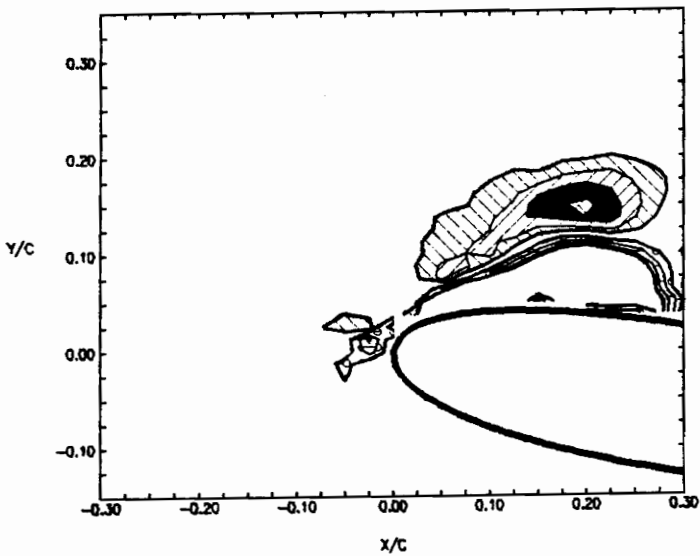
Figure 4.2.20 Velocity vectors and vorticity contours at time level 20 (20/50 of period, $\tau=1.24$ sec.)



BVI

VECTOR VELOCITY FIELD
REFERENCE FRAME FIXED WRT THE AIRFOIL

SINUSOIDAL PITCHING SCHEDULE
 PHASE = 145.2 (DEG)
 TIME LEVEL 21
 $t = 2.02$
 $Re = 12957.2$
 $Re = 19435.7$
 $U_\infty = 0.128 \text{ m/s}$
 $\alpha = 10.0 \text{ (DEG.)}$



VORTICITY CONTOURS

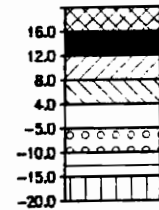
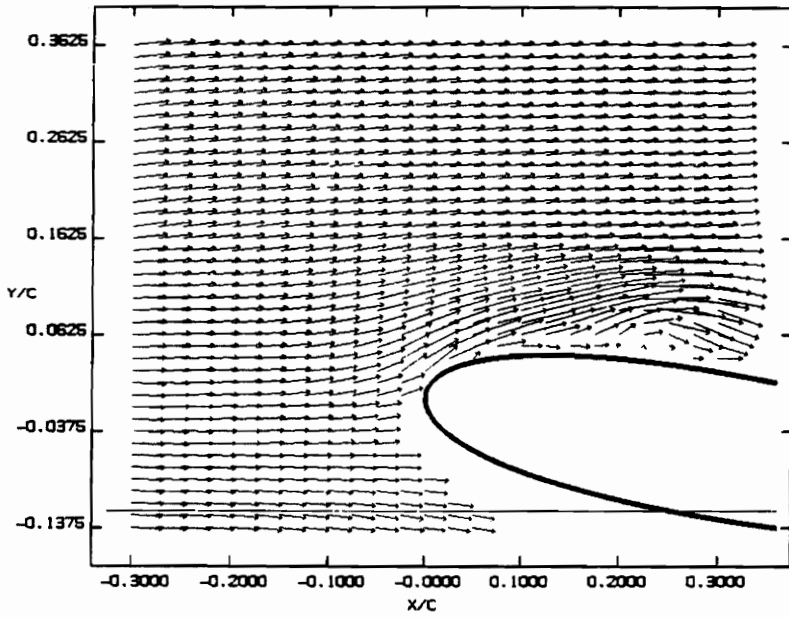


Figure 4.2.21 Velocity vectors and vorticity contours at time level 21 (21/50 of period, $\tau = 1.24 \text{ sec.}$)



BVI

VECTOR VELOCITY FIELD
REFERENCE FRAME FIXED WRT THE AIRFOIL

SINUSOIDAL PITCHING SCHEDULE

PHASE = 162.4 (DEG)

TIME LEVEL 22

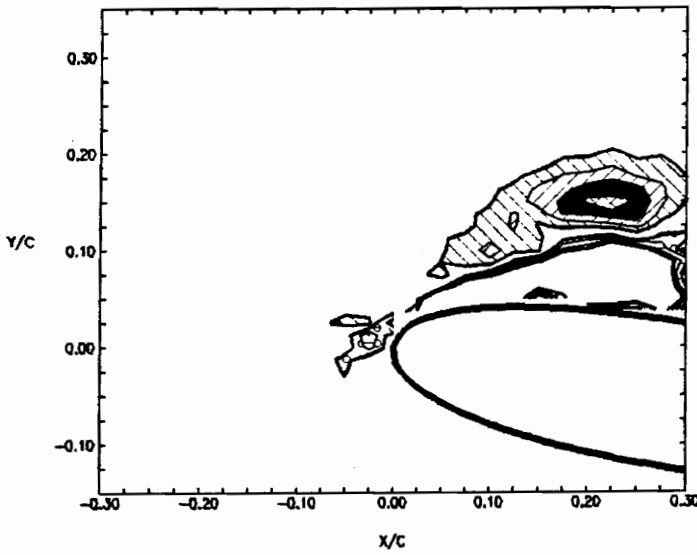
$t = 2.02$

$Re_c = 12967.2$

$Re = 19436.7$

$U_\infty = 0.128 \text{ m/s}$

$\alpha = 10.0 \text{ (DEG.)}$



VORTICITY CONTOURS

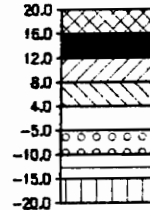
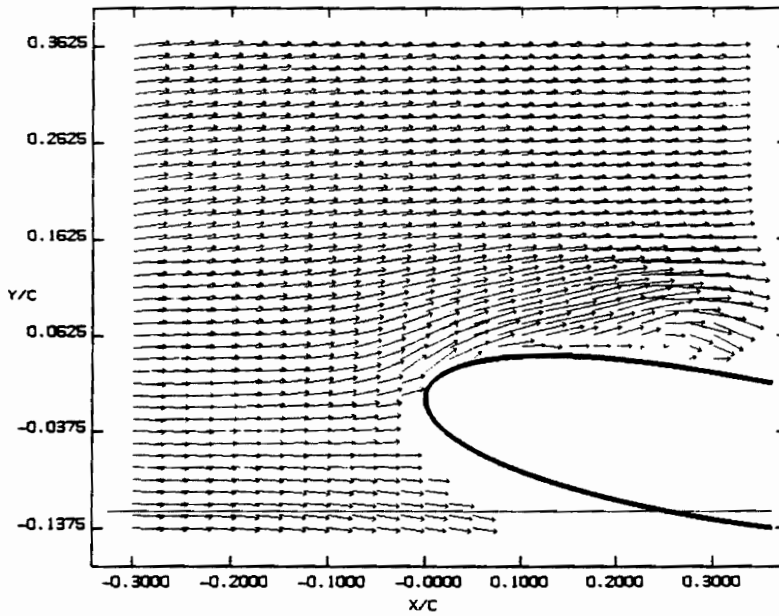


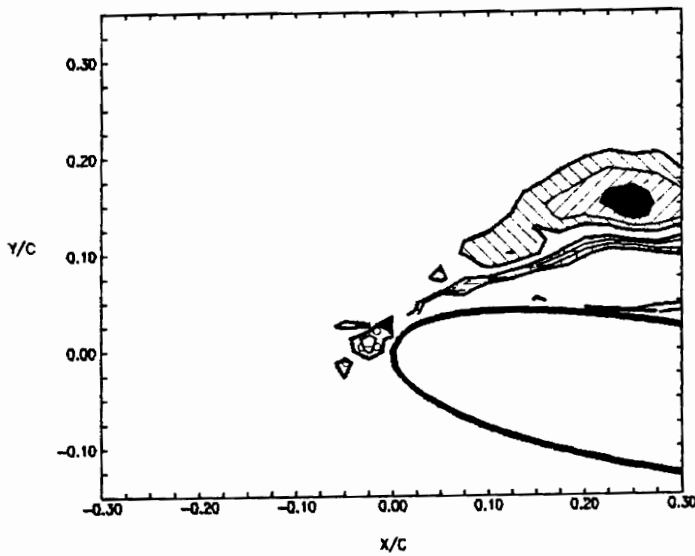
Figure 4.2.22 Velocity vectors and vorticity contours at time level 22 (22/50 of period, $\tau=1.24$ sec.)



BVI
 VECTOR VELOCITY FIELD
 REFERENCE FRAME FIXED WRT THE AIRFOIL

SINUSOIDAL PITCHING SCHEDULE
 PHASE = 159.7 (DEG)
 TIME LEVEL 23
 $t = 2.02$
 $Re = 12957.2$

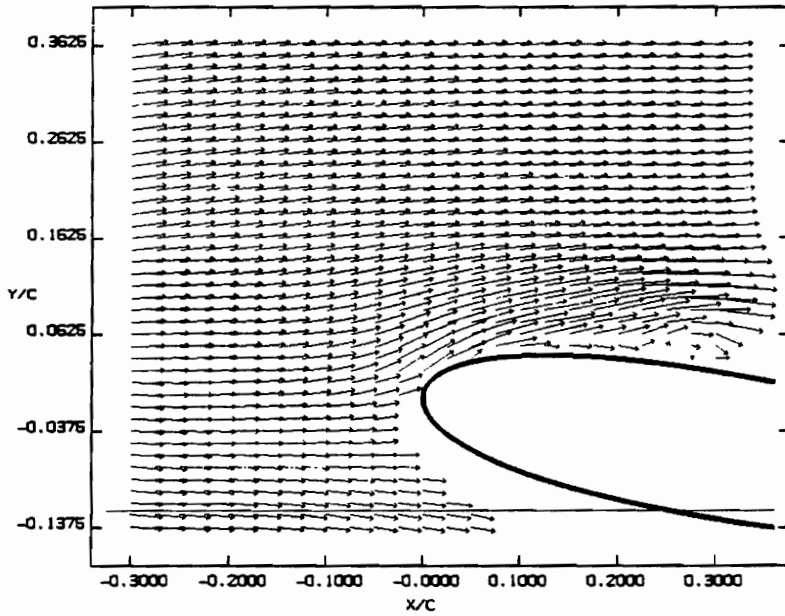
$Re = 19436.7$
 $U_\infty = 0.128 \text{ m/s}$
 $\alpha = 10.0 \text{ (DEG.)}$



VORTICITY CONTOURS

| |
|-------|
| 12.0 |
| 8.0 |
| 4.0 |
| -5.0 |
| -10.0 |
| -15.0 |
| -20.0 |

Figure 4.2.23 Velocity vectors and vorticity contours at time level 23 (23/50 of period, $\tau=1.24$ sec.)



BVI

VECTOR VELOCITY FIELD
REFERENCE FRAME FIXED WRT THE AIRFOIL

SINUSOIDAL PITCHING SCHEDULE

PHASE = 166.9 (DEG)

TIME LEVEL 24

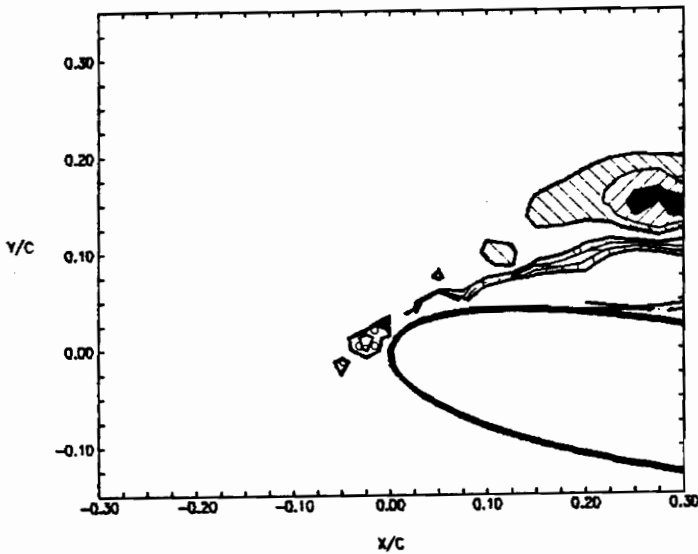
h = 2.02

Re = 12967.2

Re = 19436.7

U_∞ = 0.128 m/s

α = 10.0 (DEG.)



VORTICITY CONTOURS

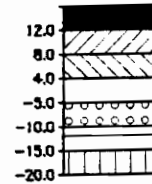
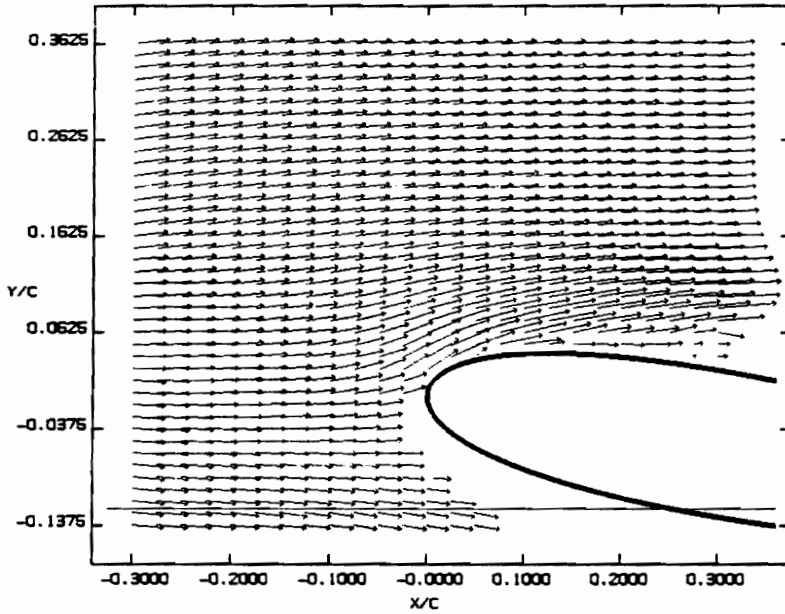


Figure 4.2.24 Velocity vectors and vorticity contours at time level 24 (24/50 of period, $\tau=1.24$ sec.)



BVI

VECTOR VELOCITY FIELD
REFERENCE FRAME FIXED WRT THE AIRFOIL

SINUSOIDAL PITCHING SCHEDULE

PHASE = 174.2 (DEG)

TIME LEVEL 25

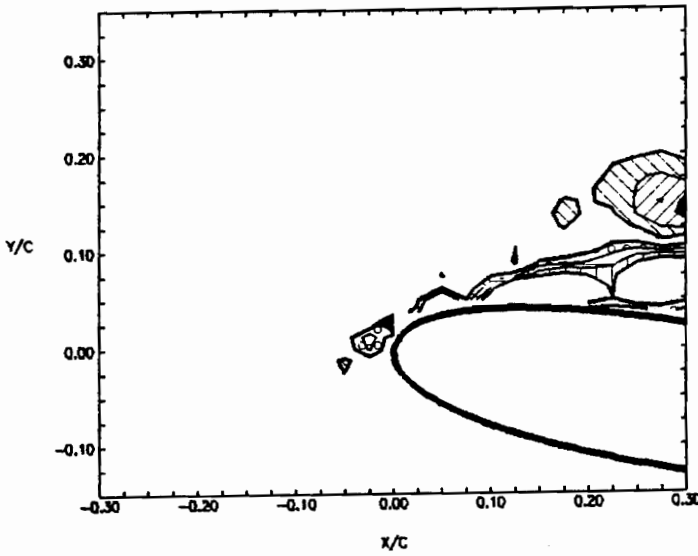
$k = 2.02$

$Re_c = 12957.2$

$Re = 19436.7$

$U_\infty = 0.128 \text{ m/s}$

$\alpha = 10.0 \text{ (DEG.)}$



VORTICITY CONTOURS

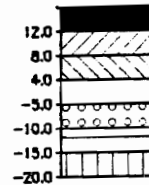
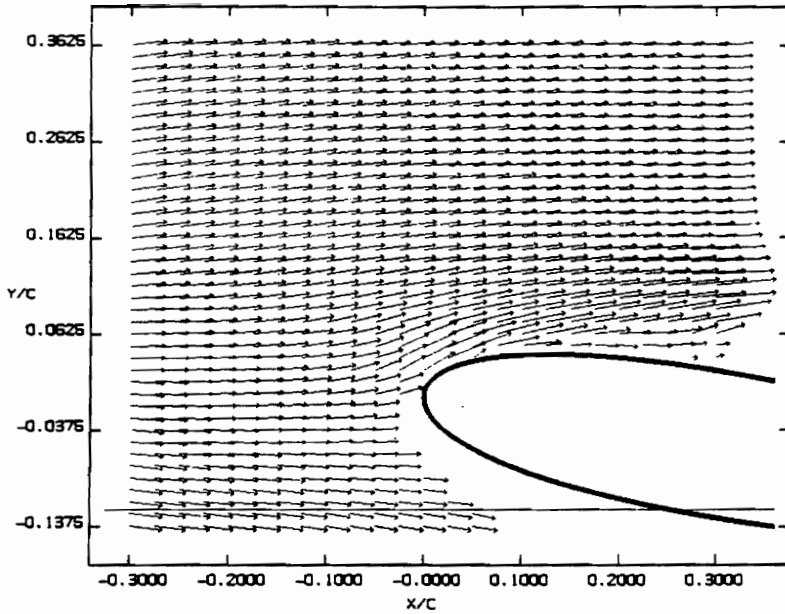


Figure 4.2.25 Velocity vectors and vorticity contours at time level 25 (25/50 of period, $\tau=1.24$ sec.)



BVI

VECTOR VELOCITY FIELD
REFERENCE FRAME FIXED WRT THE AIRFOIL

SINUSOIDAL PITCHING SCHEDULE

PHASE = 181.5 (DEG)

TIME LEVEL 26

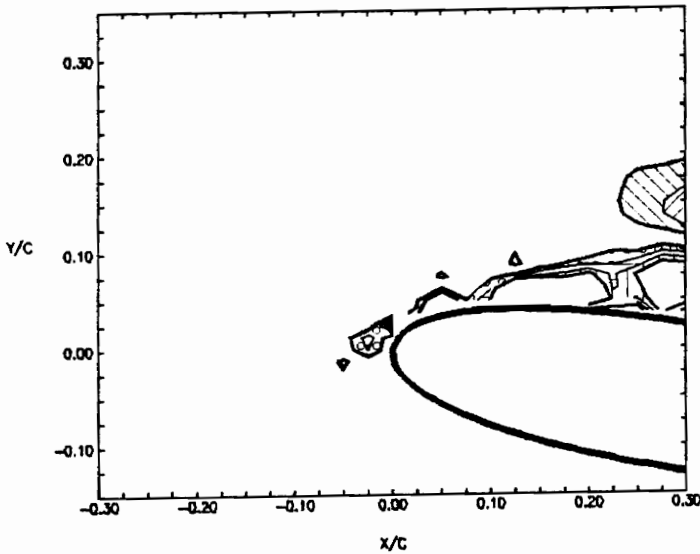
$k = 2.02$

$R_{\theta} = 12957.2$

$R_{\omega} = 19435.7$

$U_{\infty} = 0.128 \text{ m/s}$

$\alpha = 10.0 \text{ (DEG.)}$



VORTICITY CONTOURS

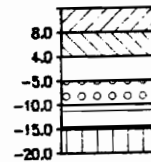
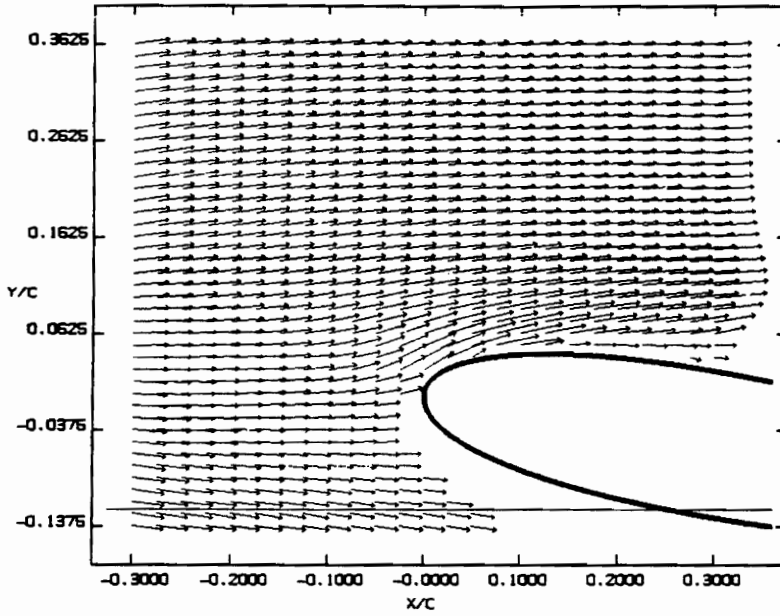


Figure 4.2.26 Velocity vectors and vorticity contours at time level 26 (26/50 of period, $\tau=1.24$ sec.)



BVI

VECTOR VELOCITY FIELD
REFERENCE FRAME FIXED WRT THE AIRFOIL

SINUSOIDAL PITCHING SCHEDULE

PHASE = 188.7 (DEG)

TIME LEVEL 27

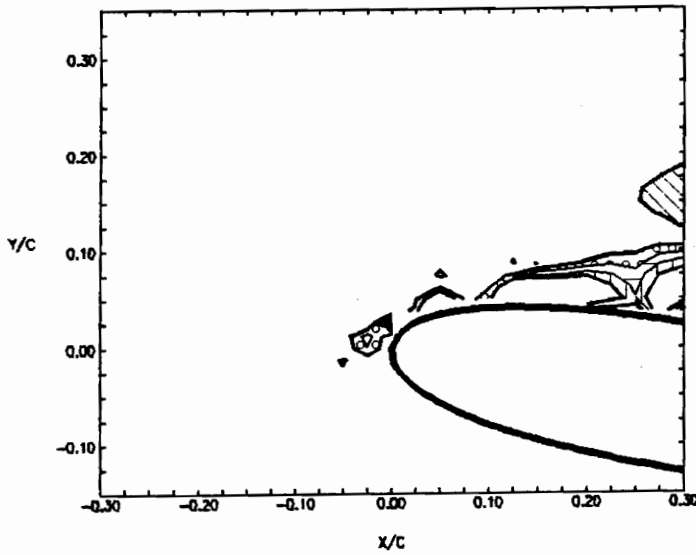
t = 2.02

Re_{∞} = 12957.2

Re = 19435.7

U_{∞} = 0.128 m/s

α = 10.0 (DEG.)



VORTICITY CONTOURS

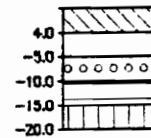
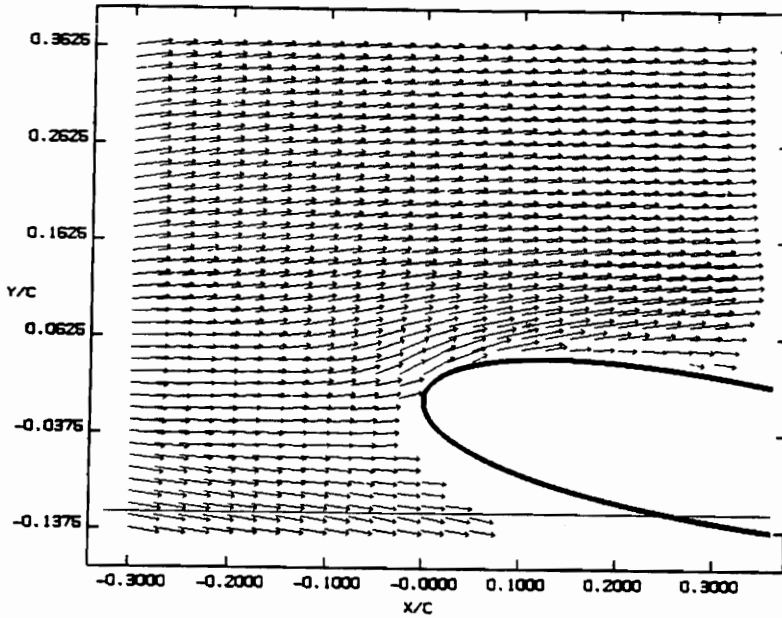


Figure 4.2.27 Velocity vectors and vorticity contours at time level 27 (27/50 of period, $\tau=1.24$ sec.)



BVI

VECTOR VELOCITY FIELD
REFERENCE FRAME FIXED WRT THE AIRFOIL

SINUSOIDAL PITCHING SCHEDULE

PHASE = 196.0 (DEG)

TIME LEVEL 28

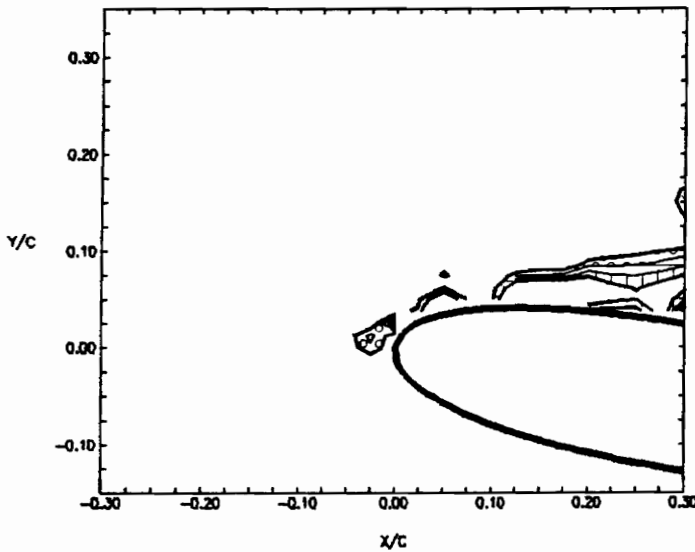
t = 2.02

Re = 12967.2

Ro = 19436.7

U_∞ = 0.128 m/s

α = 10.0 (DEG.)



VORTICITY CONTOURS

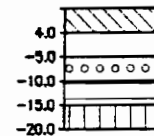
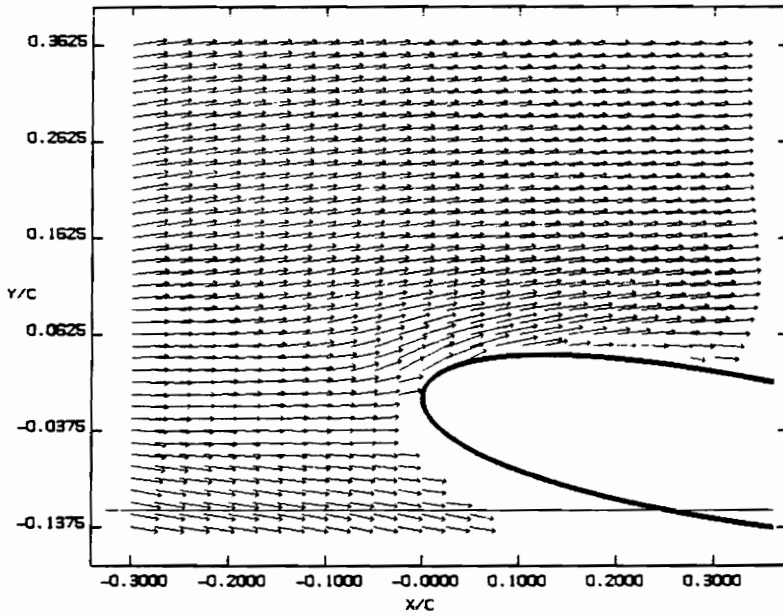


Figure 4.2.28 Velocity vectors and vorticity contours at time level 28 (28/50 of period, $\tau=1.24$ sec.)



BVI

VECTOR VELOCITY FIELD
REFERENCE FRAME FIXED WRT THE AIRFOIL

SINUSOIDAL PITCHING SCHEDULE

PHASE = 203.2 (DEG)

TIME LEVEL 29

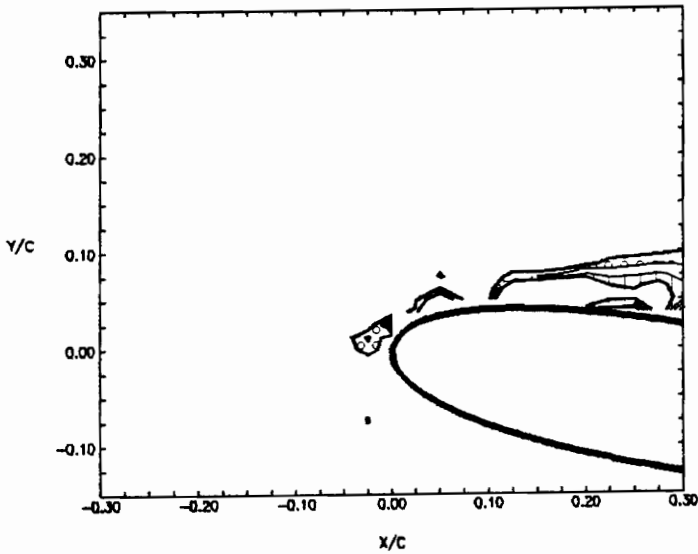
$\lambda = 2.02$

$Re = 12957.2$

$Re = 19435.7$

$U_\infty = 0.128 \text{ m/s}$

$\alpha = 10.0 \text{ (DEG.)}$



VORTICITY CONTOURS

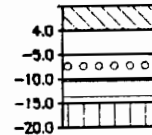
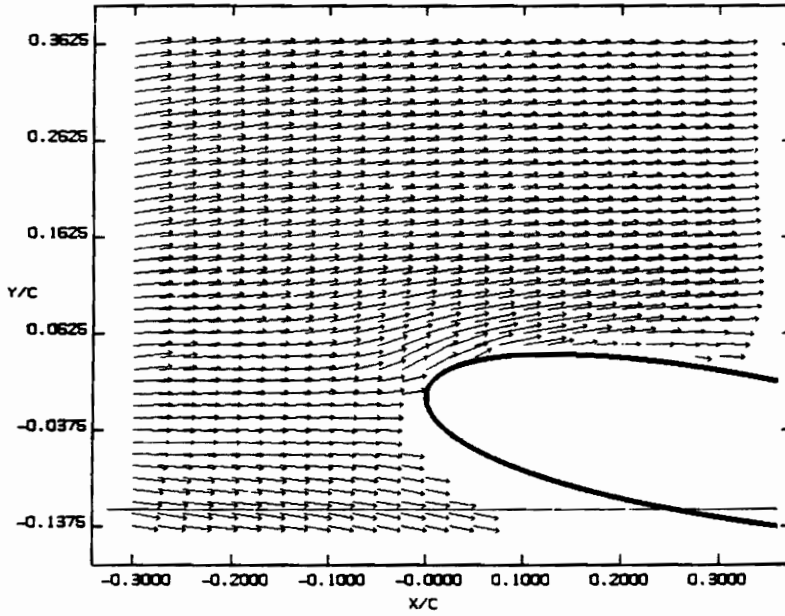


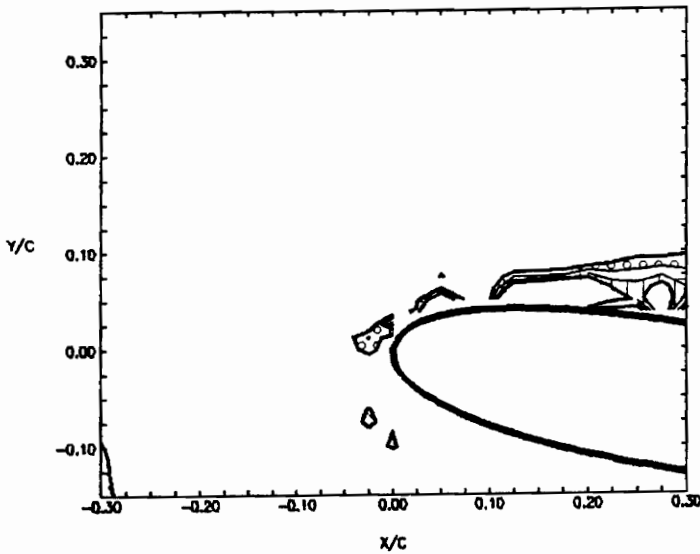
Figure 4.2.29 Velocity vectors and vorticity contours at time level 29 (29/50 of period, $\tau = 1.24 \text{ sec.}$)



BVI

VECTOR VELOCITY FIELD
REFERENCE FRAME FIXED WRT THE AIRFOIL

SINUSOIDAL PITCHING SCHEDULE
 PHASE = 210.5 (DEG)
 TIME LEVEL 30
 $t = 2.02$
 $Re = 12957.2$
 $Re = 19436.7$
 $U_\infty = 0.128 \text{ m/s}$
 $\alpha = 10.0 \text{ (DEG.)}$



VORTICITY CONTOURS

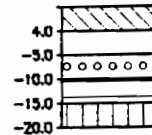
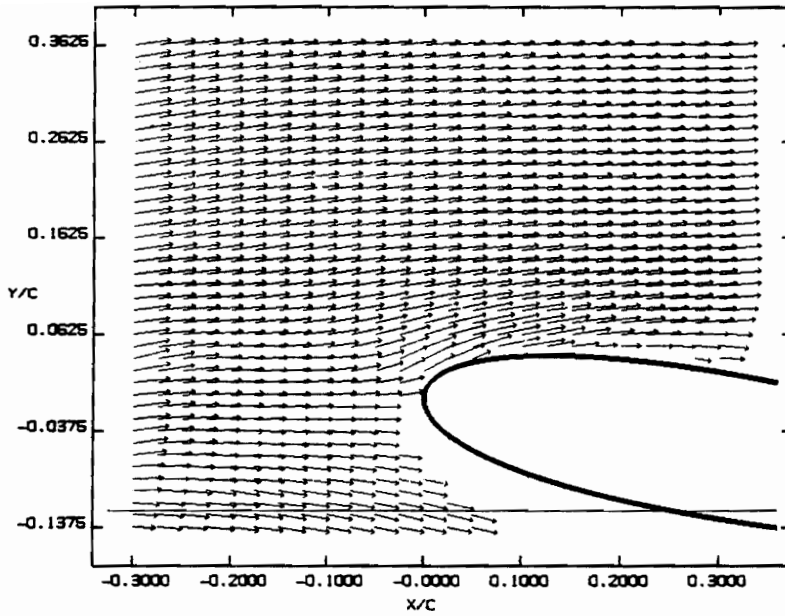


Figure 4.2.30 Velocity vectors and vorticity contours at time level 30 (30/50 of period, $\tau = 1.24 \text{ sec.}$)



BVI

VECTOR VELOCITY FIELD
REFERENCE FRAME FIXED WRT THE AIRFOIL

SINUSOIDAL PITCHING SCHEDULE

PHASE = 217.8 (DEG)

TIME LEVEL 31

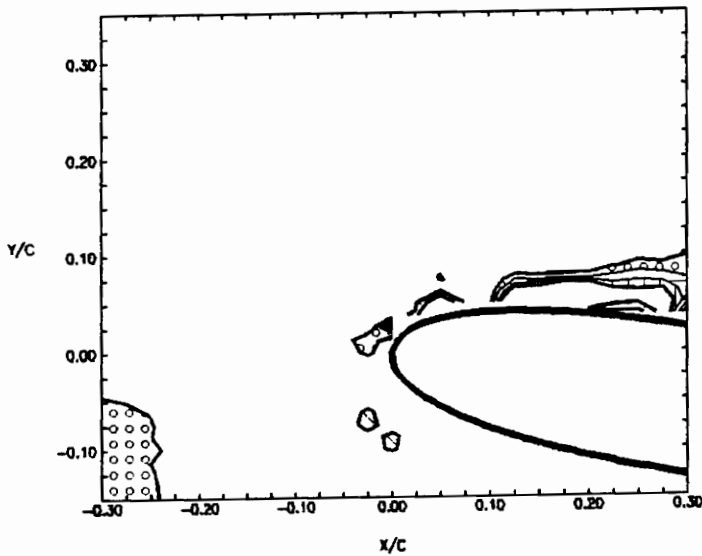
$k = 2.02$

$Re = 12967.2$

$Re = 19436.7$

$U_\infty = 0.128 \text{ m/s}$

$\alpha = 10.0 \text{ (DEG.)}$



VORTICITY CONTOURS

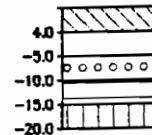
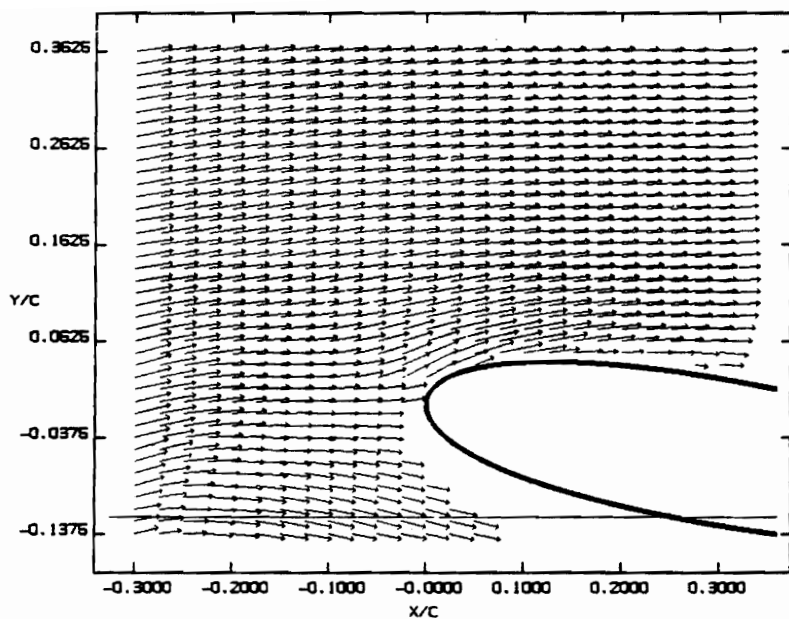


Figure 4.2.31 Velocity vectors and vorticity contours at time level 31 (31/50 of period, $\tau = 1.24 \text{ sec.}$)



BVI

VECTOR VELOCITY FIELD
REFERENCE FRAME FIXED WRT THE AIRFOIL

SINUSOIDAL PITCHING SCHEDULE

PHASE = 225.0 (DEG)

TIME LEVEL 32

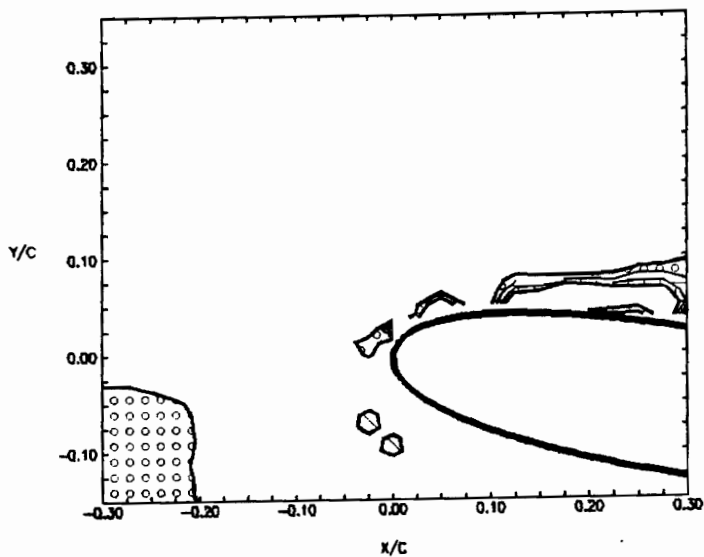
h = 2.02

Re_c = 12957.2

Re = 19435.7

U_∞ = 0.128 m/s

α = 10.0 (DEG.)



VORTICITY CONTOURS

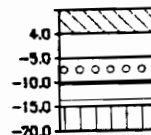
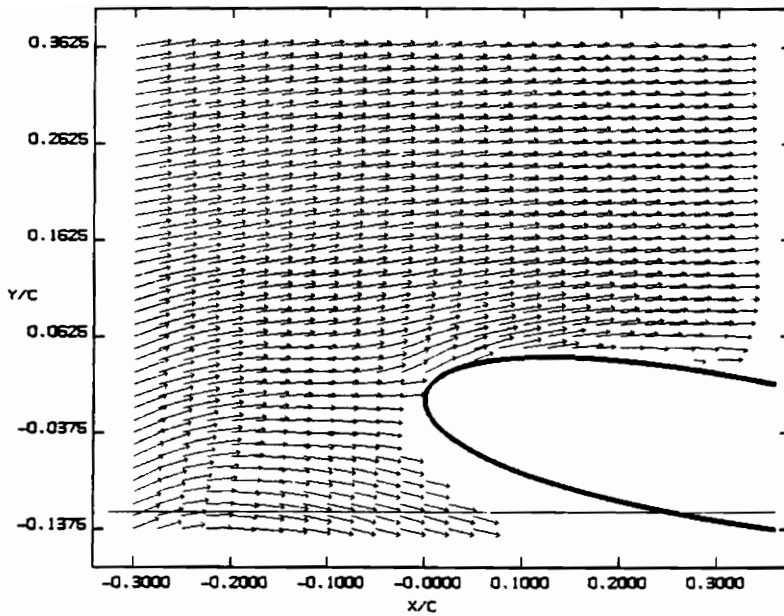


Figure 4.2.32 Velocity vectors and vorticity contours at time level 32 (32/50 of period, $\tau=1.24$ sec.)



BVI

VECTOR VELOCITY FIELD
REFERENCE FRAME FIXED WRT THE AIRFOIL

SINUSOIDAL PITCHING SCHEDULE

PHASE = 232.3 (DEG)

TIME LEVEL 33

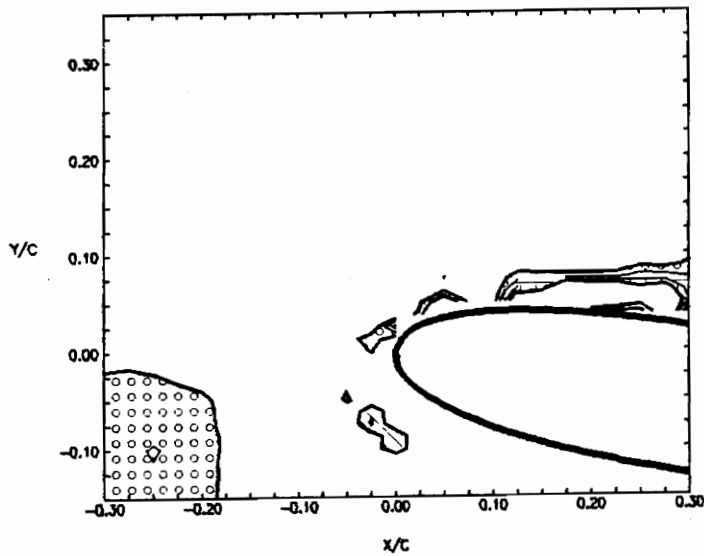
t = 2.02

Re_c = 12957.2

Re = 19435.7

U_∞ = 0.128 m/s

α = 10.0 (DEG.)



VORTICITY CONTOURS

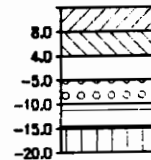
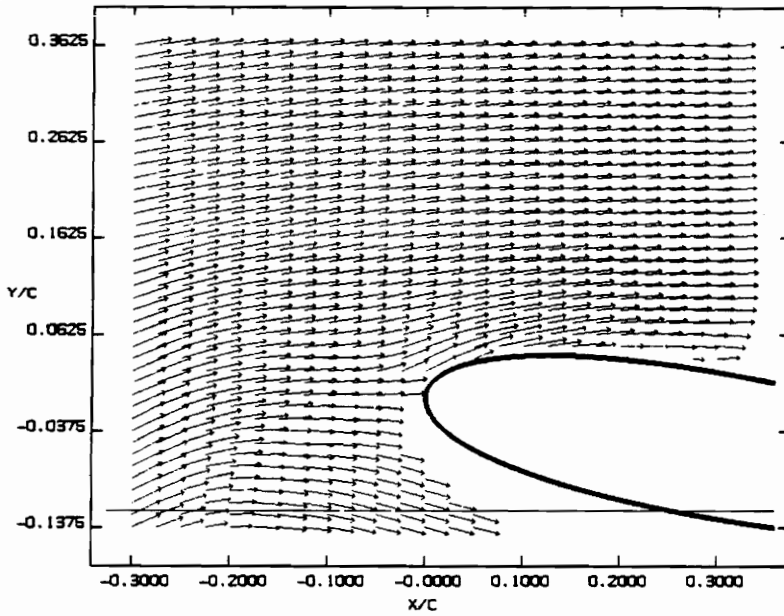


Figure 4.2.33 Velocity vectors and vorticity contours at time level 33 (33/50 of period, $\tau=1.24$ sec.)



BVI

VECTOR VELOCITY FIELD
REFERENCE FRAME FIXED WRT THE AIRFOIL

SINUSOIDAL PITCHING SCHEDULE

PHASE = 239.5 (DEG)

TIME LEVEL 34

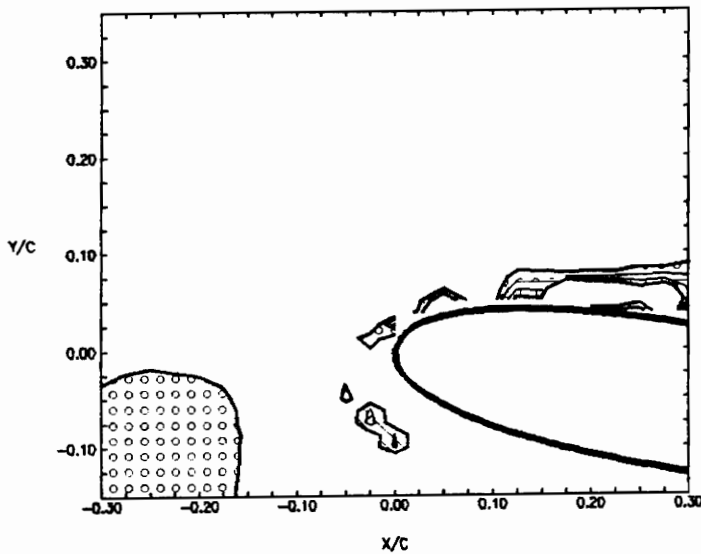
h = 2.02

Re = 12957.2

Re = 19436.7

U_{∞} = 0.128 m/s

α = 10.0 (DEG.)



VORTICITY CONTOURS

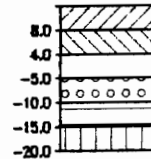
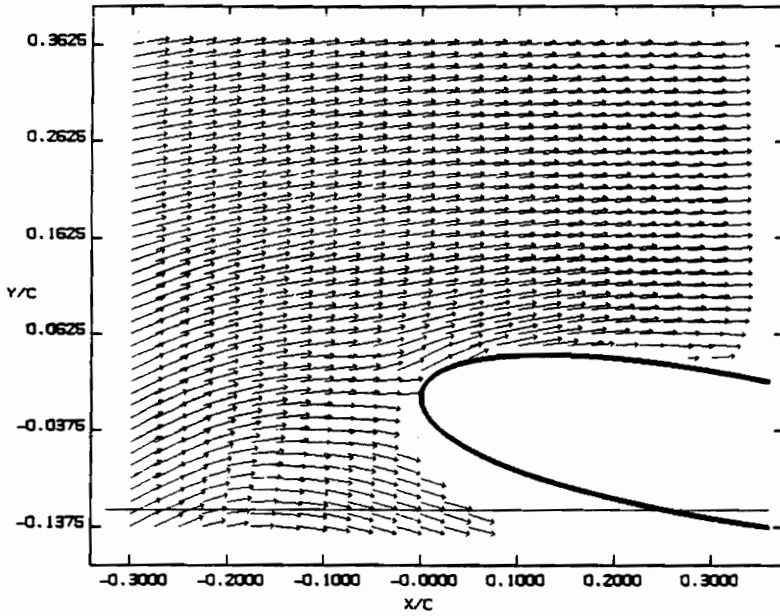


Figure 4.2.34 Velocity vectors and vorticity contours at time level 34 (34/50 of period, $\tau = 1.24$ sec.)



BVI

VECTOR VELOCITY FIELD
REFERENCE FRAME FIXED WRT THE AIRFOIL

SINUSOIDAL PITCHING SCHEDULE

PHASE = 246.8 (DEG)

TIME LEVEL 35

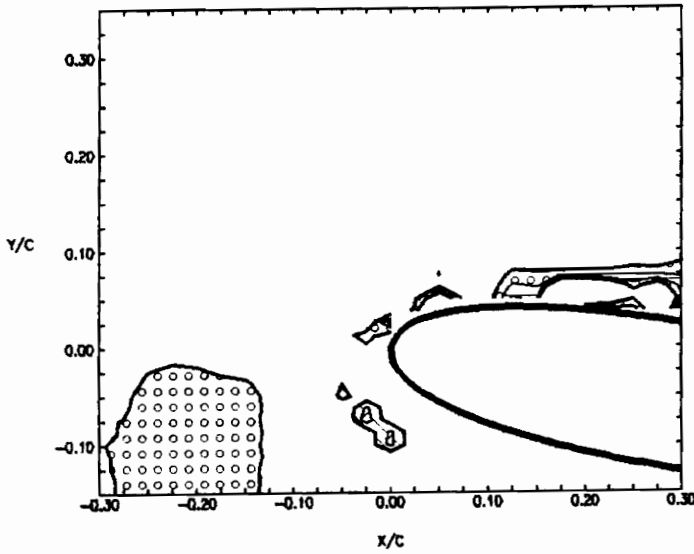
t = 2.02

Re_c = 12967.2

Re = 19435.7

U_∞ = 0.128 m/s

α = 10.0 (DEG.)



VORTICITY CONTOURS

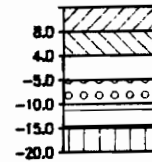
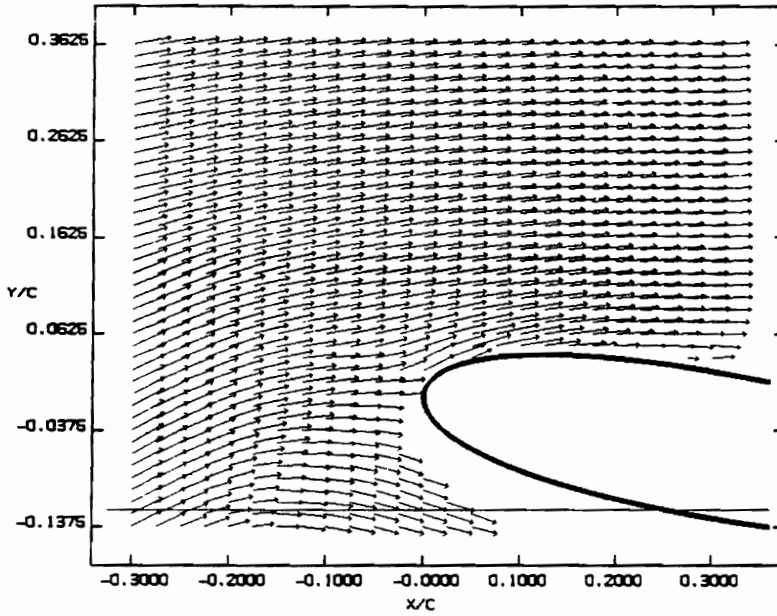


Figure 4.2.35 Velocity vectors and vorticity contours at time level 35 (35/50 of period, $\tau=1.24$ sec.)



BVI

VECTOR VELOCITY FIELD
REFERENCE FRAME FIXED WRT THE AIRFOIL

SINUSOIDAL PITCHING SCHEDULE

PHASE = 254.0 (DEG)

TIME LEVEL 36

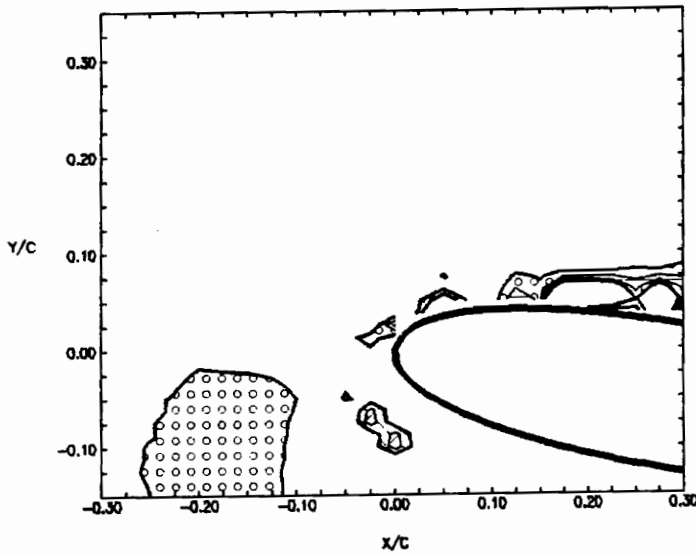
$t = 2.02$

$Re_c = 12957.2$

$Re = 19435.7$

$U_\infty = 0.128 \text{ m/s}$

$\alpha = 10.0 \text{ (DEG.)}$



VORTICITY CONTOURS

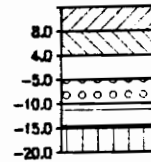
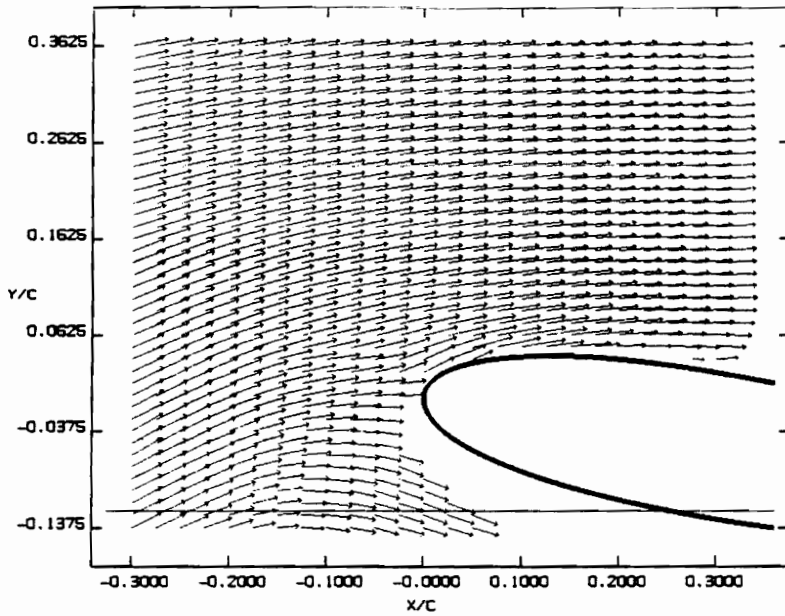


Figure 4.2.36 Velocity vectors and vorticity contours at time level 36 (36/50 of period, $\tau = 1.24 \text{ sec.}$)



BVI

VECTOR VELOCITY FIELD
REFERENCE FRAME FIXED WRT THE AIRFOIL

SINUSOIDAL PITCHING SCHEDULE

PHASE = 261.3 (DEG)

TIME LEVEL 37

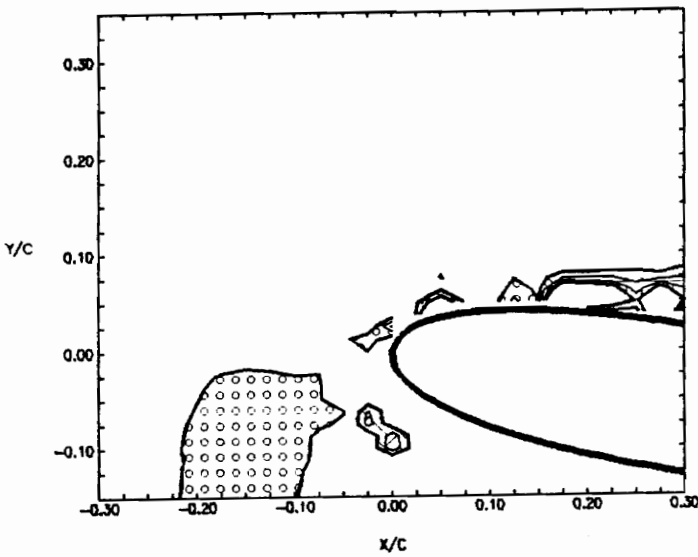
$k = 2.02$

$Re = 12957.2$

$Re = 19435.7$

$U_\infty = 0.128 \text{ m/s}$

$\alpha = 10.0 \text{ (DEG.)}$



VORTICITY CONTOURS

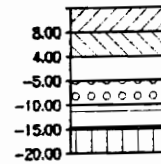


Figure 4.2.37 Velocity vectors and vorticity contours at time level 37 (37/50 of period, $\tau = 1.24 \text{ sec.}$)

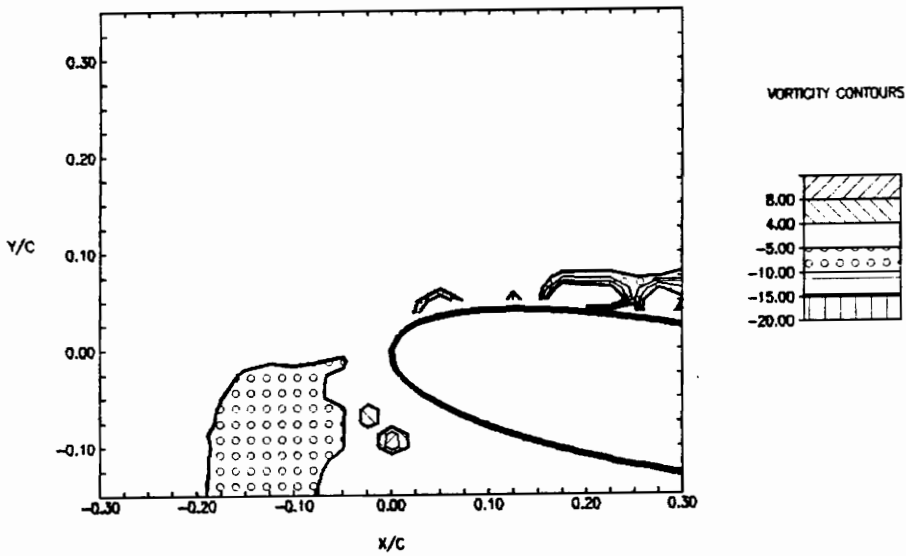
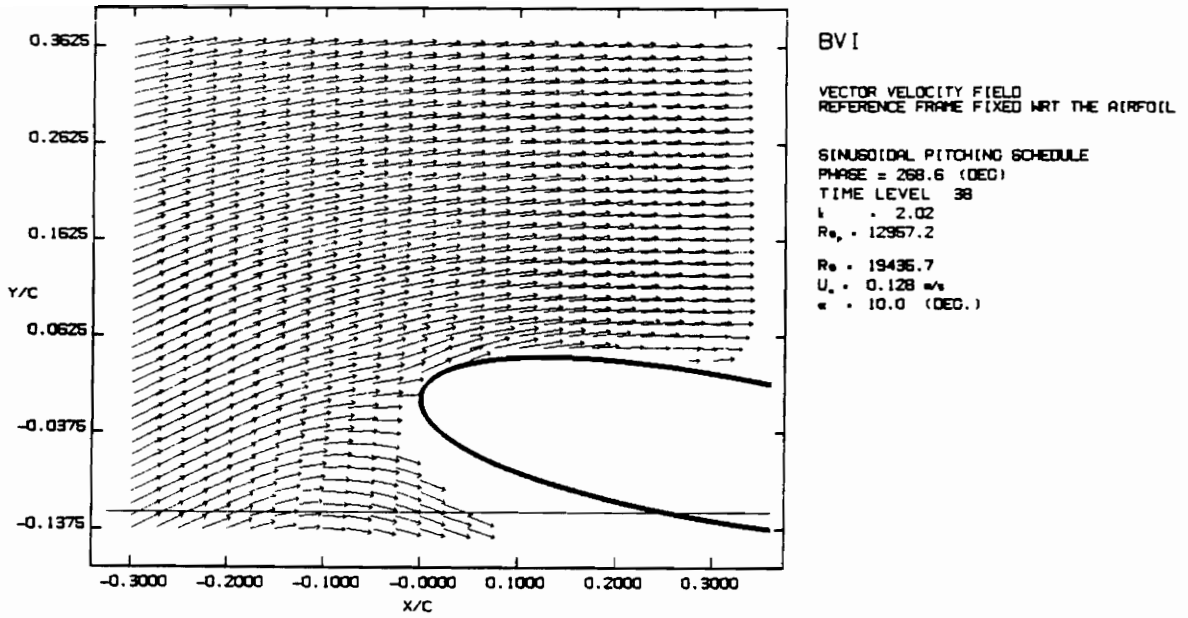
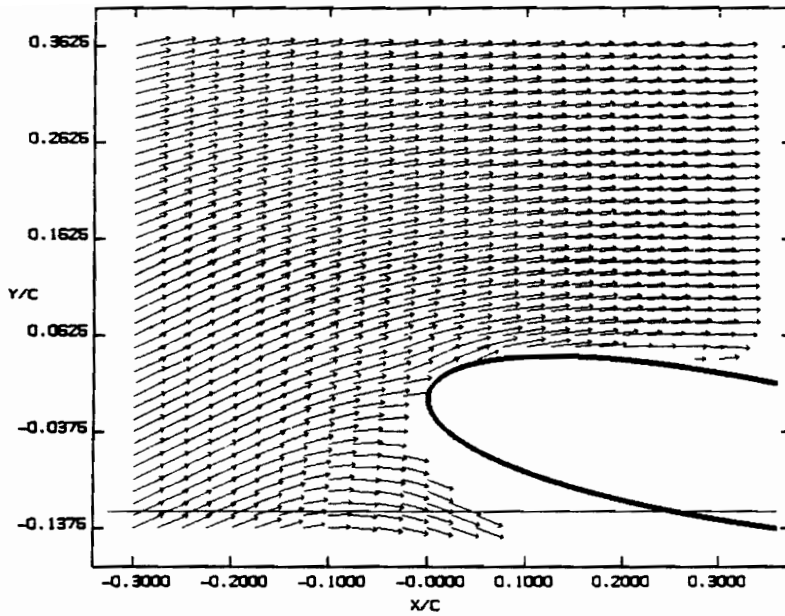


Figure 4.2.38 Velocity vectors and vorticity contours at time level 38 (38/50 of period, $\tau=1.24$ sec.)



BVI

VECTOR VELOCITY FIELD
REFERENCE FRAME FIXED WRT THE AIRFOIL

SINUSOIDAL PITCHING SCHEDULE

PHASE = 276.8 (DEG)

TIME LEVEL 39

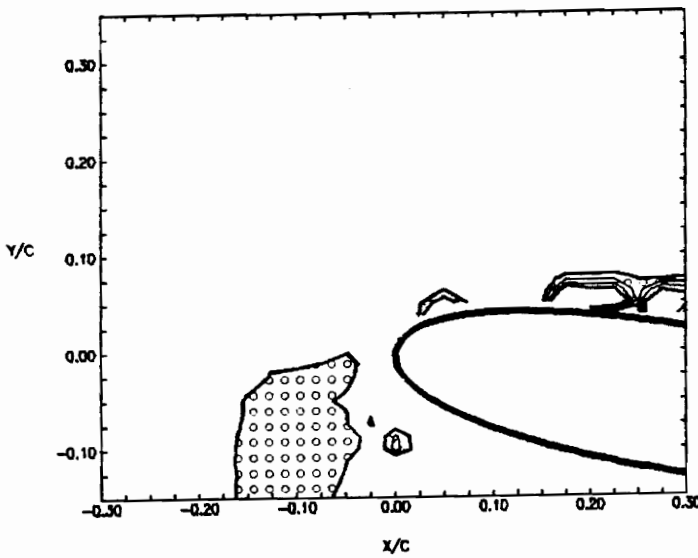
b = 2.02

Re_b = 12967.2

Re = 19436.7

U_∞ = 0.128 m/s

α = 10.0 (DEG.)



VORTICITY CONTOURS

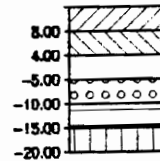
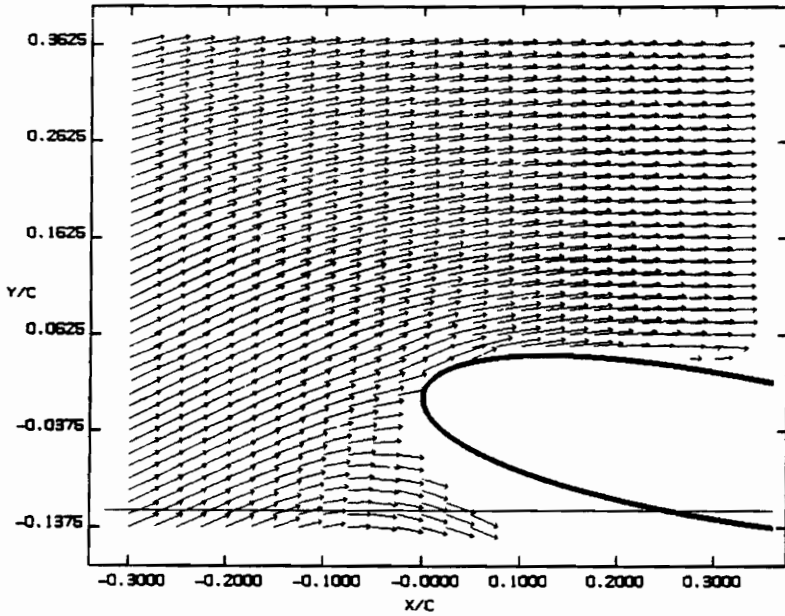


Figure 4.2.39 Velocity vectors and vorticity contours at time level 39 (39/50 of period, $\tau = 1.24$ sec.)



BVI

VECTOR VELOCITY FIELD
REFERENCE FRAME FIXED WRT THE AIRFOIL

SINUSOIDAL PITCHING SCHEDULE

PHASE = 283.1 (DEG)

TIME LEVEL 40

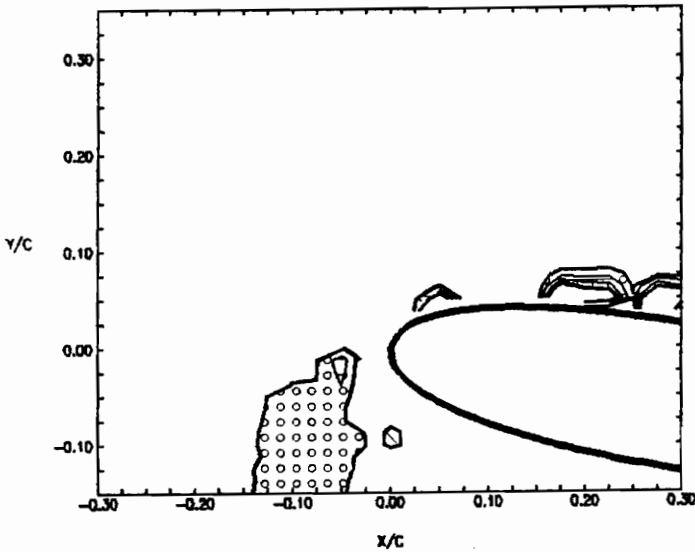
t = 2.02

Re_{∞} = 12967.2

Re = 19436.7

U_{∞} = 0.128 m/s

α = 10.0 (DEG.)



VORTICITY CONTOURS

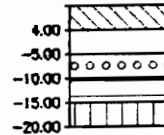
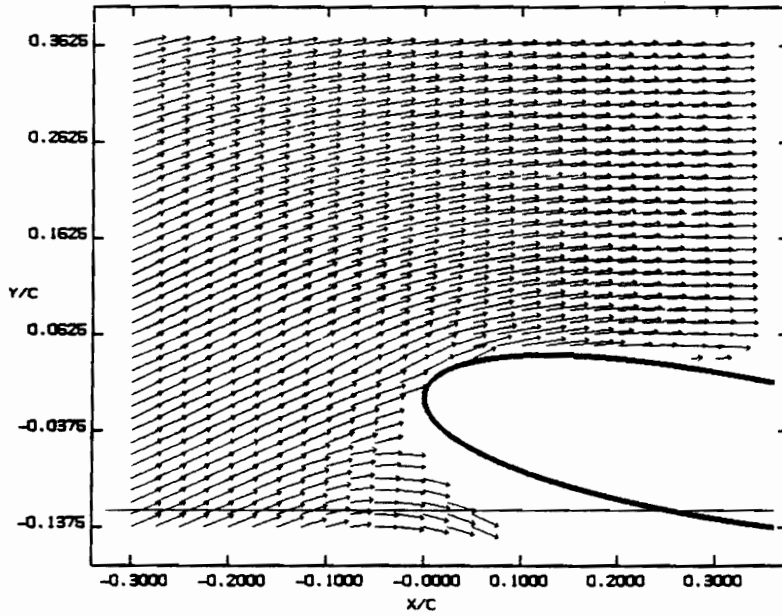


Figure 4.2.40 Velocity vectors and vorticity contours at time level 40 (40/50 of period, $\tau=1.24$ sec.)



BVI

VECTOR VELOCITY FIELD
REFERENCE FRAME FIXED WRT THE AIRFOIL

SINUSOIDAL PITCHING SCHEDULE

PHASE = 290.3 (DEG)

TIME LEVEL 41

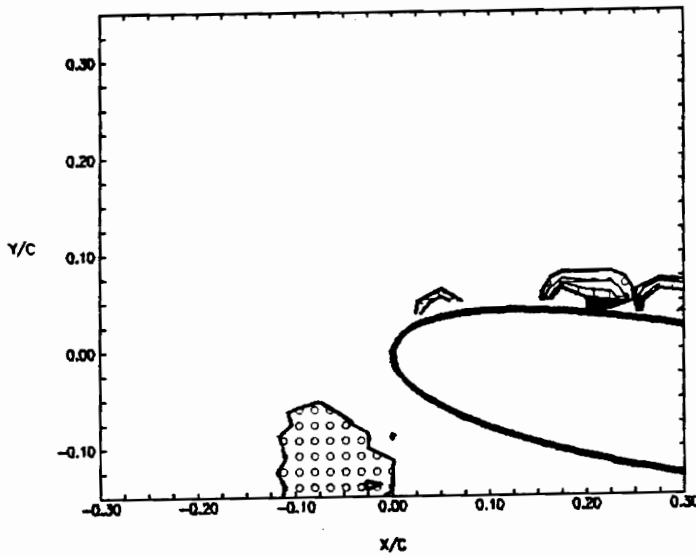
t = 2.02

Re = 12957.2

Re = 19435.7

U_{∞} = 0.128 m/s

α = 10.0 (DEG.)



VORTICITY CONTOURS

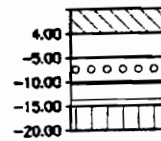
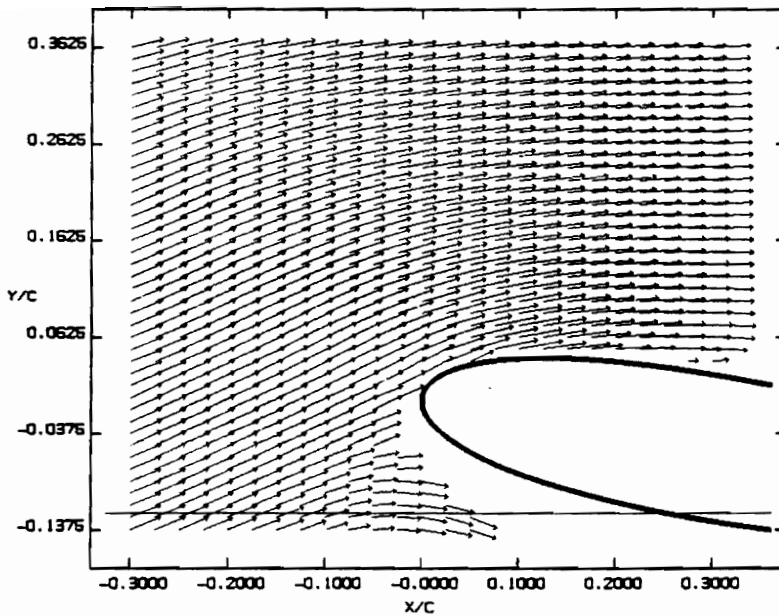


Figure 4.2.41 Velocity vectors and vorticity contours at time level 41 (41/50 of period, $\tau=1.24$ sec.)



BVI

VECTOR VELOCITY FIELD
REFERENCE FRAME FIXED WRT THE AIRFOIL

SINUSOIDAL PITCHING SCHEDULE

PHASE = 297.6 (DEG)

TIME LEVEL 42

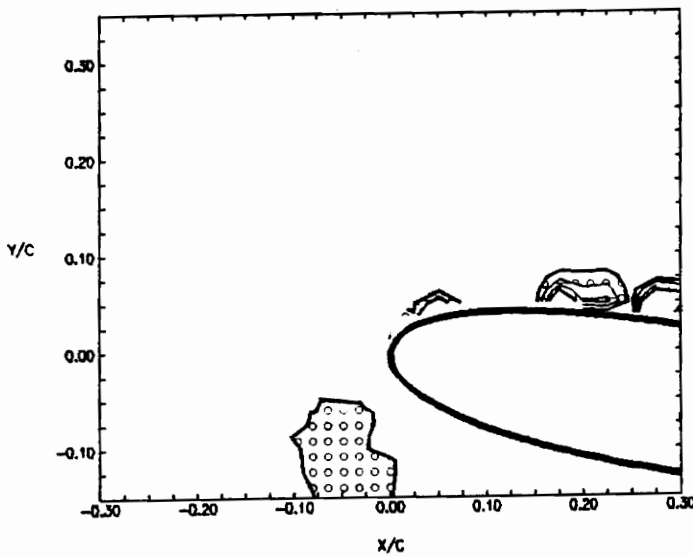
t = 2.02

Re_c = 12957.2

Re = 19435.7

U_∞ = 0.128 m/s

α = 10.0 (DEG.)



VORTICITY CONTOURS

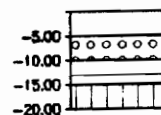
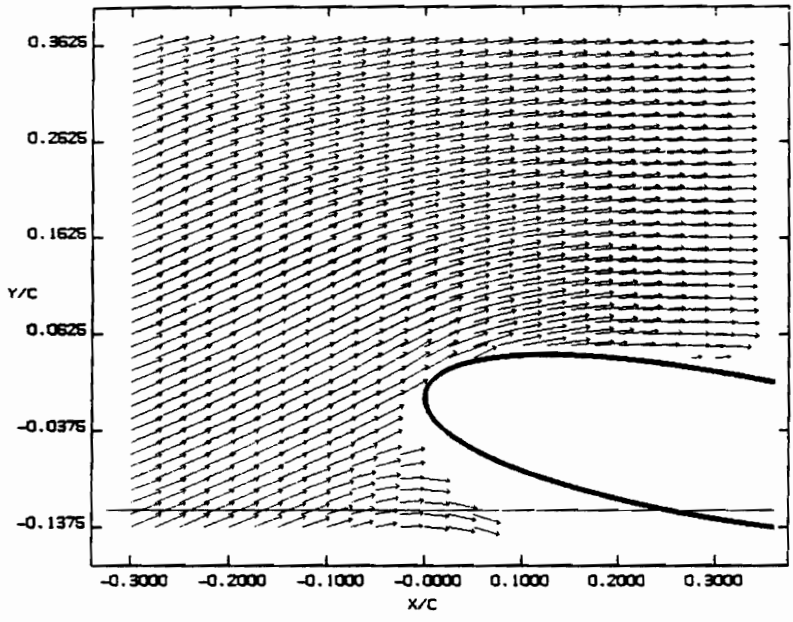


Figure 4.2.42 Velocity vectors and vorticity contours at time level 42 (42/50 of period, $\tau=1.24$ sec.)

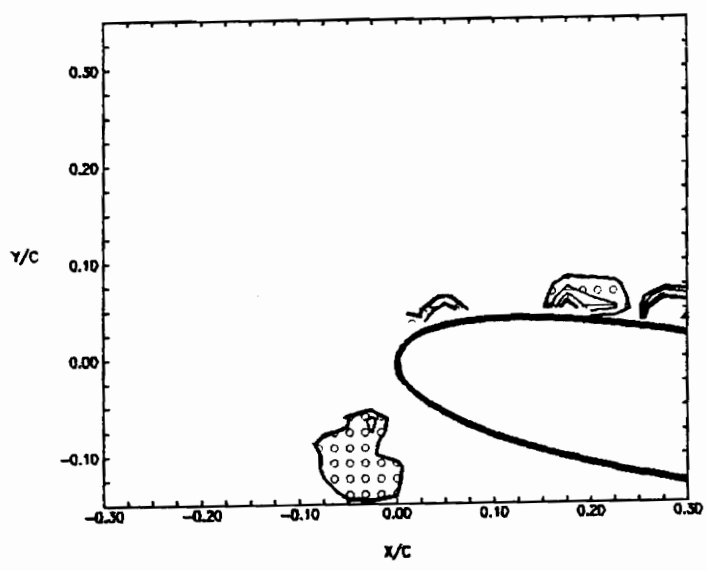


BVI

VECTOR VELOCITY FIELD
 REFERENCE FRAME FIXED WRT THE AIRFOIL

SINUSOIDAL PITCHING SCHEDULE
 PHASE = 304.9 (DEG)
 TIME LEVEL 43
 $t = 2.02$
 $Re = 12957.2$

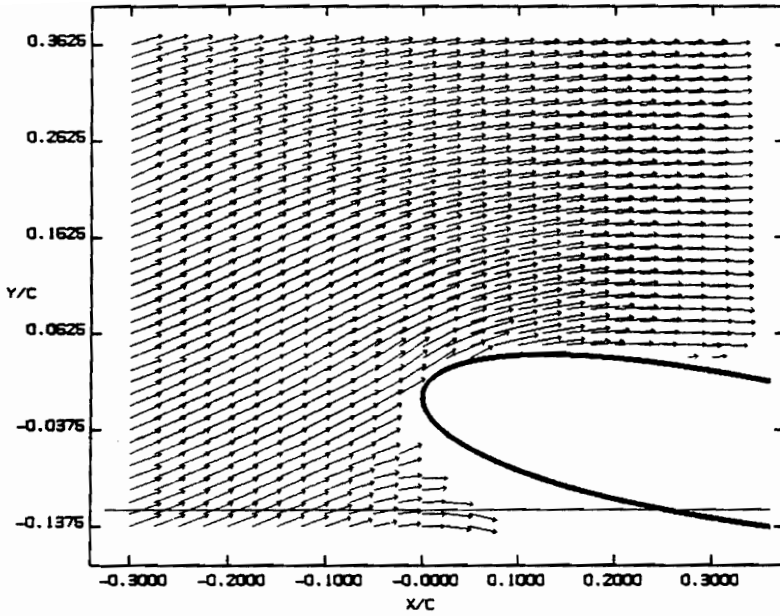
$Re = 19495.7$
 $U_\infty = 0.128 \text{ m/s}$
 $\alpha = 10.0 \text{ (DEG.)}$



VORTICITY CONTOURS

| |
|--------|
| -5.00 |
| -10.00 |
| -15.00 |
| -20.00 |

Figure 4.2.43 Velocity vectors and vorticity contours at time level 43 (43/50 of period, $\tau = 1.24 \text{ sec.}$)



BVI

VECTOR VELOCITY FIELD
REFERENCE FRAME FIXED WRT THE AIRFOIL

SINUSOIDAL PITCHING SCHEDULE

PHASE = 312.1 (DEG)

TIME LEVEL 44

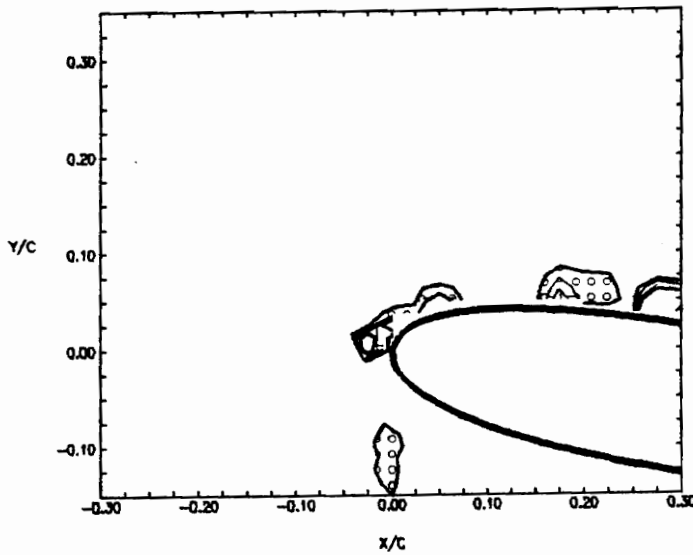
l = 2.02

Re = 12957.2

Re = 19435.7

U_{∞} = 0.128 u_0

α = 10.0 (DEG.)



VORTICITY CONTOURS

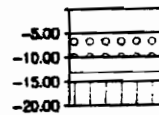
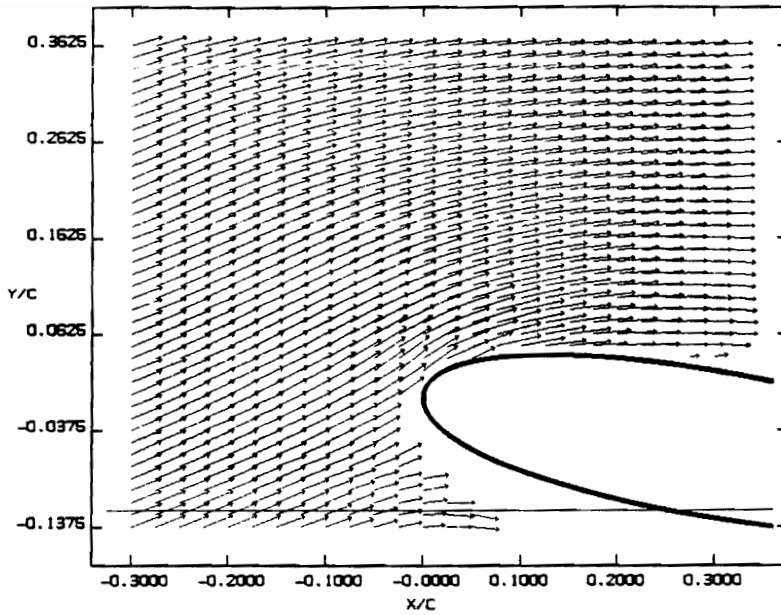


Figure 4.2.44 Velocity vectors and vorticity contours at time level 44 (44/50 of period, $\tau=1.24$ sec.)



BVI

VECTOR VELOCITY FIELD
REFERENCE FRAME FIXED WRT THE AIRFOIL

SINUSOIDAL PITCHING SCHEDULE

PHASE = 319.4 (DEG)

TIME LEVEL 45

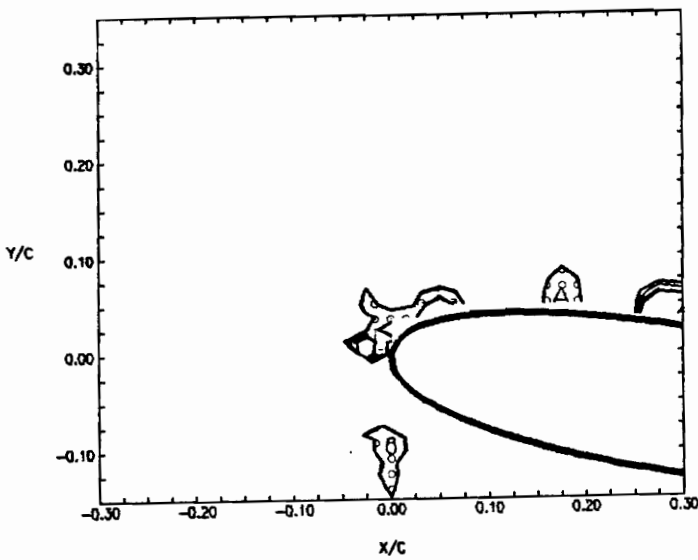
t = 2.02

Re = 12967.2

Re = 19435.7

U_∞ = 0.128 m/s

α = 10.0 (DEG.)



VORTICITY CONTOURS

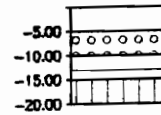
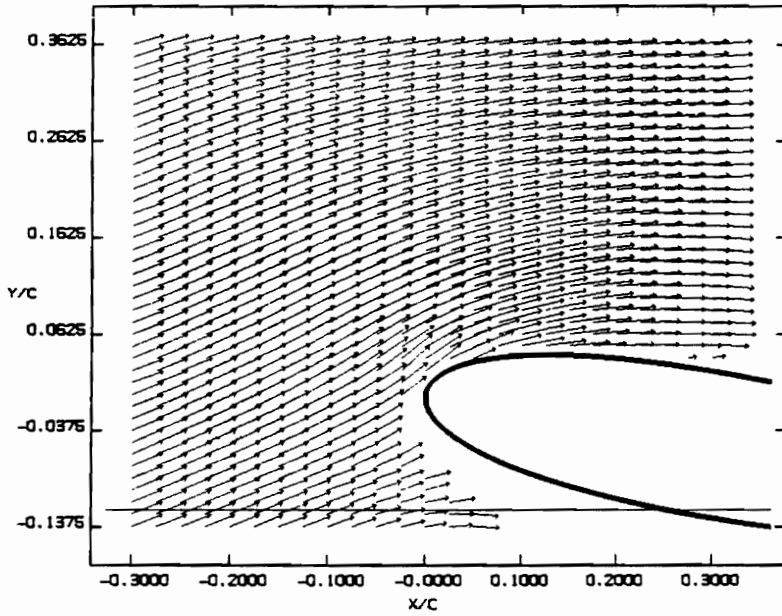


Figure 4.2.45 Velocity vectors and vorticity contours at time level 45 (45/50 of period, $\tau=1.24$ sec.)



BVI

VECTOR VELOCITY FIELD
REFERENCE FRAME FIXED WRT THE AIRFOIL

SINUSOIDAL PITCHING SCHEDULE

PHASE = 326.6 (DEG)

TIME LEVEL 46

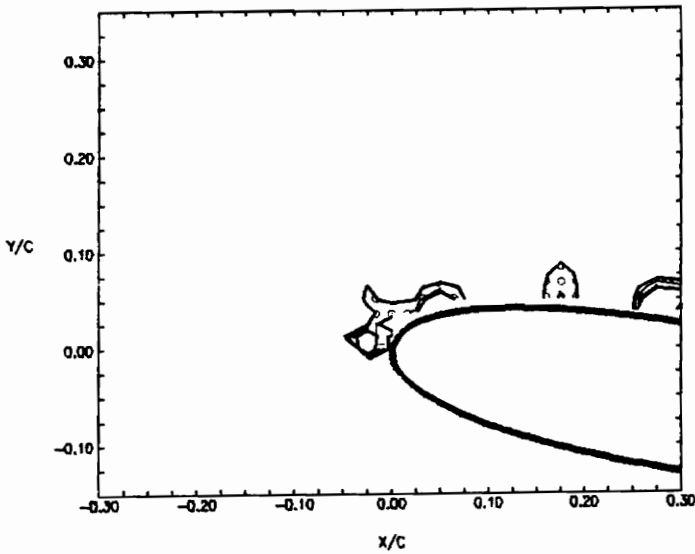
$t = 2.02$

$Re = 12967.2$

$Re = 19436.7$

$U_\infty = 0.128$ m/s

$\alpha = 10.0$ (DEG.)



VORTICITY CONTOURS

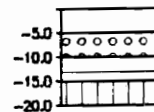


Figure 4.2.46 Velocity vectors and vorticity contours at time level 46 (46/50 of period, $\tau=1.24$ sec.)

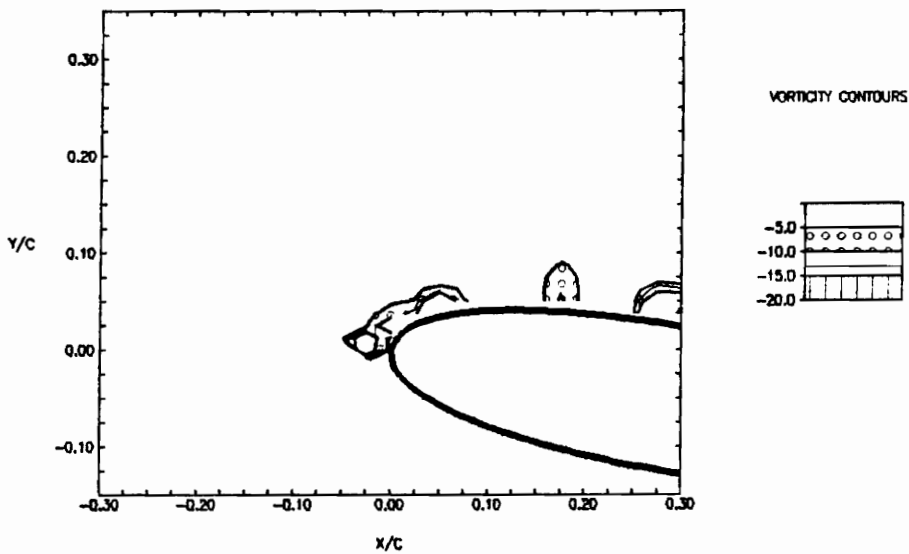
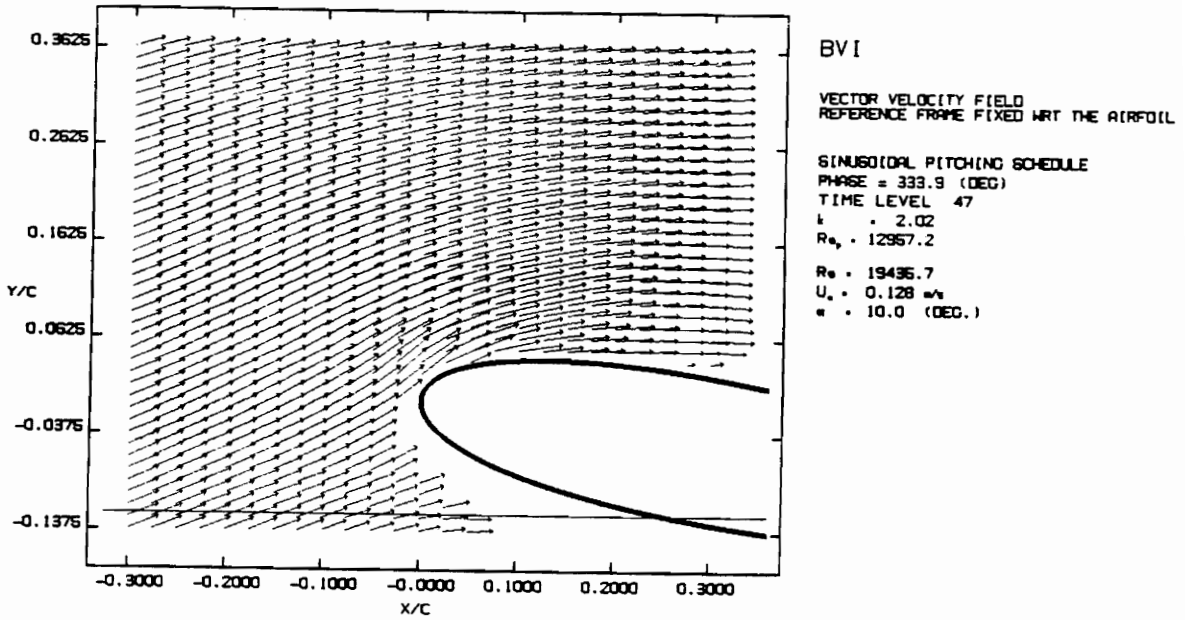
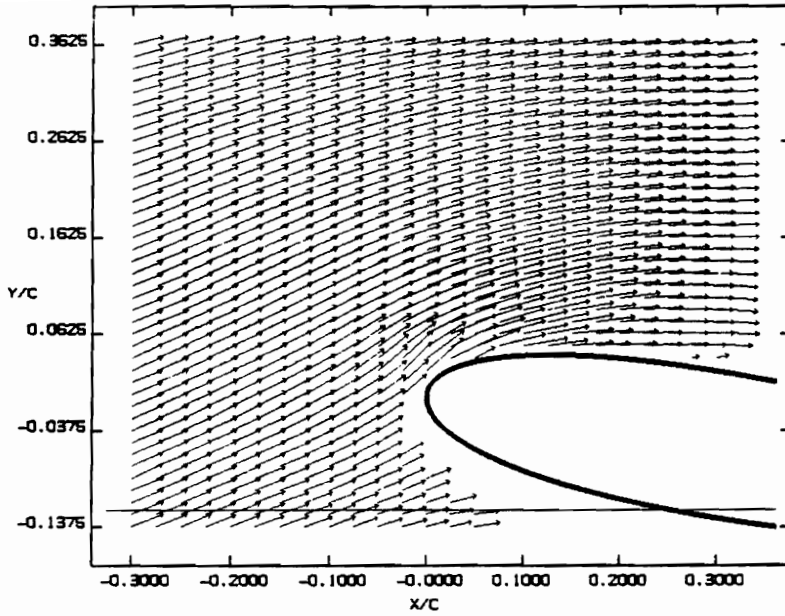


Figure 4.2.47 Velocity vectors and vorticity contours at time level 47 (47/50 of period, $\tau=1.24$ sec.)



BVI

VECTOR VELOCITY FIELD
REFERENCE FRAME FIXED WRT THE AIRFOIL

SINUSOIDAL PITCHING SCHEDULE

PHASE = 341.2 (DEG)

TIME LEVEL 48

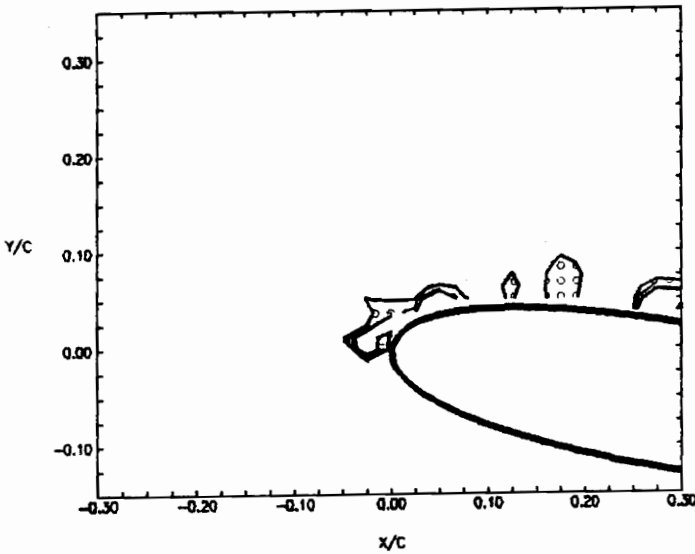
$k = 2.02$

$Re = 12967.2$

$Re = 19436.7$

$U_\infty = 0.128 \text{ m/s}$

$\alpha = 10.0 \text{ (DEG.)}$



VORTICITY CONTOURS

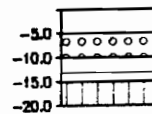
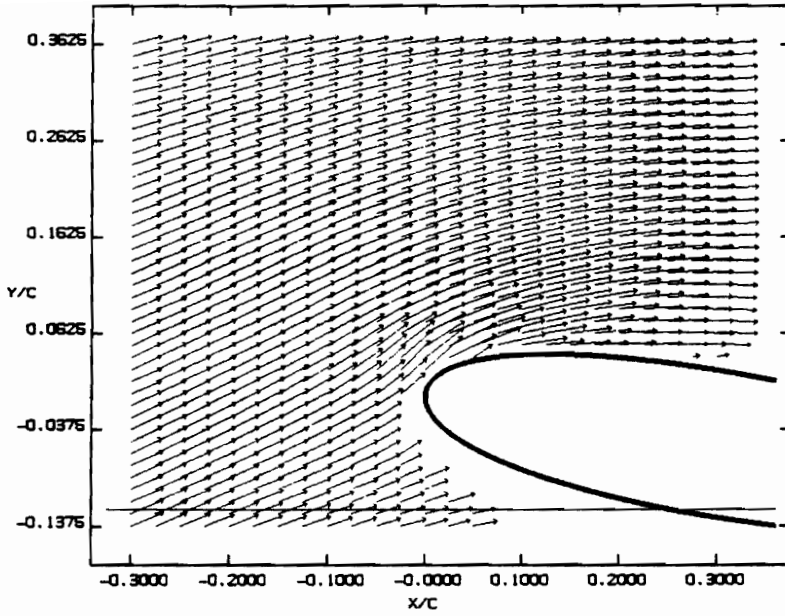


Figure 4.2.48 Velocity vectors and vorticity contours at time level 48 (48/50 of period, $\tau=1.24 \text{ sec.}$)



BVI

VECTOR VELOCITY FIELD
REFERENCE FRAME FIXED WRT THE AIRFOIL

SINUSOIDAL PITCHING SCHEDULE

PHASE = 348.4 (DEG)

TIME LEVEL 49

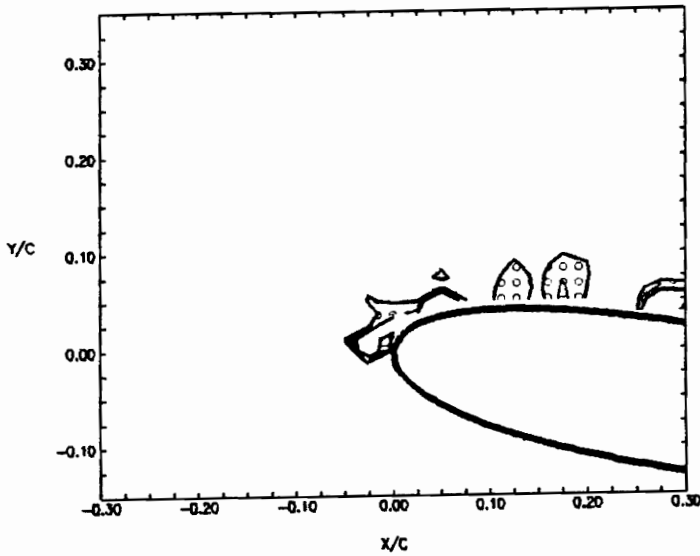
k = 2.02

Re_c = 12967.2

Re = 19436.7

U_∞ = 0.128 m/s

α = 10.0 (DEG.)



VORTICITY CONTOURS

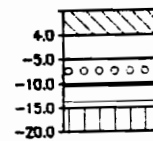
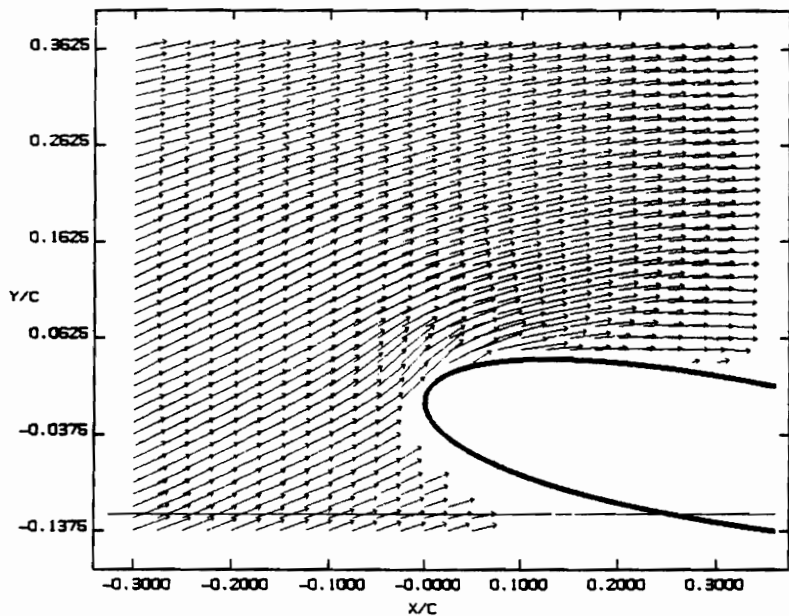


Figure 4.2.49 Velocity vectors and vorticity contours at time level 49 (49/50 of period, $\tau=1.24$ sec.)



BVI

VECTOR VELOCITY FIELD
REFERENCE FRAME FIXED WRT THE AIRFOIL

SINUSOIDAL PITCHING SCHEDULE

PHASE = 355.7 (DEG)

TIME LEVEL 50

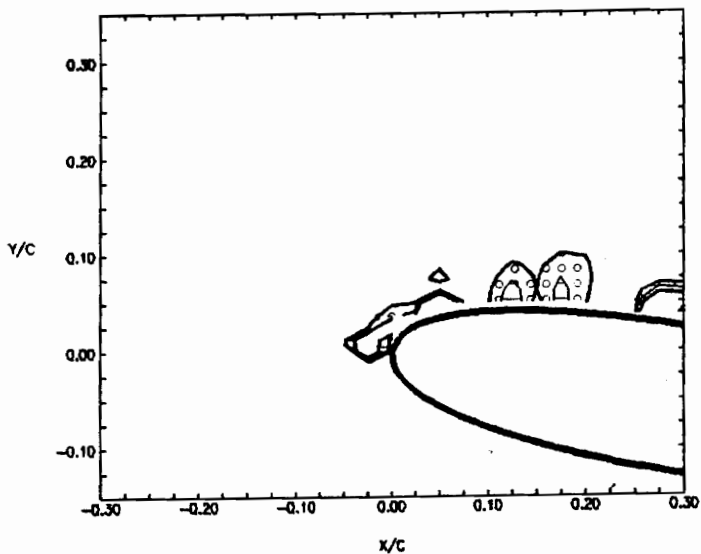
t = 2.02

Re = 12957.2

Re = 19435.7

U_{∞} = 0.128 m/s

α = 10.0 (DEG.)



VORTICITY CONTOURS

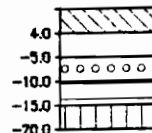


Figure 4.2.50 Velocity vectors and vorticity contours at time level 50 (50/50 of period, $\tau=1.24$ sec.)

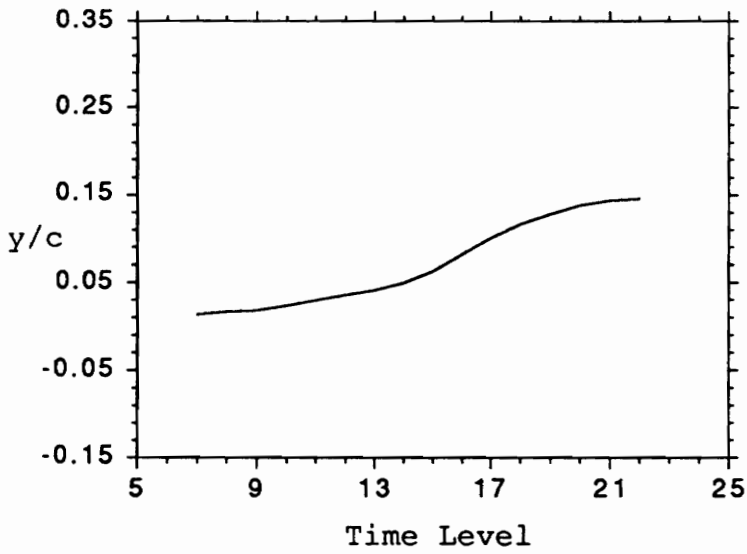
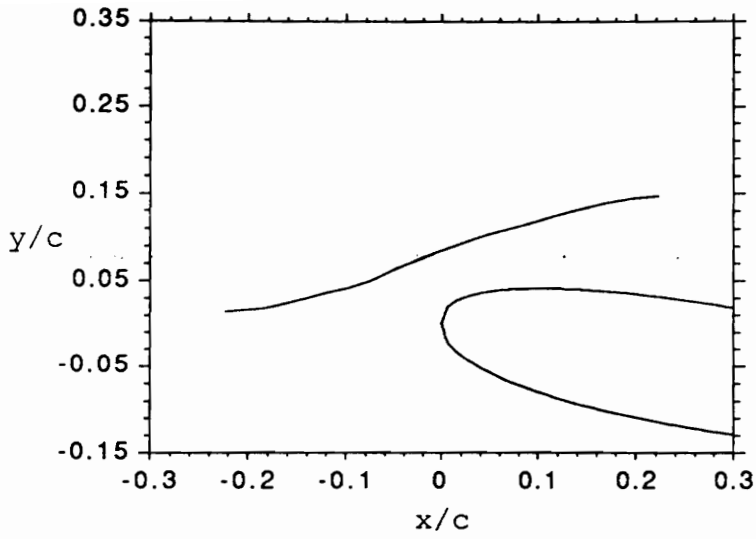


Figure 4.2.51 The average location of the vortex in the x-y plane, relative to the airfoil, and the time-y plane

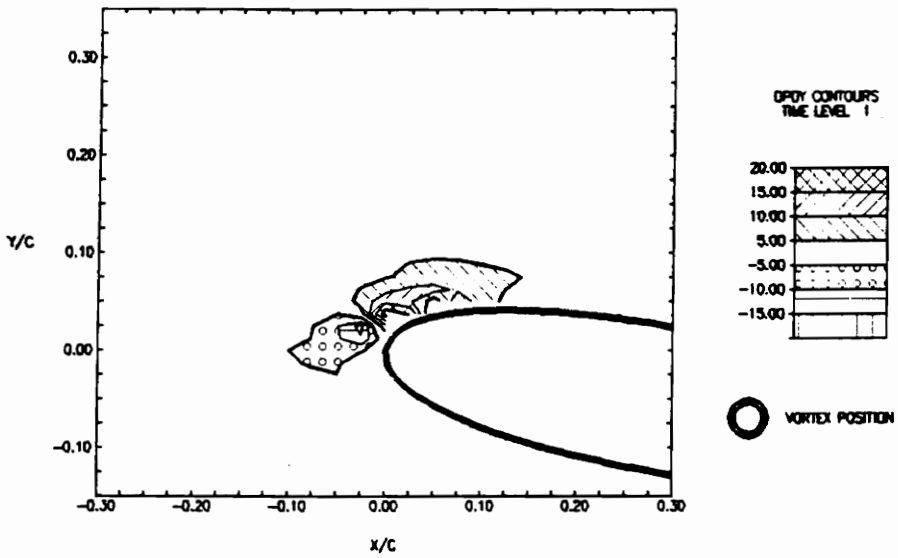
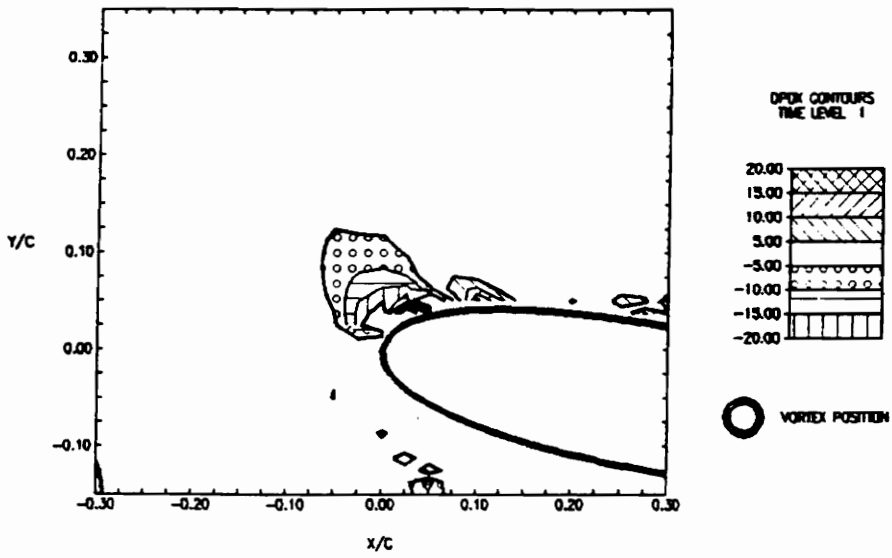


Figure 4.3.1 Pressure gradient contours, $\partial p/\partial x$ and $\partial p/\partial y$, at time level 1 (1/50 of period, $\tau=1.24$ sec.)

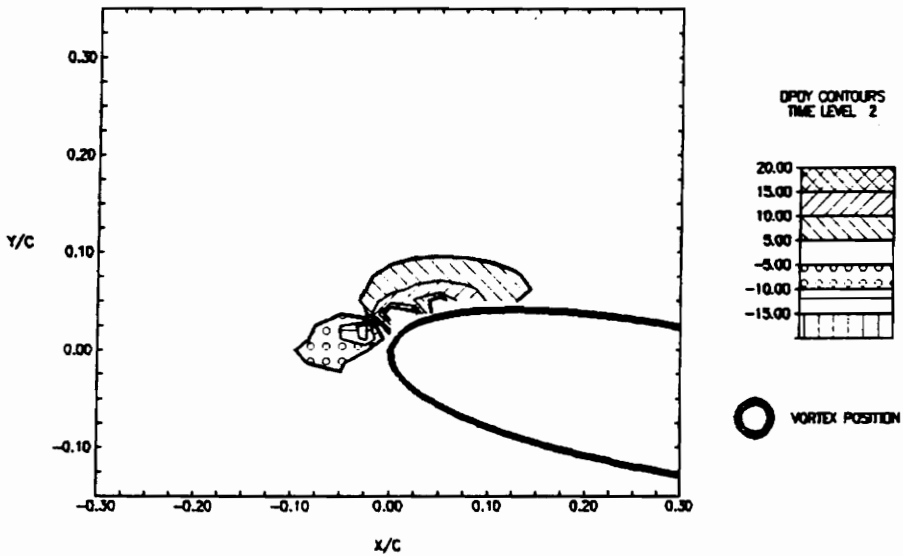
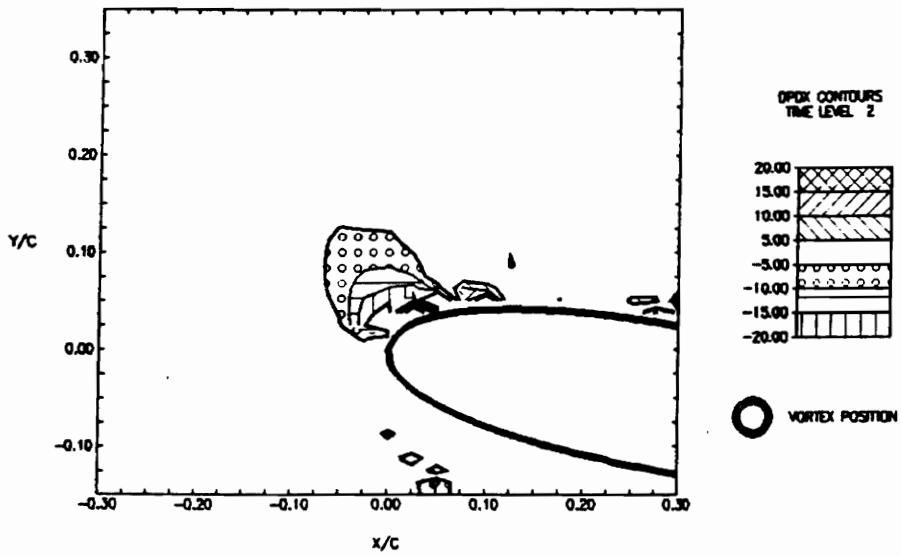


Figure 4.3.2 Pressure gradient contours, $\partial p/\partial x$ and $\partial p/\partial y$, at time level 2 (2/50 of period, $\tau=1.24$ sec.)

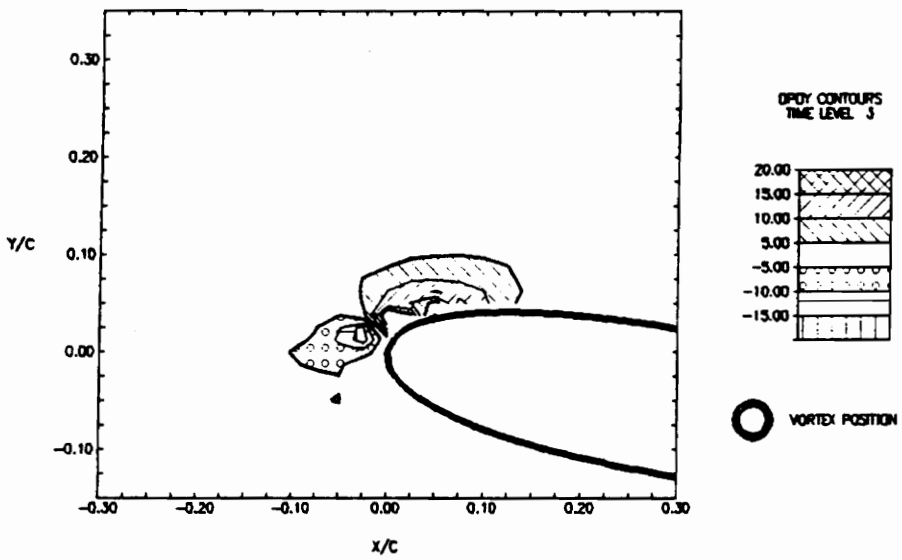
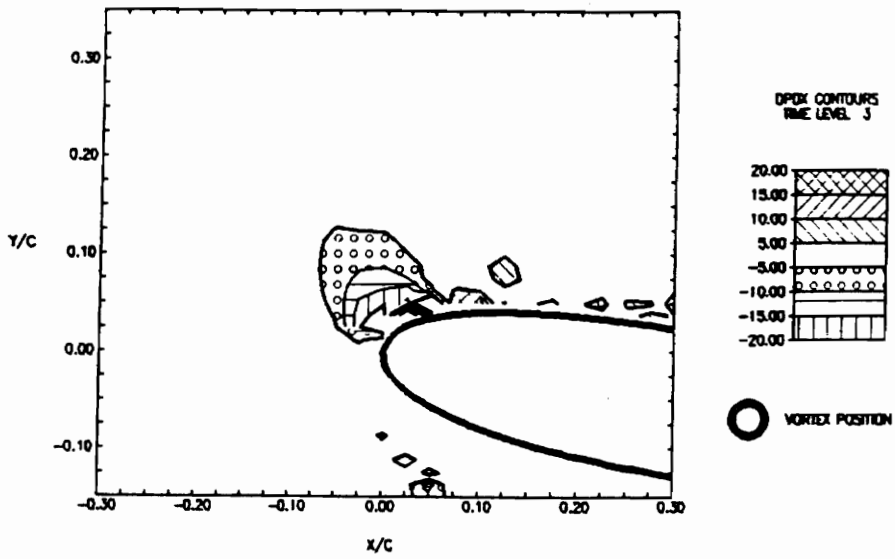


Figure 4.3.3 Pressure gradient contours, $\partial p/\partial x$ and $\partial p/\partial y$, at time level 3 (3/50 of period, $\tau=1.24$ sec.)

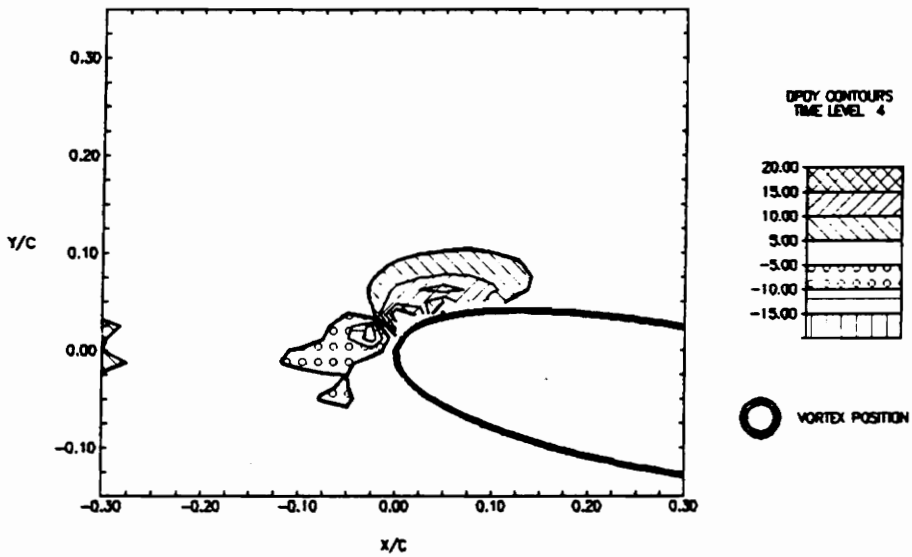
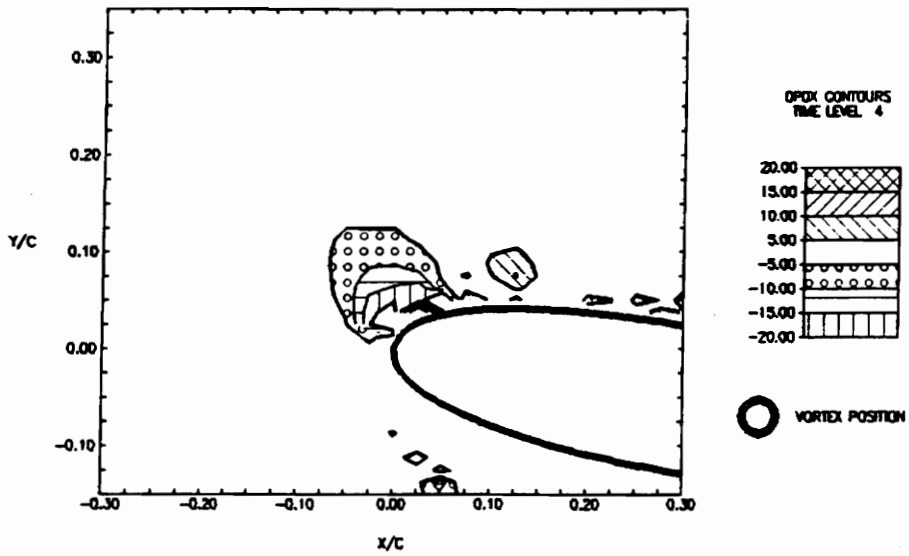


Figure 4.3.4 Pressure gradient contours, $\partial p/\partial x$ and $\partial p/\partial y$, at time level 4 (4/50 of period, $\tau=1.24$ sec.)

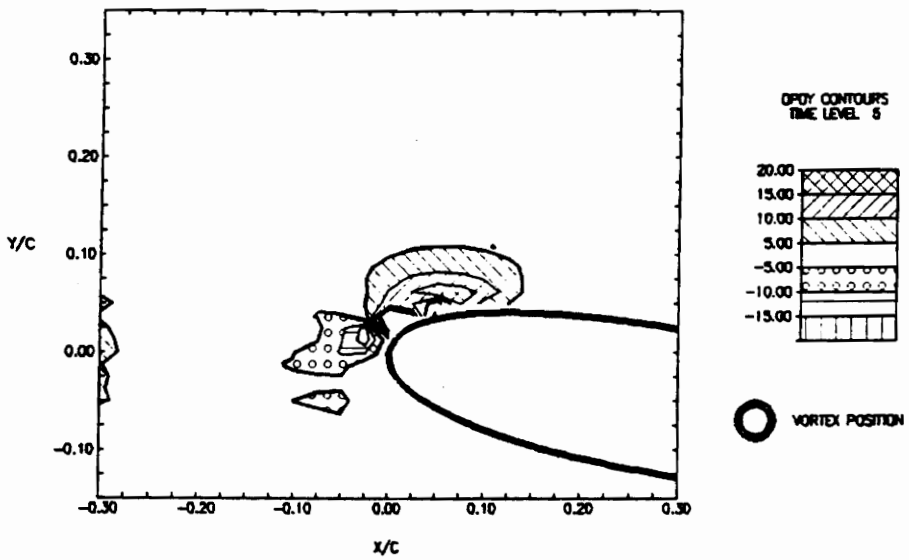
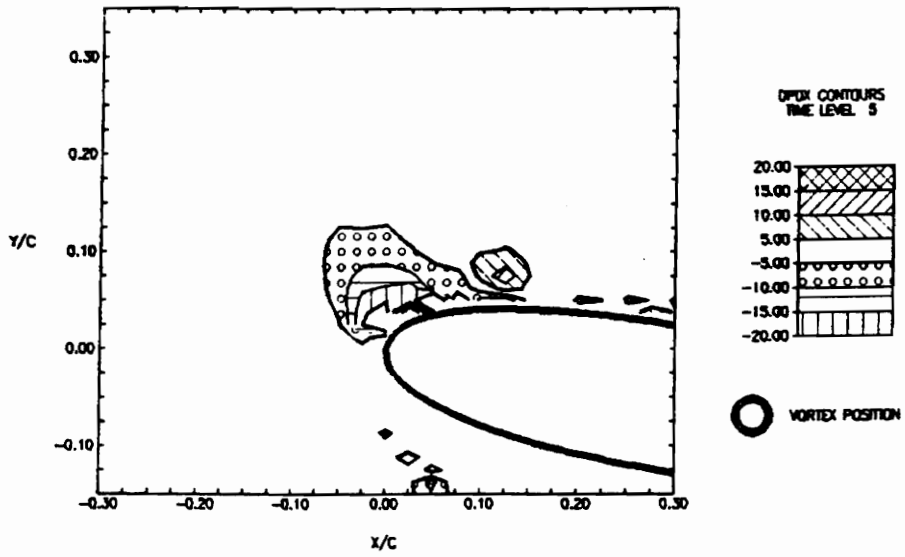


Figure 4.3.5 Pressure gradient contours, $\partial p/\partial x$ and $\partial p/\partial y$, at time level 5 (5/50 of period, $\tau=1.24$ sec.)

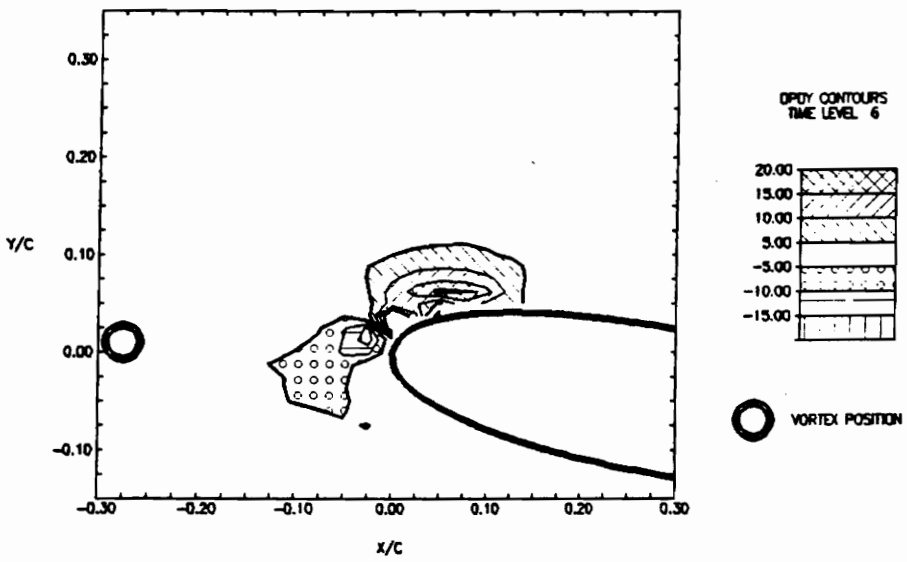
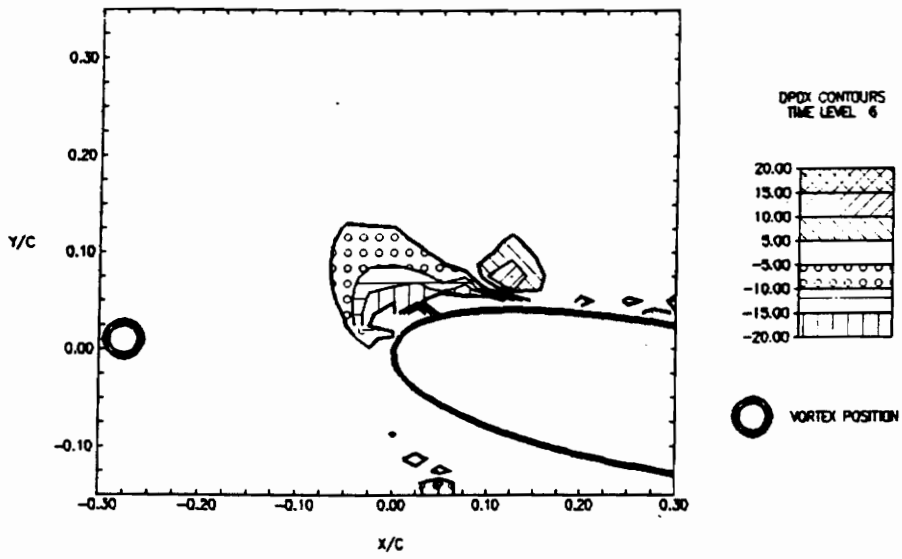


Figure 4.3.6 Pressure gradient contours, $\partial p/\partial x$ and $\partial p/\partial y$, at time level 6 (6/50 of period, $\tau=1.24$ sec.)

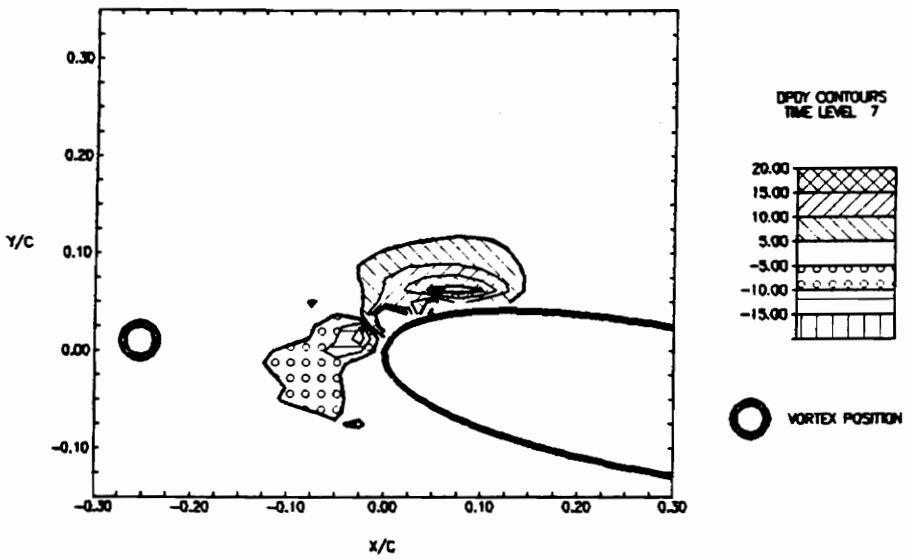
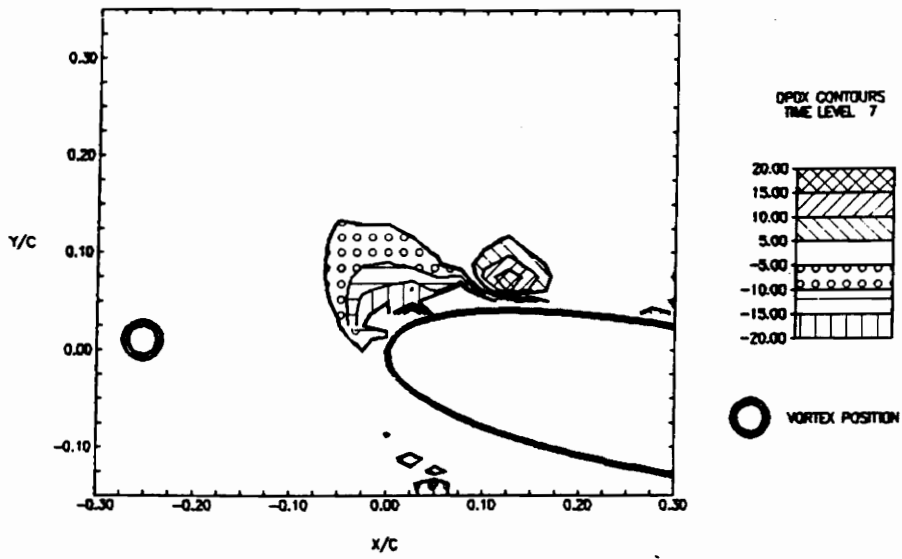


Figure 4.3.7 Pressure gradient contours, $\partial p/\partial x$ and $\partial p/\partial y$, at time level 7 (7/50 of period, $\tau=1.24$ sec.)

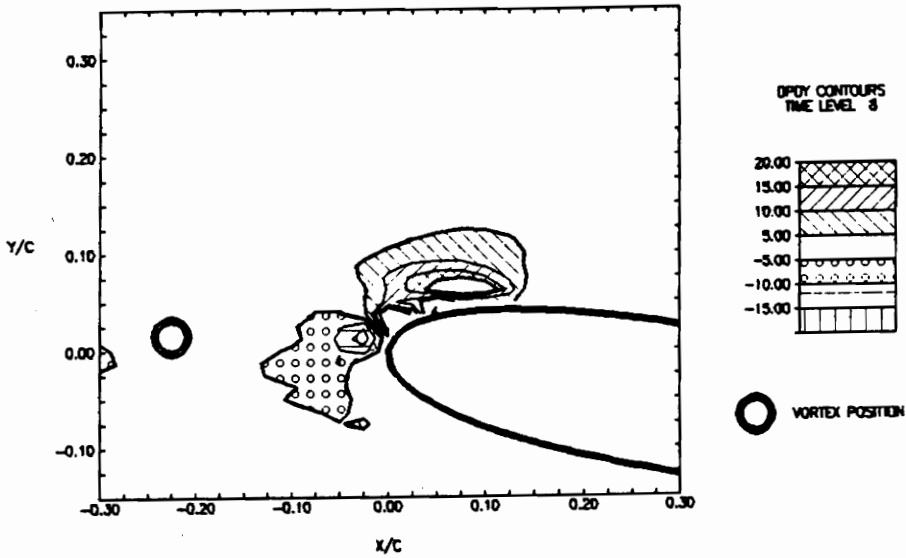
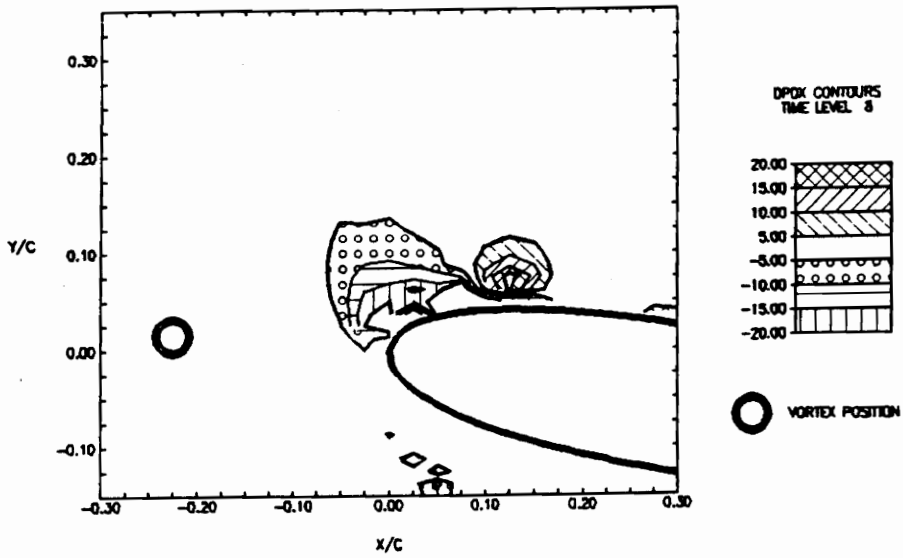


Figure 4.3.8 Pressure gradient contours, $\partial p/\partial x$ and $\partial p/\partial y$, at time level 8 (8/50 of period, $\tau=1.24$ sec.)

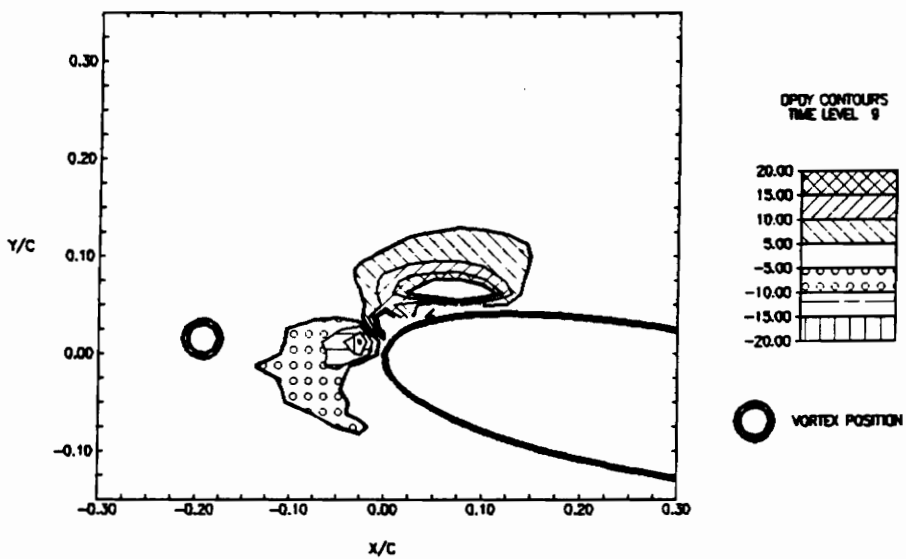
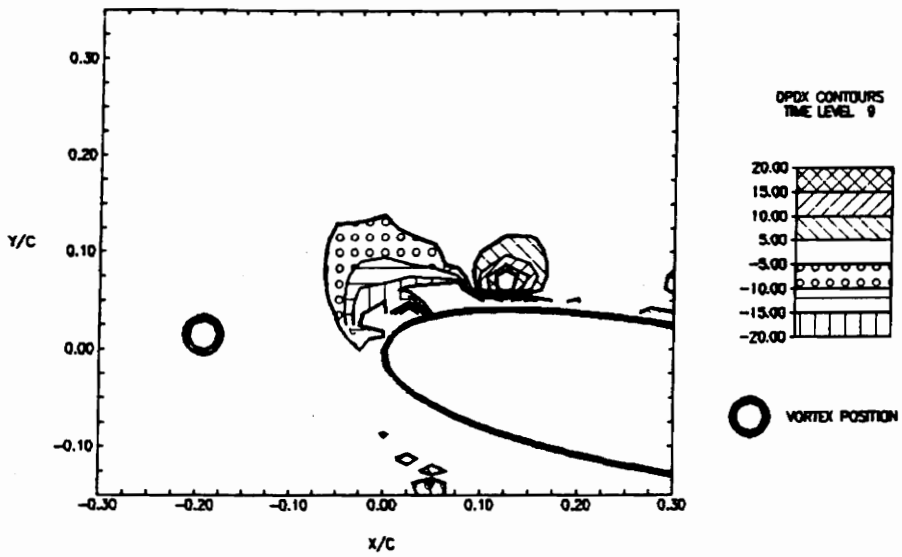


Figure 4.3.9 Pressure gradient contours, $\partial p/\partial x$ and $\partial p/\partial y$, at time level 9 (9/50 of period, $\tau=1.24$ sec.)

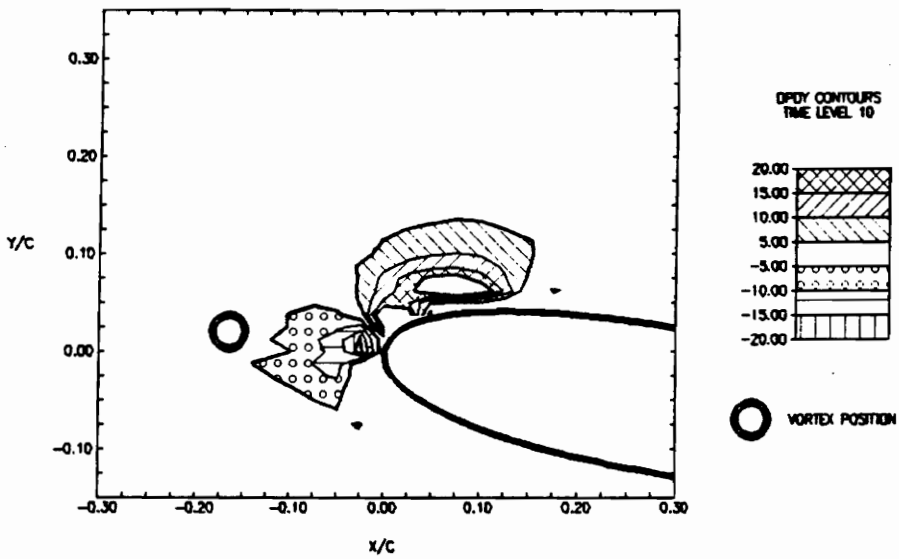
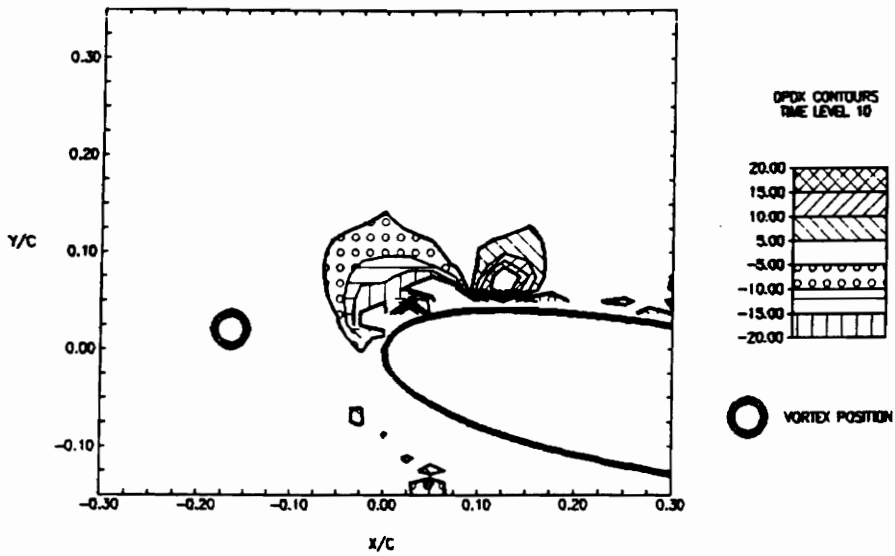


Figure 4.3.10 Pressure gradient contours, $\partial p/\partial x$ and $\partial p/\partial y$, at time level 10 (10/50 of period, $\tau=1.24$ sec.)

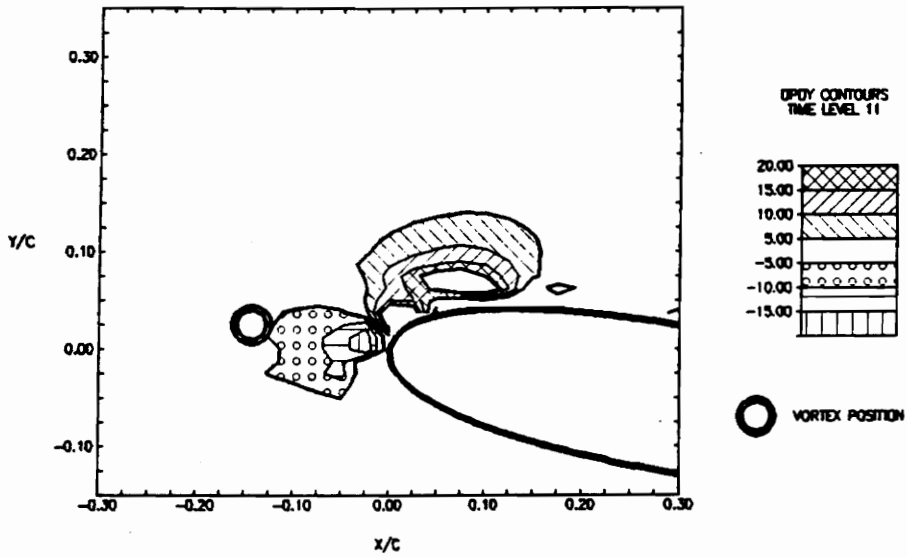
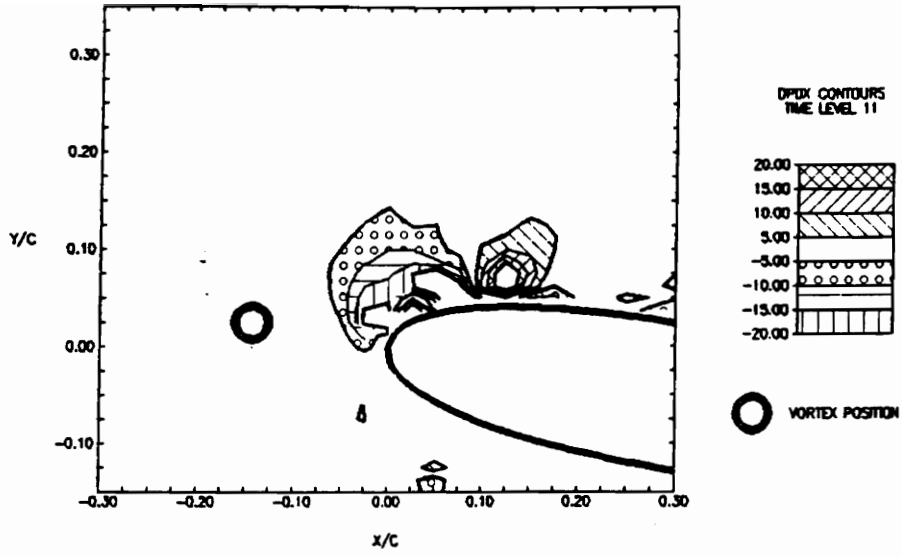


Figure 4.3.11 Pressure gradient contours, $\partial p/\partial x$ and $\partial p/\partial y$, at time level 11 (11/50 of period, $\tau=1.24$ sec.)

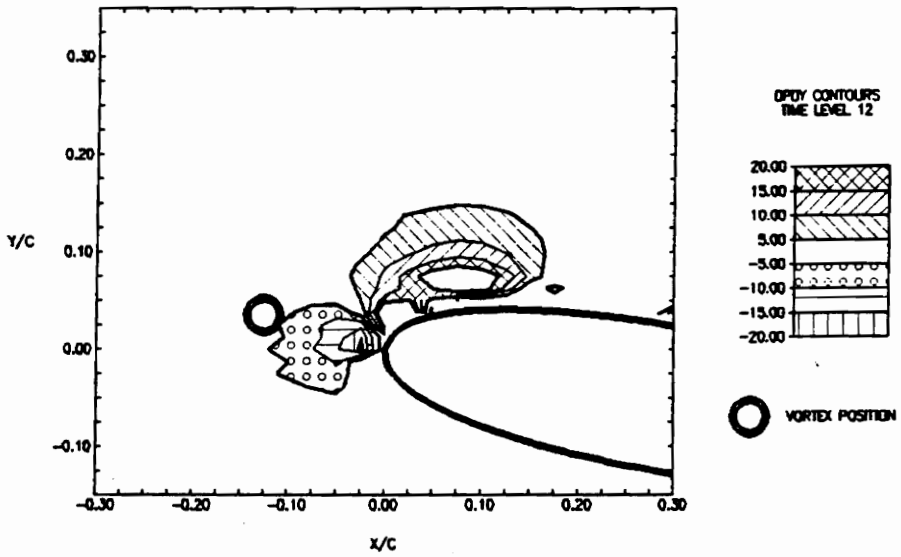
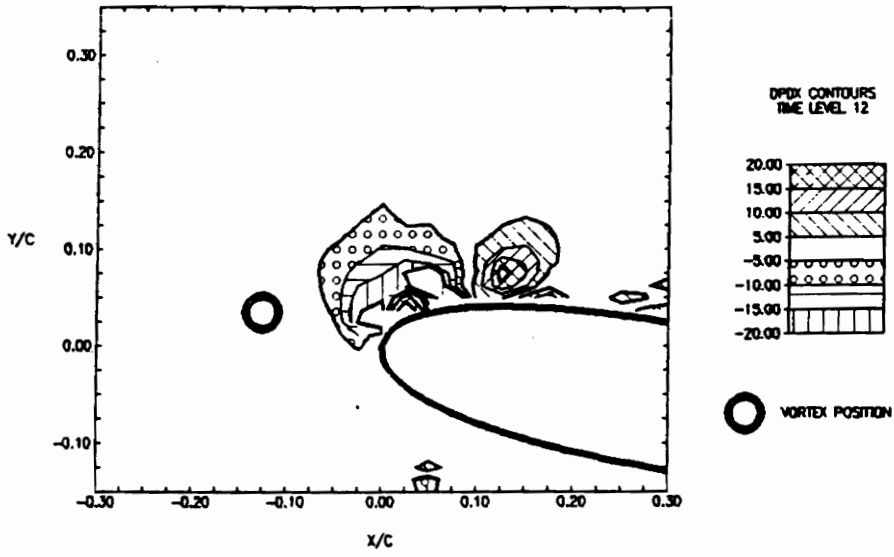


Figure 4.3.12 Pressure gradient contours, $\partial p/\partial x$ and $\partial p/\partial y$, at time level 12 (12/50 of period, $\tau=1.24$ sec.)

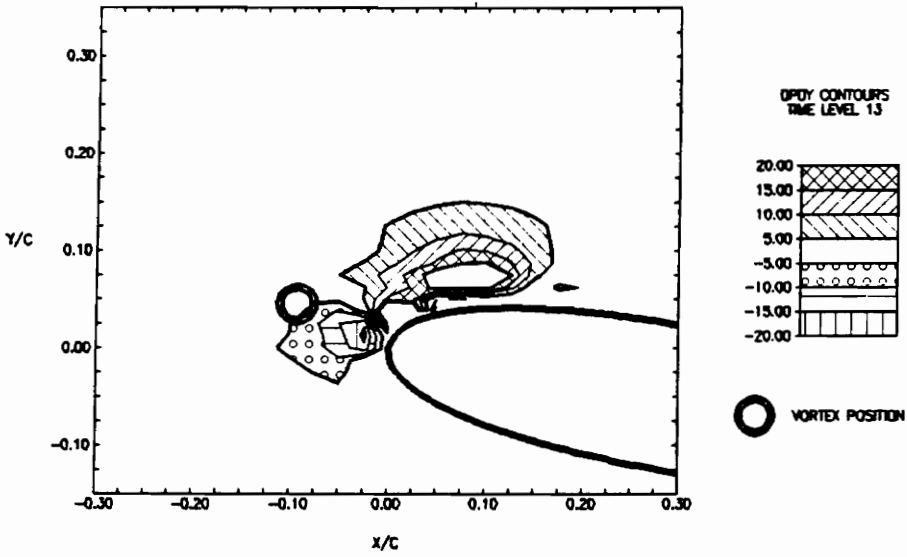
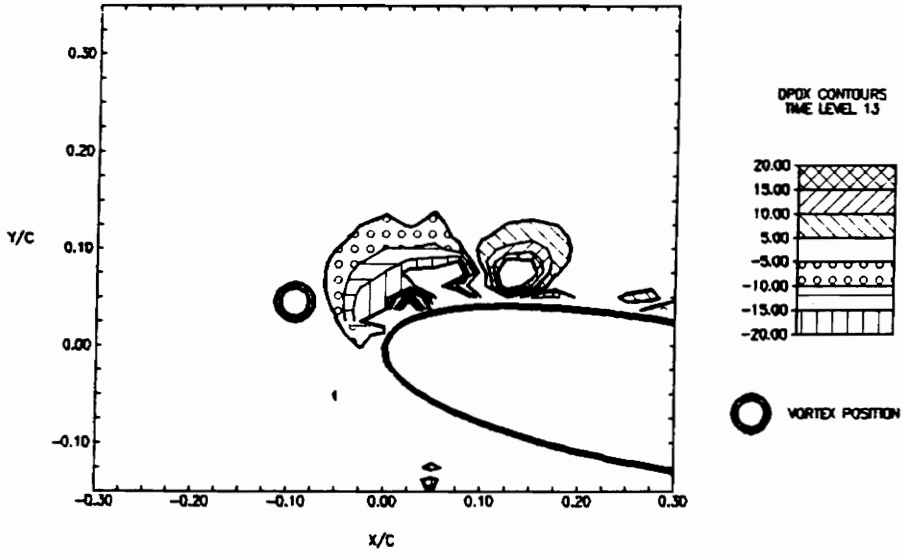


Figure 4.3.13 Pressure gradient contours, $\partial p/\partial x$ and $\partial p/\partial y$, at time level 13 (13/50 of period, $\tau=1.24$ sec.)

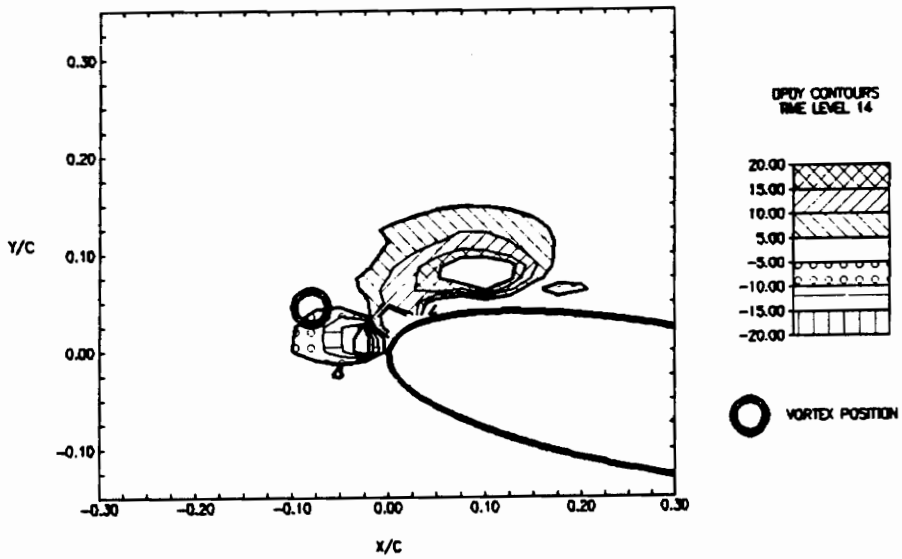
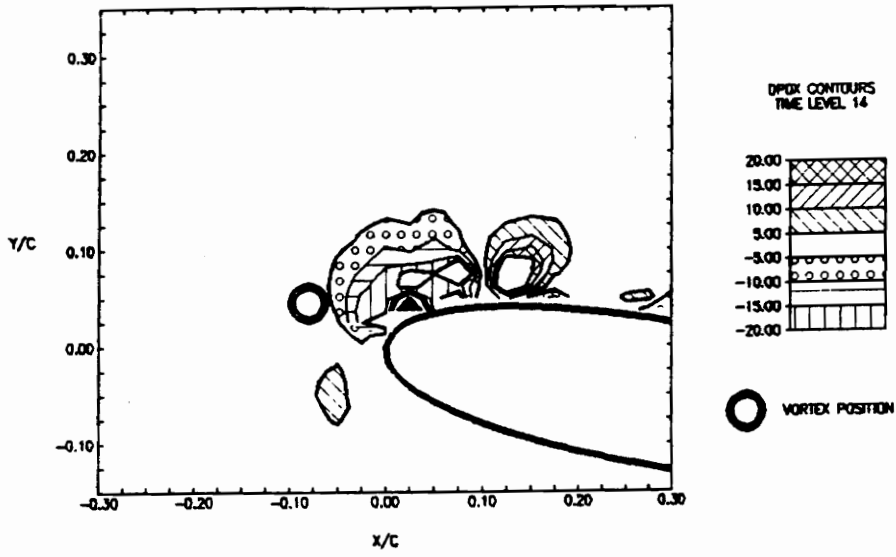


Figure 4.3.14 Pressure gradient contours, $\partial p/\partial x$ and $\partial p/\partial y$, at time level 14 (14/50 of period, $\tau=1.24$ sec.)

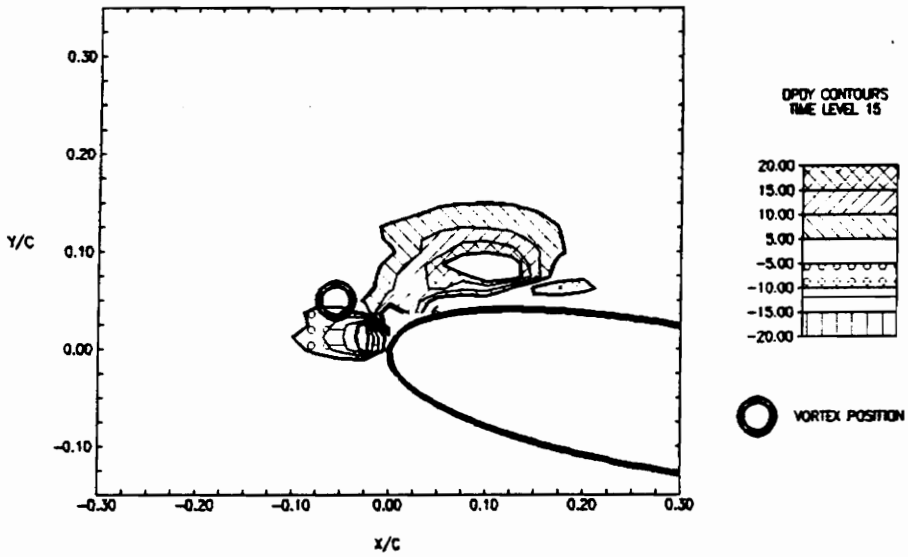
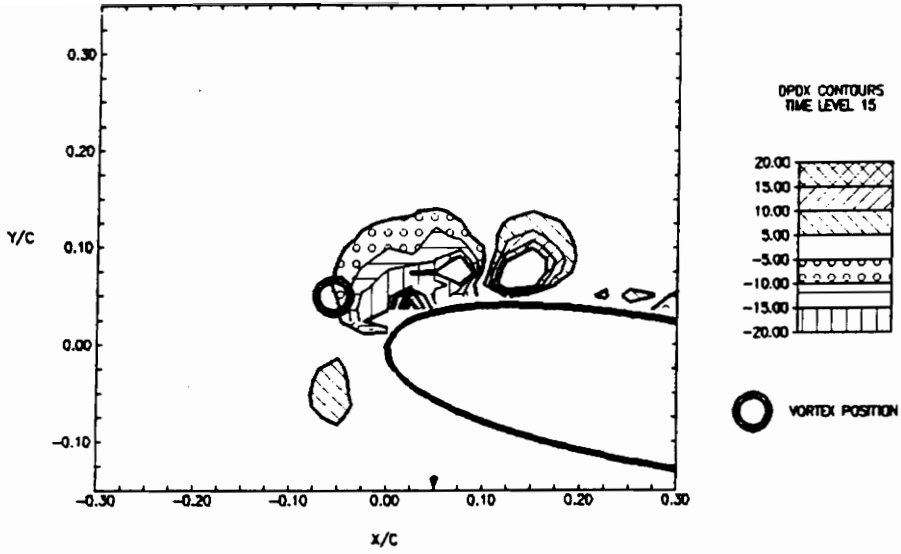


Figure 4.3.15 Pressure gradient contours, $\partial p/\partial x$ and $\partial p/\partial y$, at time level 15 (15/50 of period, $\tau=1.24$ sec.)

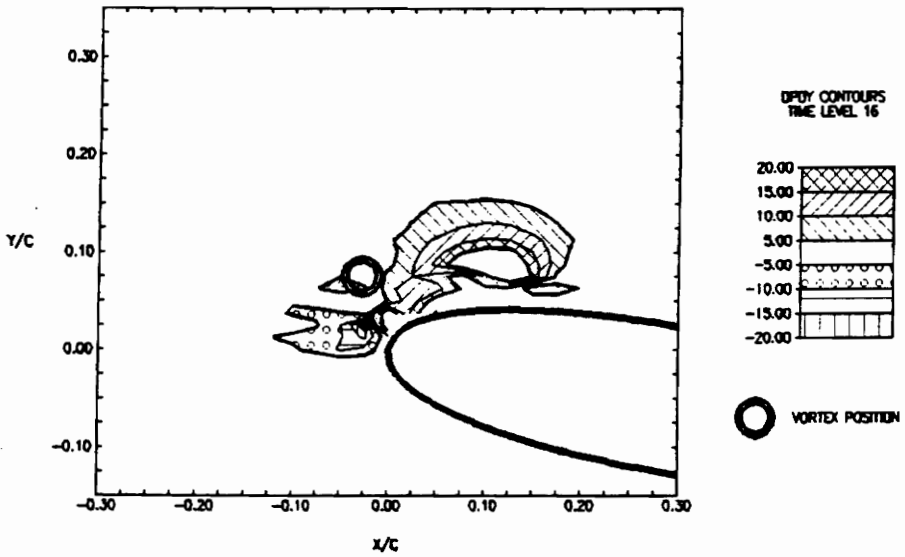
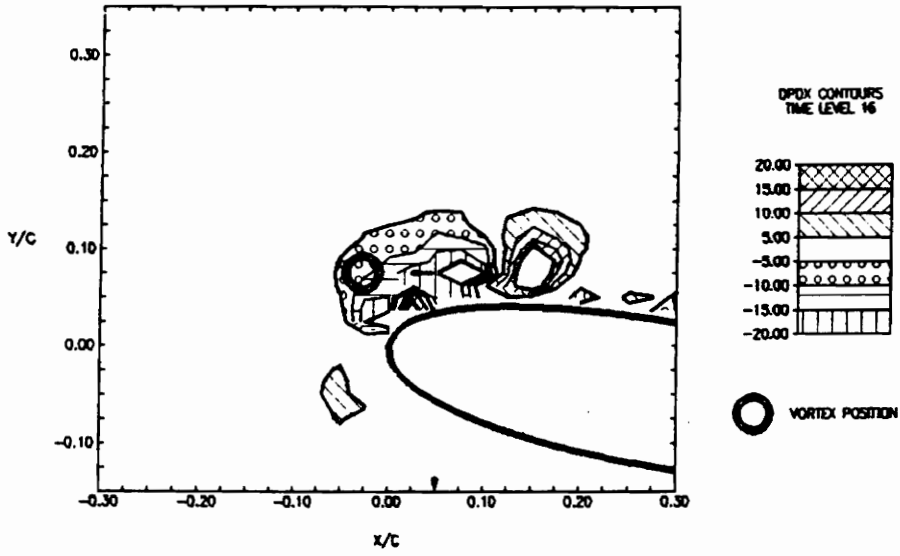


Figure 4.3.16 Pressure gradient contours, $\partial p/\partial x$ and $\partial p/\partial y$, at time level 16 (16/50 of period, $\tau=1.24$ sec.)

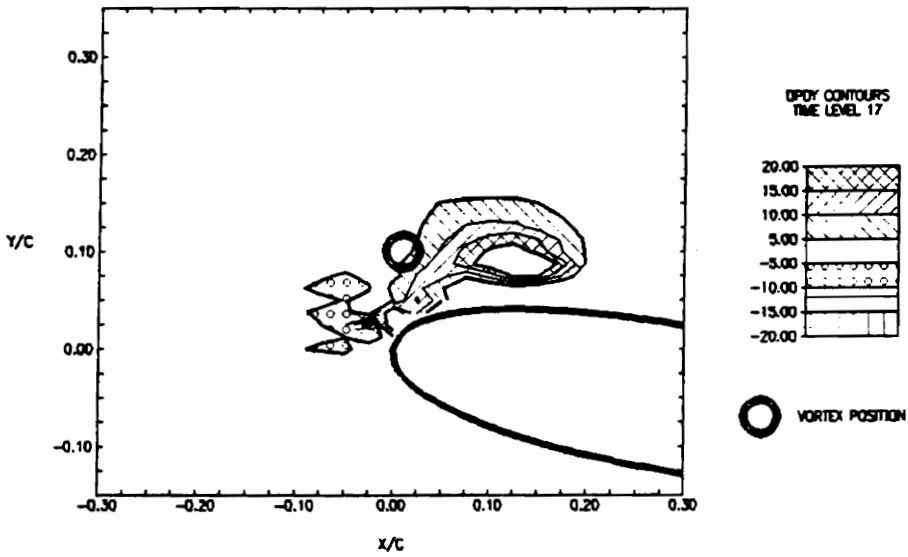
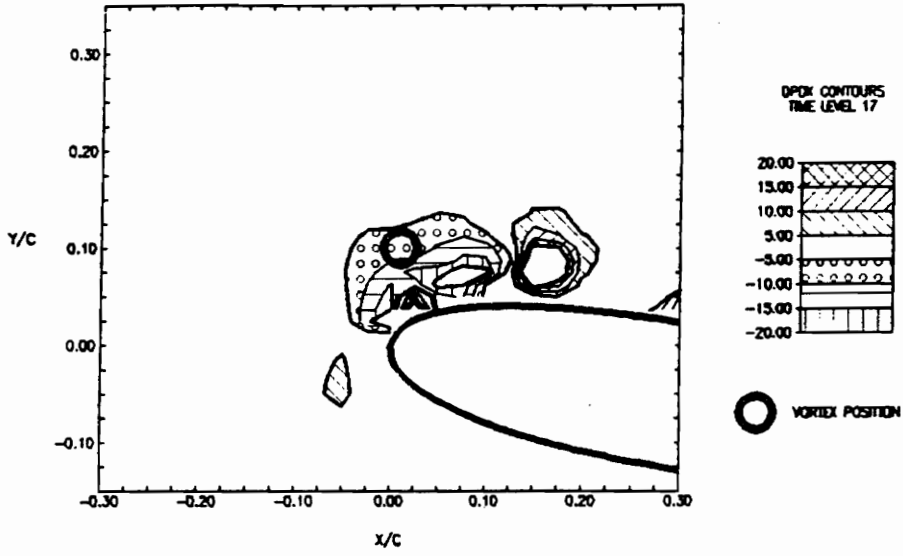


Figure 4.3.17 Pressure gradient contours, $\partial p / \partial x$ and $\partial p / \partial y$, at time level 17 (17/50 of period, $\tau = 1.24$ sec.)

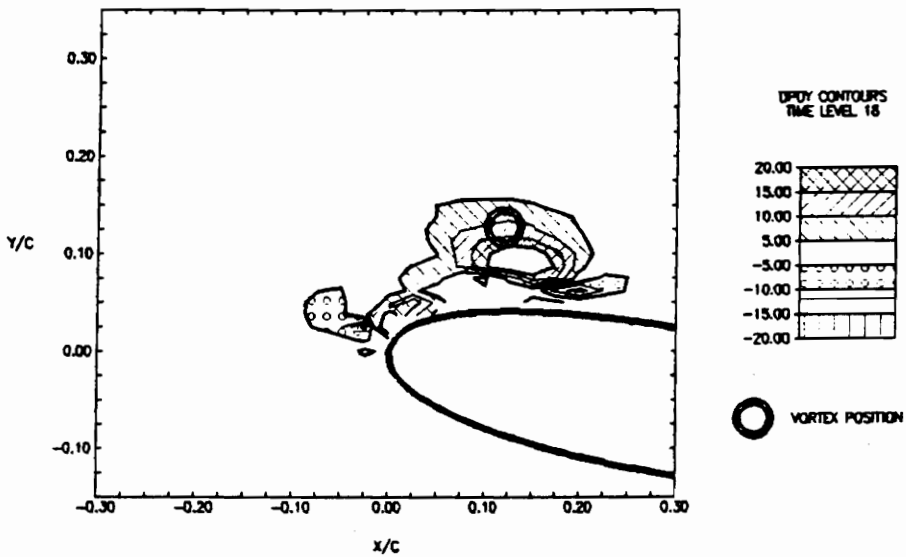
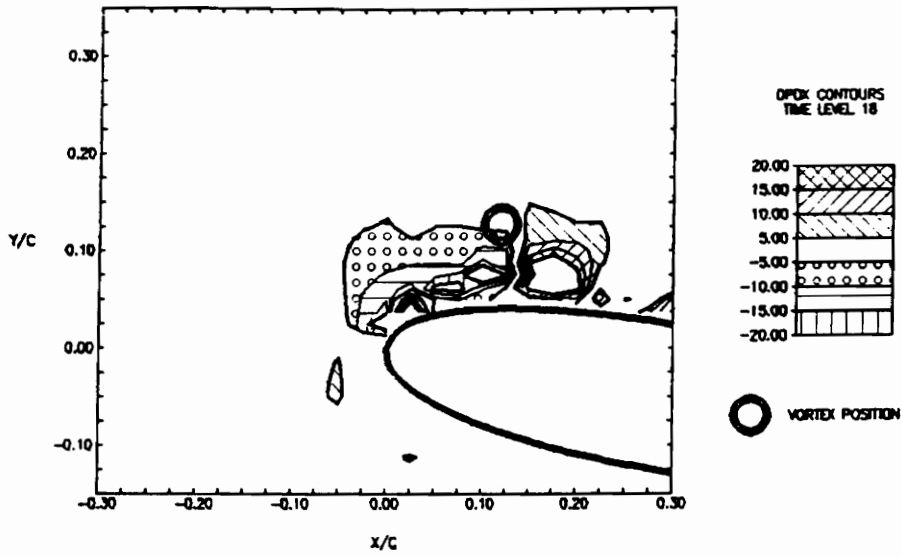


Figure 4.3.18 Pressure gradient contours, $\partial p/\partial x$ and $\partial p/\partial y$, at time level 18 (18/50 of period, $\tau=1.24$ sec.)

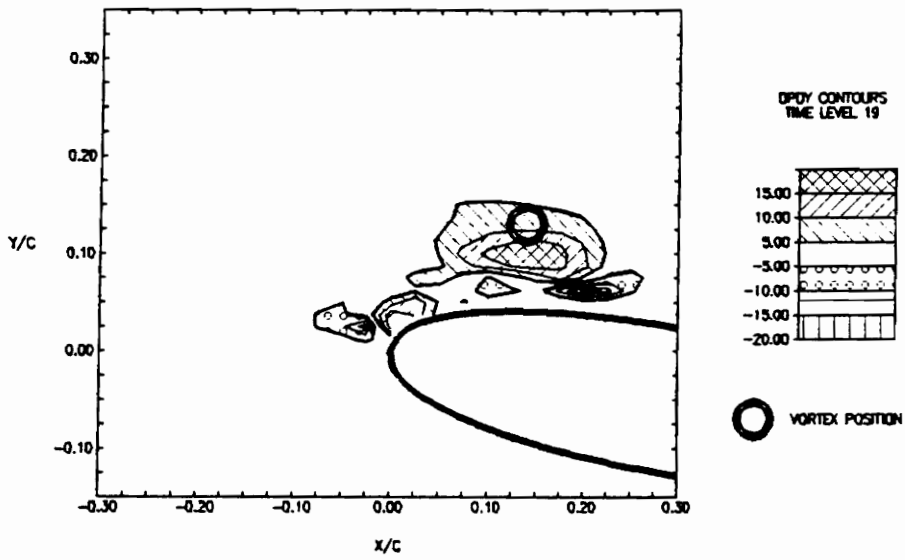
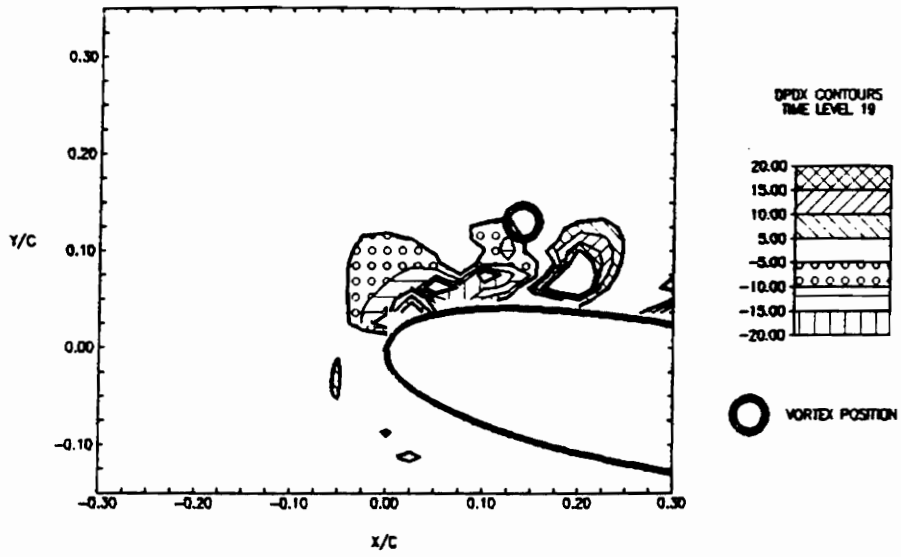


Figure 4.3.19 Pressure gradient contours, $\partial p/\partial x$ and $\partial p/\partial y$, at time level 19 (19/50 of period, $\tau=1.24$ sec.)

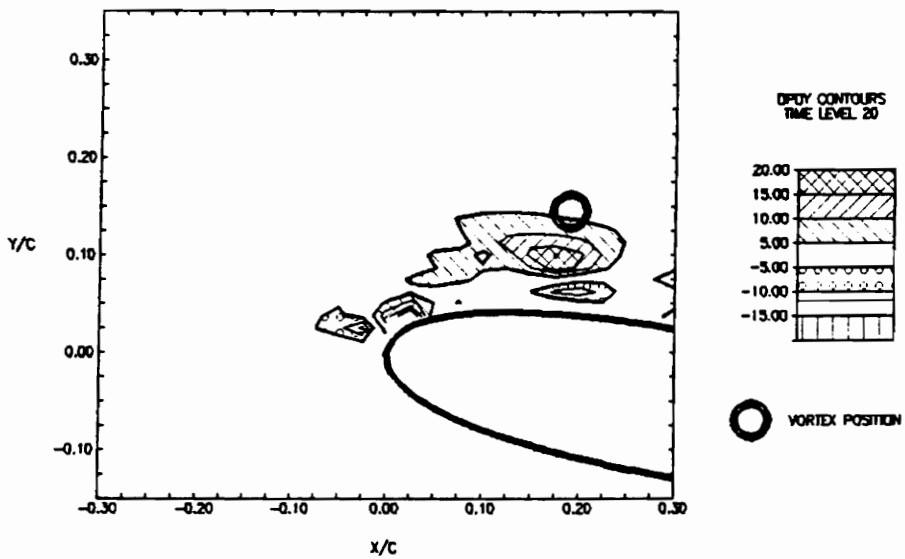
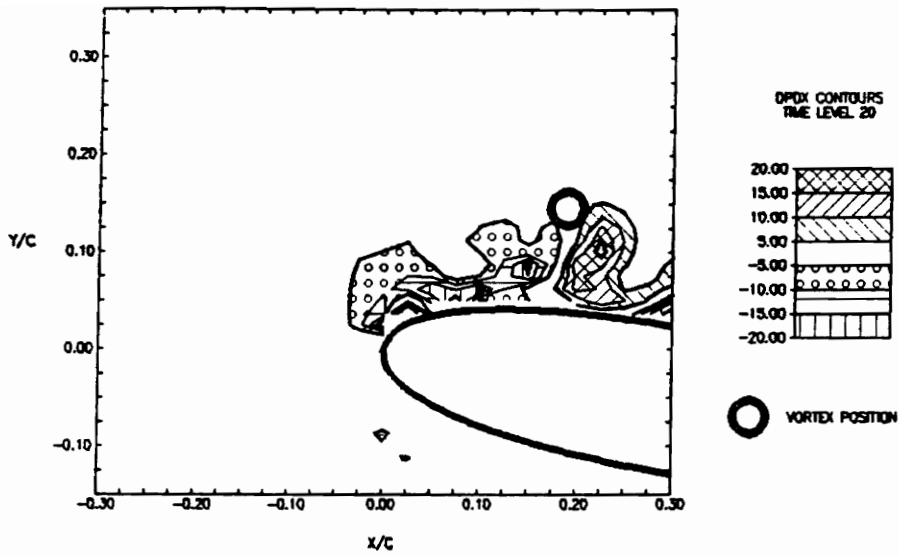


Figure 4.3.20 Pressure gradient contours, $\partial p/\partial x$ and $\partial p/\partial y$, at time level 20 (20/50 of period, $\tau=1.24$ sec.)

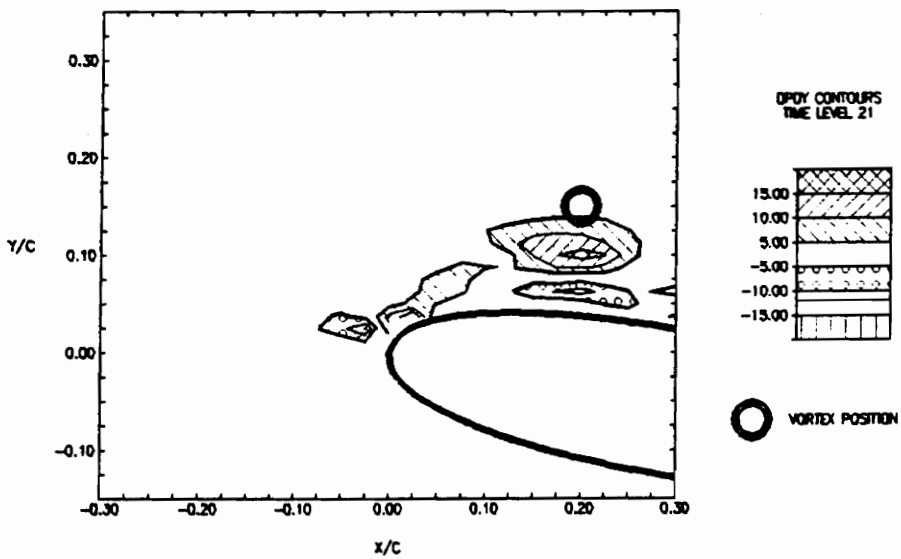
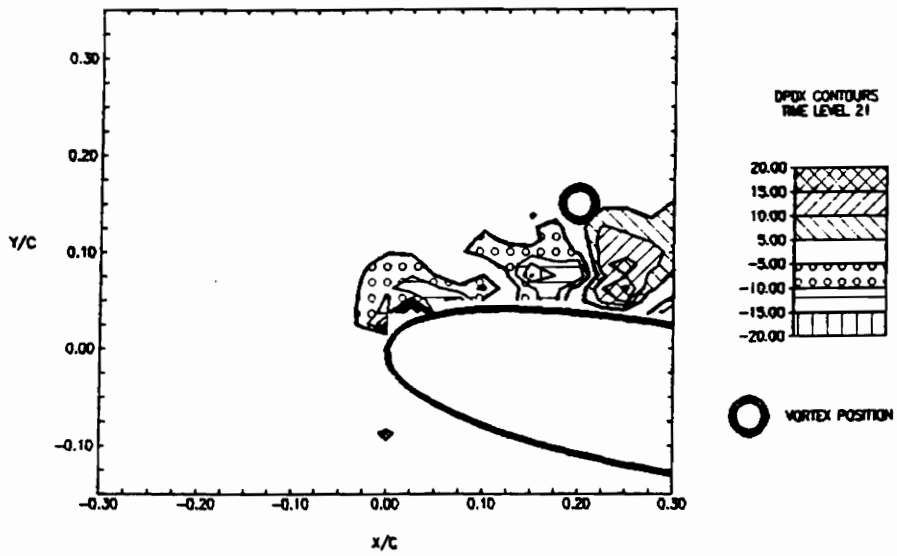


Figure 4.3.21 Pressure gradient contours, $\partial p/\partial x$ and $\partial p/\partial y$, at time level 21 (21/50 of period, $\tau=1.24$ sec.)

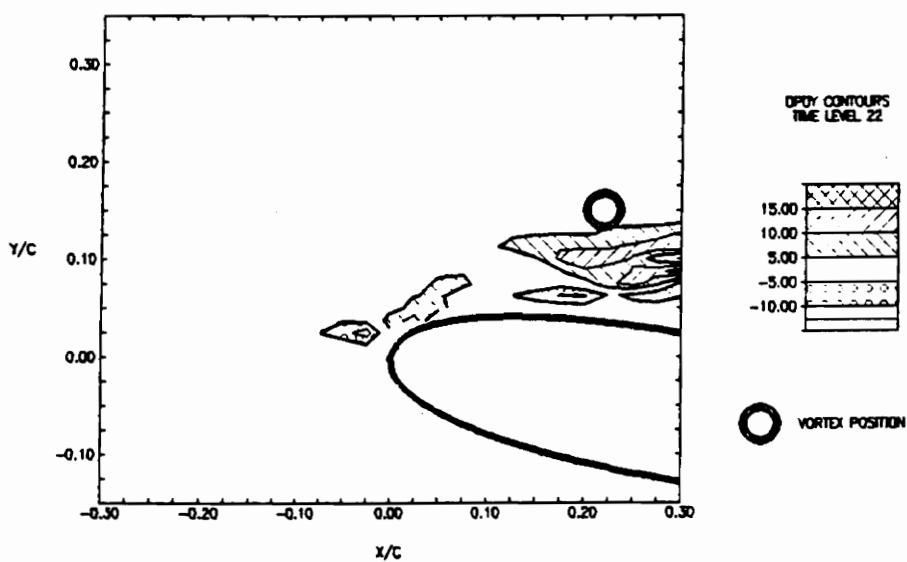
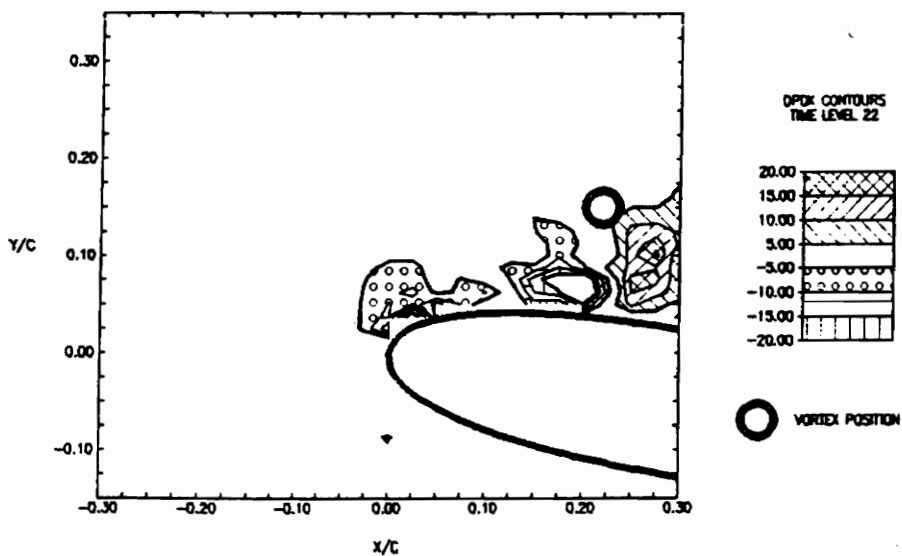


Figure 4.3.22 Pressure gradient contours, $\partial p/\partial x$ and $\partial p/\partial y$, at time level 22 (22/50 of period, $\tau=1.24$ sec.)

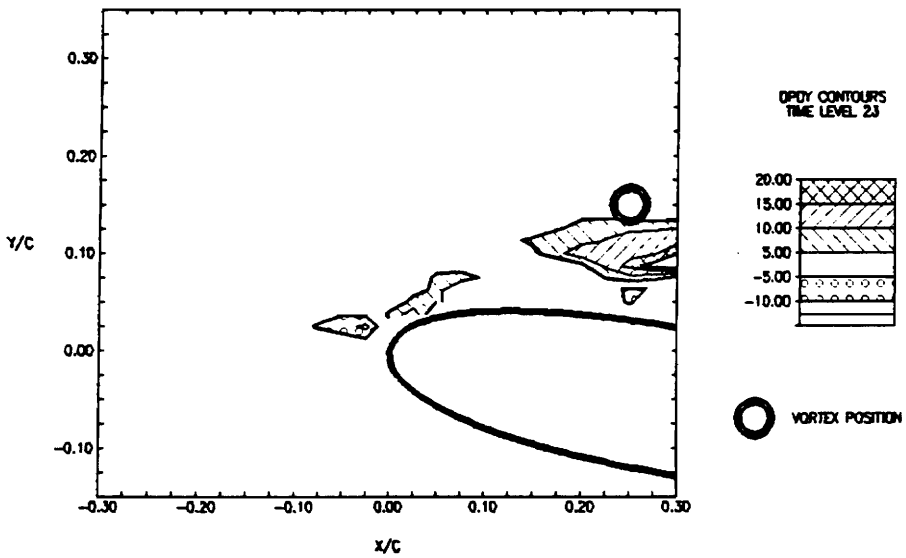
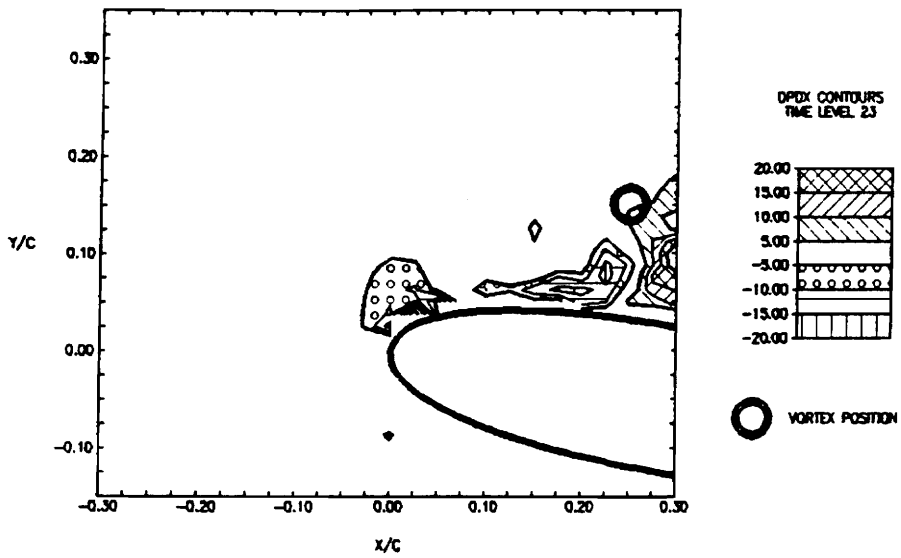


Figure 4.3.23 Pressure gradient contours, $\partial p/\partial x$ and $\partial p/\partial y$, at time level 23 (23/50 of period, $\tau=1.24$ sec.)

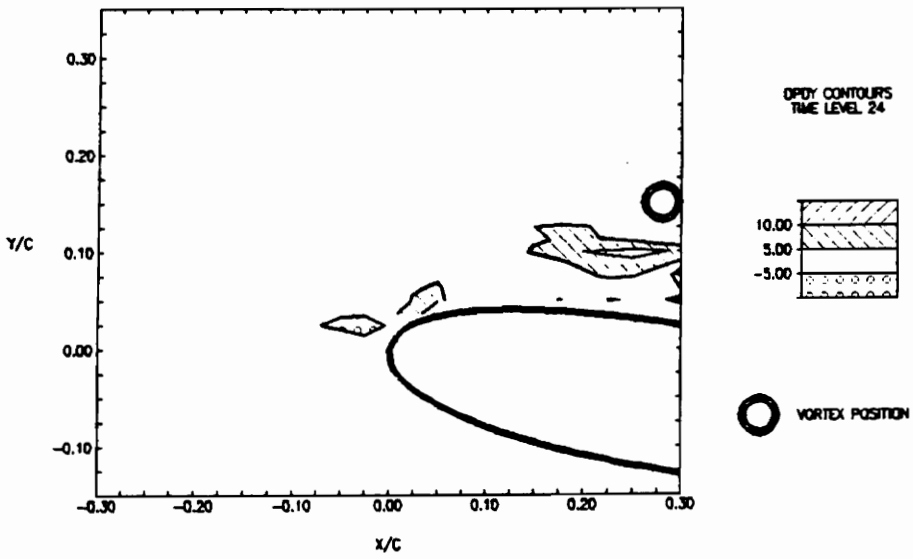
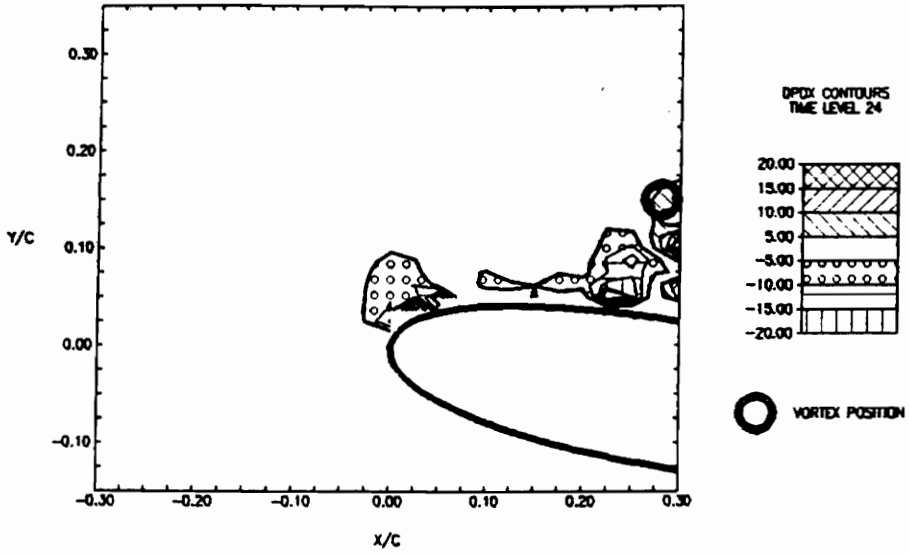


Figure 4.3.24 Pressure gradient contours, $\partial p/\partial x$ and $\partial p/\partial y$, at time level 24 (24/50 of period, $\tau=1.24$ sec.)

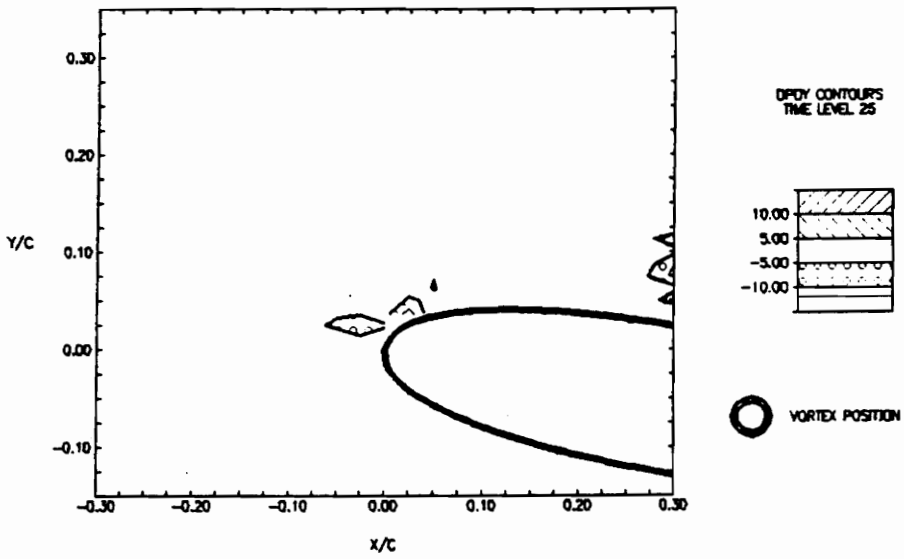
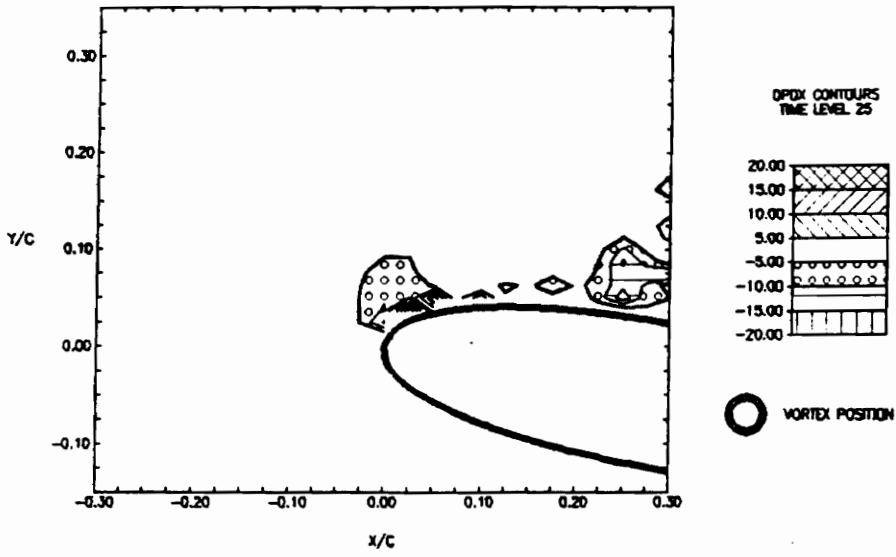


Figure 4.3.25 Pressure gradient contours, $\partial p/\partial x$ and $\partial p/\partial y$, at time level 25 (25/50 of period, $\tau=1.24$ sec.)

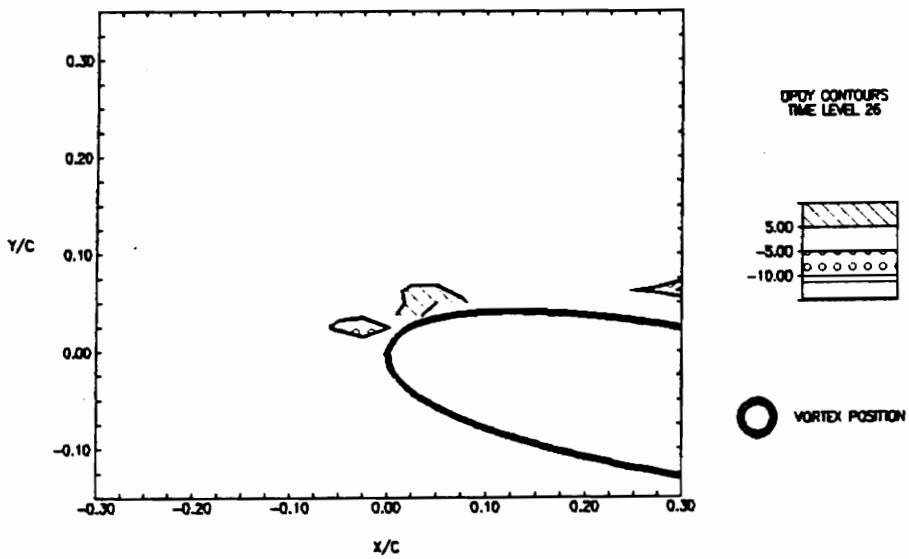
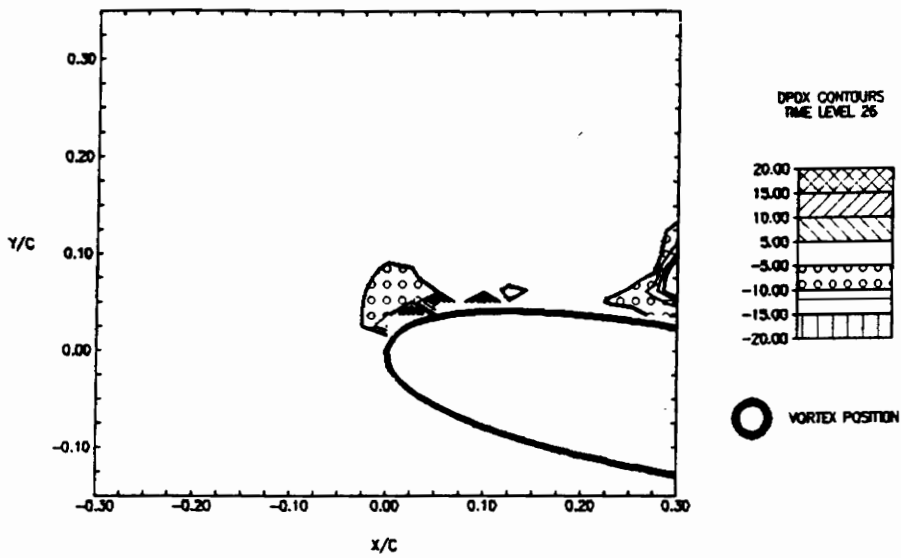


Figure 4.3.26 Pressure gradient contours, $\partial p/\partial x$ and $\partial p/\partial y$, at time level 26 (26/50 of period, $\tau=1.24$ sec.)

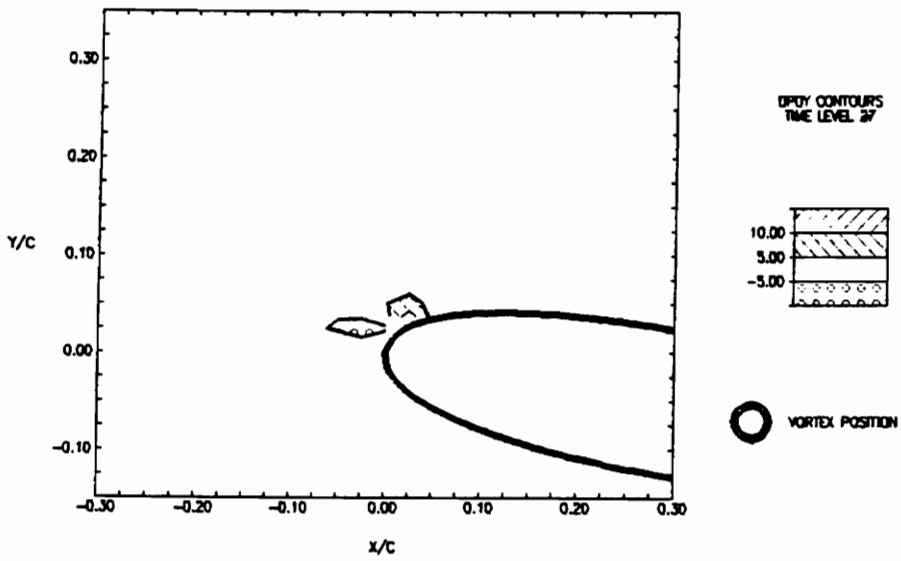
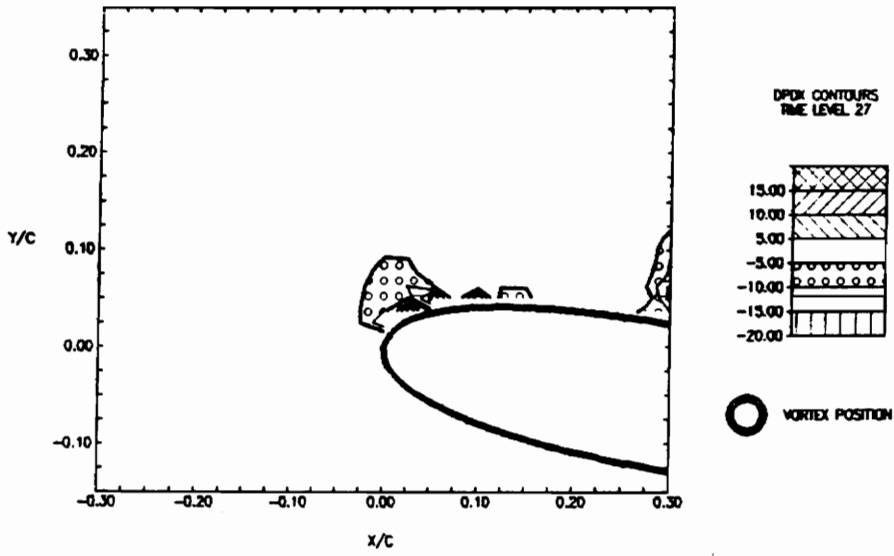


Figure 4.3.27 Pressure gradient contours, $\partial p/\partial x$ and $\partial p/\partial y$, at time level 27 (27/50 of period, $\tau=1.24$ sec.)

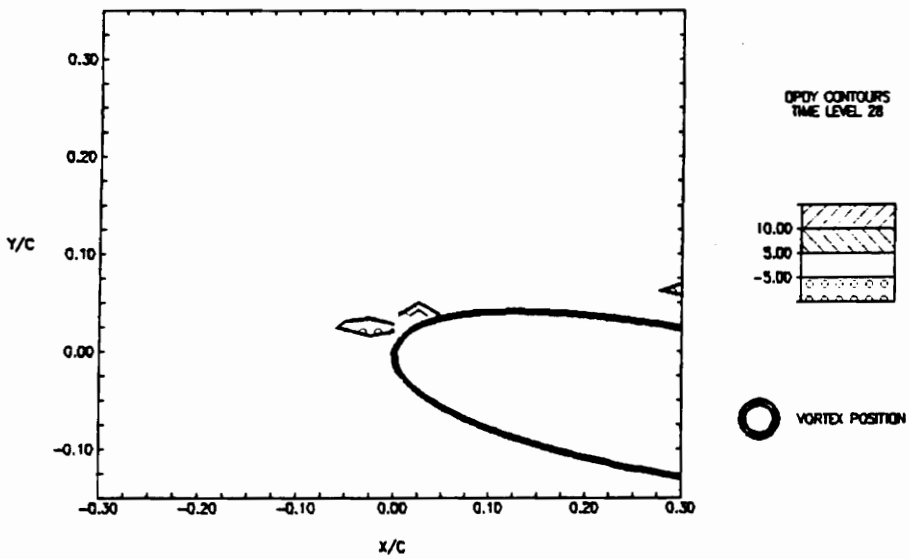
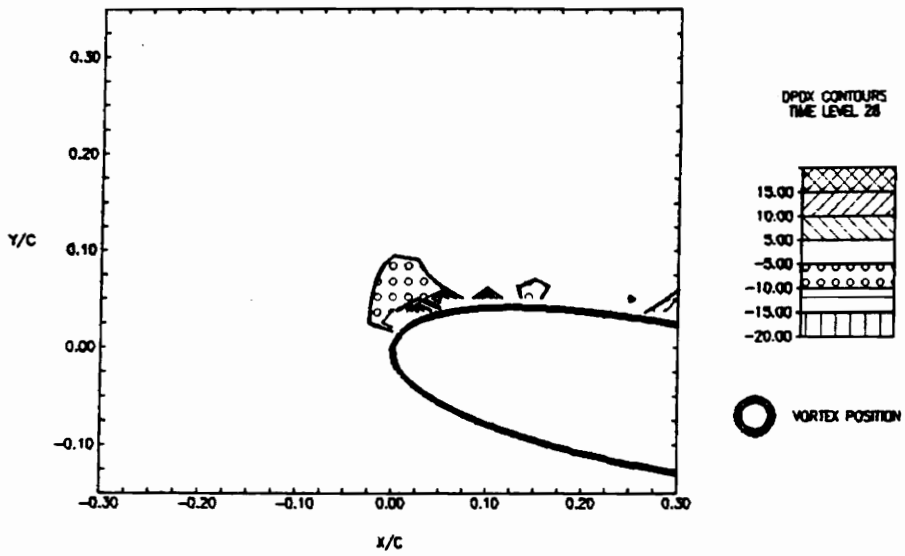


Figure 4.3.28 Pressure gradient contours, $\partial p/\partial x$ and $\partial p/\partial y$, at time level 28 (28/50 of period, $\tau=1.24$ sec.)

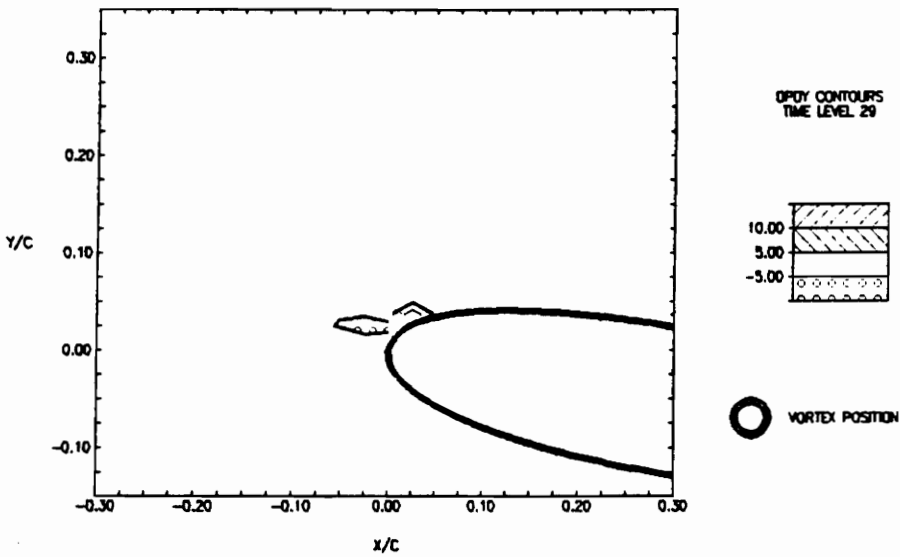
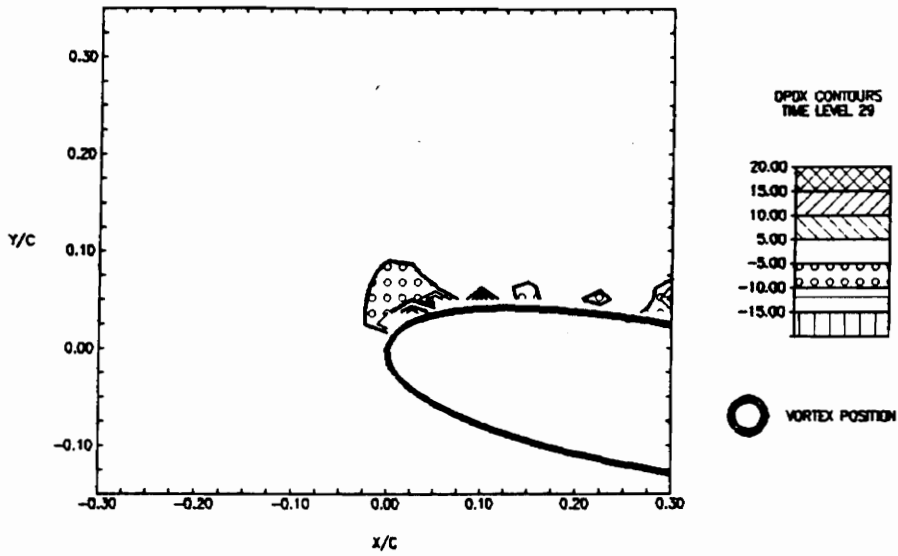


Figure 4.3.29 Pressure gradient contours, $\partial p/\partial x$ and $\partial p/\partial y$, at time level 29 (29/50 of period, $\tau=1.24$ sec.)

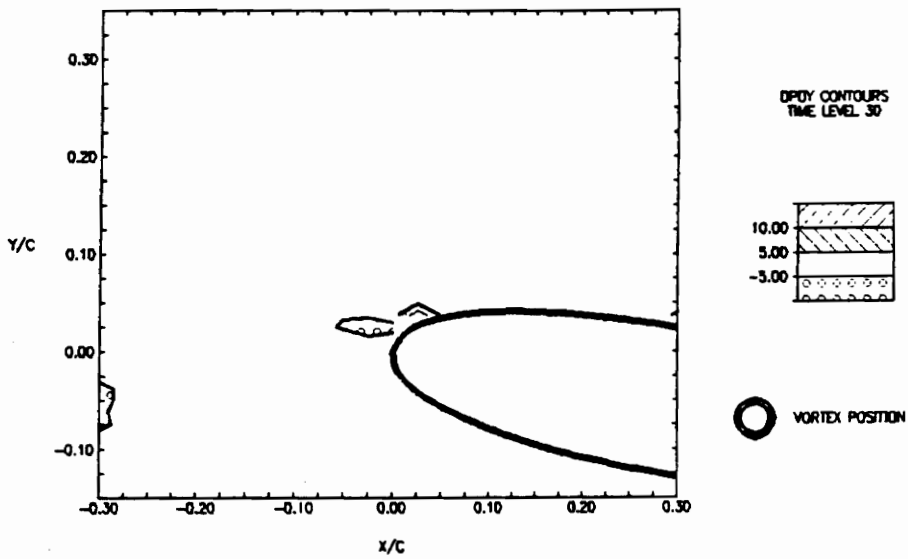
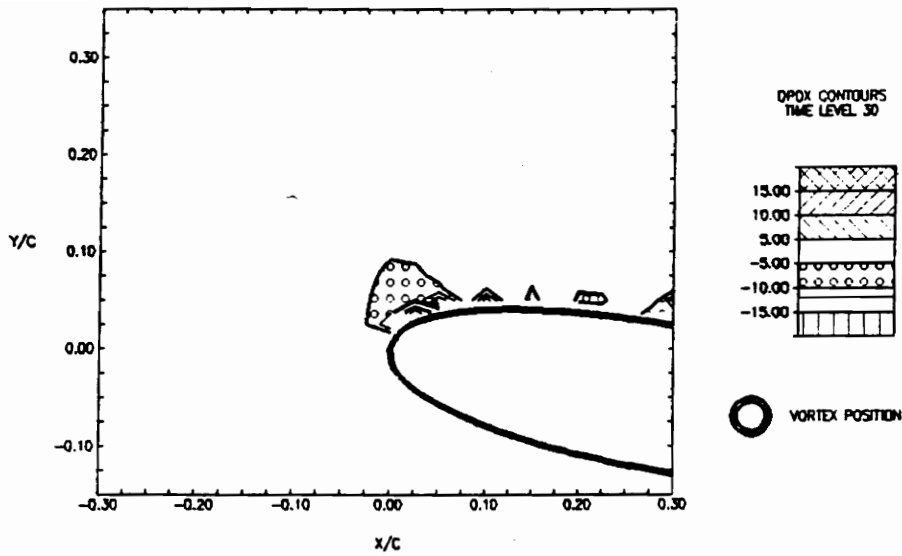


Figure 4.3.30 Pressure gradient contours, $\partial p/\partial x$ and $\partial p/\partial y$, at time level 30 (30/50 of period, $\tau=1.24$ sec.)

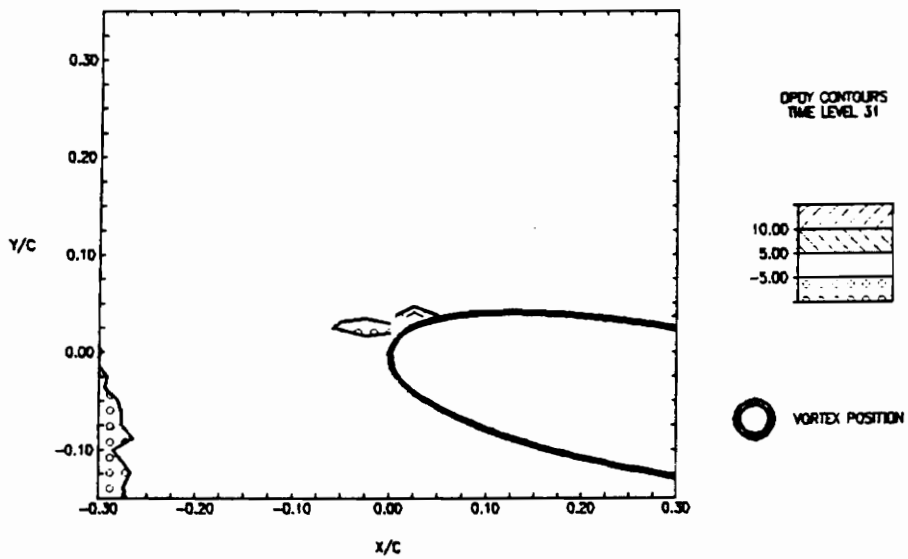
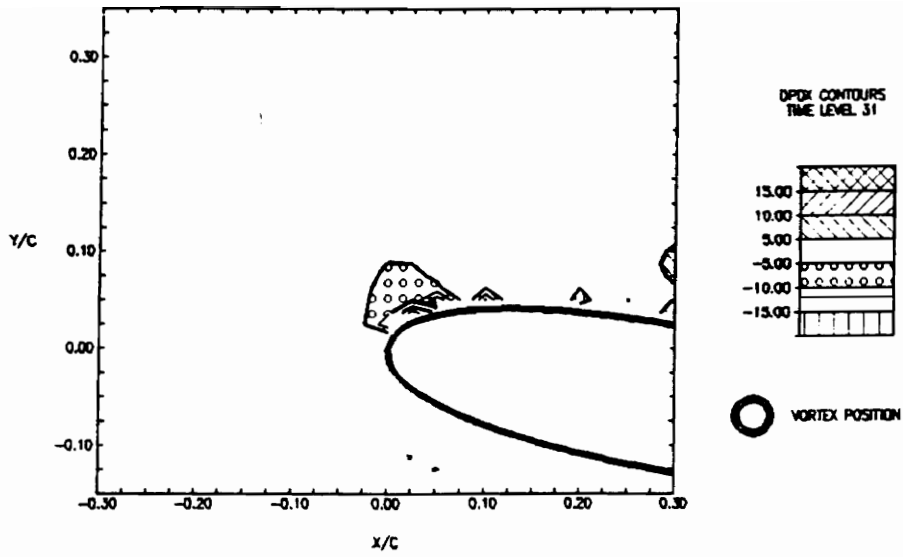


Figure 4.3.31 Pressure gradient contours, $\partial p/\partial x$ and $\partial p/\partial y$, at time level 31 (31/50 of period, $\tau=1.24$ sec.)

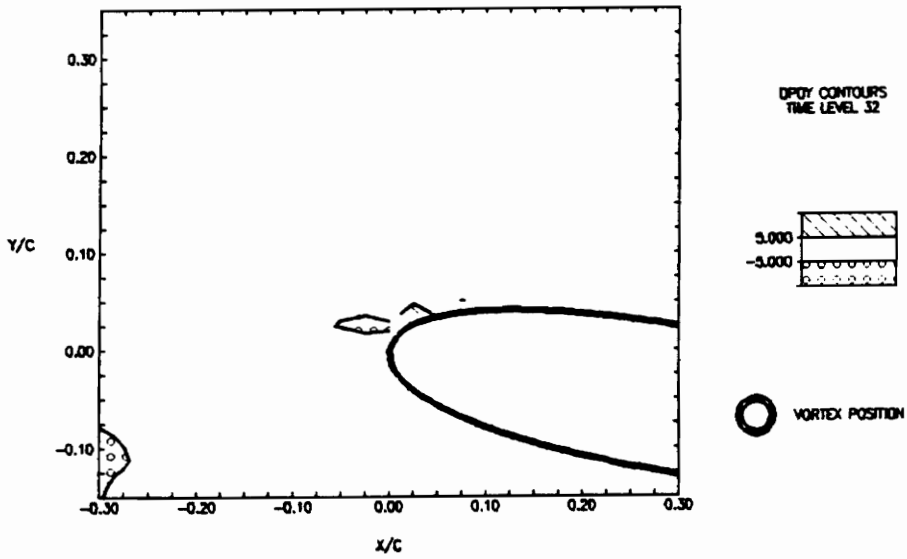
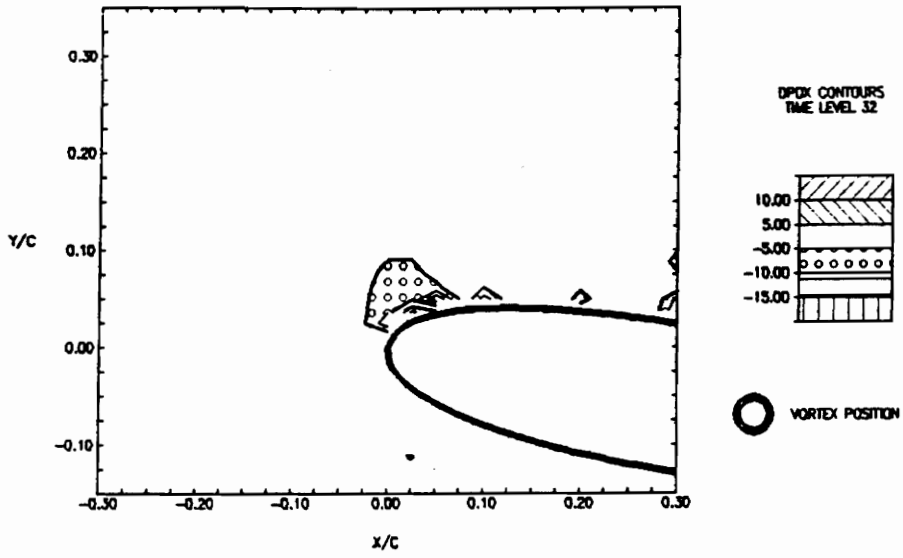


Figure 4.3.32 Pressure gradient contours, $\partial p/\partial x$ and $\partial p/\partial y$, at time level 32 (32/50 of period, $\tau=1.24$ sec.)

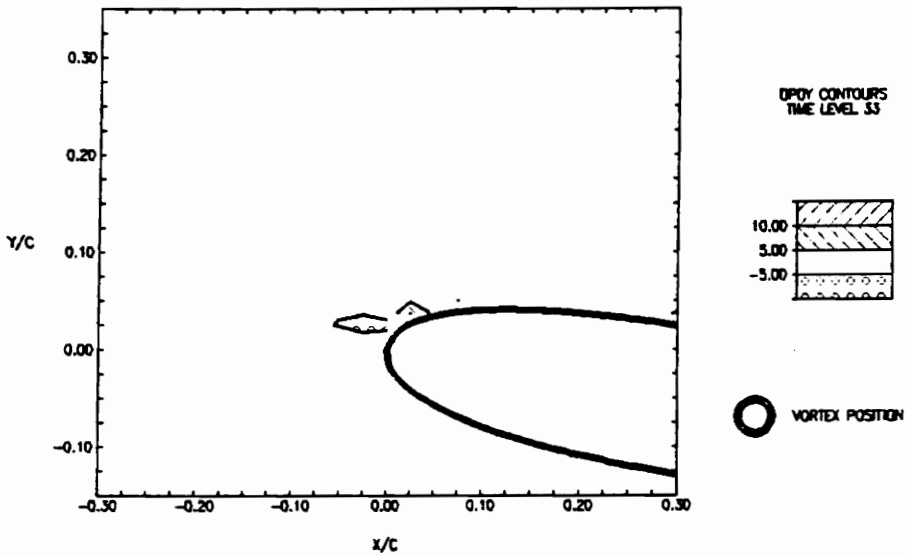
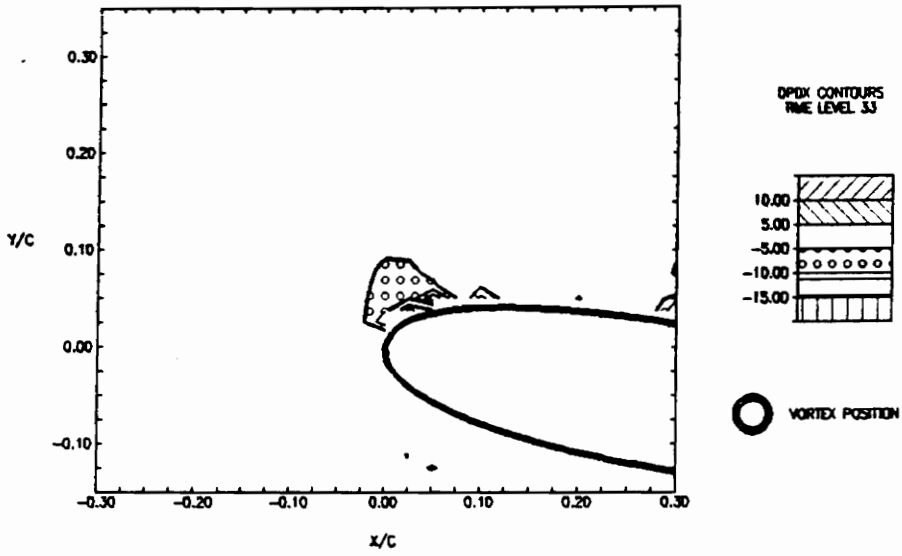


Figure 4.3.33 Pressure gradient contours, $\partial p / \partial x$ and $\partial p / \partial y$, at time level 33 (33/50 of period, $\tau=1.24$ sec.)

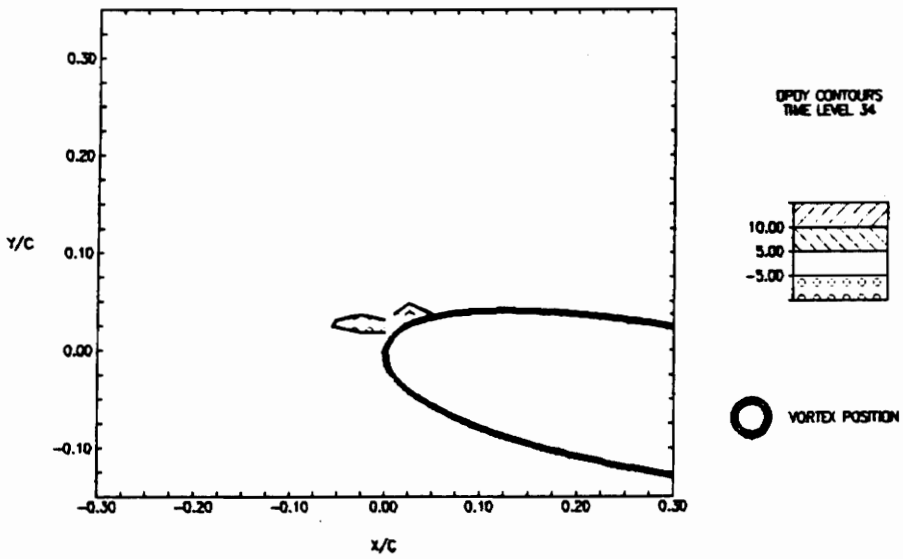
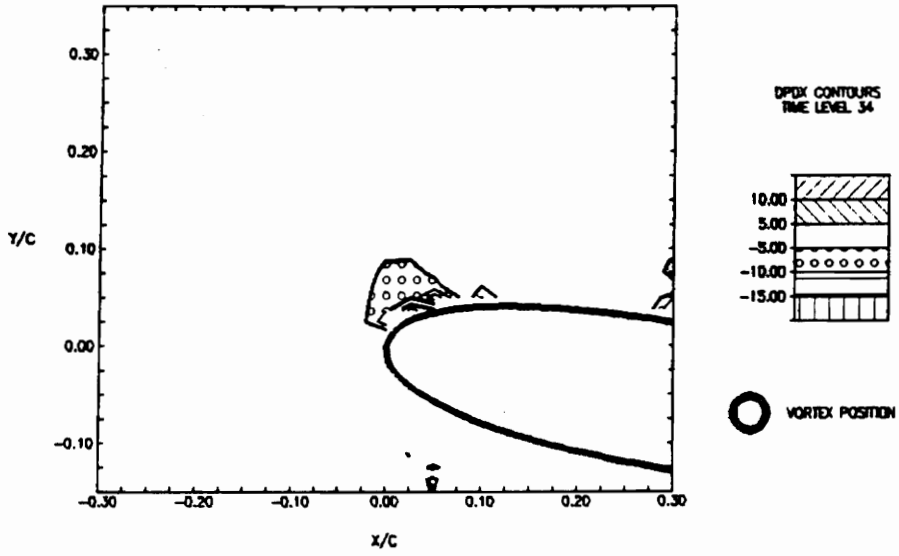


Figure 4.3.34 Pressure gradient contours, $\partial p / \partial x$ and $\partial p / \partial y$, at time level 34 (34/50 of period, $\tau = 1.24$ sec.)

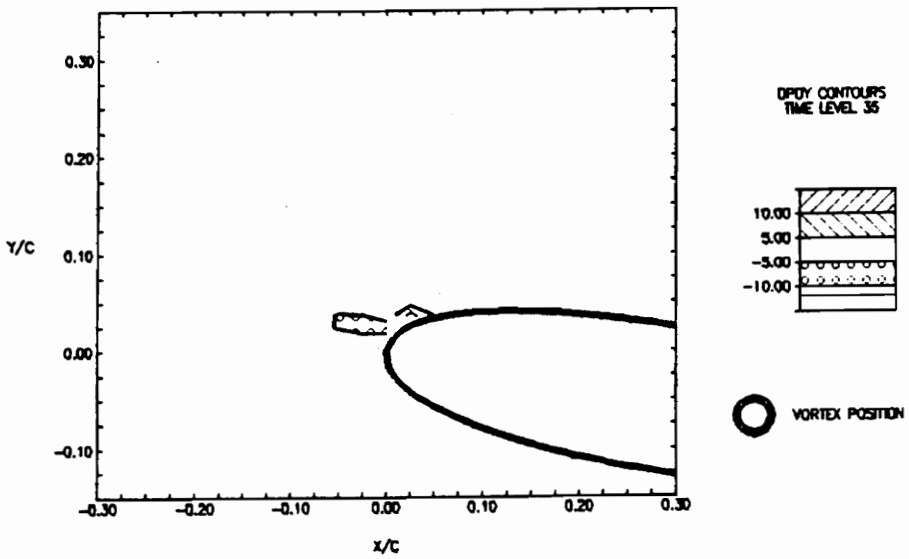
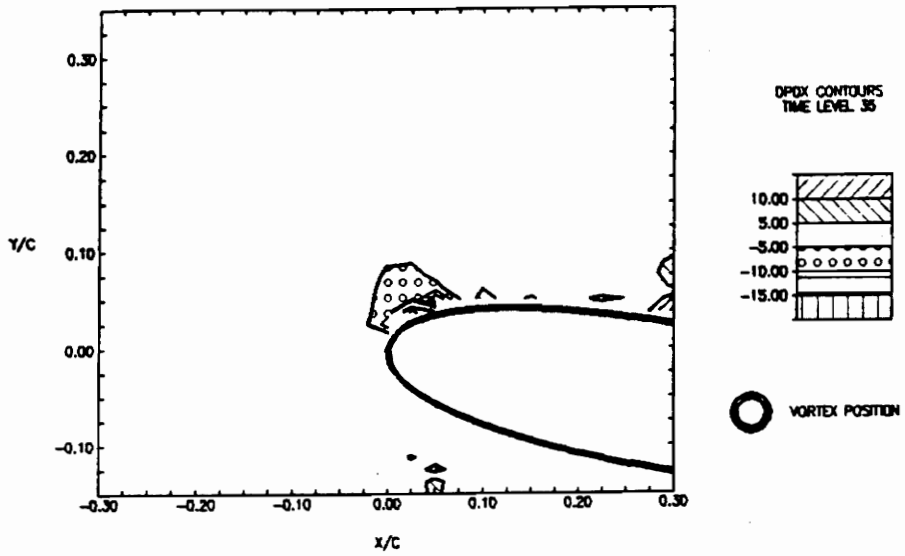


Figure 4.3.35 Pressure gradient contours, $\partial p/\partial x$ and $\partial p/\partial y$, at time level 35 (35/50 of period, $\tau=1.24$ sec.)

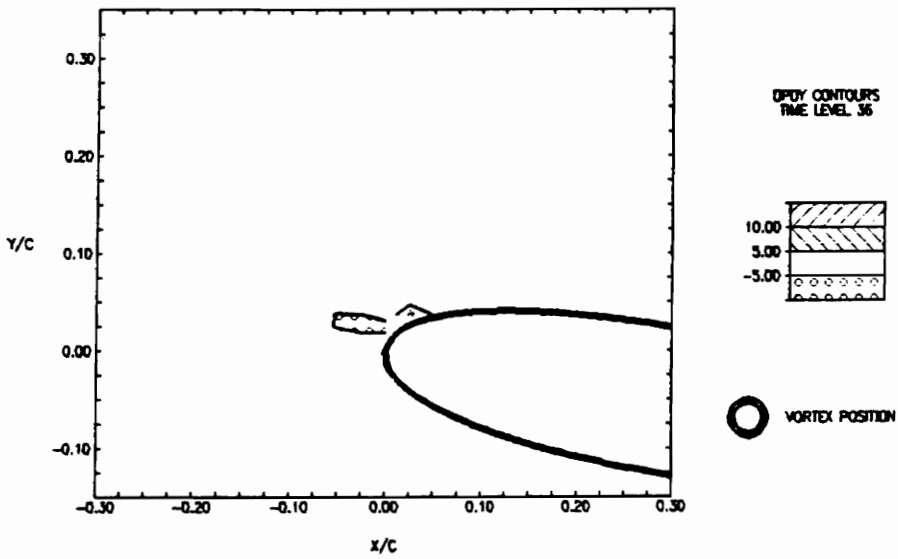
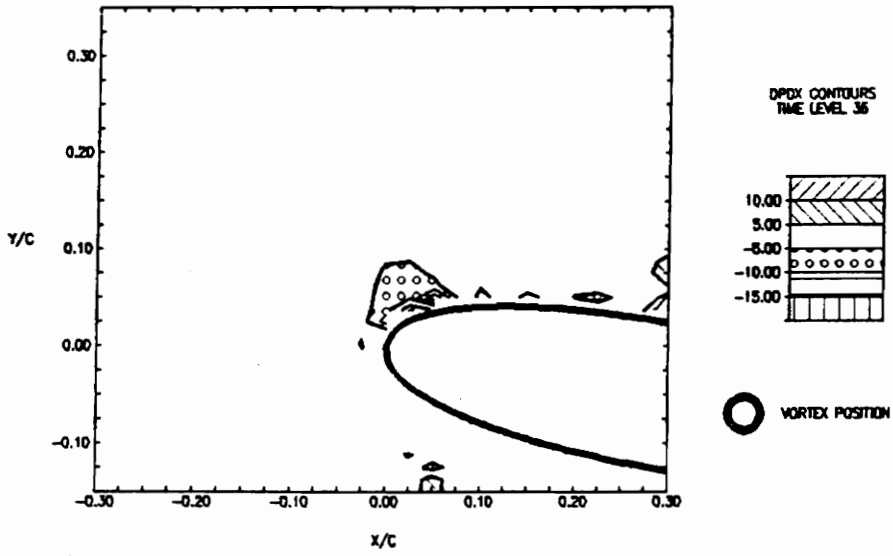


Figure 4.3.36 Pressure gradient contours, $\partial p/\partial x$ and $\partial p/\partial y$, at time level 36 (36/50 of period, $\tau=1.24$ sec.)

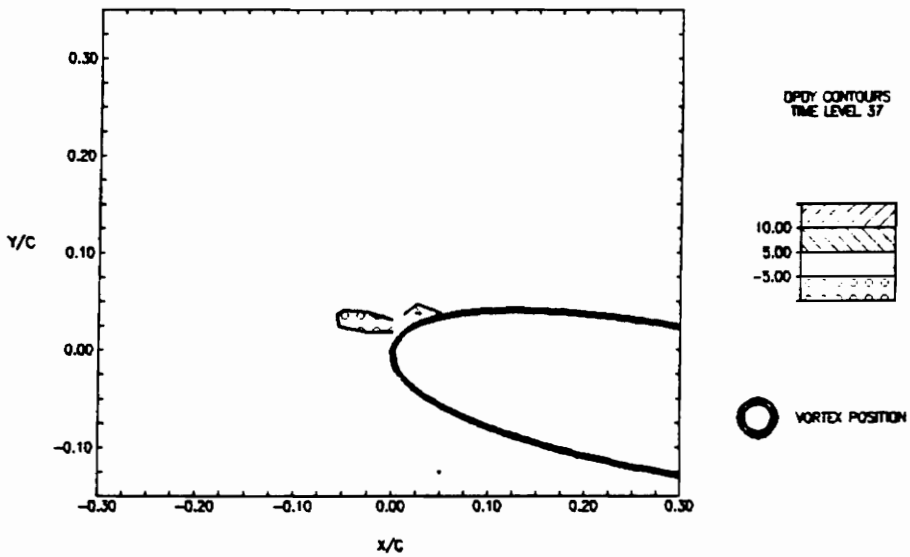
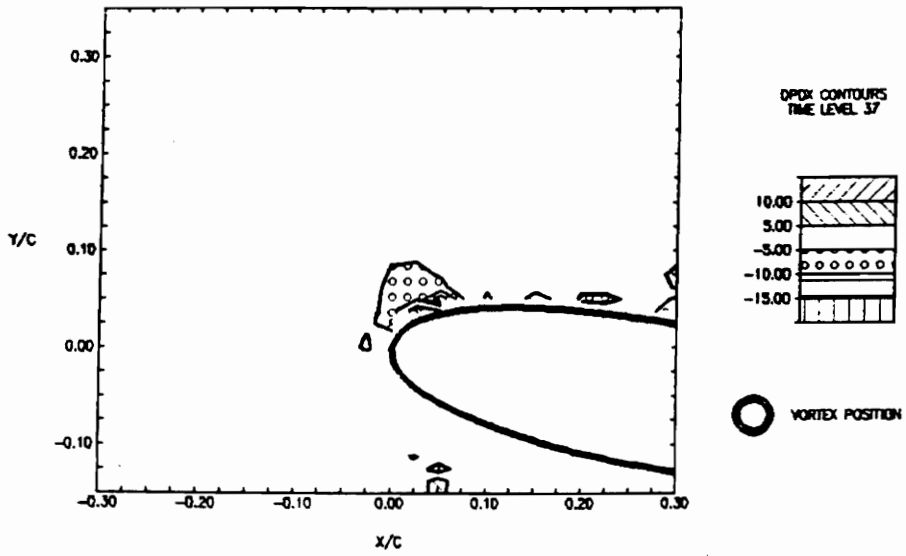


Figure 4.3.37 Pressure gradient contours, $\partial p/\partial x$ and $\partial p/\partial y$, at time level 37 (37/50 of period, $\tau=1.24$ sec.)

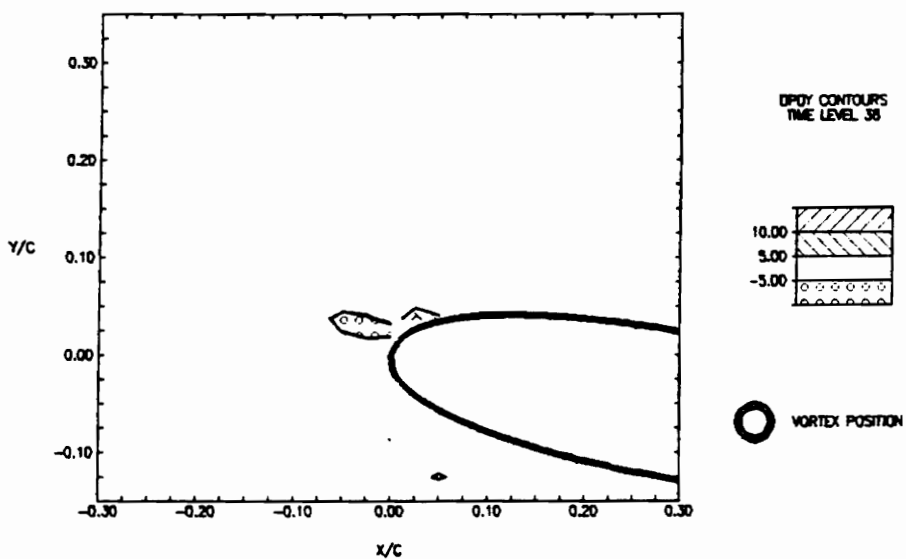
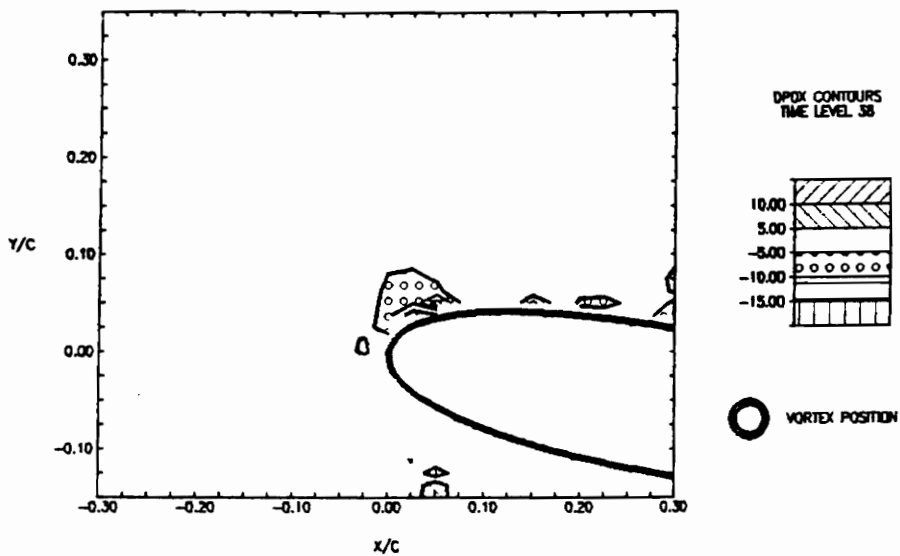


Figure 4.3.38 Pressure gradient contours, $\partial p/\partial x$ and $\partial p/\partial y$, at time level 38 (38/50 of period, $\tau=1.24$ sec.)

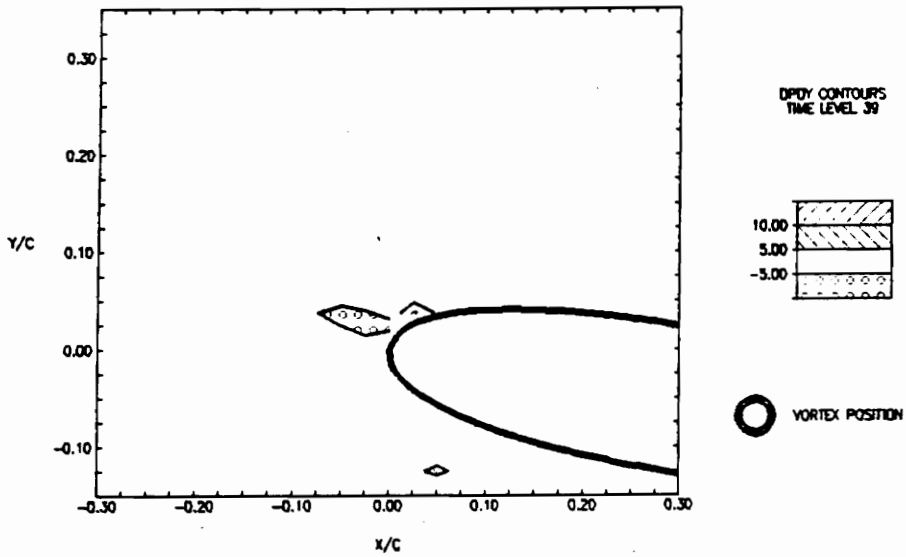
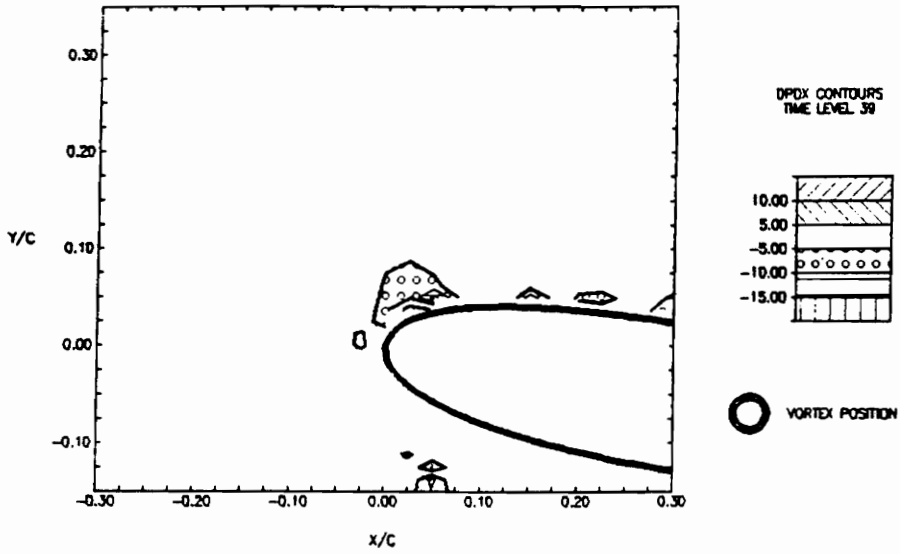


Figure 4.3.39 Pressure gradient contours, $\partial p/\partial x$ and $\partial p/\partial y$, at time level 39 (39/50 of period, $\tau=1.24$ sec.)

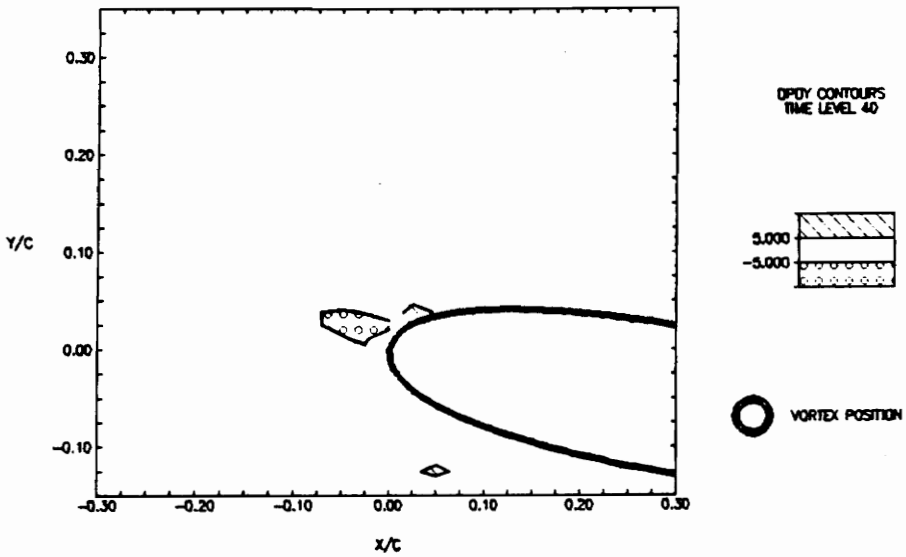
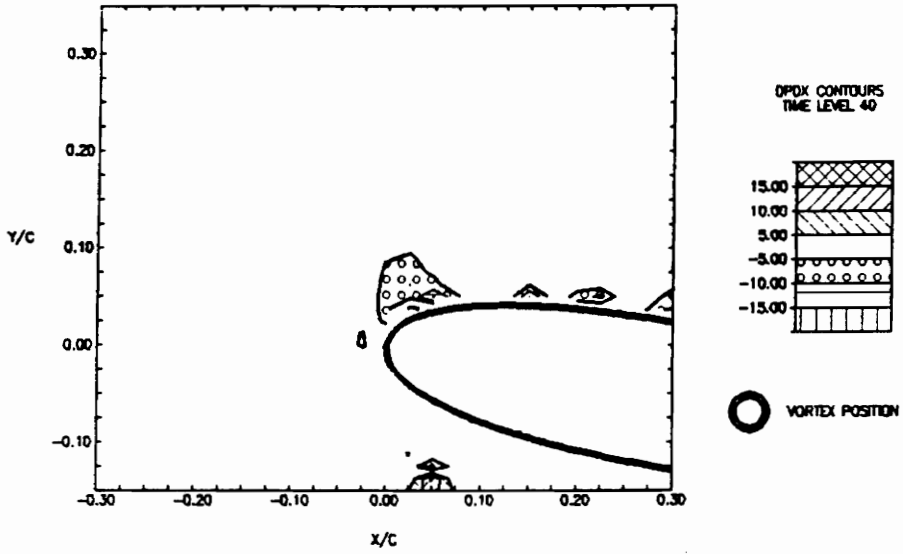


Figure 4.3.40 Pressure gradient contours, $\partial p/\partial x$ and $\partial p/\partial y$, at time level 40 (40/50 of period, $\tau=1.24$ sec.)

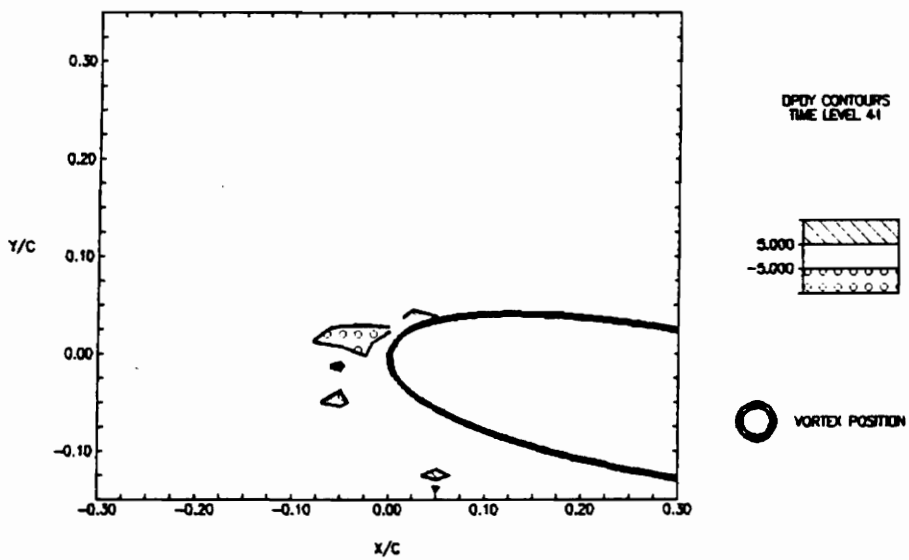
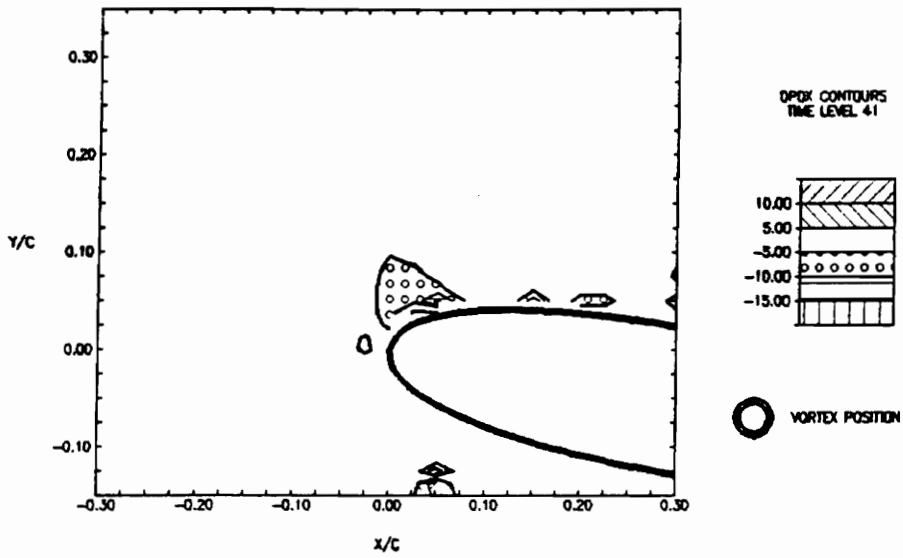


Figure 4.3.41 Pressure gradient contours, $\partial p/\partial x$ and $\partial p/\partial y$, at time level 41 (41/50 of period, $\tau=1.24$ sec.)

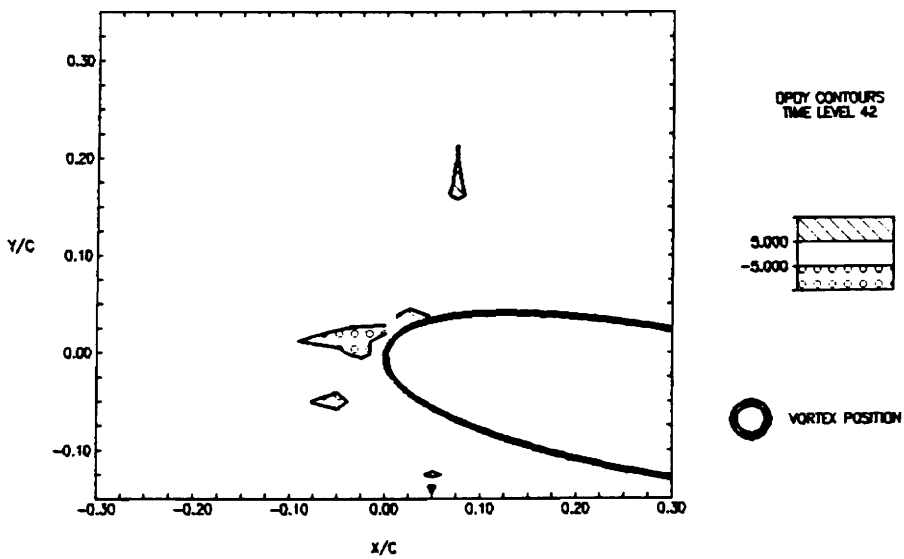
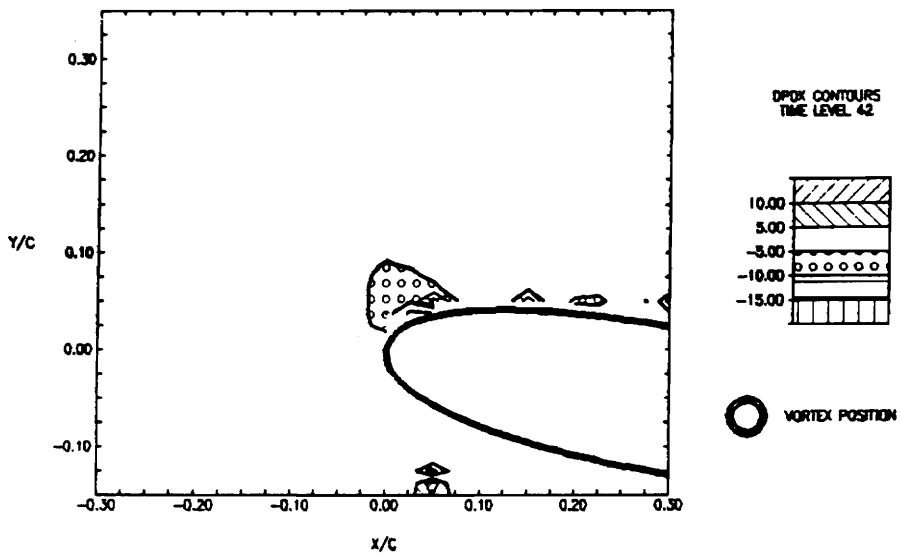


Figure 4.3.42 Pressure gradient contours, $\partial p/\partial x$ and $\partial p/\partial y$, at time level 42 (42/50 of period, $\tau=1.24$ sec.)

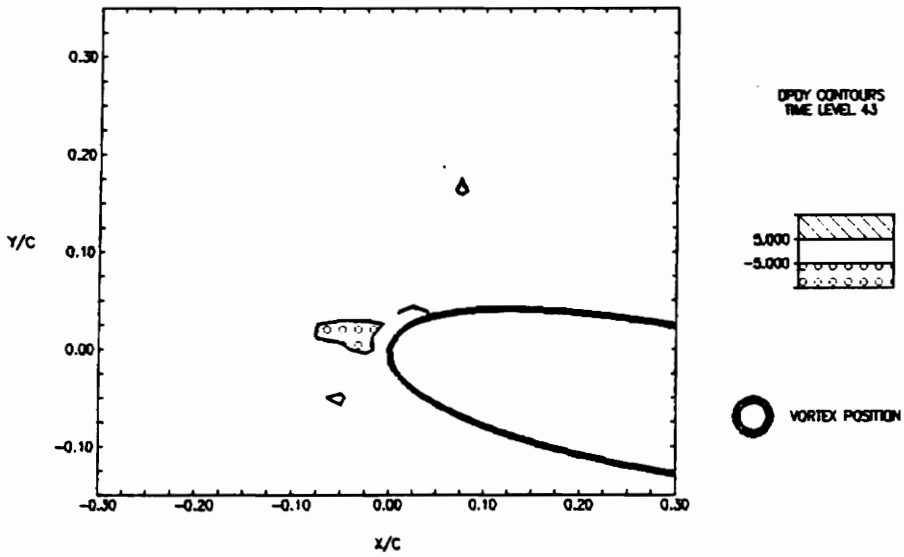
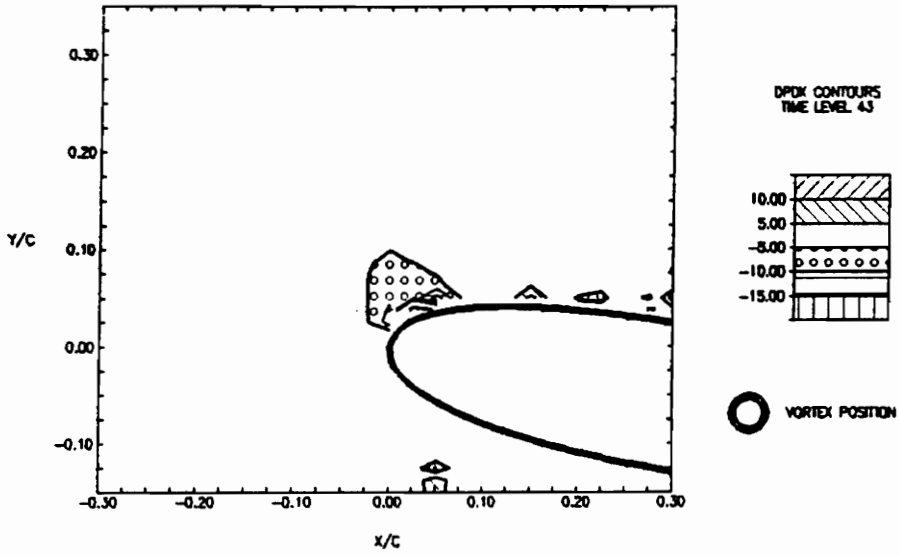


Figure 4.3.43 Pressure gradient contours, $\partial p/\partial x$ and $\partial p/\partial y$, at time level 43 (43/50 of period, $\tau=1.24$ sec.)

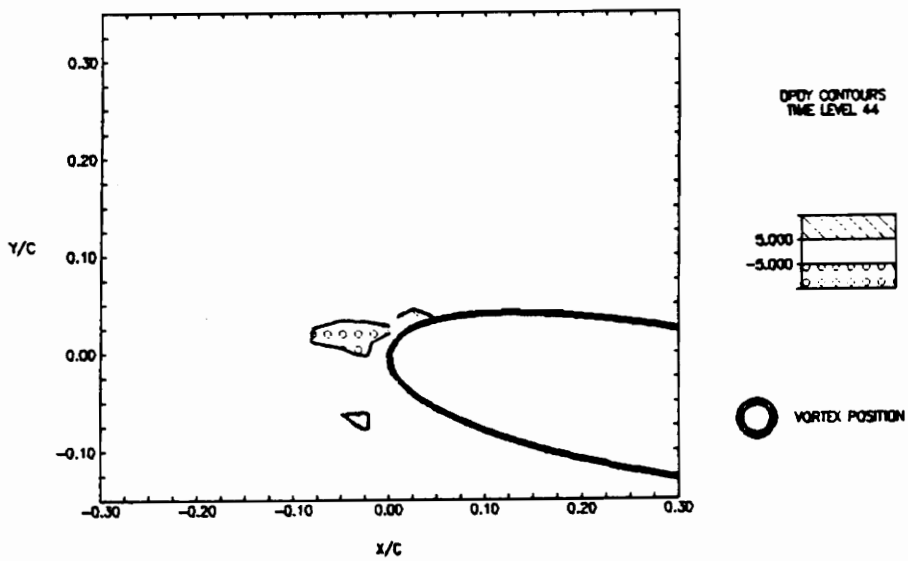
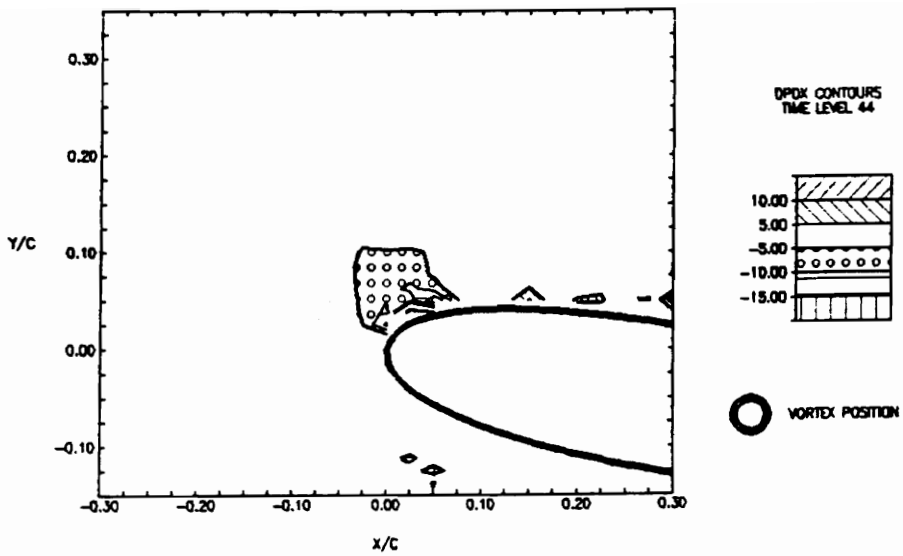


Figure 4.3.44 Pressure gradient contours, $\partial p/\partial x$ and $\partial p/\partial y$, at time level 44 (44/50 of period, $\tau=1.24$ sec.)

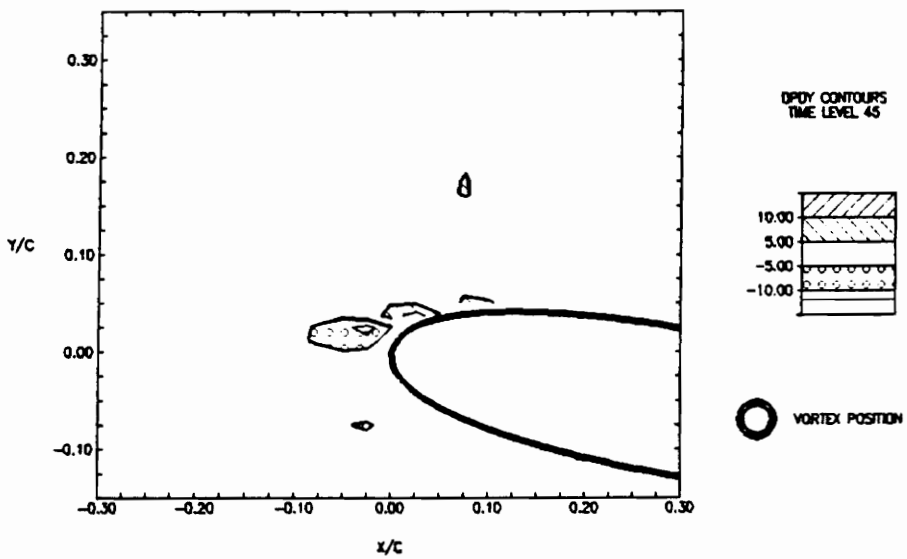
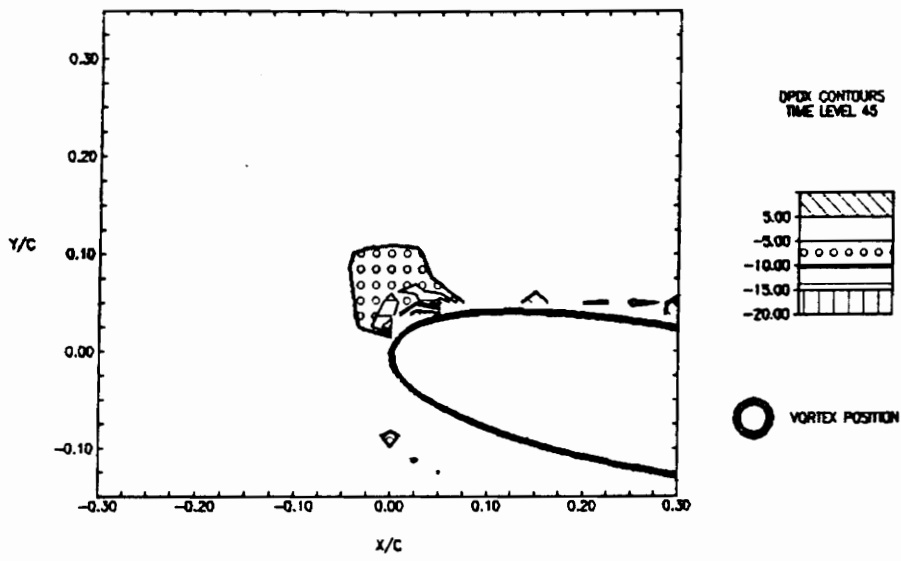


Figure 4.3.45 Pressure gradient contours, $\partial p/\partial x$ and $\partial p/\partial y$, at time level 45 (45/50 of period, $\tau=1.24$ sec.)

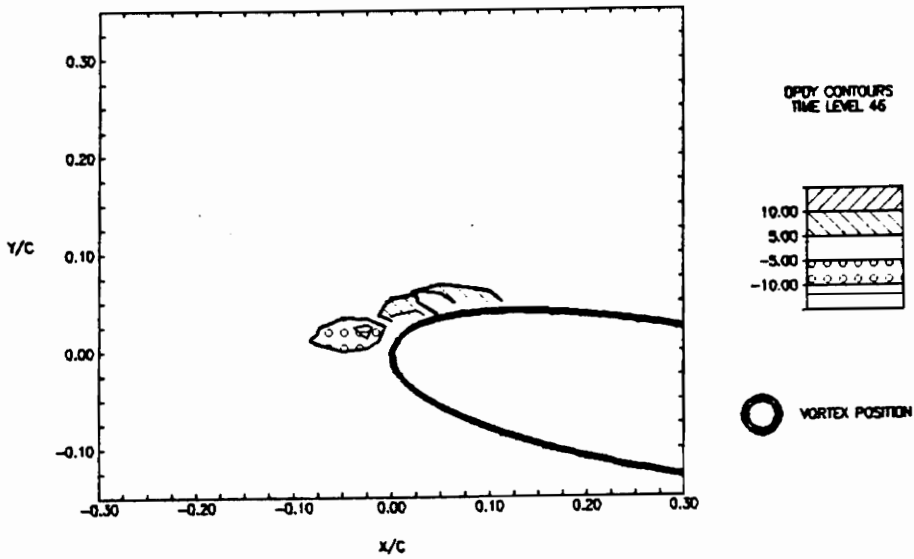
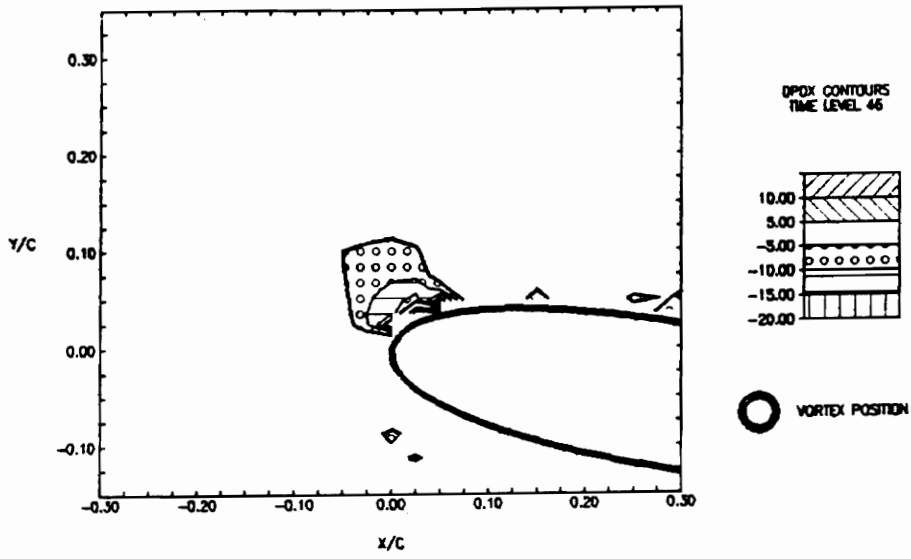


Figure 4.3.46 Pressure gradient contours, $\partial p/\partial x$ and $\partial p/\partial y$, at time level 46 (46/50 of period, $\tau=1.24$ sec.)

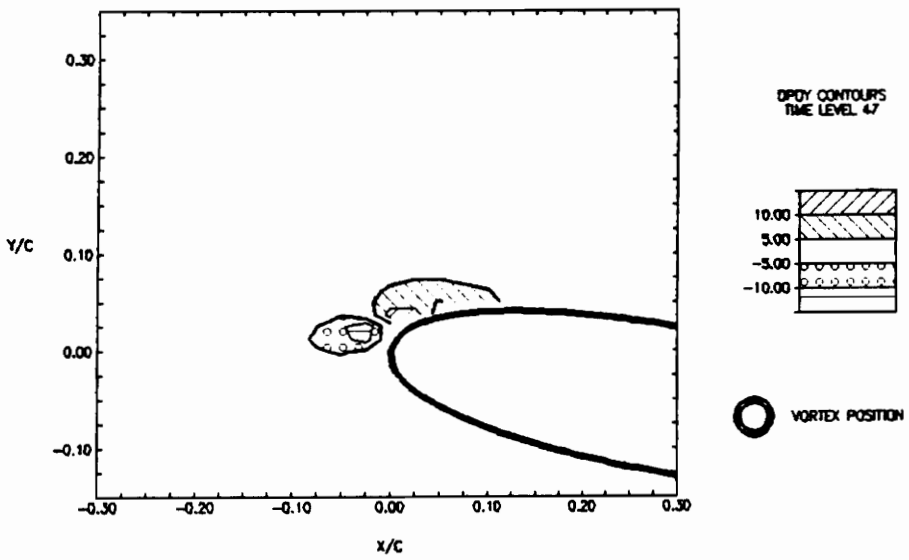
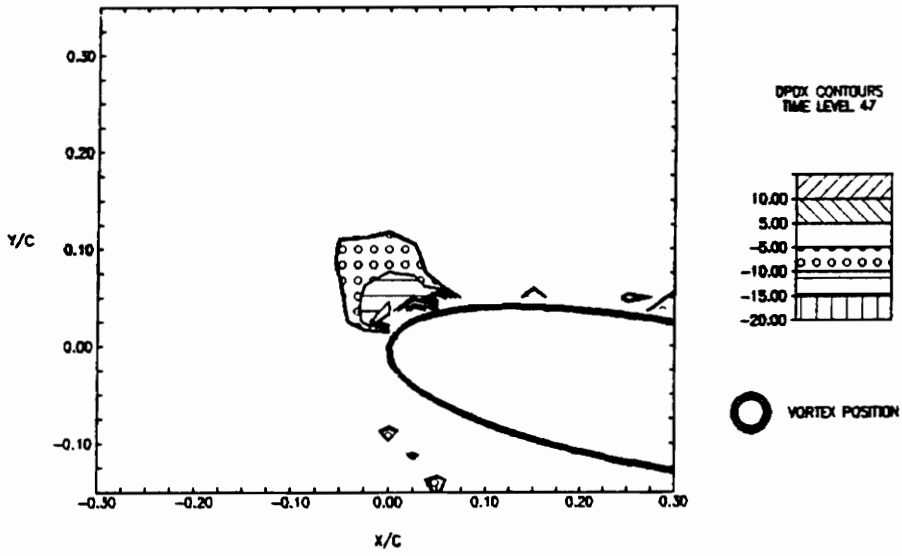


Figure 4.3.47 Pressure gradient contours, $\partial p/\partial x$ and $\partial p/\partial y$, at time level 47 (47/50 of period, $\tau=1.24$ sec.)

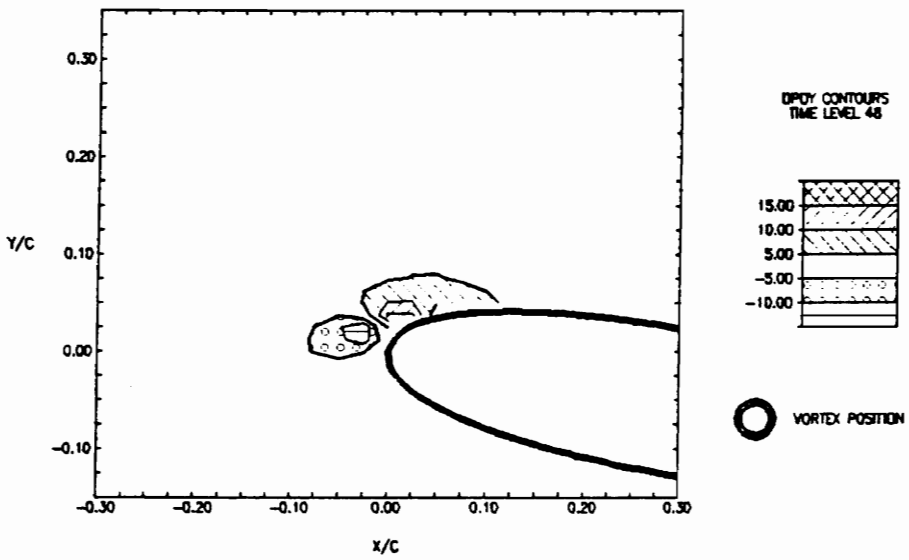
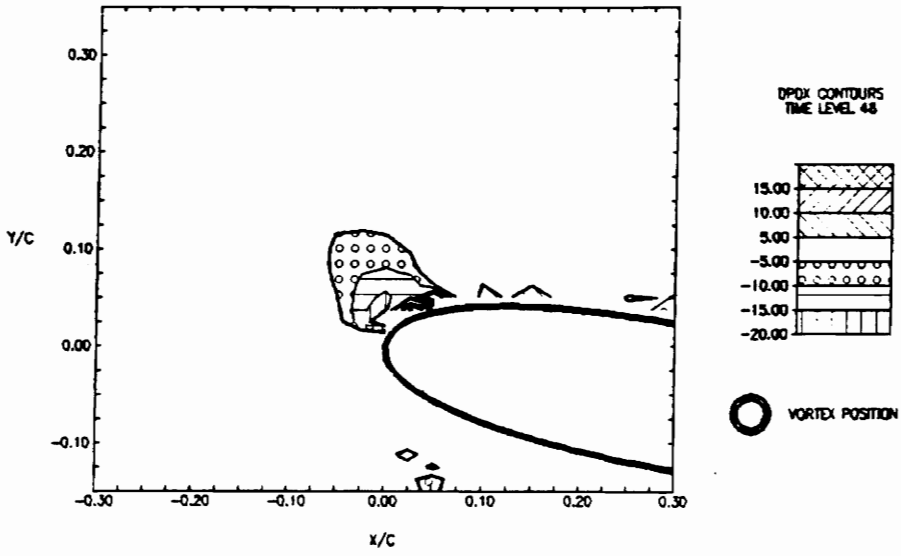


Figure 4.3.48 Pressure gradient contours, $\partial p/\partial x$ and $\partial p/\partial y$, at time level 48 (48/50 of period, $\tau=1.24$ sec.)

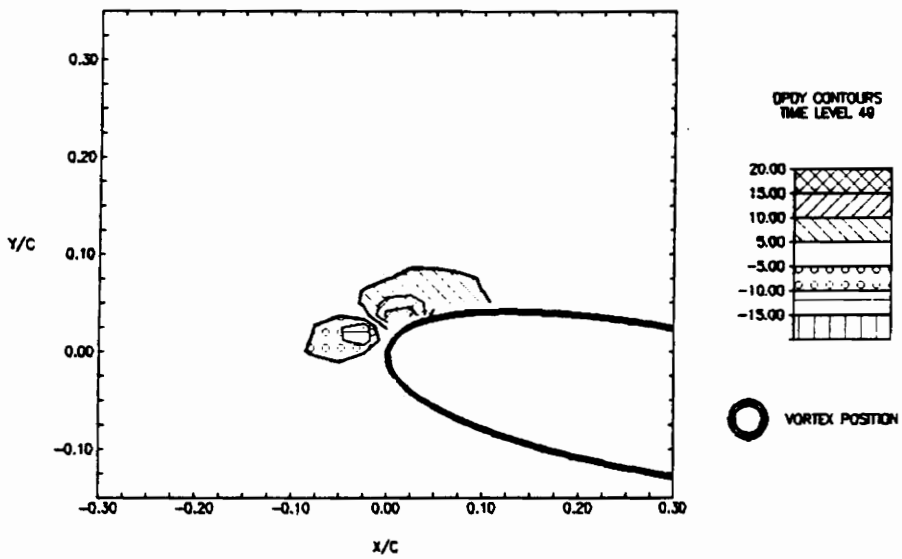
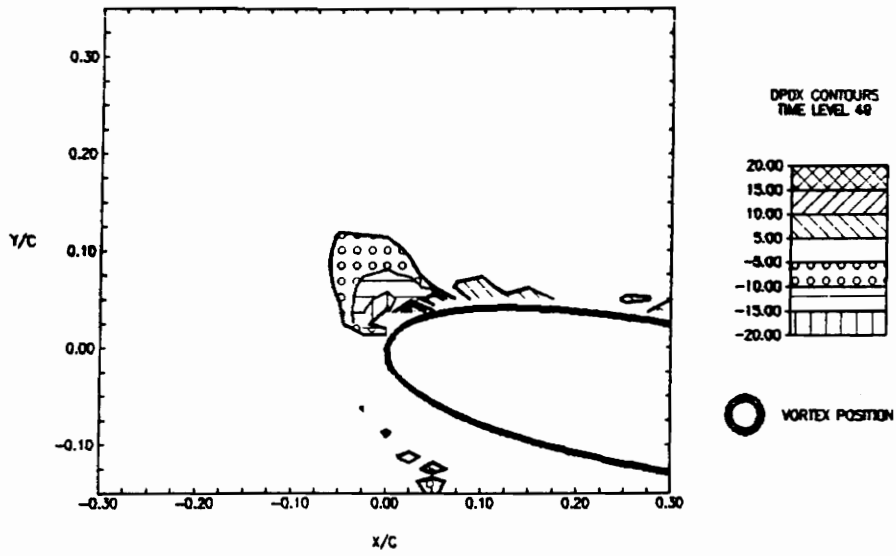


Figure 4.3.49 Pressure gradient contours, $\partial p/\partial x$ and $\partial p/\partial y$, at time level 49 (49/50 of period, $\tau=1.24$ sec.)

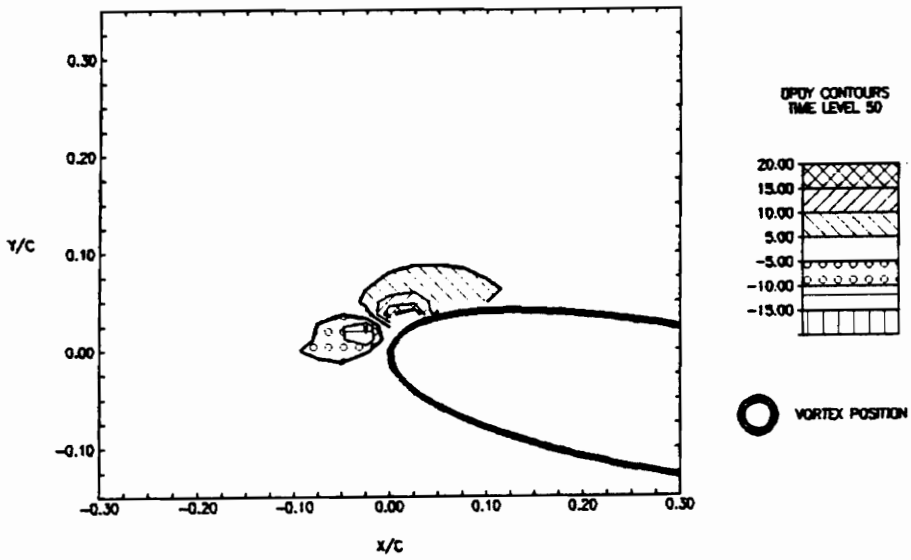
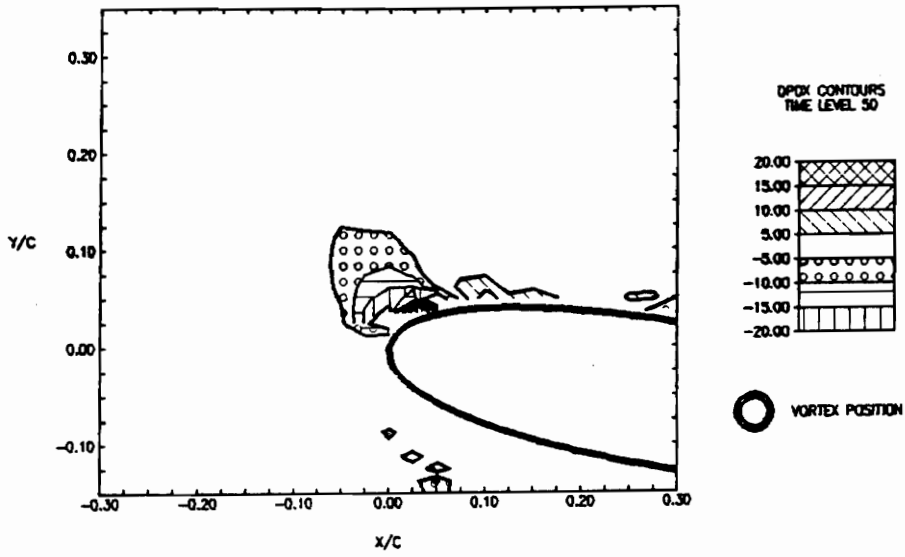


Figure 4.3.50 Pressure gradient contours, $\partial p/\partial x$ and $\partial p/\partial y$, at time level 50 (50/50 of period, $\tau=1.24$ sec.)

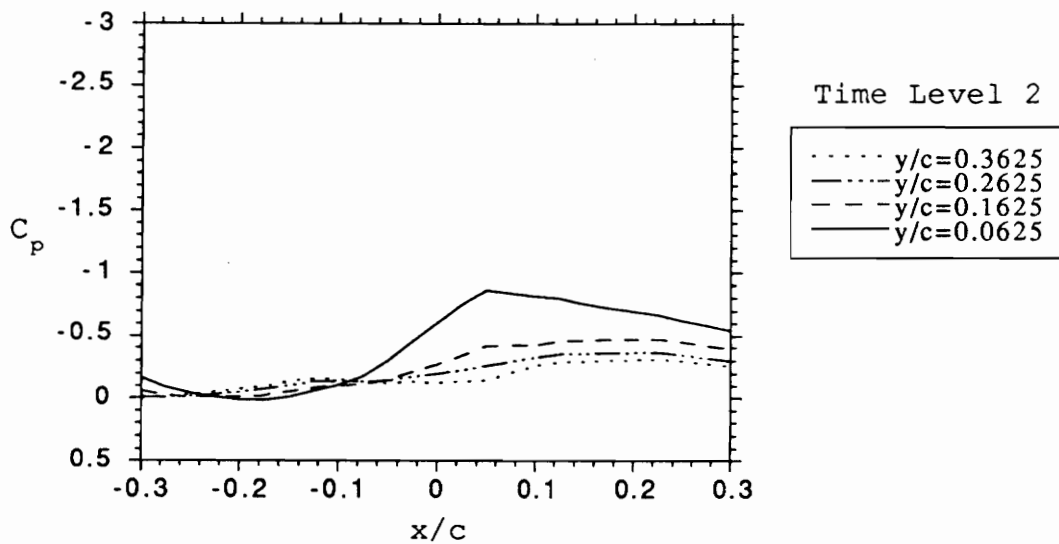
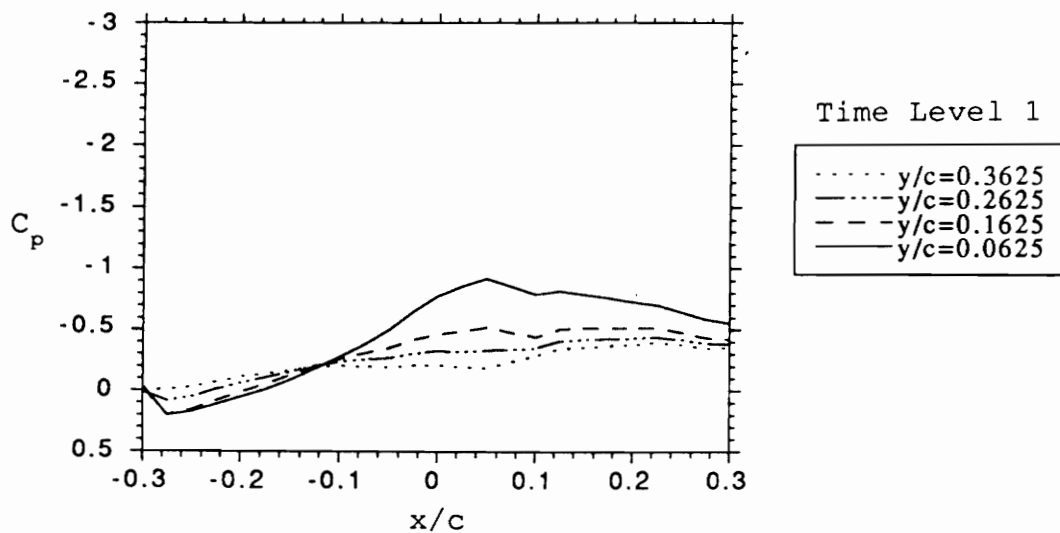


Figure 4.3.51 Pressure coefficients at four y/c locations, at time levels 1 and 2 (1/50 and 2/50 of period, $\tau=1.24$ sec.)

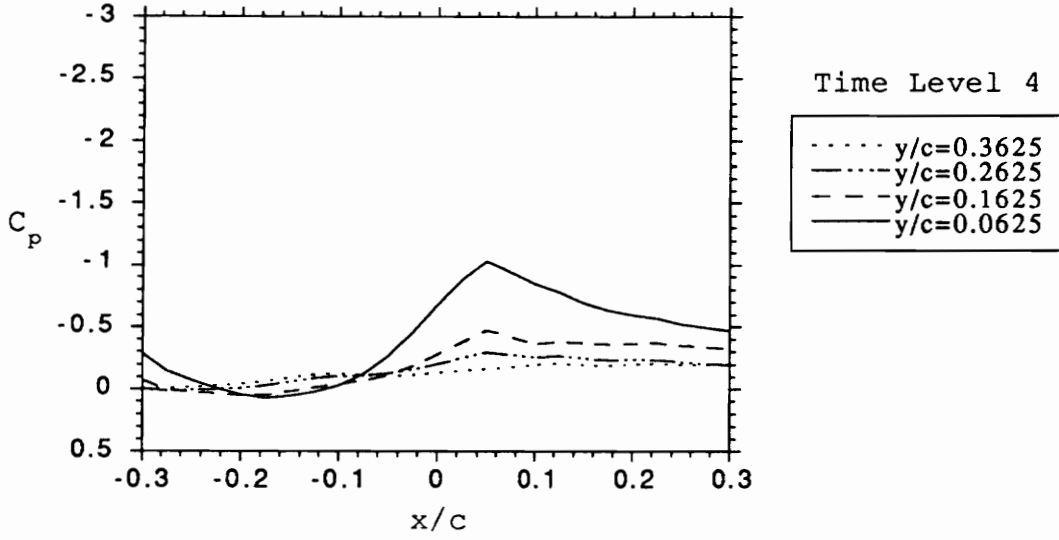
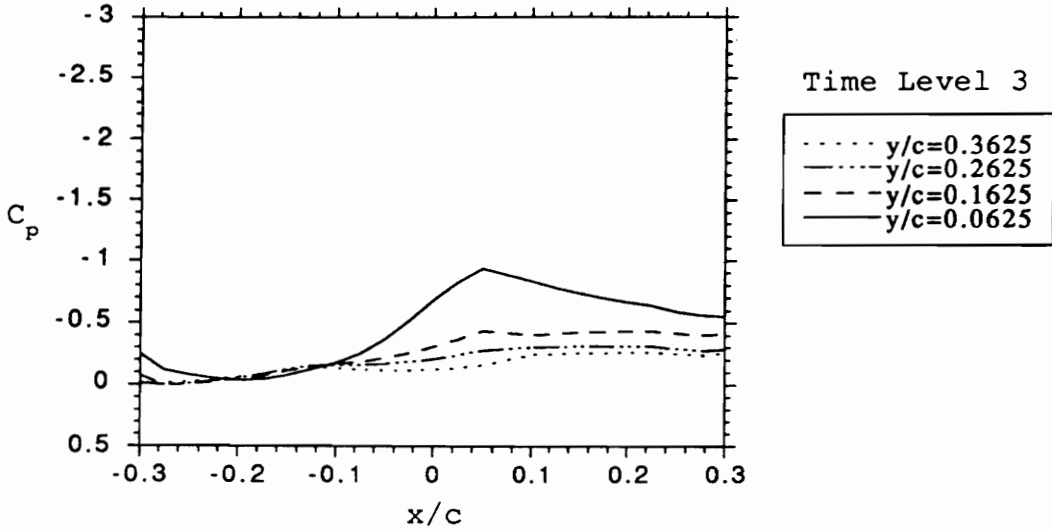


Figure 4.3.52 Pressure coefficients at four y/c locations, at time levels 3 and 4 (3/50 and 4/50 of period, $\tau=1.24$ sec.)

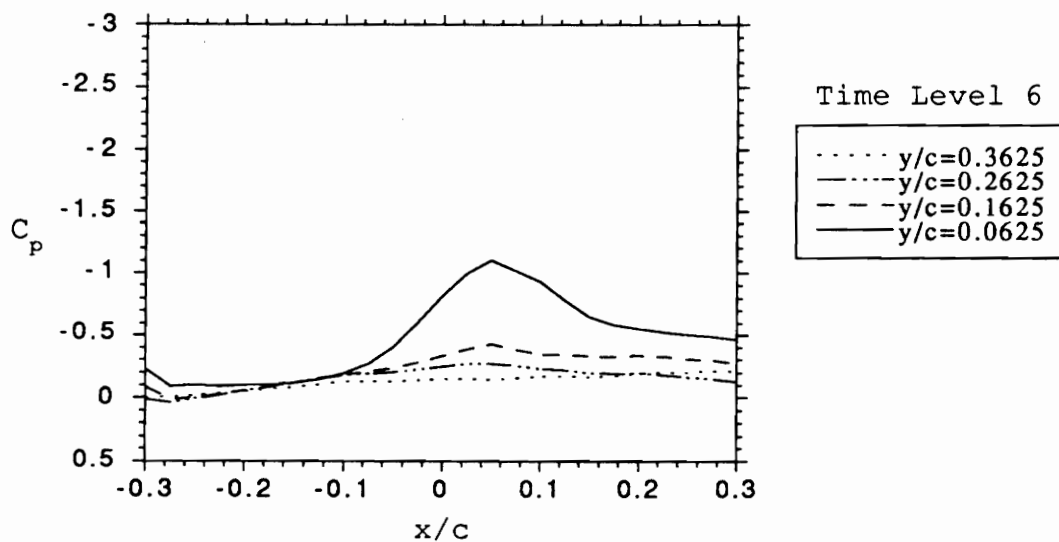
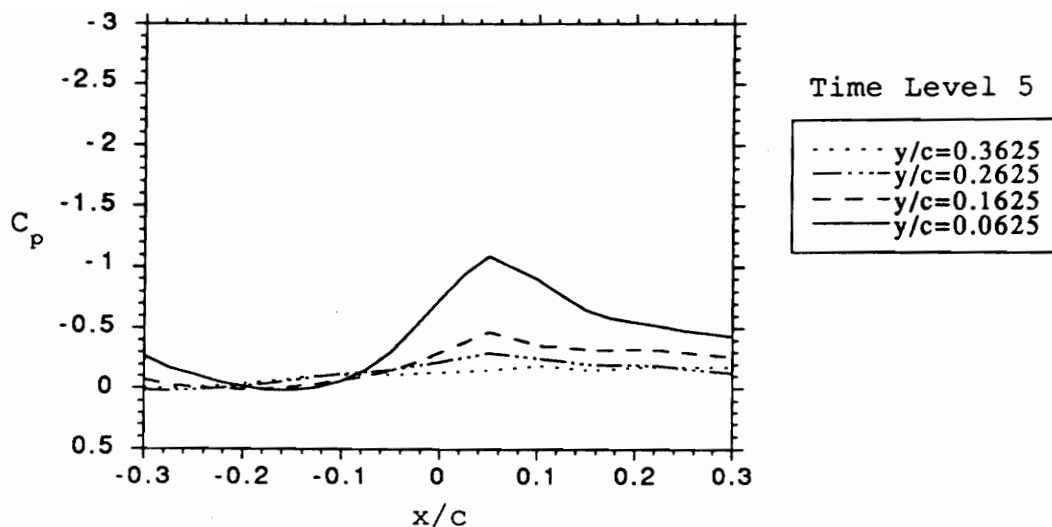


Figure 4.3.53 Pressure coefficients at four y/c locations, at time levels 5 and 6 (5/50 and 6/50 of period, $\tau=1.24$ sec.)

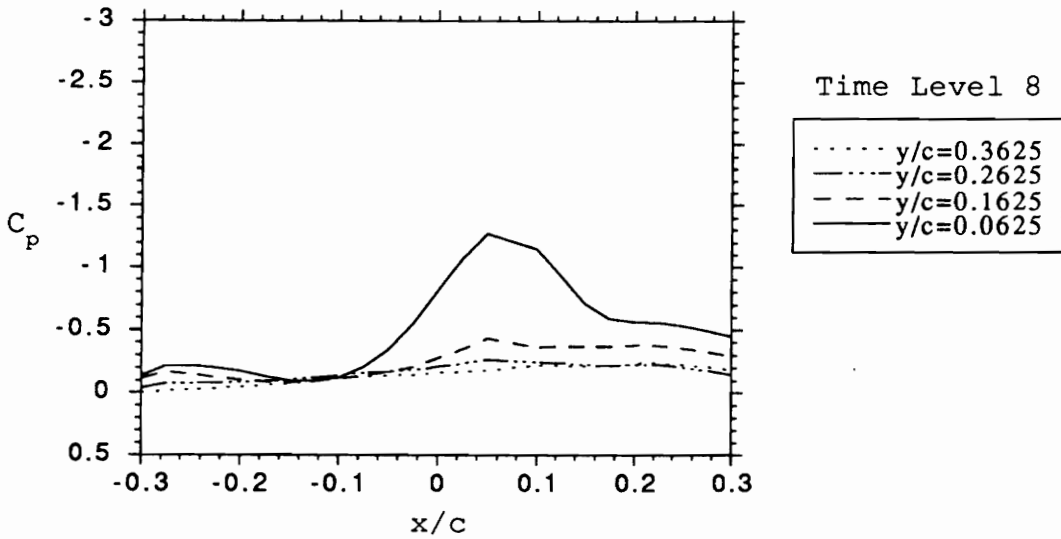
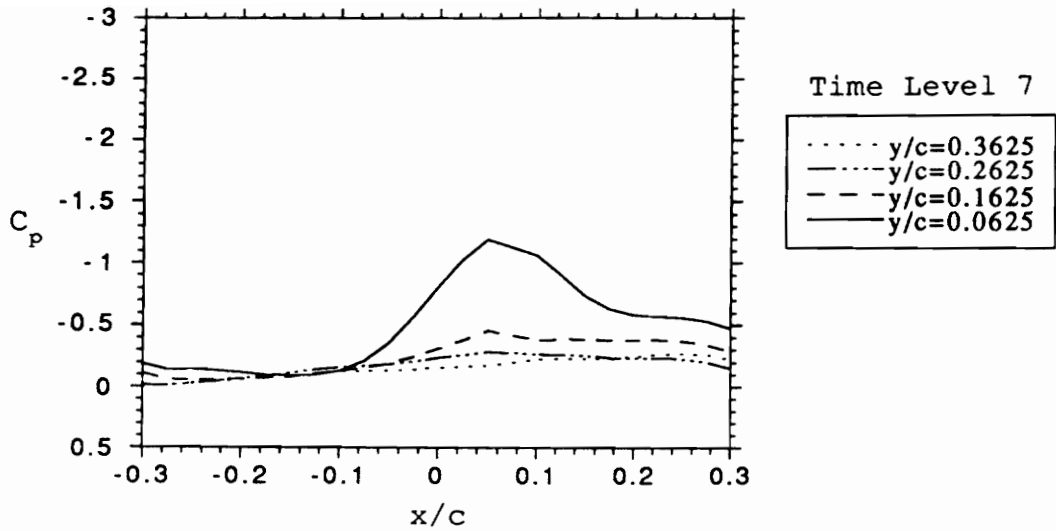


Figure 4.3.54 Pressure coefficients at four y/c locations, at time levels 7 and 8 (7/50 and 8/50 of period, $\tau=1.24$ sec.)

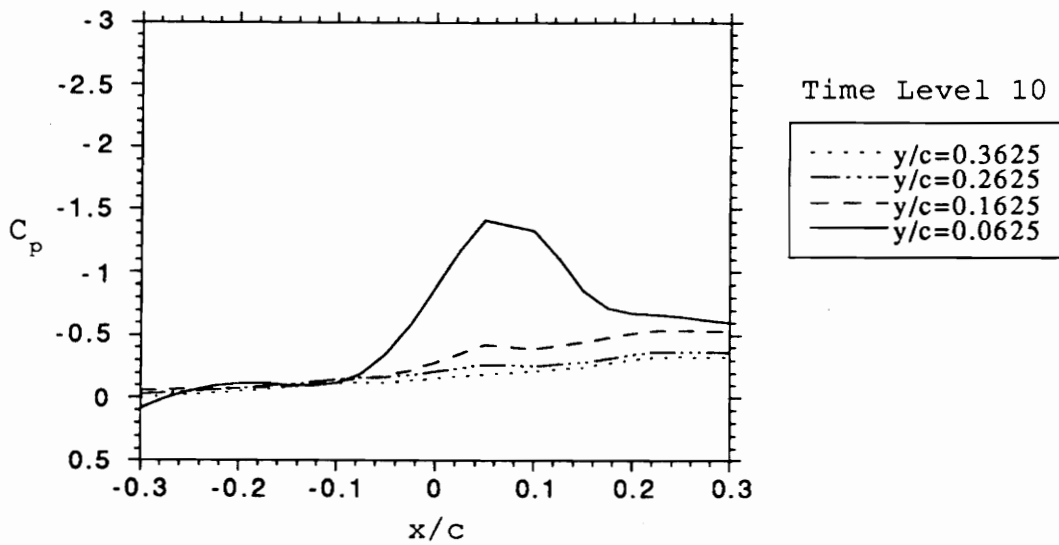
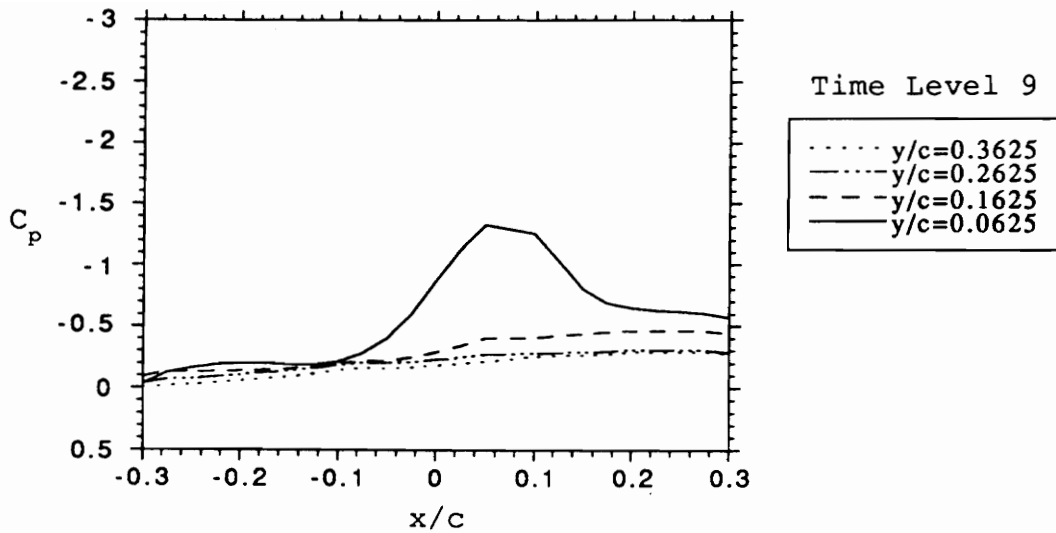


Figure 4.3.55 Pressure coefficients at four y/c locations, at time levels 9 and 10 (9/50 and 10/50 of period, $\tau=1.24$ sec.)

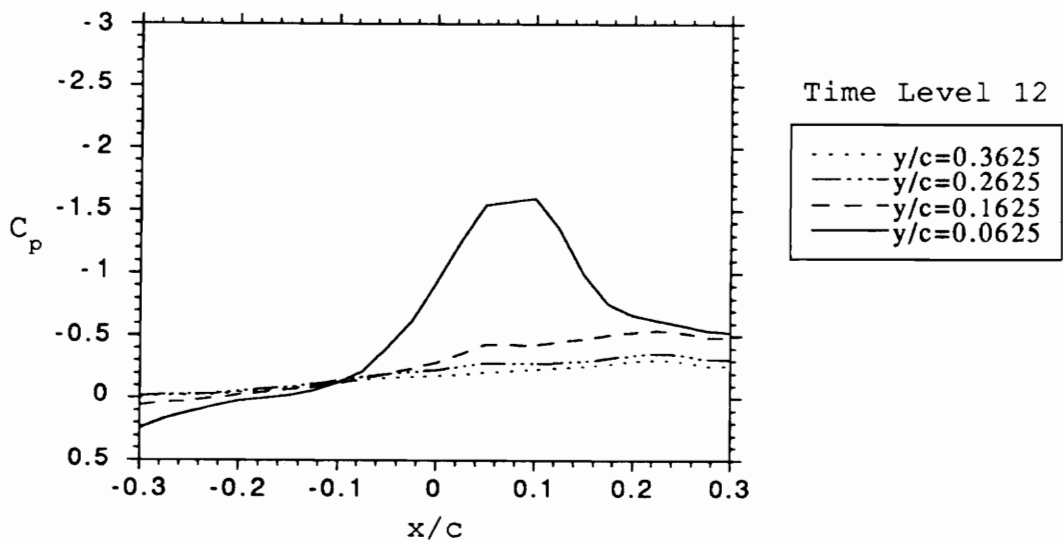
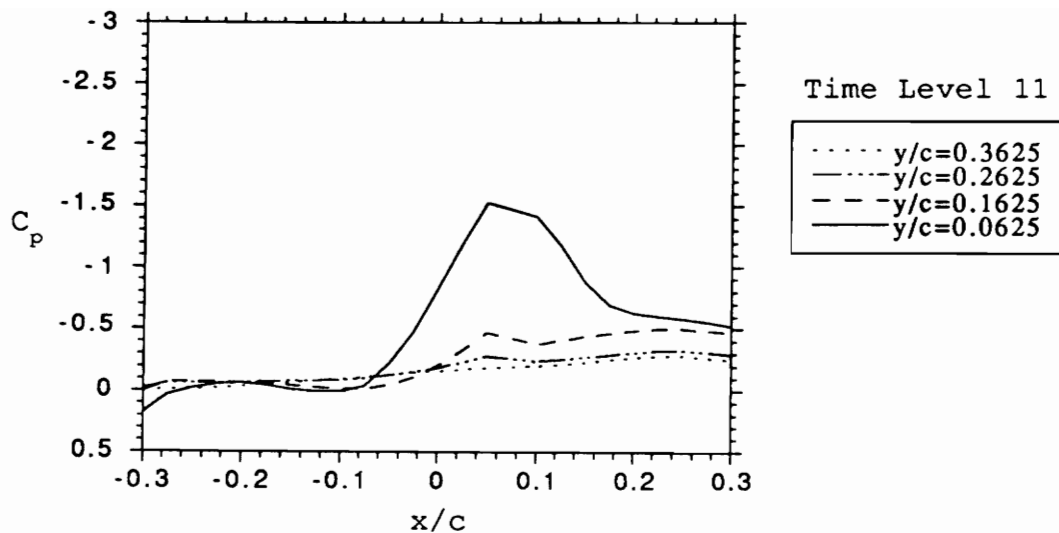


Figure 4.3.56 Pressure coefficients at four y/c locations, at time levels 11 and 12 (11/50 and 12/50 of period, $\tau=1.24$ sec.)

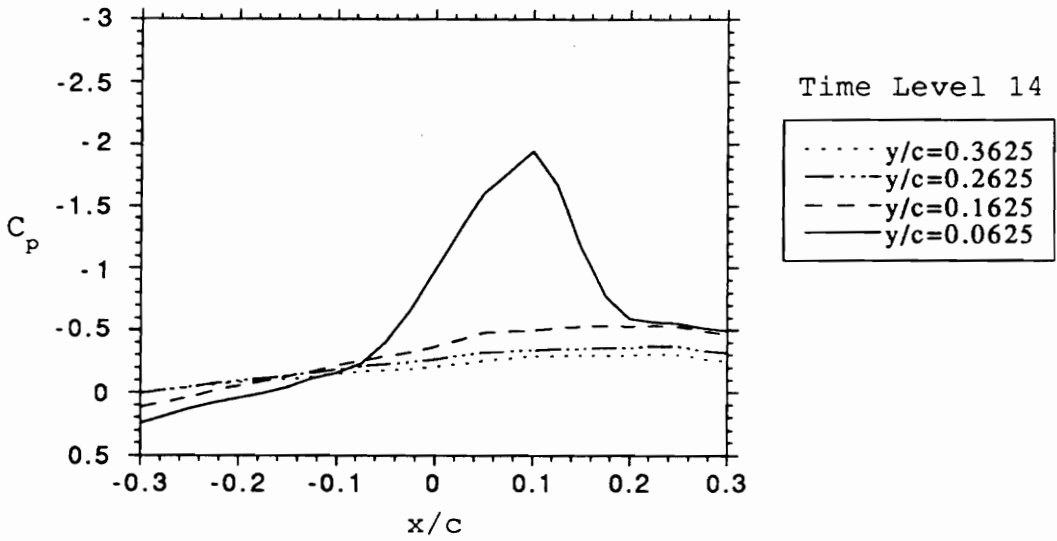
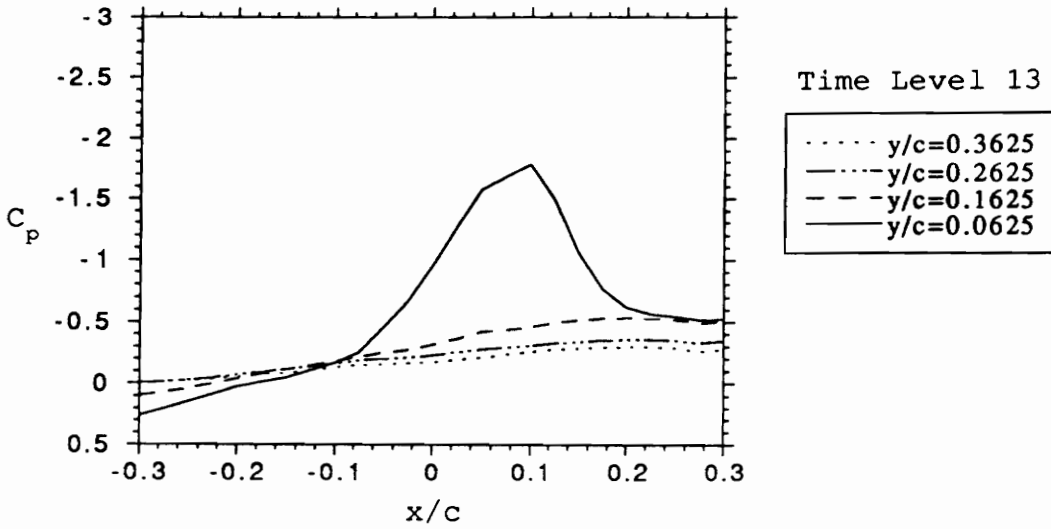


Figure 4.3.57 Pressure coefficients at four y/c locations, at time levels 13 and 14 (13/50 and 14/50 of period, $\tau=1.24$ sec.)

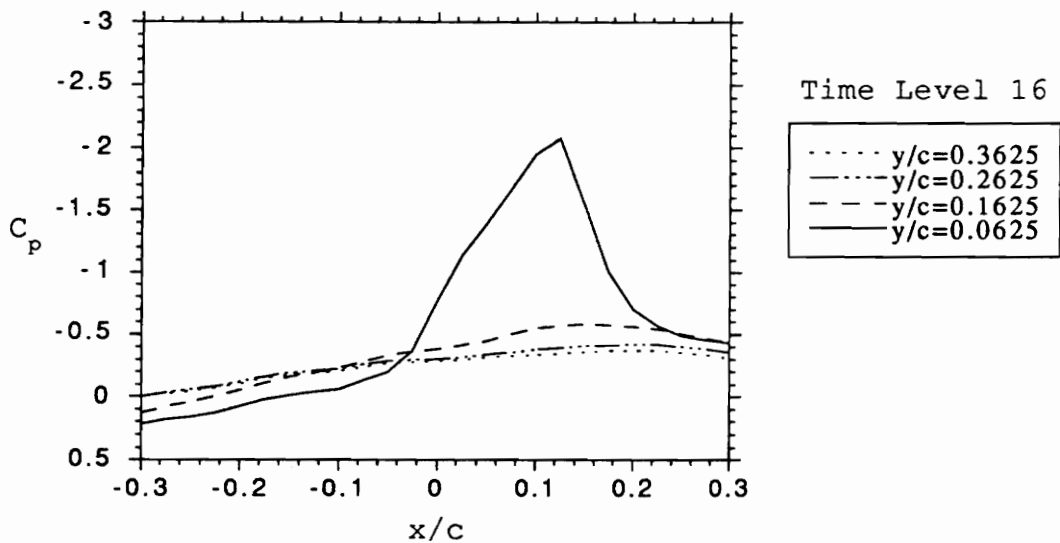
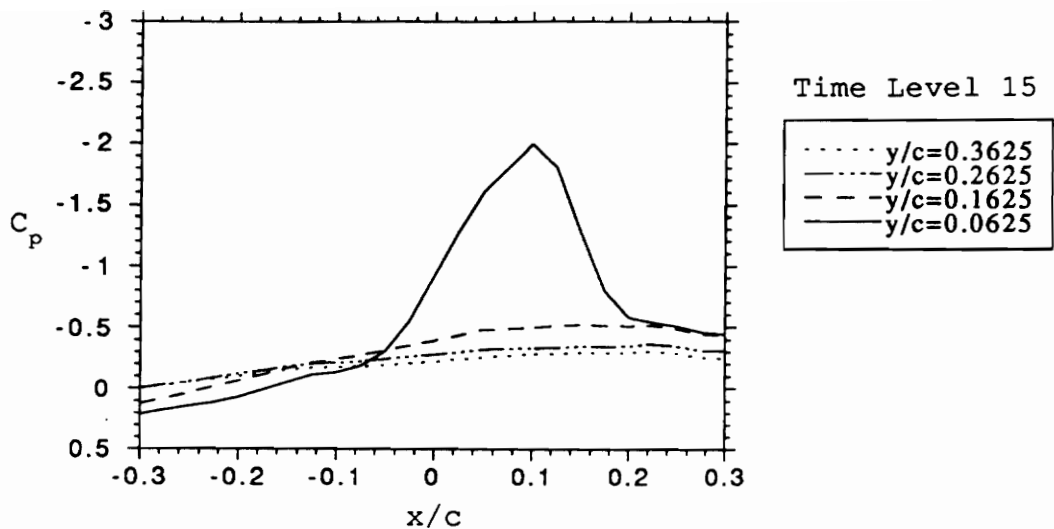


Figure 4.3.58 Pressure coefficients at four y/c locations, at time levels 15 and 16 (15/50 and 16/50 of period, $\tau=1.24$ sec.)

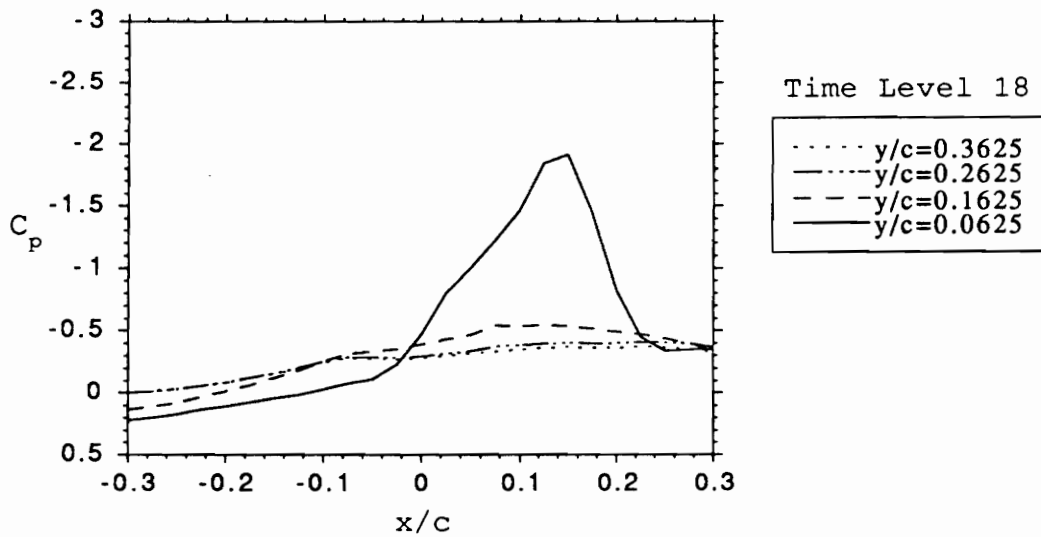
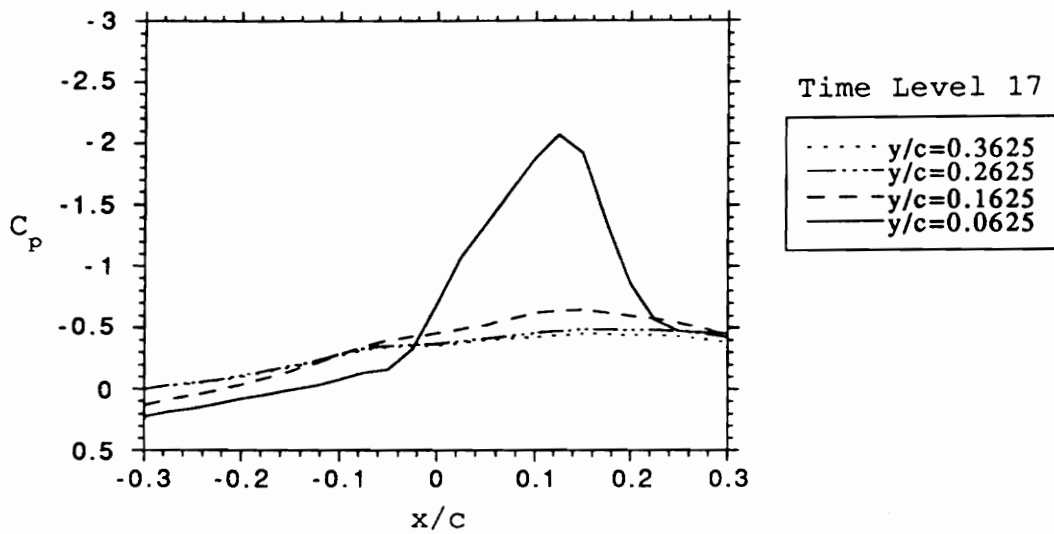


Figure 4.3.59 Pressure coefficients at four y/c locations, at time levels 17 and 18 (17/50 and 18/50 of period, $\tau=1.24$ sec.)

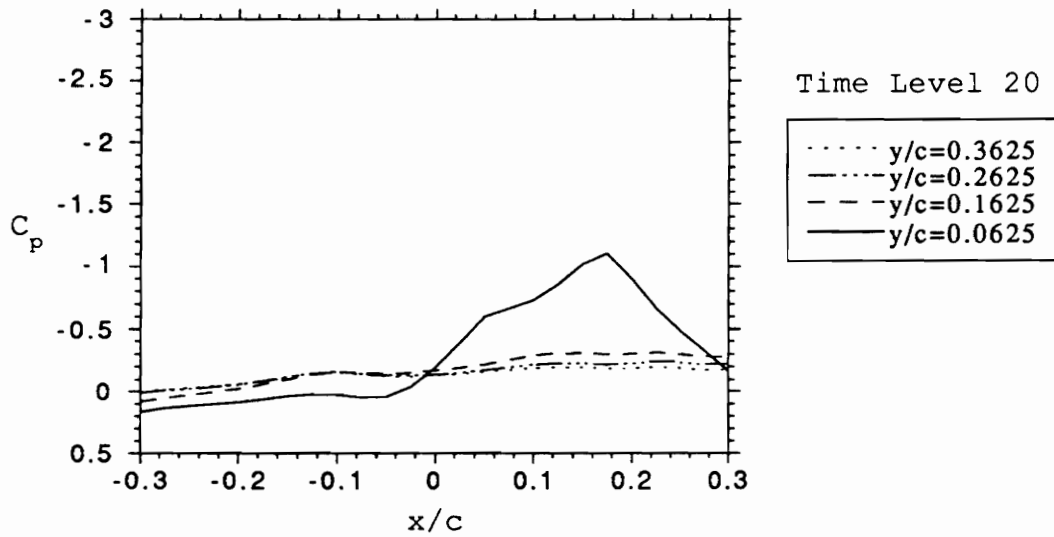
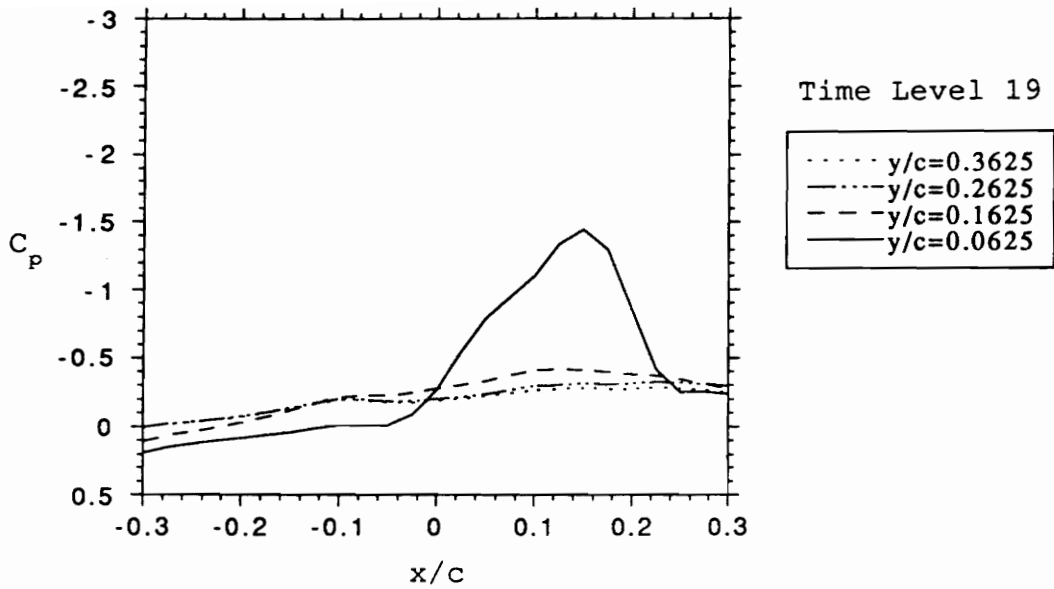


Figure 4.3.60 Pressure coefficients at four y/c locations, at time levels 19 and 20 (19/50 and 20/50 of period, $\tau=1.24$ sec.)

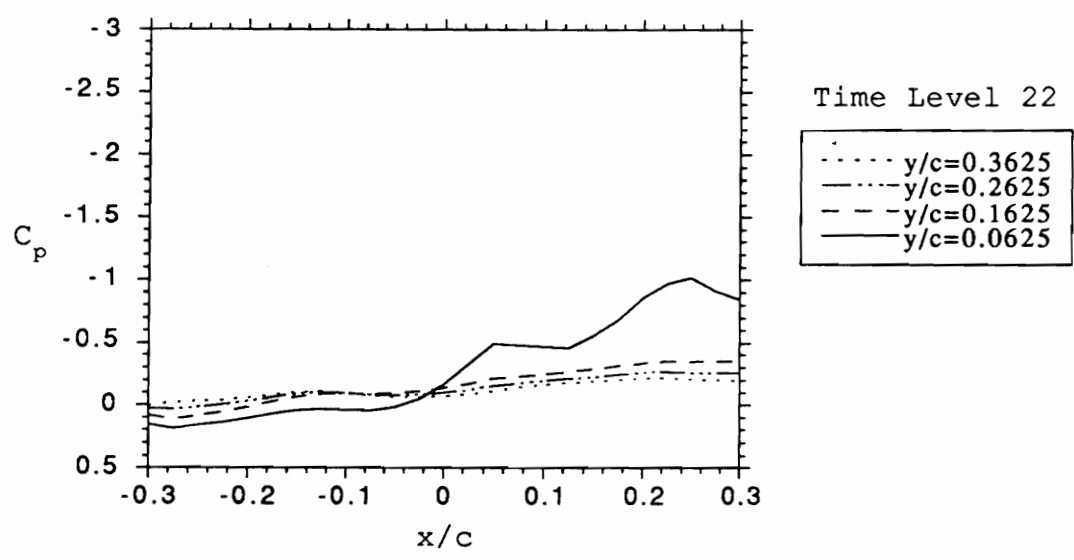
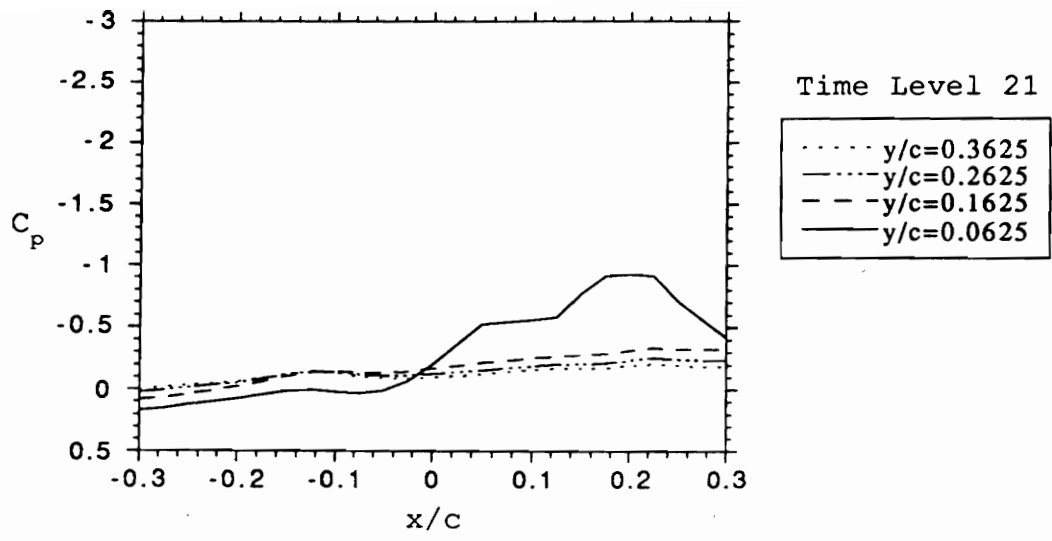


Figure 4.3.61 Pressure coefficients at four y/c locations, at time levels 21 and 22 (21/50 and 22/50 of period, $\tau=1.24$ sec.)

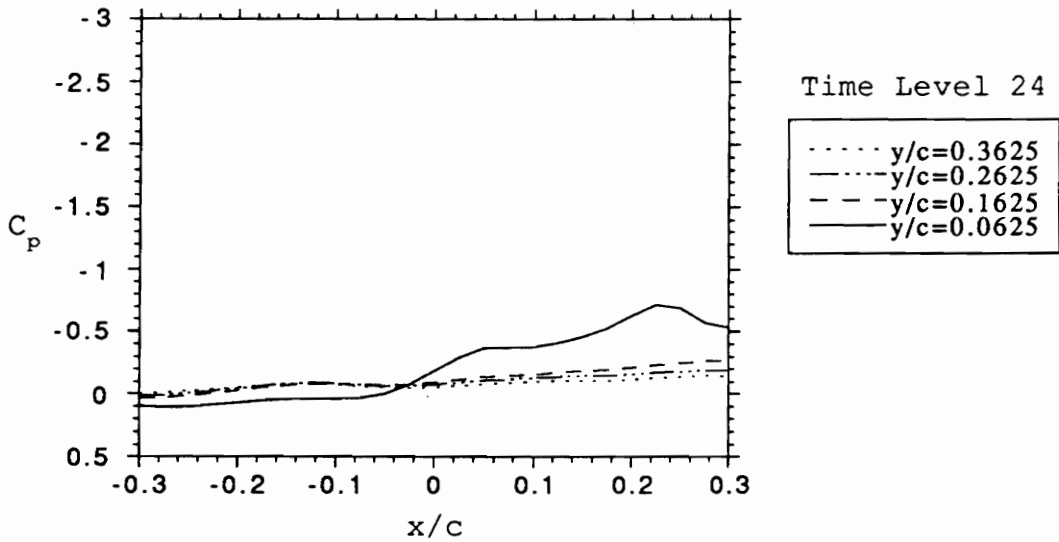
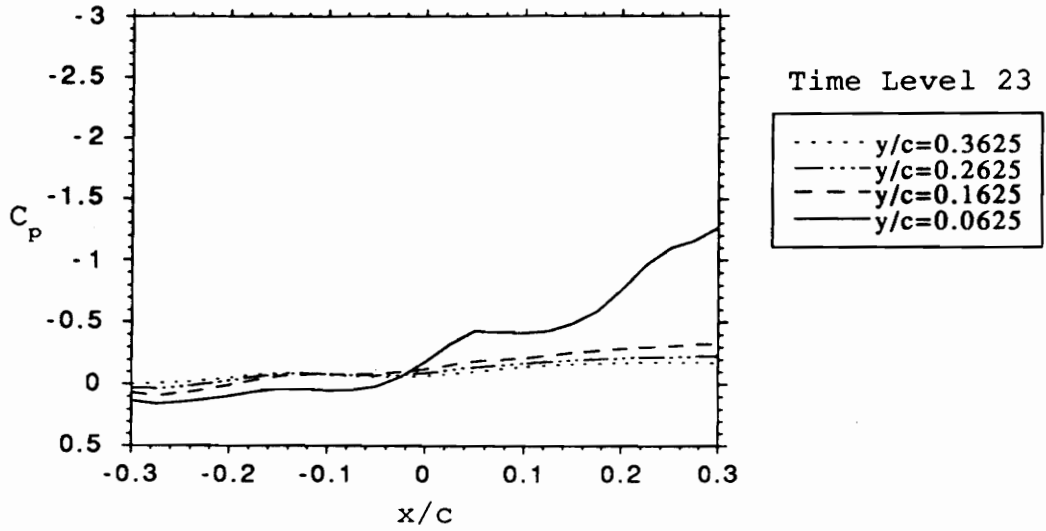


Figure 4.3.62 Pressure coefficients at four y/c locations, at time levels 23 and 24 (23/50 and 24/50 of period, $\tau=1.24$ sec.)

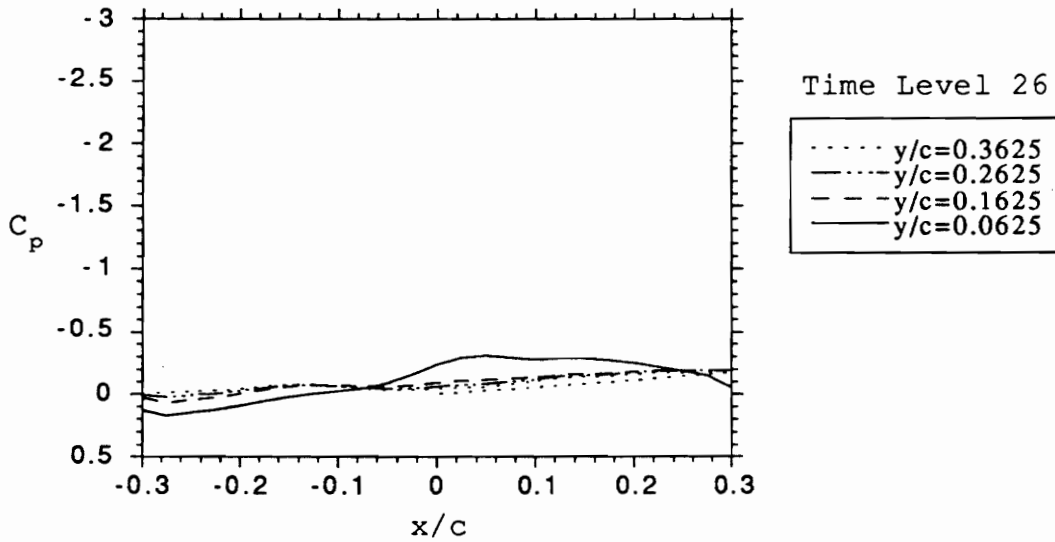
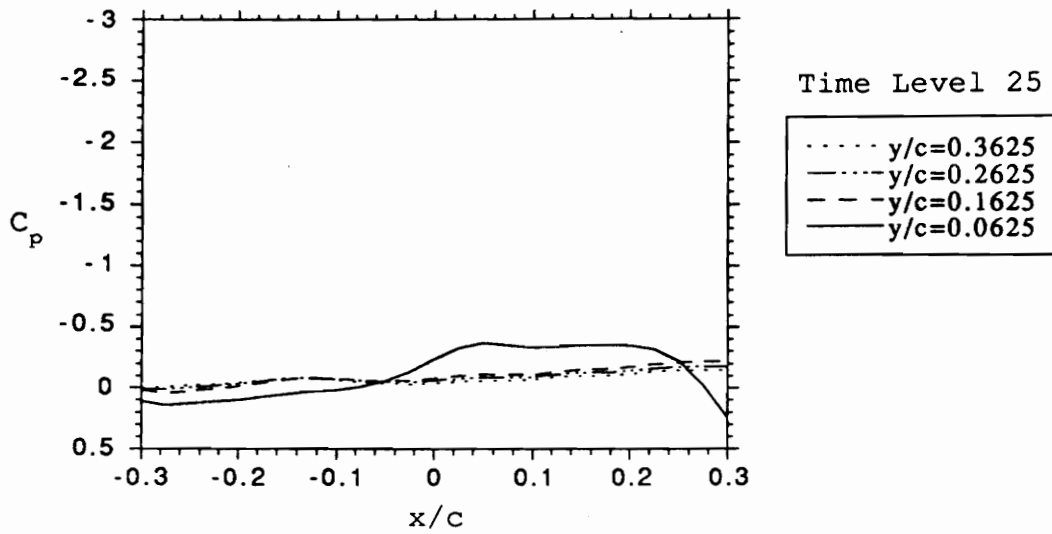


Figure 4.3.63 Pressure coefficients at four y/c locations, at time levels 25 and 26 (25/50 and 26/50 of period, $\tau=1.24$ sec.)

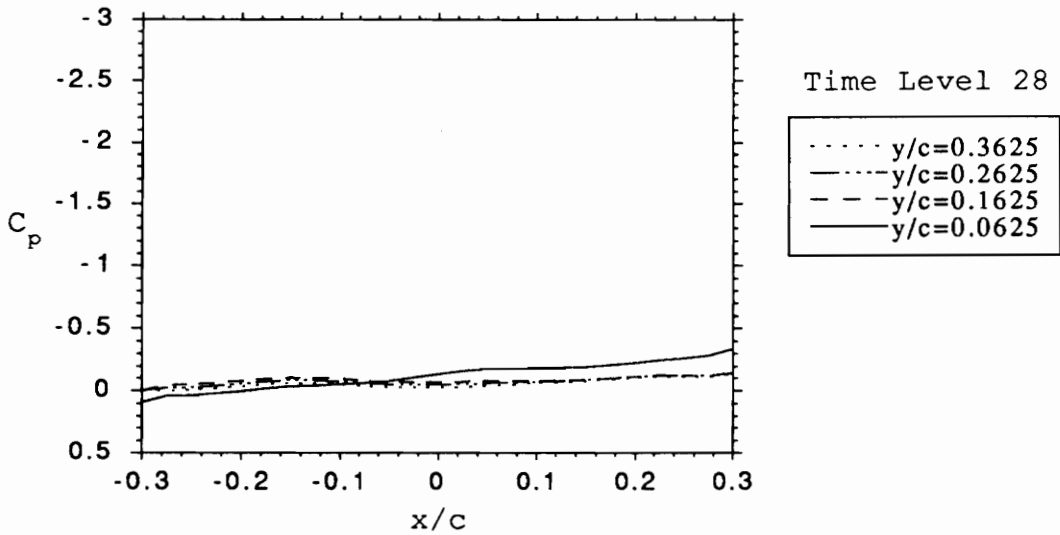
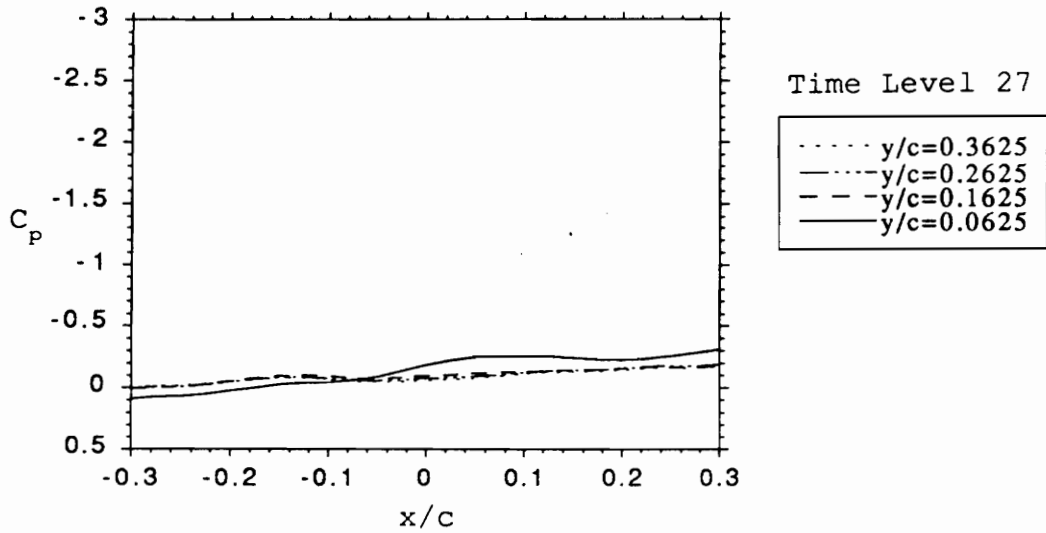


Figure 4.3.64 Pressure coefficients at four y/c locations, at time levels 27 and 28 (27/50 and 28/50 of period, $\tau=1.24$ sec.)

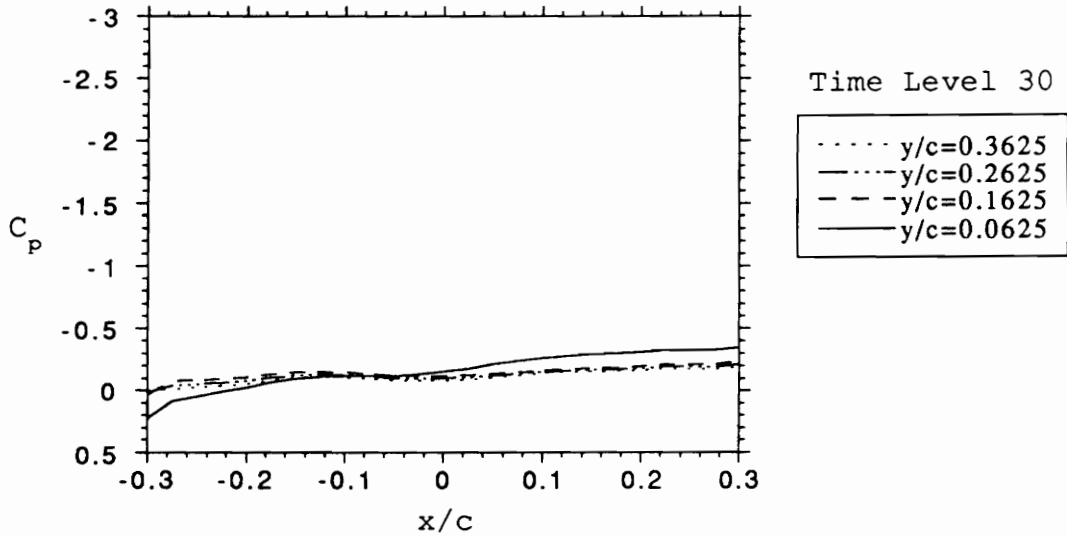
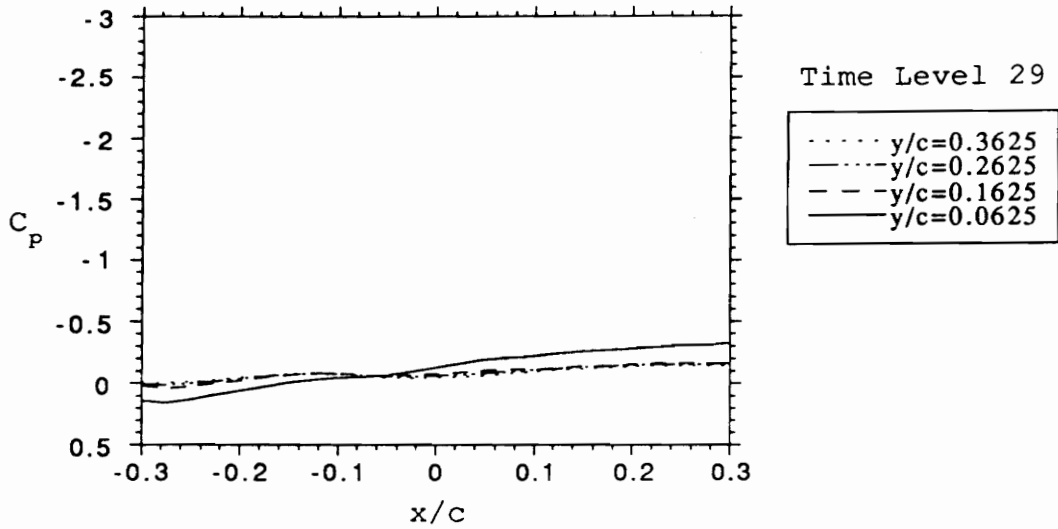


Figure 4.3.65 Pressure coefficients at four y/c locations, at time levels 29 and 30 (29/50 and 30/50 of period, $\tau=1.24$ sec.)

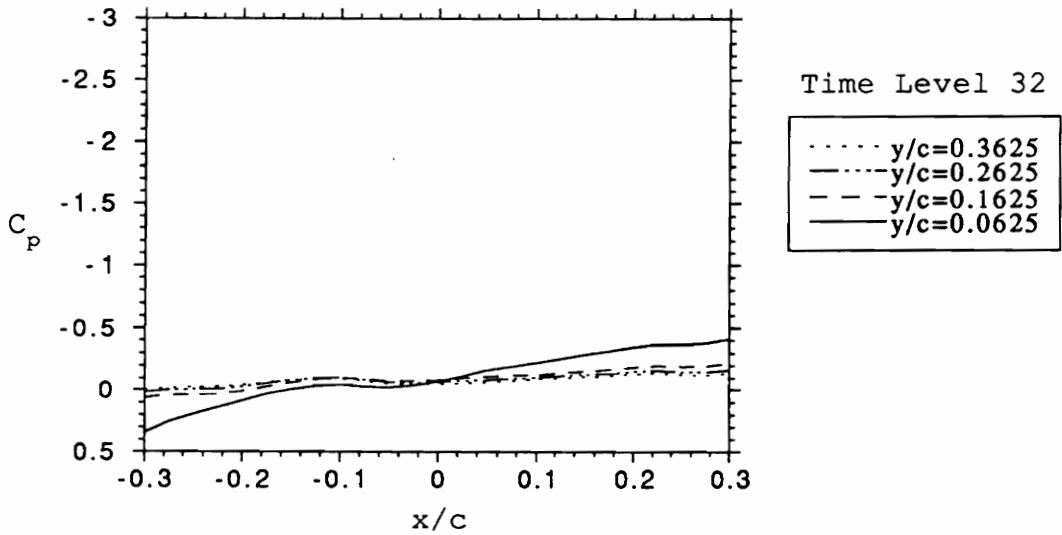
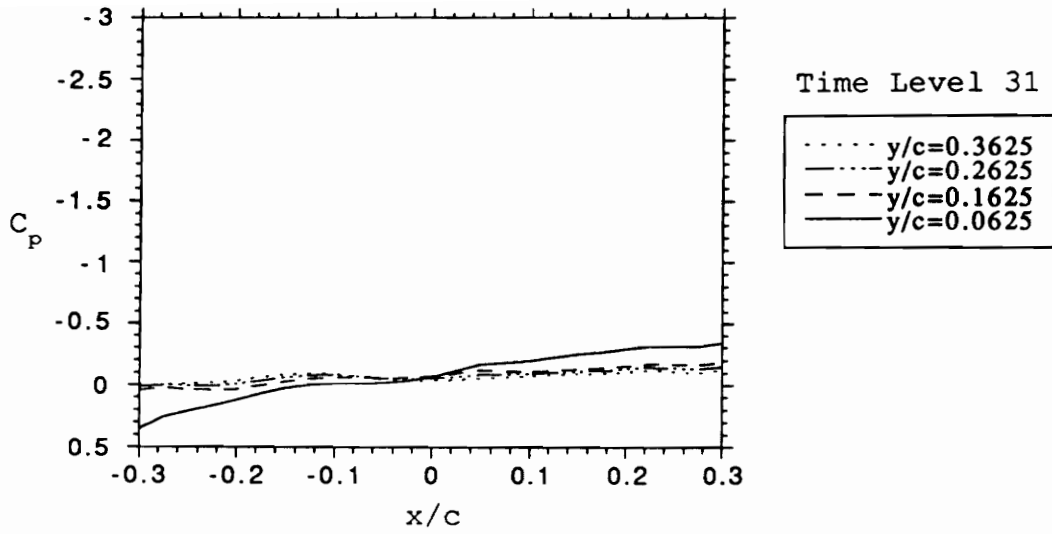


Figure 4.3.66 Pressure coefficients at four y/c locations, at time levels 31 and 32 (31/50 and 32/50 of period, $\tau=1.24$ sec.)

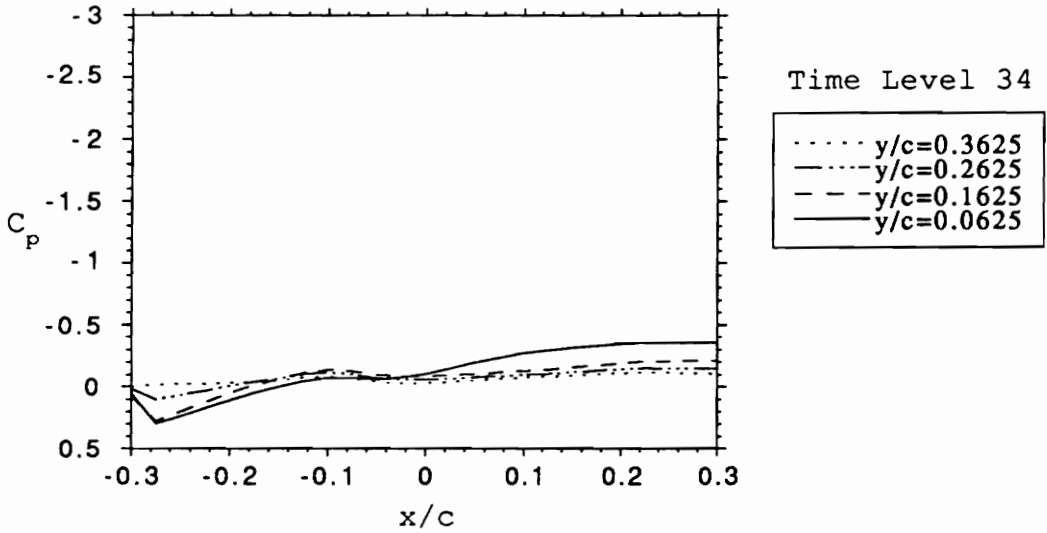
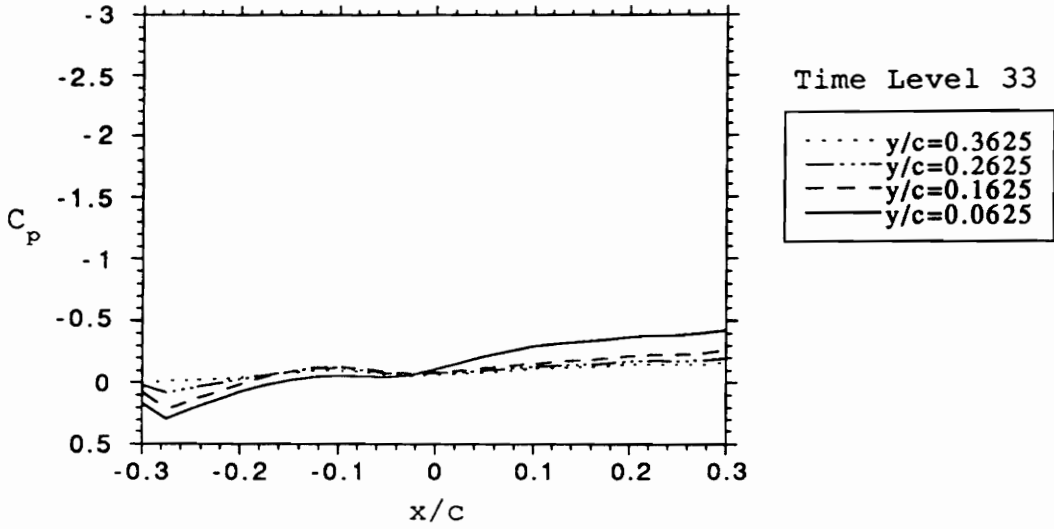


Figure 4.3.67 Pressure coefficients at four y/c locations, at time levels 33 and 34 (33/50 and 34/50 of period, $\tau=1.24$ sec.)

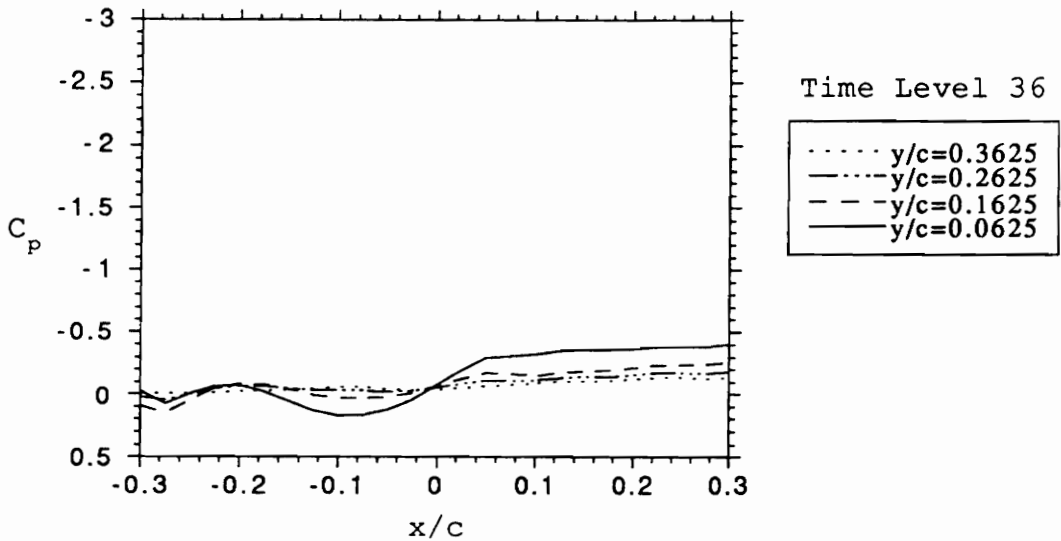
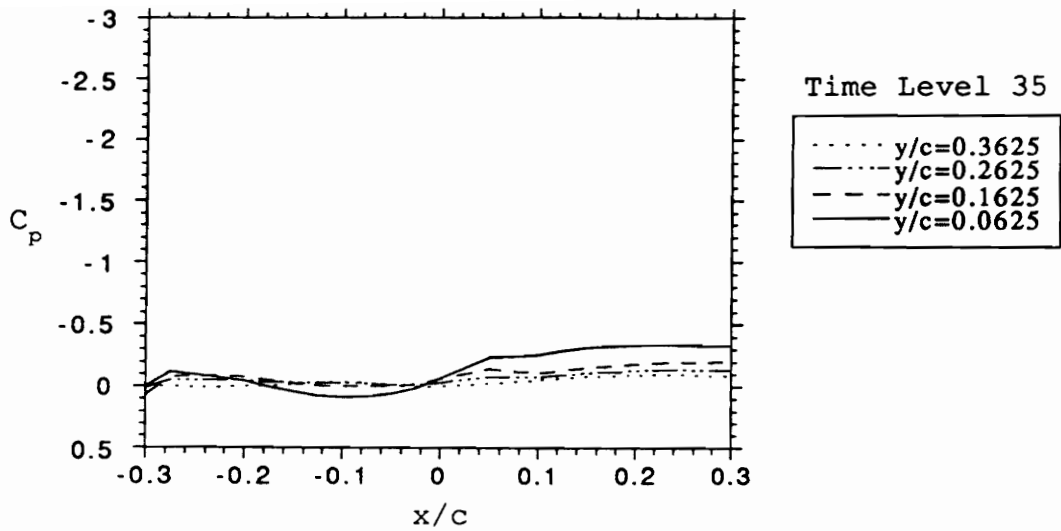


Figure 4.3.68 Pressure coefficients at four y/c locations, at time levels 35 and 36 (35/50 and 36/50 of period, $\tau=1.24$ sec.)

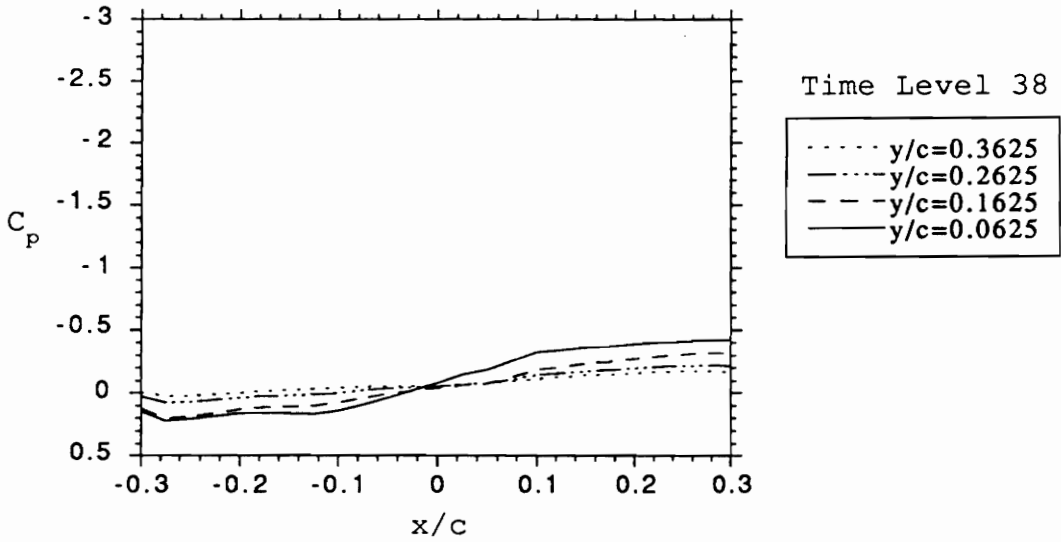
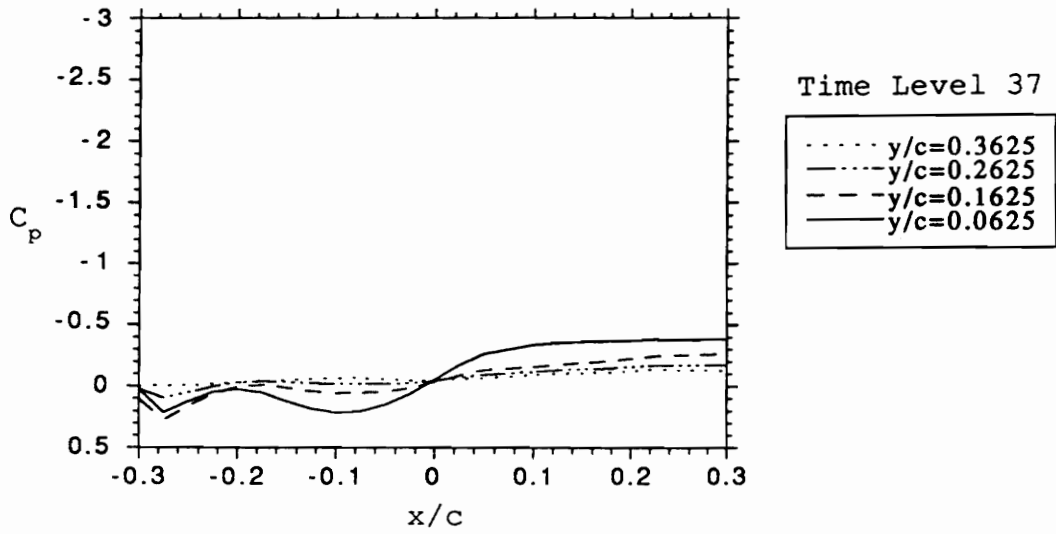


Figure 4.3.69 Pressure coefficients at four y/c locations, at time levels 37 and 38 (37/50 and 38/50 of period, $\tau=1.24$ sec.)

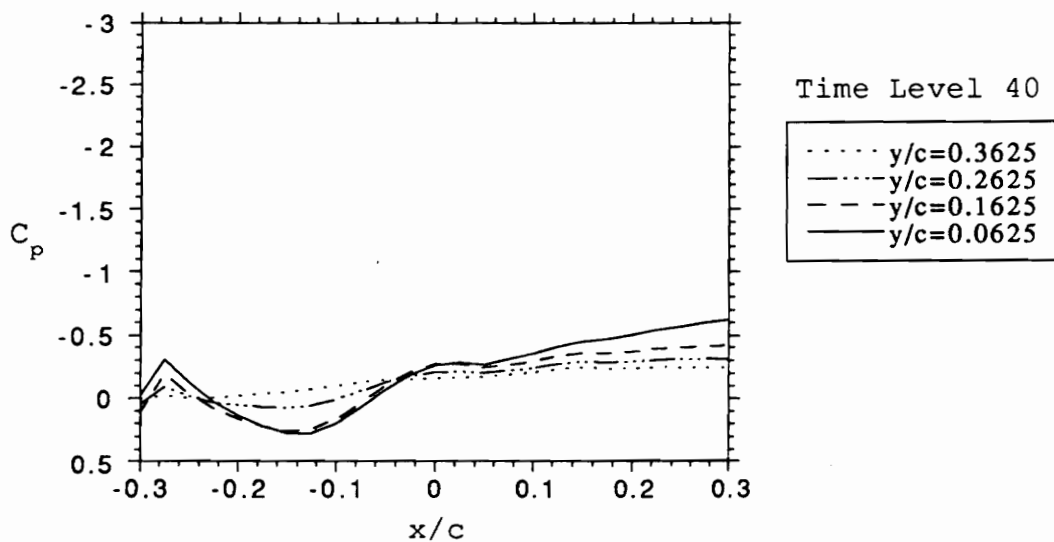
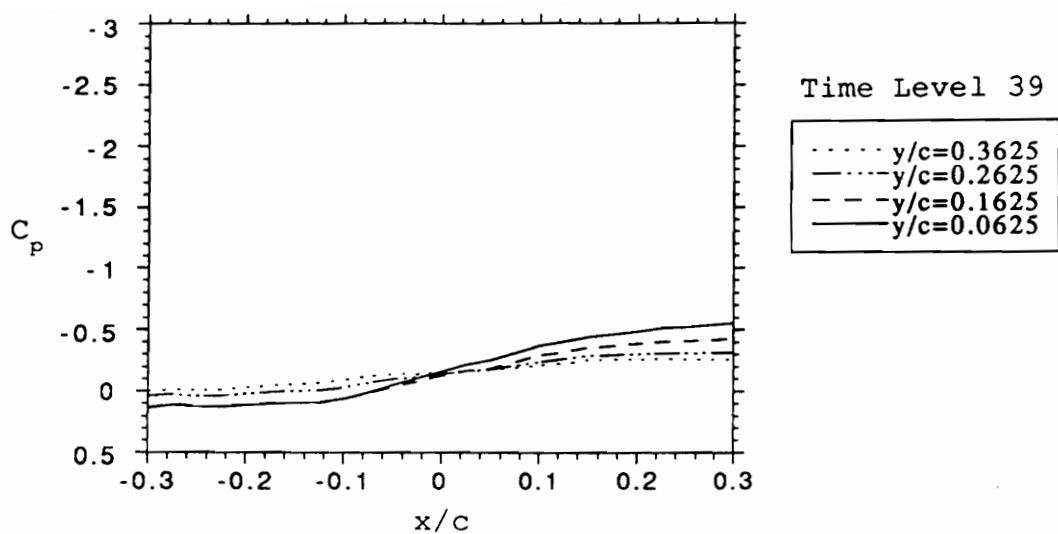


Figure 4.3.70 Pressure coefficients at four y/c locations, at time levels 39 and 40 (39/50 and 40/50 of period, $\tau=1.24$ sec.)

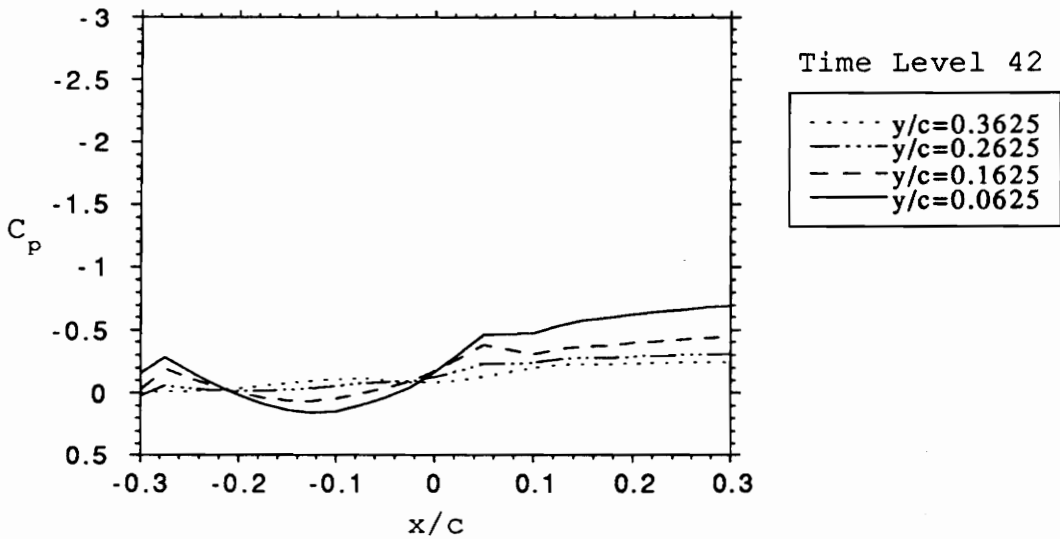
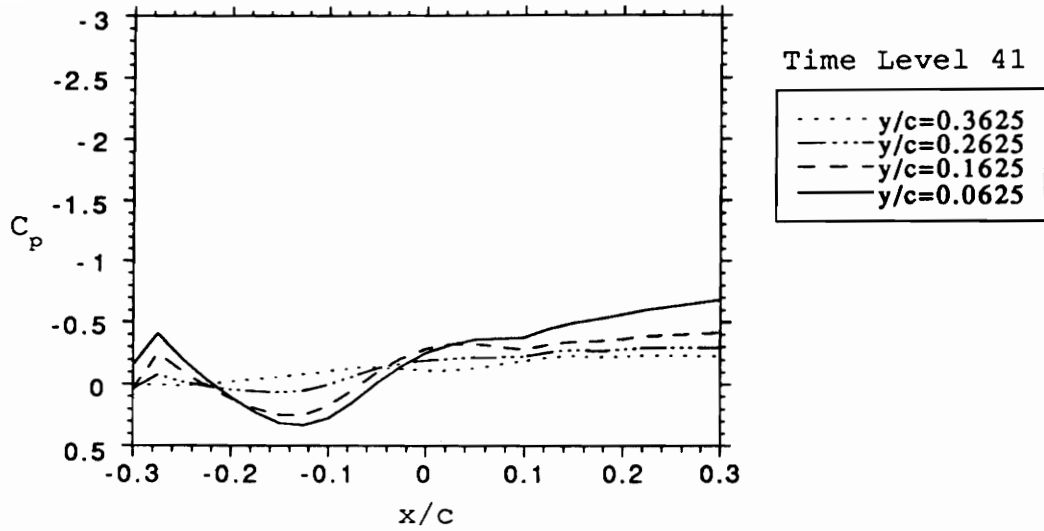


Figure 4.3.71 Pressure coefficients at four y/c locations, at time levels 41 and 42 (41/50 and 42/50 of period, $\tau=1.24$ sec.)

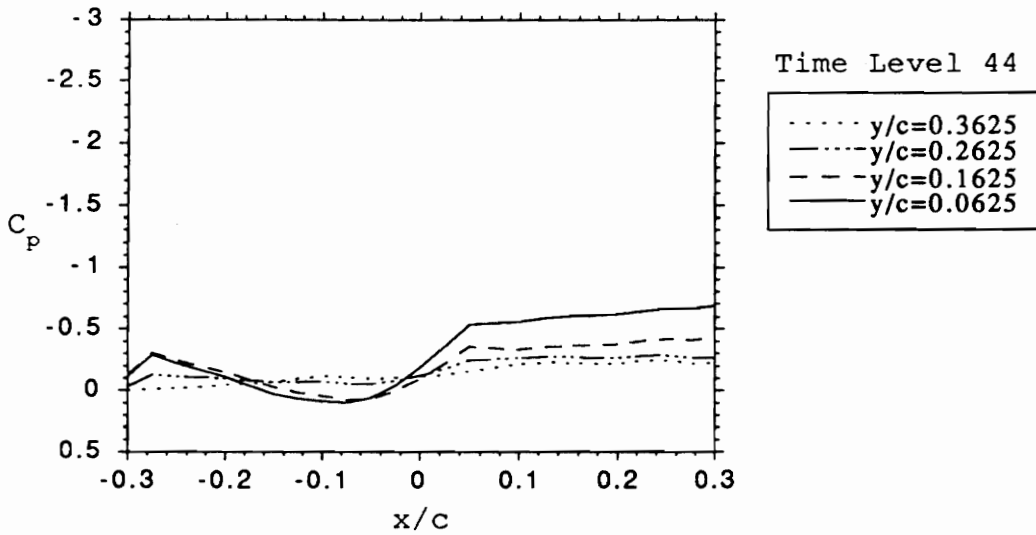
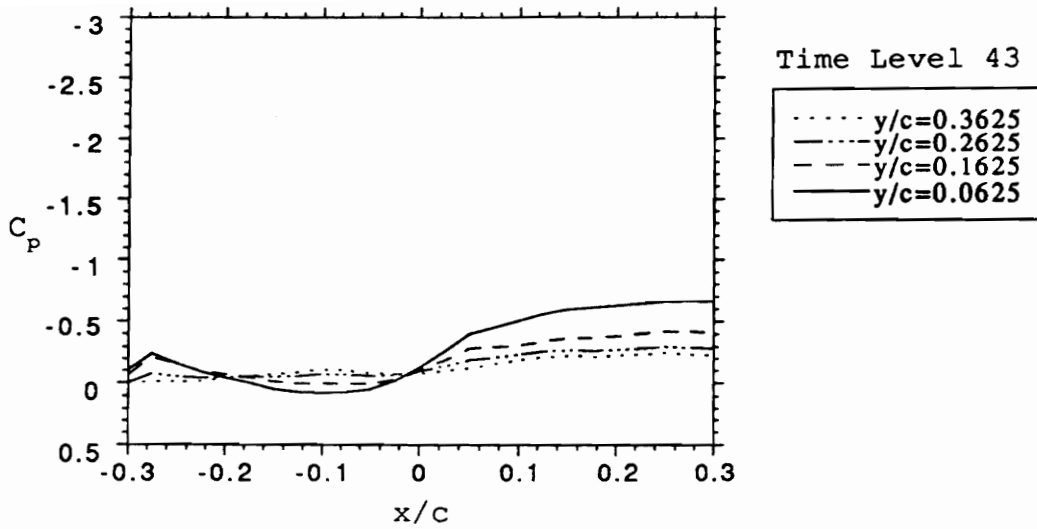


Figure 4.3.72 Pressure coefficients at four y/c locations, at time levels 43 and 44 (43/50 and 44/50 of period, $\tau=1.24$ sec.)

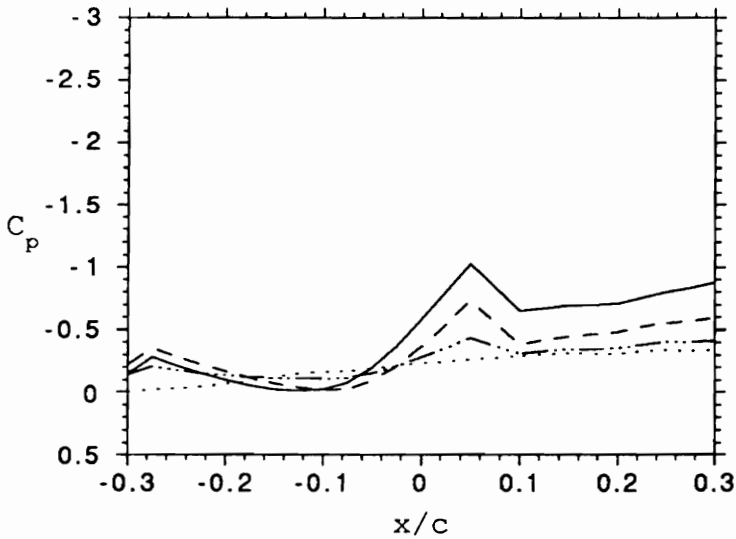
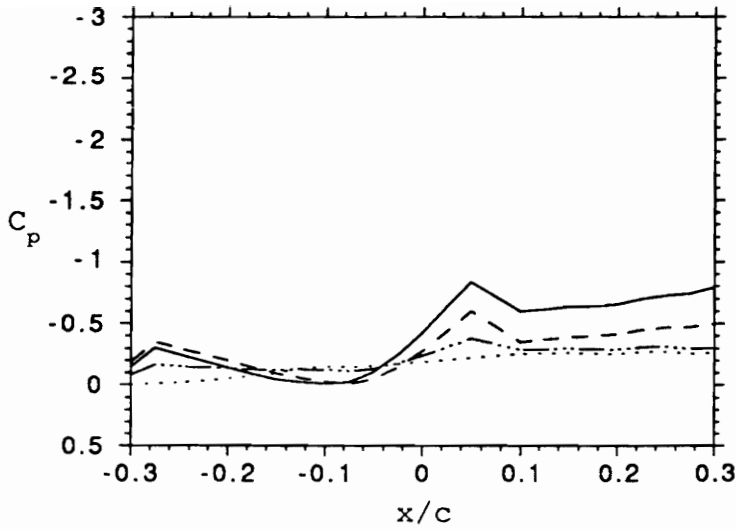


Figure 4.3.73 Pressure coefficients at four y/c locations, at time levels 45 and 46 (45/50 and 46/50 of period, $\tau=1.24$ sec.)

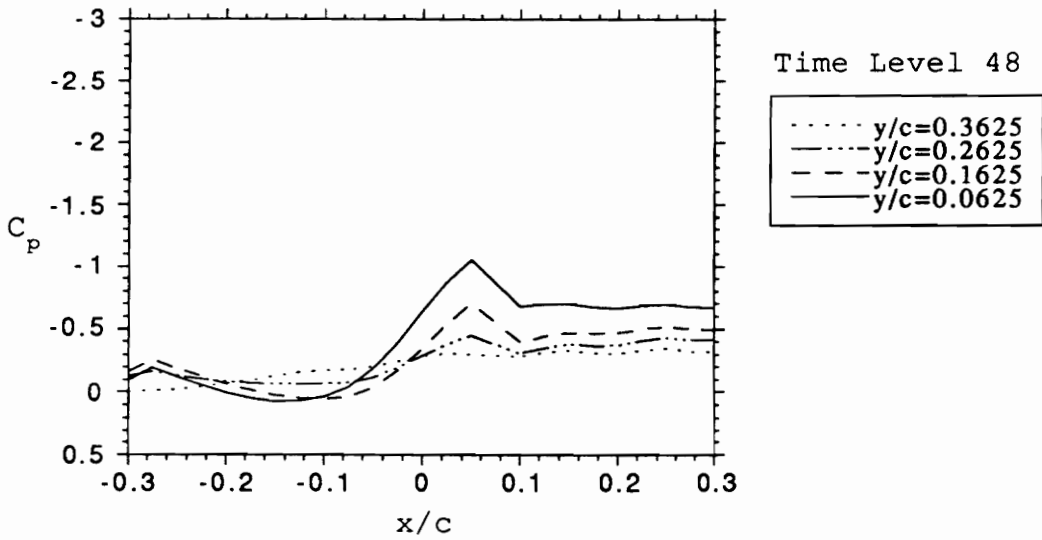
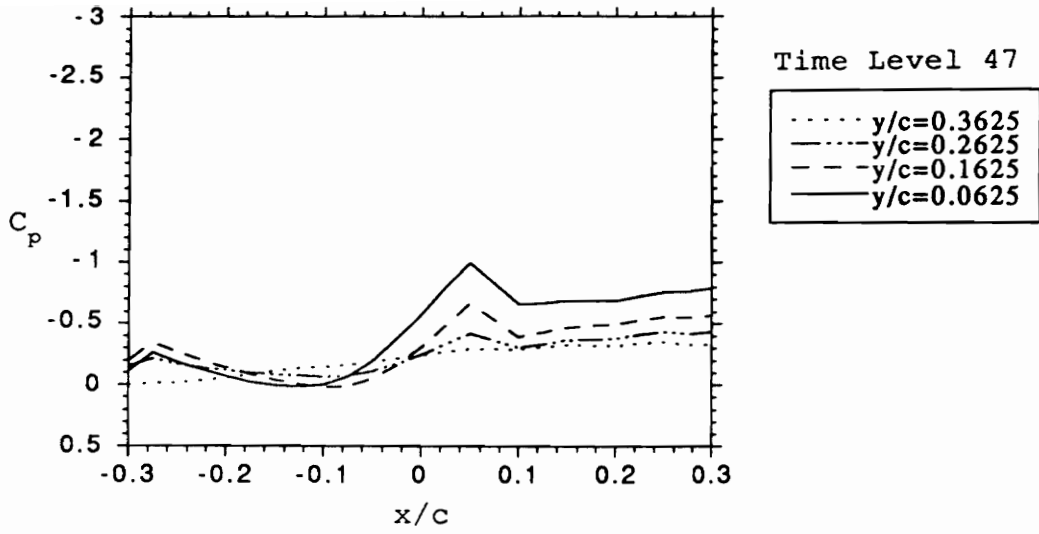


Figure 4.3.74 Pressure coefficients at four y/c locations, at time levels 47 and 48 (47/50 and 48/50 of period, $\tau=1.24$ sec.)

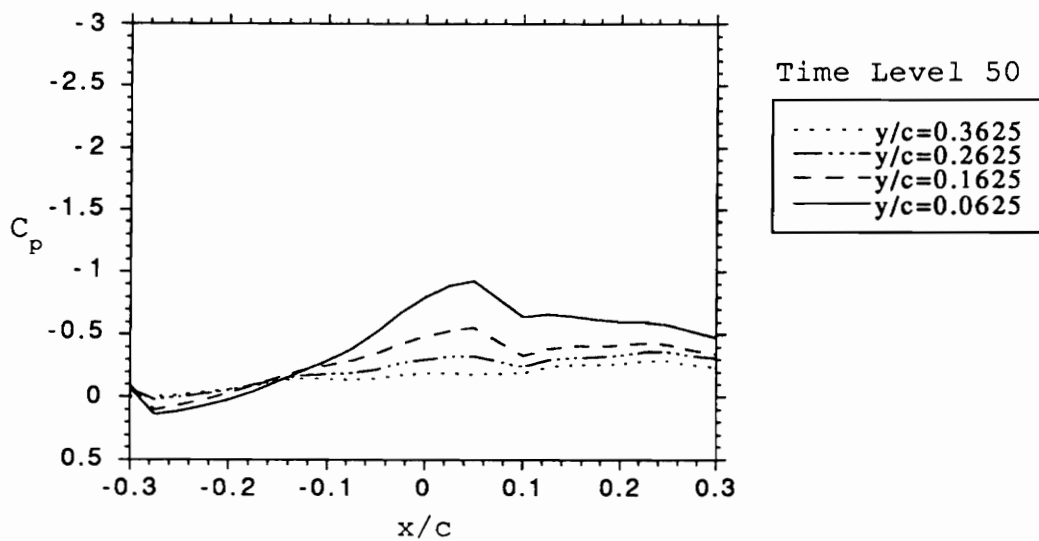
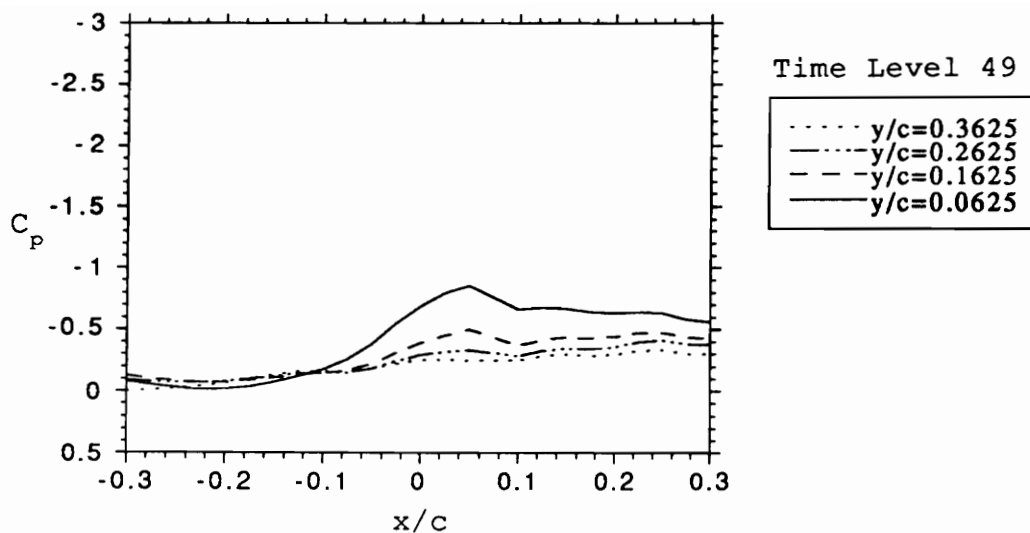


Figure 4.3.75 Pressure coefficients at four y/c locations, at time levels 49 and 50 (49/50 and 50/50 of period, $\tau=1.24$ sec.)

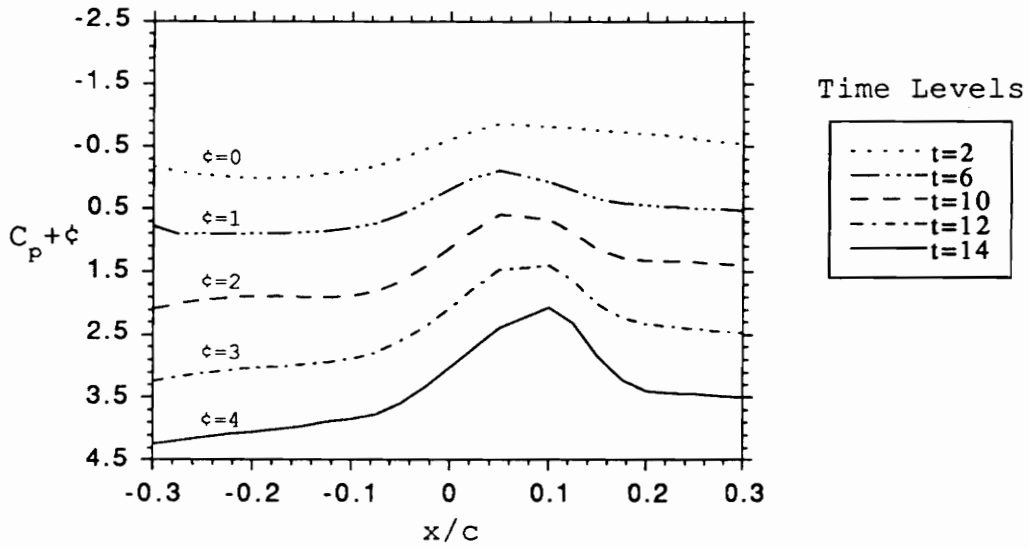
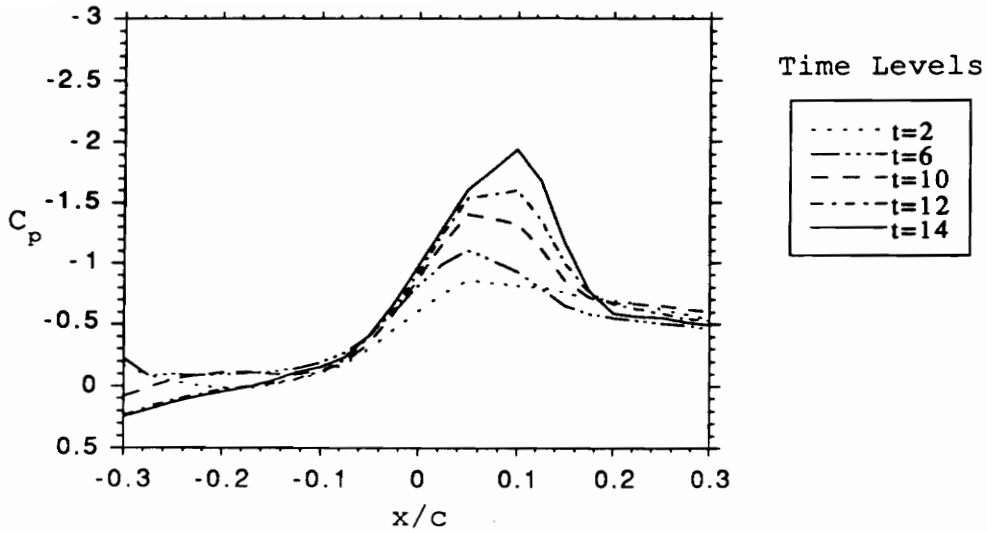


Figure 4.3.76 At $y/c = 0.0625$, pressure coefficients for time levels 2, 6, 10, 12, and 14 are combined. Also, the same curves are shifted by an integer constant.

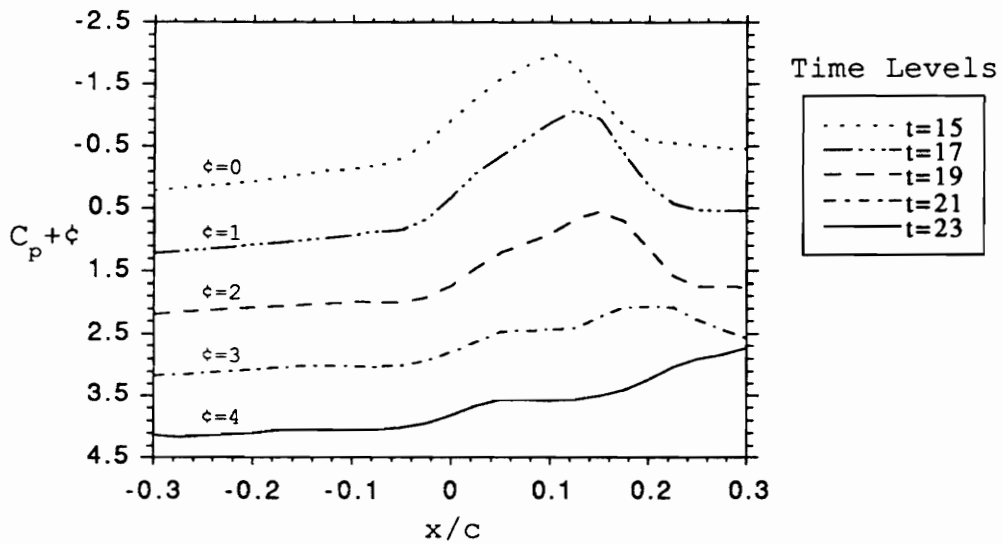
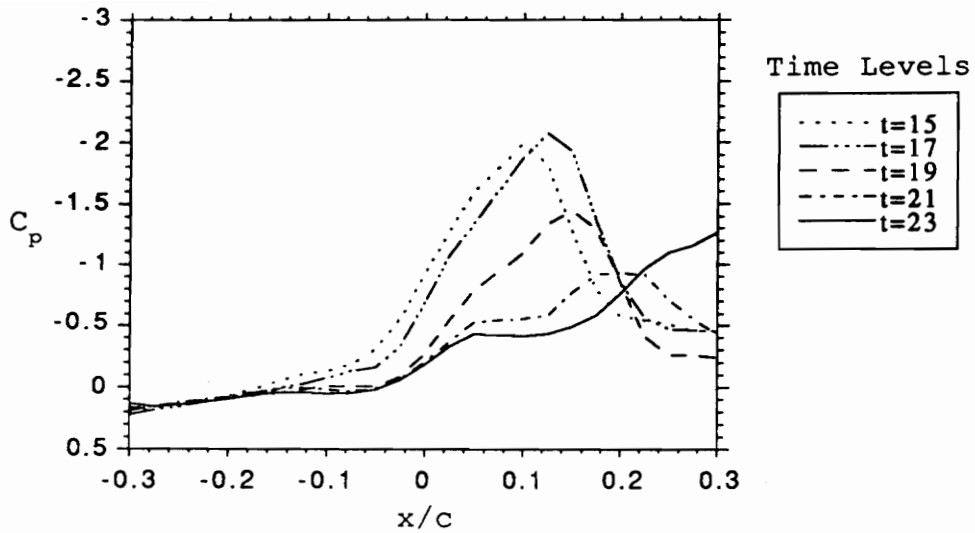


Figure 4.3.77 At $y/c = 0.0625$, pressure coefficients for time levels 15, 17, 19, 21, and 23 are combined. Also, the same curves are shifted by an integer constant.

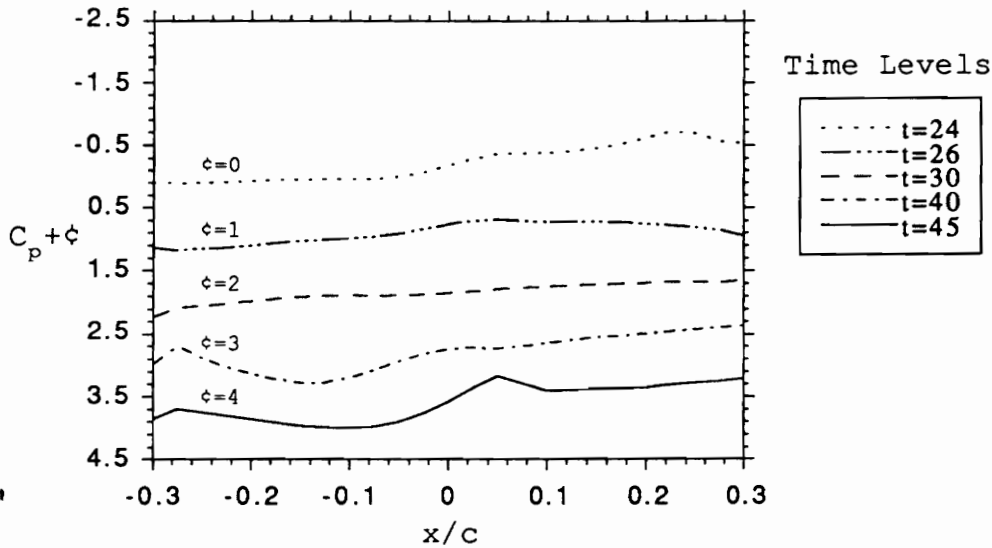
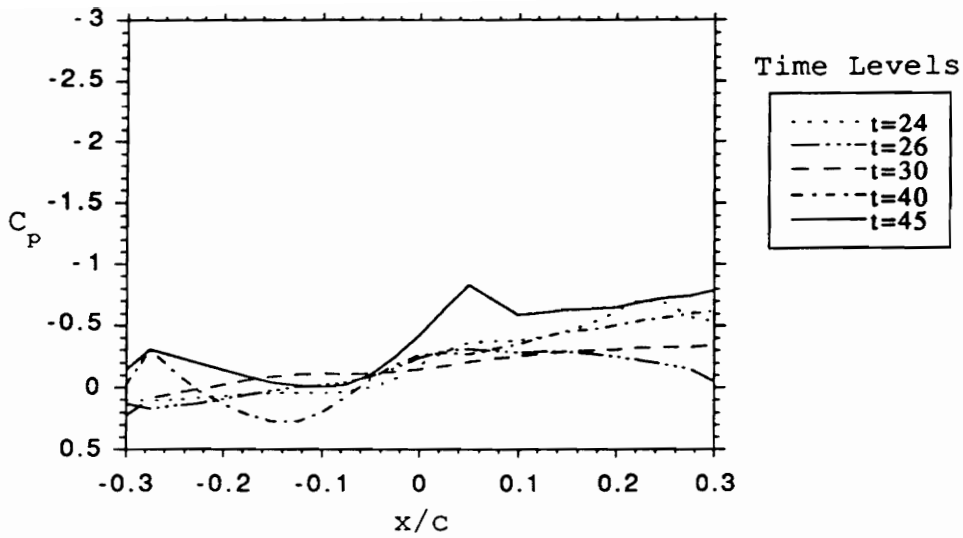


Figure 4.3.78 At $y/c = 0.0625$, pressure coefficients for time levels 24, 26, 30, 40, and 45 are combined. Also, the same curves are shifted by an integer constant.

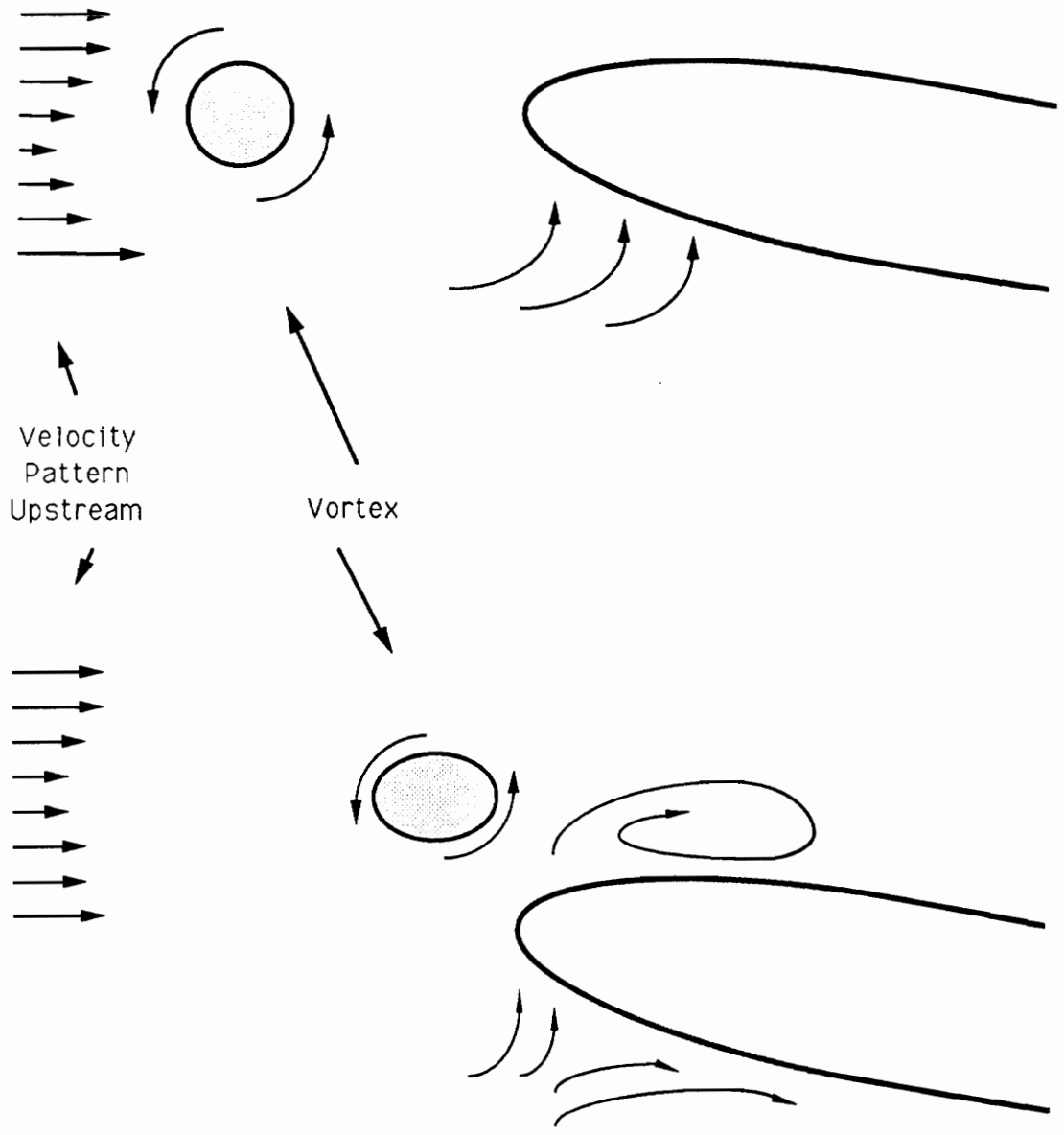


Figure 4.4.1 The affect of the vortex on the airfoil when it is far away and in the nose region

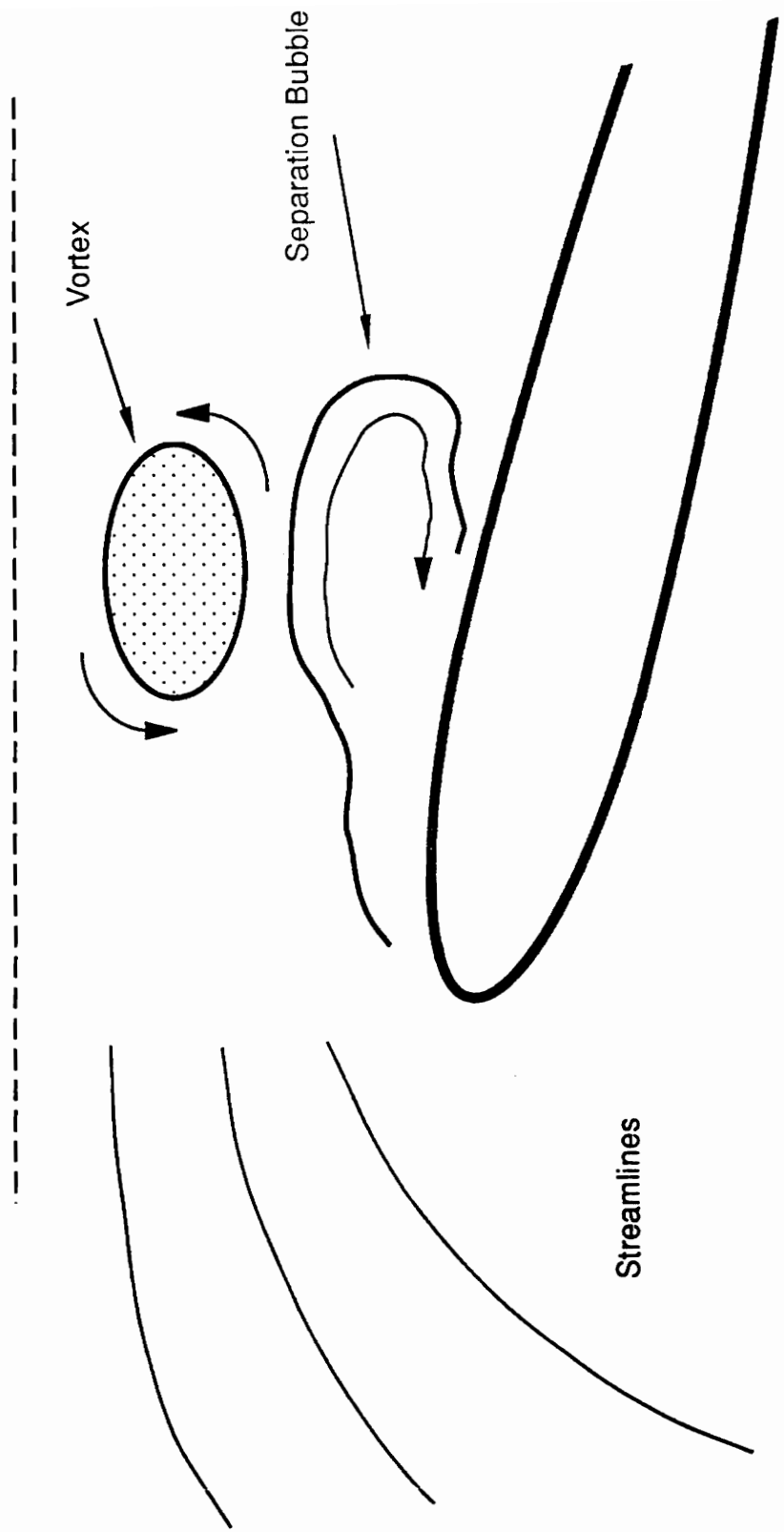


Figure 4.4.2 The affect of the vortex when it is fully above the airfoil

Vita

At the age of 25, the author saw a light in the darkness. He strove toward that light only to find that it was a star on the other side of the void of ignorance. He has built ladders and stairs to reach that star, all failing to reach the height. He is currently using a pogo-stick. That star is no less alluring today.

Matthew Michael Pesce, son of Ralph and Mary, is committed to touching that star, although most of the time he is stuck in the void.